PRO-APOPTOTIC BID FACILITATES ATR FUNCTION FOLLOWING REPLICATIVE STRESS

By

Yang Liu

Dissertation

Submitted to the Faculty of the

Graduate School of Vanderbilt University

in partial fulfillment of the requirements

for the degree of

DOCTOR OF PHILOSOPHY

in

Cell and Developmental Biology

December, 2011

Nashville, Tennessee

Approved:

Sandra S. Zinkel, M.D., Ph.D.

Kathleen L. Gould, Ph.D.

David Cortez, Ph.D.

Elizabeth Yang, M.D., Ph.D.

Laura A. Lee, M.D., Ph.D.

To my parents

ACKNOWLEDGEMENTS

First of all, I thank my thesis advisor, Sandra Zinkel. Doctor Zinkel is a nice and fantastic scientist and she instructs me in every aspect of academic activities. She is an outstanding scientist and her devotion to science infects everyone in our lab. Her office door is always open so that I can discuss and consult scientific issues with her expediently. She encourages me to think independently, critically, and creatively and supports me to attend various academic meetings. She taught me all kinds of research designs and experimental techniques in the field of cell biology, biochemistry and hematology. I thank her give me the opportunity to continue her post-doc work to investigate the function and mechanism of pro-apoptotic BID in the DNA damage response. She is a truly exceptional mentor.

I thank my thesis dissertation committee: Professor Kathy Gould, Professor David Cortez, Doctor Elizabeth Yang, and Doctor Laura Lee. As the leading scientists in biomedical research field, my committee members provide me sustained support in both scientific thinking and project progression. Without committees' excellent supervision, I could not have made such progress in my thesis project. I sincerely appreciate committees' instruction and suggestion. Especially, I should thank Professor Cortez. He shared many valuable reagents and constructs with me and gave me many invaluable ideas and suggestions. Thanks for keeping me focused with objective criticism and encouragement. I

sincerely appreciate committees' time and effort on my project.

I thank all of people in our laboratory. Especially, I thank Qiong Shi, Clinton Bertram, and Alexis Aiello. As a senior research scientist, Qiong taught me many experimental techniques, from tissue culture to co-immunoprecipitation. She helped me finish the BID-ATRIP interaction by co-immunoprecipitation assay and construct U2OS cell lines stably expressing wild-type and various mutated BID. She also shared me much invaluable knowledge and information about life style in US. Clinton helped me finish BID-RPA co-localization assay by confocal microscopy and Alexis helped me finish part of methylcellulose culture of HU-stressed bone marrow cells. Aubrey Wernick is a mouse expert and breeds all kinds of mice used in our lab. Subhrajit Biswas, Christopher Buckman, and Patrice Wagner gave me many useful suggestions on experiments as well as on presentation skills. I also thank all of the people who worked in Zinkel's lab before. I appreciate everyone's contribution to our laboratory.

I thank all of labs collaborate with us: the laboratories of Professor Walter Chazin, Professor David Cortez, Professor Ellen Fanning, Professor Scott Hiebert, Professor Jennifer Pietenpol, Professor Christine Eischen, and Doctor Elizabeth Yang. Especially, I thank Sivaraja Vaithiyalingam in Professor Chazin's lab. Dr. Vaithiyalingam helped me finish BID-RPA70N interaction by NMR technique and simulate BID-RPA70N complex. He also taught me how to prepare a ^{15}N-labled protein. I thank Professor Cortez for the anti-ATRIP antibody, various ATRIP

mutants and constructs, the U2OS cells expressing HA-ATRIP, and the RPA70N construct harboring R41E/R43E mutation. I thank Professor Fanning to share me the information about RPA as well as the expression vector of His-tagged RPA70NAB, AB, N, and 32C domain. I thank Professor Pietenpol to share GST-CDC25C protein and Nucleofector System. I appreciate everyone's support to my projects sincerely.

I thank Department of Cell and Developmental Biology, Vanderbilt-Ingram Cancer Center, Vanderbilt Cell Imaging Shared Resource, and VMC Flow Cytometry Core. I thank the research funds to support my research at Vanderbilt University.

Last but not least, I thank my parents, Huifen Yang and Zhongge Liu to give me invaluable support and encourage. And I thank my friends Tongjin Zhao (UT Southwestern) and Jun Zhang (UNC) to give me great suggestions in science.

TABLE of CONTENTS

Page

LIST OF TABLES

Table Page

LIST OF FIGURES

LIST OF ABBREVIATIONS

9-1-1	RAD9-HUS1-RAD1
aa	Amino acid
ATM	Ataxia-telangiectasia mutated
ATR	ATM- and RAD3-related
ATRIP	ATR-interacting protein
BAK	BCL2-antagonist/killer
BAX	BCL2-associated X protein
BCL-2	B-cell lymphoma 2
BID	BH3 interacting domain death agonist
BM	Bone marrow
BrdU	Bromodeoxyuridine
CDK	Cyclin-dependent kinase
CFU	Colony forming unit
CHK1	Checkpoint kinase 1
CHX	Cycloheximide
CLP	Common lymphoid progenitors
CMP	Common myeloid progenitors
DDR	DNA damage response
DMEM	Dulbecco’s modified Eagle’s medium
DSB	DNA double strand breaks

DTT	Dithiothreitol
EDTA	Ethylenediaminetetraacetic acid
EGTA	Ethylene glycol tetraacetic acid
EPO	Erythropoietin
ETOP	Etoposide
FBS	Fetal bovine serum
GEMM	Granulocyte, erythrocyte, macrophage, megakaryocyte
GM	Granulocyte macrophage
GMP	Granulocyte-monocyte progenitors
HSC	Hematopoietic stem cells
HSQC	Heteronuclear single quantum coherence
HU	Hydroxyurea
IH5	Inside Helix 5
IL3	Interleukin 3
IL6	Interleukin 6
IMDM	Iscove's modified Dulbecco's medium
IP	Immunoprecipitation
IPTG	Isopropyl-β-D-1-thiogalactopyranoside
IR	Ionizing radiation
KD	Knockdown
LSK	Lineage-/c-kit+/sca-1+

MBP	Maltose binding protein
MCL-1	Myeloid cell leukemia sequence 1
MEP	Megakaryocyte-erythroid progenitors
MPC	Myeloid progenitor cells
MRN	MRE11-RAD50-NBS1
Mw	Molecular weight
NMR	Nuclear magnetic resonance
PBS	Phosphate Buffered Saline
PDI	Protein disulfide isomerase
PIKK	Phosphoinositide-3 kinase-related kinase
PMSF	Phenylmethylsulfonyl fluoride)
RPA	Replication protein A
RPA-ID	RPA interacting domain
SCF	Stem cell factor
SDS-PAGE	Sodium dodecyl sulfate polyacrylamide gel electrophoresis
siRNA	Small interfering RNA
ssDNA	Single-stranded DNA
TNF	Tumor necrosis factor
TopBP1	Topoisomerase (DNA) II-binding protein 1
TRAIL	TNF-related apoptosis-inducing ligand
UV	Ultraviolet radiation

CHAPTER I

INTRODUCTION

Multicellular organisms utilize a series of mechanisms to maintain the tissue homeostasis, including maintenance of genomic integrity and regulation of programmed cell death. Defects in the DNA damage/repair pathway and/or apoptosis pathway have been demonstrated to associate with various human diseases, such as malignancy, autoimmune disease, and neurological disease (1). First identified as a pro-apoptotic member in the cell death pathway, BH3 interacting domain death agonist (BID) has recently been demonstrated to play a role to maintain genomic stability and execute DNA damage checkpoints following DNA damage treatments (2,3). To clarify the function of BID in the cellular response to DNA damage, especially the response to DNA damage induced by replicative stress, I used genetic and biochemical tools in this thesis to investigate the function and mechanism of BID in the Ataxia-telangiectasia mutated and RAD3-related (ATR)-mediated signaling pathways. The function of BID in the ATR-directed DNA damage response is investigated at multiple levels, from structural biology to animal models (4-6). The significance of the dual functions of BID in both DNA damage and cell death pathways will be discussed.

Apoptosis and BCL-2 family

Programmed cell death and Apoptosis

Programmed cell death is a highly regulated intracellular program used by various metazoans to initiate and execute cell death following various cellular stresses and/or extrinsic signals (7). Thus far, three types of programmed cell death have been identified and demonstrated in eukaryotic cells, i.e., apoptosis (Type I), autophagy (Type II), and programmed necrosis (Type III) (8). Apoptosis is the principle mechanism in metazoans to remove damaged or redundant cells by breaking down cell components into apoptotic bodies (9), which are recognized and engulfed by phagocytic cells to avoid inflammation around the dying cells(10). The most important molecular marker of apoptosis is the activation of various caspases (11). When apoptosis is inhibited by pharmacological agents or in certain genetic backgrounds, stressed cells might initiate programmed necrosis or necroptosis to execute caspase-independent cell death by activation of various RIP kinases (12). Different from apoptosis and necrosis, autophagy is a “survival” process involving the degradation of redundant or impaired intracellular components through lysosomal machinery as a response to cellular stress, such as starvation (13). Physiological level of autophagy is important for cellular homeostasis while excessive autophagy promotes cell death (14). Apoptosis, autophagy and programmed necrosis possess distinct characteristics with respect

to cellular morphology and molecular mechanism, however, certain key factors function in multiple cell death pathways and might control the cell fate in different types of programmed cell death.

As the best studied programmed cell death, apoptosis is elaborately regulated at multiple levels to control cell fate following various endogenous or extrinsic signals (Fig. 1-1A). Typically, the cellular stresses or death signals are sensed by various BCL-2 (B-cell lymphoma 2) family proteins, which relay the death signals to mitochondria, an essential integration machinery of cellular metabolism and apoptosis (7). Following cellular stresses or death signals, pro-apoptotic members harboring only one BH3 domain (BH3-only pro-apoptotic members) are activated and translocate to mitochondria, which results in the oligomerization and activation of BAX/BAK (7,15,16). Once BAX/BAK is activated, mitochondrial outer membrane permeabilization (MOMP) leads to the release of multiple pro-apoptotic factors from the mitochondrial inter membrane space and apoptosis is executed (17-20)(Figure 1-1). Various BH-3 only molecules can either activate BAX/BAK directly or release the inhibition on BAX/BAK from anti-apoptotic BCL-2 members indirectly (15,20-22) (Figure 1-1).

The process of mitochondrial outer membrane permeabilization results in the release of multiple pro-apoptotic proteins from the mitochondrial intermembrane space into the cytoplasm, including cytochrome *c*, SMAC (second mitochondria-derived activator of caspases)/DIABLO (direct inhibitor of apoptosis

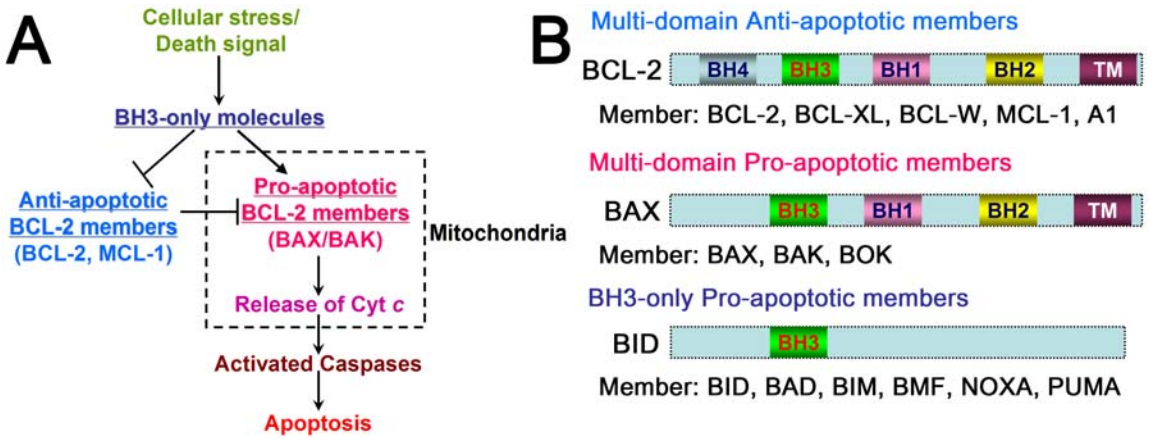

Figure 1-1. The function of BCL-2 family in apoptosis pathway. (A) Simplified apoptosis pathway. Cellular stresses or death stimuli are sensed by various BH-3 only molecules, which activate BAX/BAK directly or release the inhibition on BAX/BAK from anti-apoptotic BCL-2 members. The oligomerization of BAX/BAK results in the release of cytochrome *c*, which activates caspase-9. The resultant activation of various downstream effector caspases leads to apoptosis. (B) BCL-2 family is comprised of three subclasses, multi-domain anti-apoptotic members (e.g. BCL-2 and MCL-1), multi-domain pro-apoptotic members (e.g. BAX and BAK), and BH-3 only pro-apoptotic members (e.g. BID, BAD and BIM).

(IAP)-binding protein with low pI), OMI/HTRA2 (high-temperature-requirement protein A2), ENDONUCLEASE G, and AIF (apoptosis-inducing factor). The released cytochrome *c* binds to APAF1 (apoptotic peptidase activating factor 1) and induces a conformational change (18,19). Activated APAF1 recruits caspase-9 in the presence of ATP/dATP to form the apoptosome, which cleaves and activates downstream effector caspases, e.g. caspase-3 (18,23). The released SMAC/DIABLO and OMI/HTRA2 bind to IAP and blocks its inhibition of caspases (24-26). The released ENDONUCLEASE G and AIF translocate to the nucleus to induce DNA fragmentation and degradation (27,28). It is worthwhile to note that the initiation of apoptosis in mammalian systems is predominantly regulated by BCL-2 family proteins at the sensor/transducer level (7,29) rather than by the effectors functioning downstream mitochondria.

Based on the origin of death stimuli, the apoptotic response is initiated and mediated by either intrinsic or extrinsic cell death pathways. Intrinsic death stimuli (e.g. oncogene activation, DNA damage, and survival factor deprivation) are generated within the cells, predominantly sensed by various BH3-only molecules, and transduced to mitochondria to initiate apoptosis (7). Extrinsic death stimuli (e.g. death ligands, such as Fas ligand and TRAIL) are generated from extracellular environments, sensed by death receptors, and executed by caspases to initiate apoptosis directly (30). Interestingly, BH3-only BID mediates the crosstalk between the extrinsic pathway and the intrinsic pathway through the

generation of truncate BID by caspase 8 cleavage (31,32). Based on the function of BCL-2 family in the extrinsic pathways, two pathways have been reported in different cell types. In Type I cells (e.g. thymocytes), sufficient caspase 8 activation results in an adequate activation of downstream effector caspase (e.g. caspase 3 and caspase 7) and tBID-induced activation of BAX at the mitochondria plays a minimum role in this death receptor-induced apoptosis (33). In Type II cells (e.g. hepatocytes), the mitochondrial amplification loop is an essential process to generate sufficient activation of downstream effector caspases and caspase 8-mediated cleavage of BID plays an important role to initiate death receptor-induced apoptosis (33).

BCL-2 family

BCL-2 gene was first reported and cloned from non-Hodgkin lymphomas with t(14;18) chromosomal translocations, in which *BCL-2* gene is fused with the immunoglobulin heavy-chain locus (IgH) (34-39). In a *Bcl-2*-Ig transgenic mouse model, under the control of the IgH enhancer, the *BCL-2* gene is highly expressed at the transcriptional level to protect B cells from apoptosis following multiple physiological and pathological stimuli (40,41). *Bcl-2*-Ig transgenic mice spontaneously develop a polyclonal follicular hyperplasia comprised of B220-positive, IgM/IgD-positive B cells (41). Different from other oncogenes that induce cell proliferation (i.e., RAS and MYC), BCL-2 does not increase cell cycle

proliferation (42), suggesting that abnormal apoptosis is a novel mechanism of tumorigenesis.

After the *BCL-2* gene was cloned and investigated, a series of proteins sharing BCL-2 homology domains (BH domain) were identified by biochemical or genetic tools. The BCL-2 family is classified as three groups, multi-domain anti-apoptotic members (e.g. BCL-2 and MCL-1), multi-domain pro-apoptotic members (e.g. BAX and BAK), and BH3-only pro-apoptotic members (e.g. BID, BAD and BIM) (Figure 1-1) (7,15,43). Following cellular stresses or death signals, pro-apoptotic members harboring only one BH3 domain (BH3-only pro-apoptotic members) are activated and translocate to mitochondria to interact with other BCL-2 family members by their BH3 domain, which results in the activation of BAX/BAK (7,15,16). Once activated, BAX and BAK undergo conformational changes, which result in the homo-oligomerization of BAX/BAK to form a pore that results in mitochondrial outer membrane permeabilization (MOMP) (20,44).

Although BH3-only proteins interact with BAX/BAK by BH3 domain, different BH3-only proteins activate BAX/BAK by different mechanisms (45). BID, BIM and PUMA are able to interact with all anti-apoptotic BCL-2 family members and function as direct activators of BAX/BAK (46,47). In an *in vitro* system with isolated mitochrondria or liposome vesicles, peptides comprised of the BH3-domain of BID activate monomeric BAX to form supramolecular membrane openings in the outer mitochondrial membrane (46,47). Similar effects on

cytochrome *c* release and BAX oligomerization have also been observed for tBID, BIM and PUMA (48,49). The detailed activation mechanism of tBID in mitochrondria was uncovered by Andrew's lab in 2008 (50) using fluorescence techniques and an *in vitro* reconstitution system. tBID first associates with the membrane and then recruits BAX, followed by BAX oligomerization and membrane permeablization. In contrast, other BH3-only proteins (e.g. BAD, BIK and Noxa) function as indirect sensitizers to regulate the activation of BAX/BAK by releasing the inhibition of anti-apoptotic proteins (e.g. BCL-2 and MCL-1) on direct activators (BID and BIM). Each BH3-only sensitizer has a unique binding profile for limited anti-apoptotic BCL-2 family members and incubation of these sensitizers does not induce cytochrome *c* release from the isolated mitochrondria *in vitro* (48,51). When anti-apoptotic proteins are overexpressed, the pro-apoptotic function of direct activators is inhibited and co-expression of these sensitizers significantly diminishes the inhibition of anti-apoptotic proteins in a dose-dependent manner (48,51). However, how BH3-only molecules quantitatively activate BAX/BAK is still not clear, and the mechanisms deduced from different systems are still controversial(52,53).

As upstream sensors in apoptotic signaling pathways, various BH3-only molecules are selectively activated in response to specific cellular stresses or death stimuli by either transcriptional control or posttranslational modification(7,54). For example, following DNA damage, the activation of p53

increases the transcriptional level of *PUMA* and *NOXA* to initiate apoptosis (55). Following cytokine deprivation, *BIM* expression is up-regulated by the forkhead transcription factor FKHRL1 (56). Following survival factor withdrawal, BAD phosphorylation is blocked, which releases BAD from 14-3-3 binding and it interacts with anti-apoptotic proteins in the cytosol (57). Following death receptor stimulation, BID is cleaved by activated caspase 8 and truncated BID translocates to mitochondria to initiate apoptosis (31,32).

Table 1. Summarized spontaneous phenotypes of animal model with deficiency in BCL-2 family member.

Gene name	Protein functions	Knockout Phenotypes
A1	Anti-apoptotic	Enhanced apoptosis of peripheral blood neutrophils and mast cells (58,59)
Bad	Pro-apoptotic	Diffuse large B cell lymphoma (60)
Bax	Pro-apoptotic	Thymocytes and B cells hyperplasia, male infertile (61)
Bax/Bak	Pro-apoptotic	Persistence of interdigital webs, abnormal accumulation of small neuronal cells and lymphocytes (62)
Bcl-2	Anti-apoptotic	Growth retardation, polycystic kidney disease, fulminant apoptosis of the thymus and spleen, hypopigmented hair (63)
Bcl-w	Anti-apoptotic	Failed spermatogenesis (64)
Bcl-x	Anti-apoptotic	Defects of the survival of immature thymocytes (65)
Bid	Pro-apoptotic	Chronic myelomoncytic leukemia (66)
Bim	Pro-apoptotic	Develop plasmacytosis and autoimmune kidney disease (67-70)
Mcl-1	Anti-apoptotic	Loss of peripheral lymphocytes, loss of bone marrow early progenitor/stem cell populations (71,72)

Although various BCL-2 family proteins share similar structure and apoptotic function *in vitro*, the physiological and pathological functions of different BCL-2

members differ *in vivo* (Table 1). The spontaneous phenotypes of animal models with deficiencies in Bcl-2 family members are summarized in Table 1. *Bcl-2* -/- mice complete embryonic development, however, severe growth retardation, polycystic kidney disease, fulminant apoptosis of the thymus and spleen, and hypopigmented hair were observed in *Bcl-2* -/- mice as early as one week of age (63). Inducible deletion of *Mcl-1* in mice resulted in ablation of bone marrow and the loss of early bone marrow progenitor and stem cell populations (71,72). When both *Bax* and *Bak* gene are deleted in mice, the majority of *Bax* -/- *Bak* -/- mice died perinatally and the adult mice exhibit severe developmental defects (62). It is worthwhile to note that although the loss of *Bcl-2*, *Mcl-1* and *Bax/Bak* results in severe defects, only mild phenotypes were observed in other Bcl-2 family knockout mice (Table 1), which suggests that Bcl-2 family proteins function differentially and hierarchically *in vivo*. Interestingly, most of the severe phenotypes in Bcl-2 family knockout mice were observed in the hematopoietic system (Table 1), suggesting that the Bcl-2 family plays an important role in the maintenance of hematopoiesis *in vivo*.

Pro-apoptotic BID

First identified by protein interactive cloning with Bcl-2 and Bax, murine Bid cDNA was cloned and studied in Korsmeyer's lab in 1996 (73). Harboring only one BH3 domain, BID is a pro-apoptotic BH3-only molecule that interacts with

other BCL-2 family proteins by its BH3 domain (73). In 1998, two research groups (Wang and Yuan's lab) independently clarified the pro-apoptotic function of BID in the extrinsic cell death pathway and reported the cleavage of BID by activated caspase 8 (31,32). In 1999, the solution structures of both human and murine BID are resolved by NMR spectroscopy in two independent labs (Cowburn and Wagner's lab) (74,75). In the same year, Korsmeyer's lab successfully generated *Bid* -/- mice, which were reported to be resistant to Fas-induced hepatocellular apoptosis (76). Although *Bid* -/- mice develop quite normally, Zinkel et al in Korsmeyer's lab demonstrated that *Bid* -/- mice spontaneously develop a fatal myeloproliferative disorder resembling chronic myelomonocytic leukemia (CMML) and genomic instability was reported in *Bid* -/- tumor cells in 2003 (66). In 2005, two independent research groups (Gross and Korsmeyer's) identified a novel function of BID in the DNA damage signaling pathway and BID was demonstrated to be a novel ATM/ATR substrate following genotoxic stress (2,3). However, Strasser's lab reported a dispensable role of BID in the DNA damage-induced response in 2007 (77). To resolve this issue, more scientific groups, including Zinkel's lab, have published a series of research articles (4,78-83), which provide solid evidence demonstrating the important role of BID in the DNA damage response.

BID is unique among BH3-only proteins in linking the intrinsic (mitochondria-dependent) and death receptor-mediated apoptotic pathways

(31,32). According to the solution 3D structure, BID is comprised of eight hydrophobic α helices with a long flexible loop region between Helix 2 and Helix 3/BH3 domain (74,75) (Figure 1-2 A). Following death receptor (e.g., Fas or TNFα) treatment, the loop region of BID is cleaved by activated caspase 8 (31,32), which results in the myristoylation of Gly60 residue (84) and the exposure of hydrophobic BH3 domain (74,75). These post-translational modifications cause cytoplasmic BID to translocate to the mitochondria to cause the oligomerization of BAX/BAK and activate apoptosis. In the absence of BID, the Fas-induced hepatocellular apoptosis is abrogated in mice and cytochrome *c* release is prevented in cultured cells following anti-Fas antibody treatment (76). The biochemical and structural biology studies show that BID interacts with other BCL-2 members by hydrophobic interaction (73,85) and mutagenesis studies have demonstrated that the α-helical BH3 domain of BID is crucial for its interaction with other BCL-2 members to fulfill its proapoptotic function (73). Besides the classical model, other proteins also play additional roles in the regulation of BID's apoptotic function, including Caspase 2 (86,87), casein kinase (88), Calpain (89), Cathepsin (90), Granzyme B (91), PACS-2 (92) (Table 2).

In addition to its role in apoptotic signaling pathway, BID has also been demonstrated to play a role in the DNA-damage response and the maintenance of genomic integrity (Fig. 1-2B) (2,3). *Bid* -/- mice spontaneously develop a fatal myeloproliferative disorder resembling chronic myelomonocytic leukemia (CMML)

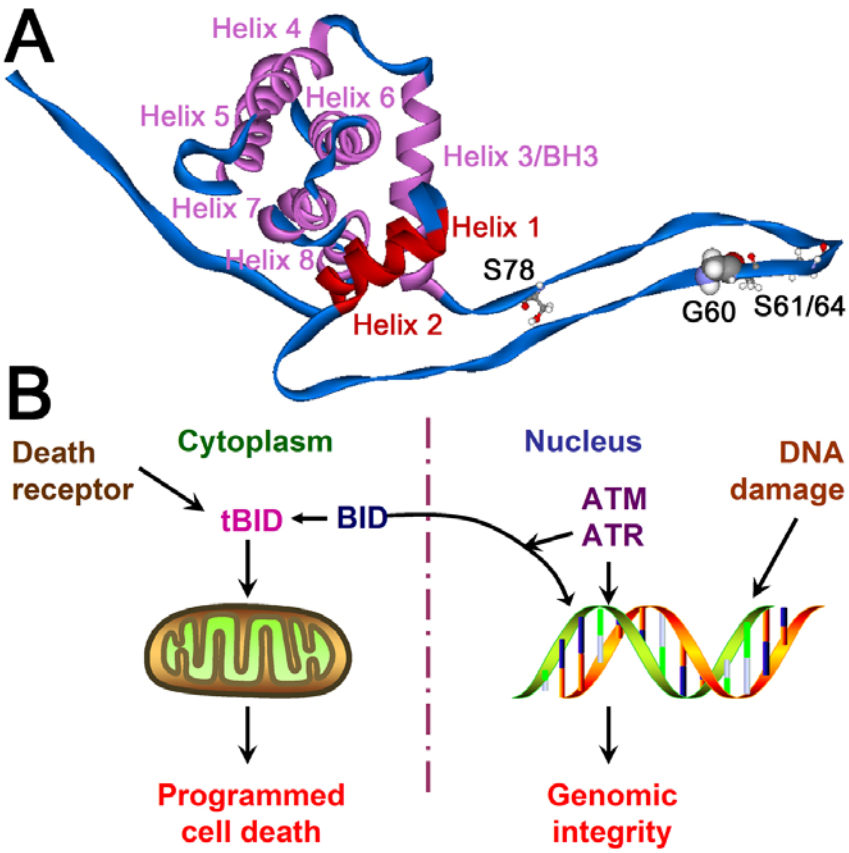

Figure 1-2. Dual functions of BID. (A) Solution NMR structure of mouse Bid (Protein data bank (PDB) entry 1DDB)(74). BID is comprised of eight hydrophobic helixes and one flexible loop region between Helix 2 and Helix 3 (BH3 domain). Following death receptor, BID is cleaved by caspase 8 at Asp59/Gly60. Following DNA damage treatment, BID is phosphorylated by ATM/ATR at Ser61/64 and Ser78. (B) Pro-apoptotic BID plays dual roles in both cell death and DNA damage signaling pathways (2). Following death receptor, cytosolic BID is cleaved by activated caspase 8. Truncated BID (tBID) translocates to mitochondria to initiate apoptosis. Following DNA damage treatment, BID is found in the nucleus and phosphorylated by activated ATM/ATR to maintain genomic integrity.

and the tumor cells in *Bid* -/- mice display trisomy of multiple chromosomes and chromosomal translocation (66). In the absence of Bid, myeloid progenitor cells and mouse embryonic fibroblasts show intra-S checkpoint defects upon DNA damage (2,3). In addition, following DNA damage treatments, Bid is found in the nucleus and its Ser61/64 and Ser78 residues in the loop region are phosphorylated by ATM (ataxia telangiectasia mutated protein)/ATR (ATM and Rad3-related protein) rapidly and the phosphorylation of BID is essential for BID's role in maintaining intra-S checkpoint (2,3,82,93).

As BID plays dual roles in both the cell death and DNA damage response, multiple interaction partners and post-translational modifications have been reported to regulate BID's function following various cellular stresses. The identified interaction partners and post-translational modifications of BID are summarized in Table 2. Interestingly, most of the post-translational modifications and functional domains lie in the flexible loop region and C-terminal helix domain of BID (Table 2). For example, besides caspase 8, caspase 2 also cleaves BID at Asp59/Gly60 site to generate tBID following heat shock and endoplasmic reticulum stress (86,87). In addition, casein kinase I and II phosphorylate BID at Thr58, Ser61, Ser64, which protect BID from cleavage by caspase 8 (88). Interestingly, cleaved BID interacts with mitochondrial cardiolipin by its Helix 6 domain to facilitate its mitochondrial targeting and pro-apoptotic activity (94-96).

In addition to *in vitro* studies, the physiological functions of BID have also been

investigated *in vivo* in a mouse model. In *Bid* -/- mice, the hepatocytes are resistant to Fas-induced apoptosis (76) and the neurons are resistant to apoptosis after oxygen/glucose deprivation and focal cerebral ischemia (97). A similar pro-apoptotic effect has also been observed in renal ischemia-reperfusion (98) and UV-damaged Langerhans cells (83). *Bid* -/- mice spontaneously develop chronic myelomonocytic leukemia (CMML) and the tumor cells display

Table 2. Identified interaction partners and post-translational modifications of BID.

Partner	Interaction	Post-translation modification/functional domain	Function
Caspase 8 (31,32)	ES	Asp 59 cleavage	Truncated BID, initiate apoptosis
Caspase 2 (86,87)	ES	Asp 59 cleavage	Truncated BID, initiate apoptosis
Calpain (89)	ES	Gly70/Arg71	Truncated BID, initiate apoptosis
Cathepsin (90)	ES	Arg65 and Arg71	Truncated BID, initiate apoptosis
Granzyme B (91)	ES	Asp 75 cleavage	Truncated BID, initiate apoptosis
ATM/ATR (2)	ES	Ser61/64, Ser78 phosphorylation	Maintain intra-S checkpoint
Casein kinase (88)	ES	Thr58, Ser61, Ser64	Protect BID from cleavage by Caspase 8
BCL2/BCL-xl/BCL-w/ MCL-1/A1 (73)	PPI	BH3 domain	Initiate apoptosis.
BAX/BAK (73)	PPI	BH3 domain	Initiate apoptosis.
PACS-2 (92)	PPI	Unknown	Facilitate translocation of BID to mitochondria
Mitochondrial Cardiolipin (94-96)	Lipid interaction	Helix 6 domain	Mitochondrial targeting and pro-apoptotic activity of tBID
ATRIP (4)	PPI	Helix 4 domain	Facilitate ATR function following replicative stress
RPA (5)	PPI	RPA-ID region	Facilitate ATR function following replicative stress

ES, enzyme-substrate interaction; PPI, protein-protein interaction

chromosomal aberrations (66). As both cell death and DNA damage signaling contribute to tissue homeostasis and genomic integrity, it is still unclear which function of BID directs the tumor suppressor function of BID *in vivo*. Interestingly, the tumor development in diethylnitrosamine-treated liver was significantly retarded in *Bid* -/- mice (99), suggesting that the tumor suppressor function of BID is to inhibit tumorigenesis rather than tumor progression.

DNA damage and ATM/ATR-mediated signaling pathways

DNA damage response

As genetic information is stored in the genome, the maintenance of genomic integrity is critical for survival. The genome is constantly threatened by DNA damaging agents from both endogenous and exogenous sources. Endogenous DNA damage is produced continuously inside the living cell, by replication errors and reactive oxygen species generated from normal metabolic byproducts (1). DNA damage also results from external agents, such as ultraviolet light, various radiation resources, carcinogens and drugs used in chemotherapy (1). DNA lesions might occur at multiple levels, from base removal or modification, nucleotide deletion or insertion, strand breaks (single- or double- stranded breaks) to cross-linked strands (1). Cells employ different repair mechanisms to restore damaged DNA, dependent on the type and severity of the DNA lesions (1,100).

The irreparable DNA lesions will be eliminated by programmed cell death to prevent potentially catastrophic mutations in multi-cellular organisms. If irreparable DNA damage is preserved in dividing cells, it might generate replication errors and accumulation of DNA mutations in daughter cells. The accumulation of DNA mutations has been demonstrated to be an important cause of various diseases, including cancer and premature aging (1).

Following DNA damage, cells initiate a series of responses to maintain genomic integrity, including DNA damage checkpoints (arrest cell cycle progression), DNA repair (restore damaged DNA), transcriptional response (change the transcription profile) and programmed cell death (eliminate irreparable cells) (1). The DNA damage is sensed by various DNA damage sensors and activates PIKK (Phosphoinositide-3 kinase-related kinase) protein kinases (e.g. ATM, ATR, DNA-PKcs). With the aid of mediators, damage signals are transduced to transducers (e.g., CHK1 and CHK2 Ser/Thr kinases) and then effectors (e.g. CDC25 phosphatases), which inactivate CDKs to arrest cell cycle progression at G1/S, intra-S or G2/M checkpoint (1). Meanwhile, the DNA lesions are repaired by various DNA repair mechanisms, including direct reversal of base damage, base excision repair, nucleotide excision repair, mismatch repair, double-strand break repair, and cross-link repair (1). It has been reported that it is the stable association of repair factors with chromatin rather than DNA damage itself that initiates the DNA damage signaling pathways (101).

The persistence of the DNA damage response, the selection of DNA repair, and the cellular sensitivity to DNA damage are quite dependent on cell type and cell cycle status (102). For example, thymocytes, neural precursor cells and myeloid progenitor cells have been reported to be exquisitely sensitive to DNA damage and undergo apoptosis following genotoxic insult (2,103,104). In contrast, hematopoietic stem cells are more resistant to IR treatment and use different types of DNA repair mechanisms based on their quiescent or proliferating status (105-107).

ATM/ATR-mediated signaling pathways

The DNA damage checkpoint signals are sensed, transduced and executed at multiple levels (Figure 1-3 A). Following genotoxic stress, checkpoint-specific damage sensors recognize the DNA lesions and activate downstream transducers with the assistance of various mediators, including 53BP1, Claspin, TopBP1 and BRCA1 (1). Two phosphoinositide-3 kinase-related protein kinases, ATM and ATR, have been identified as the primary sensors to DNA double strand breaks (DSBs) and to DNA damage that perturbs DNA replication (replicative stress), respectively (108-111). ATM and ATR are members of the PIKK family protein kinases and preferentially phosphorylate their substrates at serine or threonine residues followed by glutamine (SQ/TQ sites) (112,113). In structure, the PIKK family proteins are comprised of five characterized domains: N-terminal

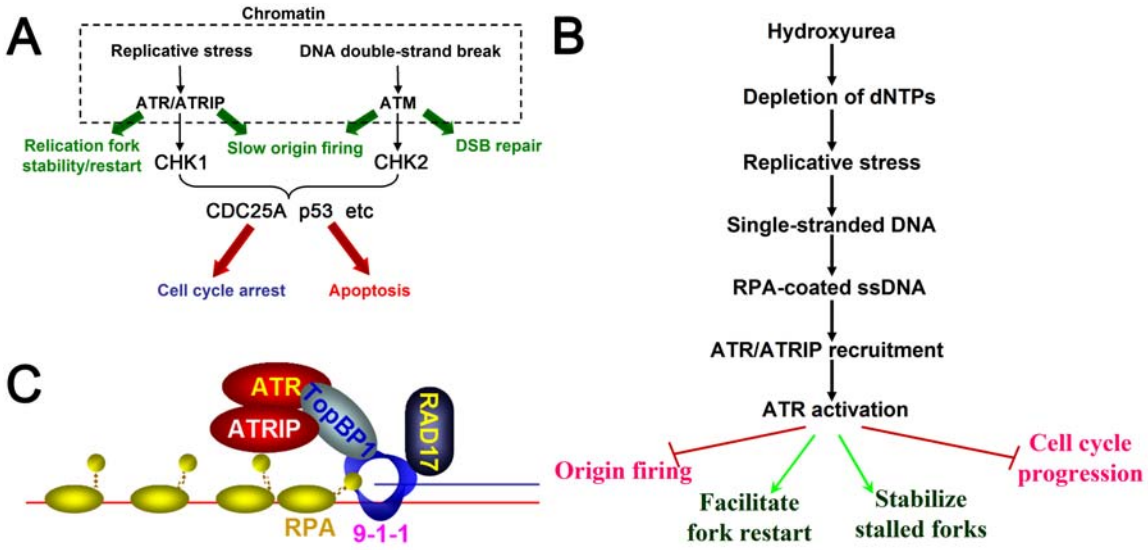

Figure 1-3. Simplified ATM/ATR-mediated signaling pathways. (A) Following genotoxic stress, DNA damage is sensed and detected by sensor (e.g., ATM, ATR). With the aid of mediators (not shown), damage signals are transduced to transducers (e.g., CHK1 and CHK2), which further activate downstream effectors (e.g., p53 and CDC25A) to execute their function directly (e.g., checkpoint, apoptosis, DNA repair). The schematic diagram (B) and model (C) of the activation process of ATR-mediated signals. As a ribonucleotide reductase inhibitor, hydroxyurea blocks the biosynthesis of deoxyribonucleotides and results in the depletion of dNTP pools. Following replicative stress, the uncoupling activities between DNA polymerase and helicase results in the generation of excessive single stranded DNA (ssDNA). The ssDNA is sensed and coated by RPA, a ssDNA-binding protein. ATR/ATRIP complex and RAD17/9-1-1 complex are then recruited to RPA-coated ssDNA independently. The 9-1-1 complex then recruits TopBP1 to associate with ATR/ATRIP, which stimulate ATR kinase activity. The activated ATR phosphorylates numerous substrates, including CHK1, to block origin firing and cell cycle progression, stabilize stalled replication forks, and facilitate fork restart.

α-helical repeat subunits known as HEAT (huntingtin, elongation factor 3, A subunit of protein phosphatase 2A, and TORI) repeats, FAT (FRAP, ATM, TRRAP), a C-terminal highly conserved kinase catalytic domain, PIKK-regulatory domain (PRD) and FATC (FAT C terminus) domain (114,115). The PRD and FATC domains are important to regulate the kinase activities of most PIKK family members (114).

Following DNA double strand breaks, ATM is recruited to dsDNA by NBS1 and activated by MRE11-RAD50-NBS1 (MRN) complex (111). Upon DNA damage, ATM autophosphorylates on Ser1981, which causes dimer dissociation and initiates cellular ATM kinase activity (109). Activated ATM phosphorylates numerous substrates to slow origin firing, initiate DNA repair, and execute DNA checkpoint signals (Figure 1-3 A). One well-established and unique substrate of ATM is the checkpoint kinase CHK2. The phosphorylation of CHK2 by ATM results in CHK2 activation and the activated CHK2 phosphorylates phosphotyrosine phosphatase CDC25 (116). The phosphorylation of CDC25A in G1 and S phase results in 14-3-3 binding, nuclear exclusion and ubiquitin-mediated degradation (117,118). As CDC25A dephosphorylates the conserved Thr14/Tyr15 inhibitory phosphorylation sites of CDK2 (119), the degradation of CDC25A results in the inactivation of CDK2 and resultant arrest of the cells in G1/S and/or intra-S checkpoint. Defects in ATM pathways are associated with Ataxia telangiectasia (120) and various cancers in human (Table

3). *Atm* -/- mice display growth retardation, infertility, hypersensitivity to γ-irradiation and develop thymic lymphomas with chromosomal abnormalities (121). Besides genotoxic stress, ATM is also activated following oxidative stress by formation of a disulfide-cross-linked dimer (122). Progressive bone marrow failure is reported in mature *Atm* -/- mice with elevated levels of reactive oxygen species and treatment with anti-oxidative agents significantly restores this deficiency (123).

Following replicative stress, ATR is recruited and activated at persistent ssDNA and many factors are involved to regulate this complicated process (Figure 1-3 B, C). Following replicative stress (e.g. depletion of dNTP pools by ribonucleotide reductase inhibitor), the uncoupling between DNA polymerase and helicase activities results in the generation of excessive single stranded DNA (ssDNA), which is sensed and coated by RPA, a ssDNA-binding protein (Figure 1-3 B) (124). ATR is recruited to RPA-coated ssDNA by its stable binding partner ATRIP via its checkpoint recruitment domain (108,125). Meanwhile, RAD17 and the RAD9-HUS1-RAD1 complex are recruited to the stalled replication folk independent of ATR-ATRIP loading (126). At the mediator level, TopBP1 is recruited to the 9-1-1 complex by its interaction with the C-terminus of RAD9 (127). The recruited TopBP1 in DNA damage sensor complex associates with the TopBP1-interaction domain of ATRIP and the PRD domain of ATR to stimulate ATR kinase activity (128,129). The activated ATR phosphorylates numerous

substrates to block origin firing and cell cycle progression, stabilize stalled replication forks, and facilitate fork restart (124). One well-established and unique substrate of ATR is checkpoint kinase CHK1 (130). With the aid of mediator Claspin, activated ATR phosphorylates CHK1 at Ser317 and Ser345 (131,132). The phosphorylation of CHK1 results in its structure change and exposes its active site (133). The activated CHK1 releases from chromatin (134,135) and phosphorylates CDC25 (136,137) to initiate a cell cycle checkpoint. The checkpoint signal is terminated by phosphatase-dependent dephosphorylation (138) and proteasome-dependent degradation of CHK1 (139).

Different from ATM, ATR plays important roles in maintenance of genomic integrity in proliferating cells, especially in S phase (124). Mutations in the *ATR* gene have been identified to associate with human Seckel syndrome patients (140) (Table 3). Early embryonic lethality has been reported in *Atr* -/- embryo (E7.5-E8.5), and *Atr* -/- blastocytes fail to expand and die of caspase dependent apoptosis (141,142). *Atr* conditional knockout mice show defects in tissue homeostasis with aging-related phenotypes and exhaustion of tissue-specific stem and progenitor cells (143-145). Besides ATR, the core factors in the ATR pathway are essential for the viability of replicating yeast and mammalian cells, including RPA, ATRIP and CHK1 (108,129,130,146,147). Nevertheless, damage-induced ATR-mediated signaling pathway might function differently compared with its role in normal cell cycle. Although the DNA damage response

Table 3. Identified diseases associated with deficiency in ATM/ATR-mediated DNA response.

Gene	Protein functions	Diseases in clinic
ATM	PIKK; DNA damage and DNA repair of DSBs (Sensor)	ataxia-telangiectasia; breast cancer; other cancers
ATR	PIKK; DNA damage of ssDNA; DNA replication (Sensor)	Seckel syndrome; cancer predisposition
MRE11	Homologous recombination, telomere length maintenance, and DSB repair (Sensor)	ataxia-telangiectasia-like disease; Alzheimer's disease
NBS1	DNA damage and DNA repair of DSBs (Sensor)	Nijmegen breakage syndrome; cancer predisposition
CHK2	Protein kinase (Transducer)	Li-Fraumeni syndrome; breast cancer
p53	Tumor suppressor; transcription factor; cell cycle checkpoint; DNA repair; apoptosis (Effector)	Li-Fraumeni syndrome; mutation in more than 50% tumors
CDC25	Proto-oncogene; phosphatase; cell cycle checkpoint (Effector)	Overexpression in various cancers

was severely impaired, cells harboring mutated RPA70 (148) or ATRIP (129) showed a quite normal cell cycle profile. Interestingly, *Atr* -/- Arabidopsis developed normally and growth retardation was only observed when the plants were challenged with replicative stress (149). The above results highlight the importance of investigating the function of ATR pathway quantitatively in unstressed and stressed condition among different model organisms.

Although ATM is primarily activated by double strand DNA breaks and ATR is primarily activated by stalled replication forks, activation of the ATM or ATR signaling pathways is not limited by a certain kind of DNA lesion. During replication fork collapse, DNA double strand breaks are also generated by endonuclease cleavage, thereby activating the ATM-mediated signaling pathway

(150). In addition, when DNA double strand breaks are processed into single-strand DNA, the ATR-dependent signaling pathway is also triggered by CtIP activation (151,152). On the other hand, in the absence of ATM, the ATR response is increased upon hydroxyurea treatment (153). In the T cell lineage, the deficiency of CHK1 is associated with an increased level of activated CHK2 and p53 (154). Thus, the cross-talk between ATM-CHK2 and ATR-CHK1 signaling pathways ensures the rapid activation of cell cycle checkpoints and DNA repair processes synergistically.

ssDNA binding protein RPA

First purified from human cell extracts as an essential component for the replication of simian virus 40 (SV40) (155-157), replication protein A (RPA) has been identified as a heterotrimeric ssDNA-binding protein with essential functions in multiple processes in eukaryotic DNA metabolism, including DNA replication, DNA damage/repair and recombination (147,158,159). As an abundant ssDNA-binding protein in eukaryotic cells, RPA protects ssDNA from various nucleases and prevents the formation of secondary structure, which will interfere with normal DNA processing (147,158,159). In addition, RPA stimulates the activity of several DNA helicases and DNA polymerases and coordinates the assembly and disassembly of DNA processing proteins through ssDNA in both initiation and elongation processes of DNA replication (158,159). Sensing

damaged DNA, RPA interacts with various DNA repair factors, such as XPA and RAD51, to assemble DNA repair complex and/or to initiate homologous recombination (160-165).

RPA is comprised of three subunits, RPA70, RPA32 and RPA14, and organized into eight domains connected by flexible linkers (Figure 1-4 A). The flexible linkers joining the domains in each subunit allow for optimal association of RPA with different lengths of ssDNA and various associated proteins during DNA processing. Six domains of RPA (N, A, B, C domain of RPA70, D domain of RPA32, and RPA14) adopt an oligonucleotide binding (OB)-fold (166,167), and the A to D domains of RPA sequentially mediate its interaction with ssDNA with a defined 5'-3' polarity (168-171). Although the DNA-binding affinities of each individual domain are weak, the synergistic effect of various domains of RPA produces a very high and specific binding affinity for ssDNA with K_d on a scale of 10^{-9} to 10^{-10} M (159,172). At least three different ssDNA binding modes have been characterized based on the length of ssDNA (i.e., 8-10 nt, 12-23 nt, and 28-30 nt) and the DNA-binding domains involved (159,171,173,174), suggesting that RPA possesses multiple dynamic structural conformations in DNA processing pathways. The flexible nature of RPA's confirmation has also been demonstrated by scanning transmission electron microscopy and gel filtration studies (175). In addition to these DNA-binding motifs, the N, A and B domain in RPA70 and the C domain in RPA32 have been identified as the well-established protein-protein

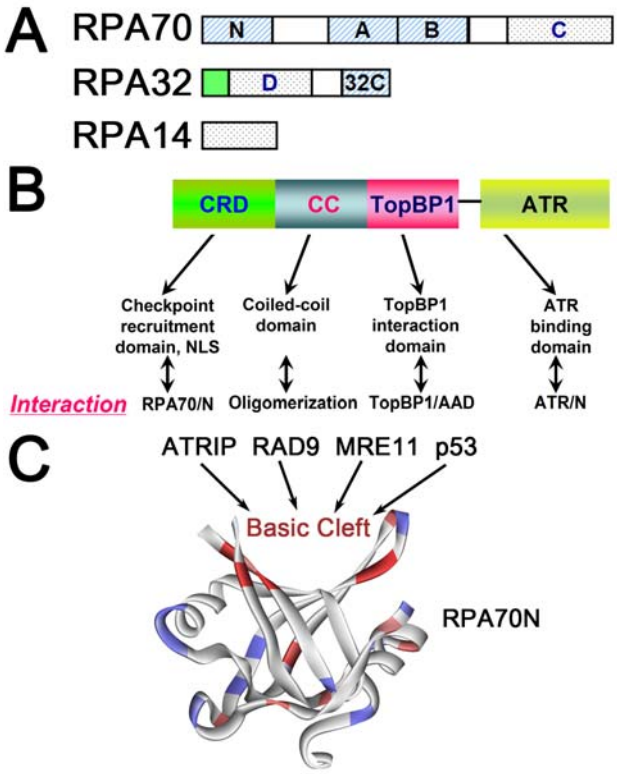

Figure 1-4. RPA recruits ATR/ATRIP to ssDNA. (A) Schematic illustration of RPA. Reticulated boxes, classical protein-protein interaction domains in RPA70 and RPA32 subunits; dotty boxes, RPA subunits interaction domains; green box, phosphoamino acid cluster in the N-terminal of RPA32. Modified from the review from Fanning et al (159) with permission. (B) Schematic illustration of ATRIP. ATRIP is comprised of an N-terminal checkpoint recruitment domain which interacts with RPA70N, a coiled-coil domain, a TopBP1-interaction domain and C-terminal ATR-binding domain. One function of the coiled-coil domain is to mediate ATRIP homo-dimerization. Modified from the review from Mordes and Cortez (176) with permission. (C) The basic cleft region of RPA70N binds with multiple DNA damage checkpoint proteins, including ATRIP and RAD9, to regulate ATR signaling. The basic and acidic amino acids are labeled with red and blue color, respectively, in the solution NMR structure of human RPA70N domain (Protein data bank entry 2B3G) (177).

interaction domains of RPA to interact with various DNA processing factors (Figure 1-4 A) (147,158,159). It is worthwhile to note that RPA might interact with certain proteins via multiple domains. For example, RPA interacts with SV40 T antigen by both RPA70A and RPA32C domains (178-180). In addition, a phosphoamino acid cluster has been characterized in the N-terminal domain of RPA32 (Figure 1-4 A). Following DNA damage treatments, the phosphorylation of Ser33 and Thr21 in this region by ATM/ATR generates a hyperphosphorylated form of RPA, which prevents ssDNA accumulation and facilitates adaptation of a DNA-replication fork to replication stress (181,182).

Following replicative stress, the uncoupled activity of DNA helicases and DNA polymerases generates excessive single-stranded DNA (ssDNA), which is sensed and coated by replication protein A (RPA) (124). Although the exact length of ssDNA in mammalian systems is unclear, the average length of ssDNA accumulated in wild type yeast is more than 330 nt following 2-hour hydroxyurea treatment (183). As one RPA molecule binds to 8-30 nt ssDNA (159), it is reasonable to speculate that one piece of extensive ssDNA might recruit a series of RPA molecules in cells (Figure 1-3 C).

The recruitment of RPA to ssDNA initiates several events to maintain genomic integrity following replicative stress. The most well-established model is RPA70N domain functions as an “antennae” to recruit a series of checkpoint proteins to ssDNA, including RAD9 and ATRIP (108,125,126,148) (Figure 1-4 B, C).

Following the independent loading of ATR/ATRIP and 9-1-1 complex on RPA-coated ssDNA (126), TopBP1, a key ATR activator, is recruited to ssDNA by interaction with ATR/ATRIP (Figure 1-4 B) and RAD9 to facilitate the formation of activated DNA damage sensor complex (127-129). The activated ATR then phosphorylates numerous substrates in replicative stress-induced DNA damage response (93). ATR and its effectors maintain genomic integrity by arresting cell cycle, slowing origin firing, stabilizing replication fork, and facilitating fork restart (124). Besides this “classical” model, RPA also maintains genomic stability by interaction with multiple DNA damage/repair proteins, including RAD51, the MRN complex and the TIM/TIPIN complex (164,184,185). Recently, annealing helicase SMARCAL1(HARP) was demonstrated to interact with RPA to prevent the generation of excessive ssDNA following replicative stress (186-189).

DNA damage-induced cell death

Once DNA damage becomes persistent and irreparable, cells will initiate programmed cell death to clear damaged cells, which maintains the genomic integrity in tissues (100). Although both DNA damage and cell death signaling pathways have been well-established, how genotoxic stress is integrated and transduced to the core apoptosis machinery is still not completely understood. Multiple complicated mechanisms are involved in the process and the decision of the cell fate seems to be dependent on the cellular as well as genetic background.

The best understood model is the p53-dependent pathways (1). Following DNA damage treatment, p53 is phosphorylated by ATM/ATR or CHK1/CHK2 (190), which releases ubiquitin ligase MDM2 from p53 and stabilizes p53 (1,191). The activated p53 functions as a transcription factor to induce the expression of a series of proapoptotic genes (e.g. *NOXA* and *PUMA*), which activate BAX/BAK in the mitochondria to initiate apoptosis (55). Meanwhile, in cytosol or mitochondria, p53 interacts with BCL-2 family proteins directly to initiate cell death independent of its transcription function (192). In addition to the classical model, genotoxic stress also induces the activation of caspase 2 in a p53-dependent manner by formation of PIDDosome to cleave BID to initiate apoptosis (193). Following irradiation, histone H1.2 has been identified as an apoptogenic factor released from chromatin to translocate to the mitochondria in a p53-dependent manner (194).

Several p53-independent mechanisms have also been reported to contribute to the DNA damage-induced apoptosis. For example, as a transcriptional regulator, BRCA1 induces apoptosis by activation of DNA damage-responsive gene *GADD45*, which further activates c-Jun N-terminal kinase/stress-activated kinase/Fas/caspase 8 pathways to initiate apoptosis (195,196). In addition, an ATR-CHK1 regulated p53/mitochondria-independent cell death pathway has recently been discovered and it is mediated in a caspase 2-dependent manner (197,198). Interestingly, following etoposide and ionizing radiation, BID has been

demonstrated to facilitate apoptosis in a p53-independent pathway and the pro-apoptotic function of BID in this setting is independent of caspase processing of the flexible loop region (79).

Mouse hematopoietic system

Hematopoiesis

Comprised of hematopoietic stem cells, progenitors, precursor cells, and various differentiated lineage-committed cells (Figure 1-5), the hematopoietic system is elaborately maintained to produce functional blood cells to satisfy the requirement of the body under various physiological and pathological conditions (199-201). Following embryo development, hematopoiesis is initiated in the yolk sac, and then occurs in the embryonic AGM (aorta-gonad-mesonephros) region (202). The definitive hematopoietic stem cells originate in the AGM and then colonize in the fetal liver until bone marrow is formed (203,204). In fetal development, the liver is the major hematopoietic organ, while hematopoiesis occurs primarily in bone marrow in postnatal development (205). In adults, various hematopoietic cells are predominately originated in bone marrow, mature in secondary lymphoid organs (i.e., spleen, thymus and lymph nodes), and function in peripheral blood and tissues (206).

All cellular blood components are derived from hematopoietic stem cells and

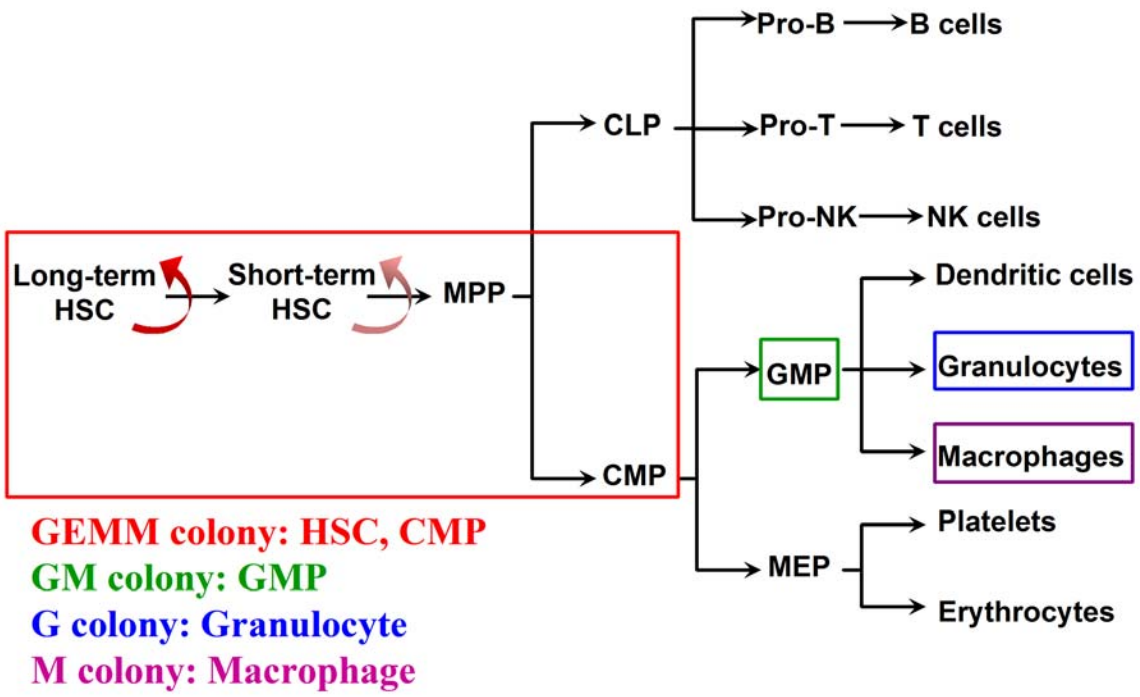

Figure 1-5. Schematic illustration of the differentiation of hematopoietic system. The hematopoietic system is comprised of hematopoietic stem cells, multipotential and lineage-restricted progenitors, and various differentiated lineage-committed cells. Supplemented with IL3, IL6, stem cell factor (SCF) and erythropoietin (EPO), hematopoietic cells are committed to differentiate through myeloid lineage in methylcellulose culture(207) and various colonies are observed according to colony morphology (208). Particularly, GEMM colonies (colony-forming unit of granulocyte/erythrocyte/macrophage/megakaryocyte) are formed from HSCs and CMPs (red frame); GM colonies (colony-forming unit of granulocyte/macrophage) are formed from GMP cells (green); G and M colonies are generated from granulocyte (blue) and macrophage (purple), respectively (209). HSC, hematopoietic stem cell; MMP, multipotent progenitor; CLP, common lymphoid progenitor; CMP, common myeloid progenitor; NK cells, nature killer cells; GMP, granulocyte macrophage progenitor; MEP, megakaryocyte erythroid progenitor.

matured through lineage-restricted differentiation (201,210). Given stimuli from certain colony stimulating factor and/or cytokines, hematopoietic cells are committed to differentiate through either the lymphoid or myeloid lineage (Figure 1-5). Lymphocytes (B cells, T cells, NK cells), derived from common lymphoid progenitors, play an essential role to mediate the adaptive immune response. Myelocytes (granulocytes, megakaryocytes and macrophages), derived from common myeloid progenitors, are involved in various physiological roles, including innate immunity and hemostasis. The differentiation and maturation of various hematopoietic cells are associated with a series of identified surface markers, which makes it possible to distinguish and characterize various cell populations in hematopoietic system by flow cytometry. For example, the HSC-enriched LSK cells (Lin-Sca1+ckit+) and MPCs (Lin-Scal-ckit+) are identified and characterized by the staining with the surface markers of Lineage (CD3, B220, Gr-1, Ter119), Sca1 and ckit (211,212). The GMP, CMP, and MEP cells in MPC population are further gated as CD34+FcγR+, CD34+FcγR-, and CD34-FcγR- population from Lin-Scal-ckit+ population, respectively, by additional surface staining with CD34 and FcγR(209) (Figure 1-5).

One in every 10^5 nucleated cells, hematopoietic stem cells are a rare population in the adult bone marrow (201). However, hematopoietic stem cells are multipotent to generate all hematopoietic cells and reconstitute hematopoietic system (201). The regeneration ability of hematopoietic stem cells has been

demonstrated and applied in bone marrow transplantation (211). Based on the self-renewal capability, the HSCs-enriched LSK population are further distinguished and characterized into long-term HSC, short-term HSC and multipotent progenitors (MPP) by surface staining of CD34 and CD135 (209,213,213,214). The self-renewal function of hematopoietic stem cells is maintained in the stem cell niche (microenvironment) in the bone marrow *in vivo* (215). Besides bone marrow, peripheral blood is another source to harvest HSCs, suggesting that HSCs might pass the bone marrow barrier and circulate in bloodstream to settle in other organs (216,217). Predominately in quiescent status, HSCs undergo either symmetric division (two daughter HSCs) to expand or asymmetric division (one HSC and one progenitor cell) to maintain HSC population (218). Although HSCs are multipotent stem cells, the self-renewal ability is limited and long-term mobilization of HSCs from quiescence into the cell cycle results in the depletion of stem cell function (218,219).

Regulation of hematopoietic stem cells

Controlled by quiescent or slowly cycling stem cells and rapidly cycling progenitor cells, the hematopoietic system is delicately regulated by various endogenous and extrinsic events to maintain hematopoietic homeostasis (200,220). In the adult, the balance among stem cells, progenitor cells and differentiated cells is controlled by a series of accumulation and elimination

factors, including proliferation, apoptosis, differentiation and self-renewal (201). Following cellular stresses or inflammatory signals, the homeostasis of the hematopoietic system is transiently disrupted by depletion of functional differentiated cells and then quickly compensated by mobilization of stem cells into the cell cycle (199,221). The activation of hematopoietic stem cells (HSCs) generates adequate progenitor cells and mature cells to recover hematopoietic homeostasis and then returns to a quiescent state (199,221). Such activation cycles, or “stem cell mobilization”, is tightly regulated, as abnormal proliferation of HSCs will deplete their self-renewal function (218). Defects in cell cycle checkpoints result in excessive mobilization of HSCs and depletes their self-renewal function in serial bone marrow transplantation (219).

Due to the rapid expansion and regeneration, the hematopoietic system is quite vulnerable to various genotoxic stresses (210). Various key factors in the DNA damage/repair pathways have been demonstrated to play an important role to maintain genomic integrity and stem cell function (222). *Atr*-conditional knockout mice demonstrated premature aging defects with significantly decreased LSK (Lin-Scal+ckit+) populations and thymic progenitors (145). Progressive bone marrow failure is observed in 24-week old *Atm* -/- mice due to a depletion of LSK cells as well as HSC function with elevated reactive oxygen species (123). Mice harboring a hypermorphic mutant allele of p53 display reduced proliferating HSC population in aging with limited HSC function (223). In addition, mice with

deficiencies in DNA repair machines, including nucleotide excision repair, telomere maintenance, non-homologous end-joining, have been demonstrated to deplete the hematopoietic stem cell function with age (224,225), suggesting that the accumulation of endogenous DNA damage limits stem cell function in a cell autonomous fashion. Interestingly, accompanied with increased DNA damage, the frequency of stem cells is increased with age (224), which is consistent with a compensatory expansion of the HSC reservoir due to the limited self-renewal function of HSCs. Besides DNA damage/repair factors, other cytoprotective properties have been proposed to protect HSCs from genotoxic stresses, including maintenance of a quiescent state by regulation of lipid raft clustering (226) and maintenance of a low metabolism level to prevent reactive oxygen species (227-229).

Ionizing irradiation (IR) and hydroxyurea (HU) have been used as two genotoxic models to investigate the DNA damage-induced response *in vitro* and *in vivo*(1). IR treatment damages all types of nucleated cells by generation of DNA double-strand breaks (DSB), which predominantly activate ATM-mediated checkpoint response (1). Interestingly, differential DNA damage response has been reported between hematopoietic stem cell and progenitor cell population following IR treatment (105,107) and the reliance on the error-prone NHEJ pathway in quiescence of HSCs has been demonstrated to contribute to hematopoietic abnormalities (105). Different from IR, hydroxyurea, a clinically

used ribonucleotide reductase inhibitor, arrests DNA replication and induces replicative stress in replicating cells but not in quiescent cells (1,230), which provide a reasonable model to selectively induce damage in progenitor cells rather than HSCs. In a mouse model, HU has been demonstrated to induce the mobilization of HSCs *in vivo* (231), presumably by a depletion of the rapidly proliferating progenitor cell population.

CHAPTER II

MATERIALS AND METHODS

Cell biology experiments

Cell lines and drug treatments

Hox11-immortalized *Bid* +/+ and *Bid* -/- MPCs (66,232), were cultured in IMDM medium (Invitrogen, Carlsbad, CA, USA) with 20% FBS, 100 U/ml penicillin-streptomycin, 2 mM glutamine, 0. 1 mM β-mercaptoethanol, and 10% conditioned medium from WEHI cells as a source of IL-3. U2OS cells, *Bid* -/- MEFs harboring HA-tagged Bid, were cultured in DMEM (Invitrogen) with 10% FBS, 100 U/ml penicillin-streptomycin, 2 mM glutamine, and 0.1 mM β-mercaptoethanol. Early passage cells (10<*P*<20) were treated with hydroxyurea (HU) (Sigma, St. Louis, MO, USA) or etoposide (ETOP) (Sigma) as indicated.

RNAi treatment and overexpression

The siRNA oligonucleotides targeting human *BID* (SI02661911, SI02662415) were purchased from Qiagen Inc. (Valencia, CA, USA). The No. 7 (SI02661911) and No. 8 (SI02662415) hBID siRNA targeting sequences are 5'-AAAGACAATGTTAAACTTATA-3' and 5'-CAGGGATGAGTGCATCACAAA-3',

respectively. For U2OS cells, the transfection of *BID* siRNA and control siRNA (1027310, target sequence: 5'-AATTCTCCGAACGTGTCACGT-3') was mediated by Lipofectamine 2000 (Invitrogen) according to the manufacturer's instructions. Unless otherwise indicated, No.7 and No.8 hBID siRNAs were mixed together and used as *BID* siRNA in experiments. After 72-hour transfection, the transfected U2OS cells were treated as indicated in the figure legends.

The siRNA oligonucleotides targeting mouse *Bid* (SI00929103) were purchased from Qiagen Inc. Mouse *Bid* siRNA target sequence is CACAGAAGATTCCATATCAAA. For MPCs, 10×10^6 cells were washed once with PBS, resuspended in 100 µl Mouse ES Cell Nucleofector Solution (Amaxa) containing 100 pmol siRNA, and transfected twice by Nucleofector Program A-30. After 72-hour transfection, the transfected MPCs were treated as indicated in the figure legends.

For overexpression, *BID* siRNA and plasmids harboring various BID constructs in pcDNA3 vectors were co-transfected into U2OS cells by Lipofectamine 2000 (Invitrogen) according to the manufacturer's instructions. After 72-hour transfection, the cells were treated with 10 mM HU for 2 hours.

Stable cell line generation

To generate U2OS cell lines stably expressing various BID mutants, pMSCVpuro (Clontech) plasmid harboring wild type or mutated BID was

transfected into 293T cells along with packaging vector using Fugene 6 (Roche) to product retrovirus. Silent mutations in the *BID* siRNA-targeted region (cDNA: G36A/T39C/G42A/C45T/C48T) were introduced in these retrovirus constructs so that the expressed mutated BID would not be knocked down by *BID* siRNA. Then, U2OS cells were infected twice with retrovirus harboring wild type or mutated BID and selected by 0.8-1 μg/ml puromycin for 48 hours. Live cells were cultured in DMEM medium containing 0.5 μg/ml puromycin.

Immunofluorescence staining

For ATRIP nuclear foci, *BID* siRNA, or control siRNA was delivered into U2OS cells by Lipofectamine 2000. After 40 hours, pcDNA3 vector containing wild type mouse Bid or H4A mutant Bid or vector alone was introduced by FuGene 6 (Roche, Nutley, NJ, USA). After another 40 hours, the cells were treated with 10 mM HU for 5 hours. Then, the cells were fixed by 3% paraformaldehyde/2% sucrose solution and permeabilized by Triton X-100 solution (0.5% Triton X-100, 20 mM HEPES pH7.4, 50 mM NaCl, 3 mM $MgCl_2$, 300 mM sucrose). ATRIP localization was detected by immunofluorescence using anti-ATRIP polyclonal antibody 403(108). The cells were examined using a Leica DM IRBE inverted wild-field microscope (Bannockburn, IL, USA).

For BID-RPA co-localization analysis, synchronized *Bid* -/- MEFs harboring HA-tagged Bid were fixed in ice cold 3:1 methanol : acetone and blocked for

1 hour with 5% Normal Goat Serum (Sigma) in PBS. RPA was detected by immunofluorescence using Rat anti-RPA32 antibody (Cell Signaling, Danvers, MA, USA) and Alexa Fluor 546 conjugated Goat anti-Rat IgG antibody (Invitrogen). HA-tagged Bid was detected by immunofluorescence using Alexa Fluor 488 conjugated mouse anti-HA IgG (Invitrogen). Microscopy was performed using a Zeiss (Thornwood, NY, USA) LSM 510 inverted confocal microscope. (Clinton Bertram in my lab helped me finish this experiment)

Immunoprecipitation

For endogenous immunoprecipitation (IP), the chromatin-enriched nuclear fractions of *Bid* +/+ MPCs or U2OS cells were collected and lysed in lysis buffer (25 mM HEPES pH 7.5, 250 mM NaCl, 2 mM EDTA, 10% glycerol, 0.5% NP-40, 1 mM PMSF, 4 μg/ml leupeptin/antipain, 0.1 mM orthovanadate, 1 mM NaF). Then, the antibody for immunoprecipitation (i.e. biotinylated anti-human/mouse BID goat polyclonal antibody (R&D Systems, Minneapolis, MN, USA, BAF860), anti-ATRIP 403(108), or anti-RPA70 (US biological, R3400)) was added to the lysate, and incubated at 4 °C for one hour. Then, beads for immunoprecipitation (i.e. Streptavidin agarose (Novagen, Gibbstown, NJ, USA), TrueBlot anti-Rabbit Ig IP Beads (cat No. 00-8800, eBioscience Inc., San Diego, CA, USA) or TrueBlot anti-mouse Ig IP Beads (cat No. 00-8811, eBioscience Inc.)) were added and samples were incubated at 4 °C for 2 hours. The beads were pelleted, washed,

boiled with 5 × Laemmli buffer and the supernatant was resolved on SDS-PAGE. (Qiong Shi in my lab helped me finish this experiment)

For domain mapping experiments, the indicated BID constructs in pcDNA3 vectors and the indicated HA-tagged ATRIP constructs in pLPCX vectors (from Dr. David Cortez) were transfected using Lipofectamine (Invitrogen) and expressed in 293T cells for 48 h. Total cell lysates were prepared and BID was immunoprecipitated by anti-BID antibody. (Qiong Shi in my lab helped me finish this experiment)

For BID-BCL2/MCL1 interaction, pcDNA3 (Invitrogen) plasmid harboring wild type or mutated BID was transfected into 293T cells by Fugene 6 (Roche) for 48 hours. Cells were lysed in lysis buffer (25 mM HEPES pH 7.5, 250 mM NaCl, 2 mM EDTA, 10% glycerol, 0.5% NP-40, 1 mM PMSF, 4 μg/ml Leupeptin/Antipain, 0.1 mM orthovanadate, 1 mM NaF). Then, BID was immunoprecipitated by biotinylated anti-human/mouse BID goat polyclonal antibody (R&D system, BAF860) and streptavidin agarose (Novagen). The beads were pelleted, washed, boiled with 3×Laemmli buffer and the supernatant was resolved on SDS-PAGE.

CHK1 IP-kinase assay

U2OS cells transfected with control siRNA or *BID* siRNA (No. 8) for 72 hours were treated with 10 mM HU for 2 hours. The cells were lysed in IP buffer (25 mM HEPES, 250 mM NaCl, 2 mM EDTA, 0.5 NP-40, 10 % glycerol, 4 μg/ml

leupeptin/antipain, 1 mM PMSF, 10 mM β-glycerophosphate, 0.1 mM orthovanadate, 1 mM NaF, pH 7.5) and CHK1 was immunoprecipitated using polyclonal anti-CHK1 antibody (Chemicon, Temecula, CA, USA, AB3539) and protein G sepharose (Invitrogen). The immunoprecipitated products were washed once with kinase buffer (10 mM HEPES, 50 mM NaCl, 50 mM β-glycerophosphate, 10 mM $MgCl_2$, 10 $MnCl_2$, 1 mM DTT, pH 7.5) and incubated with 1 μg GST-CDC25C protein (a generous gift from Dr. Jennifer Pietenpol) on ice for 5 minutes. Then, 10 μM cold ATP and 5 μCi γ^{32}P-ATP were added to the reaction. The kinase reactions were performed at room temperature for 1 hour and stopped by adding 5 × Laemmli buffer. Kinase reactions were resolved on SDS-PAGE. Gels were stained with SimplyBlue SafeStain (Invitrogen) according to the manufacturer's instructions, photographed, and dried before the autoradiography.

Quantitative Real-time PCR

The total RNA of 10×10^6 cells were extracted and purified by Trizol (Invitrogen) and 5 μg of RNA were subjected to reverse-transcription (Invitrogen) to obtain cDNA. Quantitative RT-PCR was performed (SYBR Green Jumpstart Taq Ready-Mix (Sigma)) on the iQ5 Real-Time PCR Detection System (Bio-Rad). Sequences of the primers that were used: *Actin* (5'-GGCTGTATTCCCCTCCATCG-3', 5'-CCAGTTGGTAACAATGCCATGT-3'), *Chk1* (5'-GTTAAGCCACGAGAATGTAGTGA-3', 5'-GATACTGGATATGGCCTTCCCT-3'), *Chk2* (5'-CTCGGCTATGGGCTCTTCAG,

5'-CTTCTCAACAGTGGTCCATCG-3'), *Cdc25A* (5'- ACAGCAGTCTACAGAGAATGGG-3', 5'-GATGAGGTGAAAGGTGTCTTGG-3'), *p21* (5'-CCTGGTGATGTCCGACCTG-3', 5'-CCATGAGCGCATCGCAATC-3'), and *Noxa* (5'-GCAGAGCTACCACCTGAGTTC-3', 5'-CTTTTGCGACTTCCCAGGCA-3').

Cell cycle analysis and pCHK1 intracellular staining

BrdU incorporation analysis was performed according to BrdU Flow Kits (BD Pharmingen). Briefly, MPCs ($0.5\text{-}1\times10^6$ cells/ml) and U2OS cells (20-40% confluence) were pulse labeled with 10 μM BrdU for 45 minutes, and 2 hours, respectively. Cells were fixed and permeabilized with BD Cytofix/Cytoperm Buffer, and incubated with BD Cytoperm Plus Buffer followed by an additional short fixation with BD Cytofix/Cytoperm Buffer. The incorporated BrdU was exposed by treatment with 30 μg DNase for 1 hour at 37°C and probed with FITC-conjugated anti-BrdU antibody (BD Pharmingen) for 20 minutes at room temperature. The total DNA content was stained immediately prior to flow cytometric analysis with 20 μl of 7-aminoacridine (7-AAD) solution (BD Pharmingen).

For CHK1 intracellular staining, *Bid* +/+ and/or *Bid* -/- MPCs were fixed and permeabilized with BD Cytofix/Cytoperm Buffer, and incubated with BD Cytoperm Plus Buffer followed by an additional short fixation with BD Cytofix/Cytoperm Buffer. For pCHK1 staining, cells were stained with anti-pCHK1 (S345) antibody (Cell signaling, #2348) and then Alexa Fluor 488 conjugated Goat anti-Rabbit IgG

antibody (Invitrogen). DNA was stained by 7-AAD. Then cells were analyzed by flow cytometry.

Subcellular fractionation

Subcellular fractionation of MPCs or U2OS cells was performed as previously described (233) with minor modification. In brief, 10 × 10^6 MPCs or U2OS cells were washed once with PBS and suspended in 400 µl solution A (10 mM HEPES pH7.9, 10 mM KCl, 1.5 mM $MgCl_2$, 0.34 M sucrose, 10% glycerol, 1 mM DTT, 1 mM PMSF, 10 mM NaF, 10 mM β-glycerophosphate, 1 µM microcystin) with 0.1% NP-40 on ice for 5 minutes. The cytoplasmic and nuclear fractions were collected by centrifugation at 1300 × g for 4 minutes at 4 °C The isolated nuclei were washed once with solution A and then lysed in solution B (3 mM EDTA, 0.2 mM EGTA, 1 mM DTT, 1 mM PMSF, 10 mM NaF, 10 mM β-glycerophosphate, 1 µM microcystin). After incubation on ice for 10 minutes, chromatin fractions were harvested by centrifugation at 1700 × g for 4 minutes at 4 °C. The chromatin pellet was washed once with solution B and resuspended in 100 µl RIPA buffer. After sonication for 20 s, the samples were boiled with 5 × Laemmli buffer.

Single-cell gel electrophoresis (Comet) assay

U2OS cells overexpressing HA-tagged wild type, Helix 4 mutated hBID, RPA-ID mutated hBID or IH5 mutated hBID was transfected with *BID* siRNA for 72 hours.

Silent mutations were introduced in the *BID* siRNA-target region so that only endogenous BID was knocked down by *BID* siRNA. Then, cells were treated with 10 mM HU overnight. The untreated and treated cells were collected in ice-cold PBS and alkaline Comet assay was performed by CometAssay Kit (Trevigen, Gaithersburg, MD, USA) according to the manufacturer's instructions. Briefly, cells were mixed with molten LMAgarose and pipetted onto a CometSlide. After incubation with Lysis Solution and Alkaline Solution, slides were placed in Genemate Compact Gel tank (Bioexpress, Kaysville, UT, USA). For Helix 4 mutated hBID, TBE electrophoresis was performed at 22 V for 10 minutes. For RPA-ID and IH5 mutated hBID, Alkaline Electrophoresis was performed at 21V for 30 minutes. After incubation with 70% ethanol for 5 minutes, the slides were stained with SYBR Green I. Then, samples were examined using a Leica DM IRBE inverted wild-field microscope and analyzed by CometScore Program Version 1.5.

Antibodies

The following antibodies were used in this study: anti-BID rabbit polyclonal antibody (73), anti-BID polyclonal antibody (R&D Systems, BAF860), anti-BID polyclonal antibody (Santa Cruz, FL-195), anti-CHK1 monoclonal antibody (Santa Cruz, G-4), anti-phospho-CHK1 (S345) polyclonal antibody (Cell signaling, 2341), anti-phospho-CHK1 (S317) polyclonal antibody (Cell signaling, 2344),

anti-CDC25A monoclonal antibody (Santa Cruz, F6), anti-BAX polyclonal antibody(234), anti-ACTIN monoclonal antibody (Sigma), anti-HISTONE H3 monoclonal antibody (Upstate Biotechnology, Waltham, MA, USA, 05-928), anti-IκB polyclonal antibody (Cell signaling, 9242), anti-p53 monoclonal antibody (Santa Cruz, Pab240), anti-phospho-p53(S15) polyclonal antibody (Cell signaling, 9284), anti-HA monoclonal antibody (Roche, 12CA5), and anti-ATRIP polyclonal antibody (403; a generous gift from Professor Cortez (108)), anti-ATR polyclonal antibody (Santa Cruz, N-19), anti-RPA32 monoclonal antibody (Cell signaling, 2208), anti-RPA70 monoclonal antibody (US biological, R3400), anti-MCL-1 polyclonal antibody (Rockland, Gilbertsville, PA, USA), anti-BCL-2 monoclonal antibody (Pharmingen, San Diego, CA, USA), anti-His monoclonal antibody (Cell signaling, #2365), anti-MCM3 polyclonal antibody (Bethyl Laboratories, A300-192A), anti-PCNA monoclonal antibody (BD Pharmingen, 555567) and anti-MBP monoclonal antibody (Sigma), anti-phospho-ATM (S1981) monoclonal antibody (Cell signaling, #4526), anti-ATM monoclonal antibody (Cell signaling, #2873), anti-MRE11 polyclonal antibody (Millipore, 07-638), anti-RAD9 monoclonal antibody (Santa Cruz, M-389), anti-RUNX1 antibody was a generous gift from Professor Hiebert.

Biochemical and biophysical experiments

Protein purification

The *E. coli* BL21 strains harboring ATRIP/pSV282 (a generous gift from Dr. David Cortez) were induced by 0.1 mM isopropyl-β-D-thiogalactopyranoside (IPTG) at room temperature for 8 hurs and the His-MBP-ATRIP fusion protein was purified as previous described (235). The purification of various His-tagged RPA constructs was performed as previously described (236). The construction and purification of His-tagged RPA70-PDI fusion protein was performed as previously described (235). RPA expression constructs: RPA70N cDNA harboring R41E/R43E mutant was a generous gift from Professor Cortez (148). The expression vector of His-tagged RPA70NAB, AB, N, and 32C domain was a generous gift from Professor Fanning (237). To purify these His-tagged proteins, the harvested cells were resuspended in 30 mM Tris-HCl (pH 8.0) in 1/10 volume of the culture, lysed by 1mg/ml lysozyme, and sonicated on ice for 10 minutes. The lysate was centrifuged at 12,000 rpm for 20 minutes at 4 °C and the supernatant was purified on Ni-NTA resins in a batch procedure. After being washed with 15 ml washing buffer (20 mM imidazole, 300 mM NaCl, and 50 mM NaH_2PO4, pH 8.0), the His-tagged proteins were eluted with the elution buffer (100 mM imidazole, 300 mM NaCl, and 50 mM NaH_2PO4, pH 8.0). The proteins were dialyzed against 30 mM Tris-HCl buffer (pH 8.0) and were concentrated using the Ultrafree-15 centrifugal filter. The purified proteins were stored directly at -80°C.

Wild type or mutated human and mouse BID cDNA was cloned into pGEX-6P-1 vectors and induced in BL21 strains by 1 mM IPTG at 37 °C for 4 hours. The harvested cells were resuspended in lysis buffer (50 mM Tris-HCl, 50 mM NaCl, 5 mM EDTA, 1% Triton X-100, 1 mM DTT, 1 mM PMSF, pH 8.0) and centrifugated at 20,000 g for 20 minutes at 4 °C After incubation with glutathione-agarose for 3 hours at 4 °C the supernatant was discarded and the beads were incubated with prescission protease (GE Healthcare Bioscience, Piscataway, NJ, USA) at 4 °C overnight. The BID protein was released from GST-BID fusion protein in the beads and the supernatant was dialyzed in 30 mM Tris-HCl (pH 8.0).

Protein-protein in vitro interaction

For the BID-ATRIP *in vitro* interaction, 10 μg mouse Bid and 100 μg His-MBP-ATRIP protein were incubated in binding buffer (20 mM HEPES, 100 mM KCl, 5 mM $MgCl_2$, 0.5 mM EDTA, 0.1% NP-40, pH7.5) at room temperature for 30 minutes. Then biotinylated anti-human/mouse BID goat polyclonal antibody (R&D Systems, BAF860) was added and incubated at 4 °C for 1 hour. Streptavidin agarose (Novagen) was then added and incubated at 4 °C for 2 hours. The beads were pelleted by centrifugation and washed four times with binding buffer. The beads were boiled with 5 × Laemmli buffer. The supernatant was resolved on SDS-PAGE and immunoblotted with anti-BID and anti-ATRIP antibodies.

For the BID-RPA *in vitro* interaction, 100 pmol BID and 100 pmol RPA were

incubated in binding buffer (20 mM HEPES, 100 mM KCl, 5 mM MgCl2, 0.5 mM EDTA, 0.1% NP-40, pH7.5) at room temperature for 30 minutes. Then, BID was immunoprecipitated using biotinylated goat polyclonal anti-human/mouse BID antibody (R&D system, BAF860) and streptavidin agarose (Novagen). The beads were pelleted by centrifugation and washed five times with binding buffer. The beads were boiled with 3×Laemmli buffer and the supernatant was resolved on SDS-PAGE.

ssDNA pull-down assay was performed as pervious described (238). Briefly, 5 pmol 3'-biotinylated 80-nucleotide DNA oligomer (AGATTCACCAGTCACACGACCAG TAATAAAAGGGACATTCTGGCCAACAGAGATAGAACCCTTCTGACCTGAAAGCGTAA) was incubated with streptavidin agarose (Novagen) in buffer containing 10 mM Tris-HCl (pH 7.5) and 100 mM NaCl at 4°C for 30 minutes. Then, 1 μg purified recombinant His-tagged RPA and 80 pmol pre-cleared wild type or mutated BID was incubated with beads in binding buffer A (10 mM Tris-HCl, 100 mM NaCl, 10 μg/ml BSA, 0.01% NP-40, 10% glycerol, pH 7.5) at 4°C for 1 hour. The beads were pelleted by centrifugation and washed five times with binding buffer A. The beads were resuspended in 3×Laemmli buffer, boiled, and resolved on SDS-PAGE.

For *in vitro* RPA-ATRIP interaction, 250 pmol purified recombinant GST-wt-RPA70N or GST-RPA70N/R41E/R43E was incubated with Glutathione-Agarose (Sigma) in GST-binding buffer (20 mM HEPES, 100 mM KCl,

5 mM $MgCl_2$, 0.5 mM EDTA, 0.2% NP-40, 10% glycerol, 1 mM PMSF, pH7.5) for 1 hour at room temperature. After the agarose beads were pelleted and washed once with GST-binding buffer, 140 μg nuclear lysate of U2OS cells stably expressing HA-tagged ATRIP (a generous gift from Professor Cortez) was added with purified recombinant BID simultaneously. The mixture was incubated for 1 hour at room temperature, and then the beads were pelleted by centrifugation and washed five times with GST-binding buffer. The beads were boiled with 3×Laemmli buffer and the supernatant was resolved on SDS-PAGE.

NMR analysis

NMR experiments were performed by Dr. Vaithiyalingam in Professor Chazin's lab and conducted using Bruker DRX 500-MHz and 600-MHz spectrometers equipped with z-axis gradient TXI cryoprobes. ^{15}N-^{1}H HSQC spectra were acquired using 75 μM ^{15}N-enriched RPA70N sample in buffer containing 20 mM Tris (pH 7.0), 50 mM NaCl, and 2 mM DTT. The NMR chemical shift perturbations assays were performed by adding unlabeled protein into the solution of 15N-enriched proteins until the molar ratio reached 1:4. Resonance assignments are available for RPA70N (177) and BID (BMRB entry 5340; (75)). All spectra were processed by Topspin v2.0 (Bruker, Billerica, MA) and analyzed with Sparky (University of California, San Francisco, CA).

Docking of RPA70N with hBID

A model of RPA70N-hBID complex was generated by Dr. Vaithiyalingam in Professor Chazin's lab using HADDOCK2 software (239,240). Structures of RPA and hBID were taken from the protein data bank (PDB); entry 2B3G and 2BID, respectively. Ambiguous distance restraints (AIR) were generated based on significant chemical shift perturbations or line broadening and solvent accessibility. Side chain solvent accessibilities were calculated using NACCESS (241). Residues with a solvent accessible surface more than 50% and significant chemical shift perturbations were designed as active for docking calculations. The adjacent residues with more than 50% solvent accessible surface were designed as passive residues. An ensemble of 1000 rigid body docking models was generated at the first iteration of calculation. From this calculation, the best 200 structures were selected based on the energy to perform a second iteration using semi-flexible simulated annealing protocol, and these structures were further refined in explicit solvent. The final structure solutions were clustered using HADDOCK score and the 10 lowest energy models were selected from the most populated cluster for structural analysis.

Mouse model experiments

Mice and DNA damage treatments

For HU treatment, wild type and *Bid* -/- C57/BL6 mice (6-8 weeks old) were treated with 100 mg/kg/day hydroxyurea by intraperitoneal injection for three consecutive days. Mice were sacrificed and bone marrow was harvested from femurs and tibias 24 hours after the third injection. For long-term HU treatment, after three-consecutive-day-HU treatment, mice were released from HU treatment for 7 days and subjected to HU treatment again for three consecutive days. This treatment cycle was repeated for 6 months. For IR treatment, wild type and *Bid* -/- C57/BL6 mice (6-8 weeks old) were irradiated with 2 Gy using a ^{137}Cs source. Mice were sacrificed and bone marrow was harvested 24 hours after irradiation. At least two independent experiments were performed with n = 5 in each set (See figure legend for details).

Cell staining and flow cytometry

Bone marrow cells were stained with the following antibody in staining buffer (3% FBS in PBS): biotinylated CD3 (BD pharmingen), biotinylated B220 (BD pharmingen), biotinylated TER119 (BD pharmingen), biotinylated Gr-1 (BD pharmingen), APC-conjugated anti-c-kit (BD pharmingen), PE-Cy7-conjugated anti-Sca1 (eBioscience), FITC-conjugated anti-CD34 (BD pharmingen), FITC-conjugated anti-BrdU (BD pharmingen), PE-conjugated anti-FcγRII/III (eBioscience), Pacific blue-conjugated streptavidin (Invitrogen), Alexa Fluor 488-conjugated anti-phospho-Histone H2A.X (Ser139) (Cell signaling, #9719),

PE-conjugated anti-CD45.1 (BD pharmingen), FITC-conjugated anti-CD45.2 (BD pharmingen). For lineage staining, cells were stained with biotinylated CD3, biotinylated B220, biotinylated Ter119 and biotinylated Gr-1 for 20 minutes on ice. Then, cells were stained with Pacific blue-conjugated streptavidin, APC-conjugated anti-c-kit, PE-Cy7-conjugated anti-Sca1, FITC-conjugated anti-CD34 and PE-conjugated anti-FcγRII/III for 20 minutes on ice. Cell population data were obtained by a 5-laser BD LSRII (Vanderbilt Flow Cytometry Core) and analyzed by Flowjo 8. Compensation parameter setting was performed using BD™ CompBead (BD pharmingen).

BrdU incorporation and cell death analysis

BrdU incorporation analysis was performed according to BrdU Flow Kits (BD Pharmingen). Briefly, mice were treated with 100 µl 10 mg/ml BrdU solution by intraperitoneal injection. Incorporation of BrdU was detected in bone marrow from femurs and tibias in 1 hour post injection. Erythrocytes were lysed in RBC lysis buffer (10 mM Tris-HCl, 0.83% NH_4Cl, pH 7.3) and bone marrow cells were stained with various surface markers as mentioned in the figure legends. Then, cells were fixed and permeabilized with BD Cytofix/Cytoperm Buffer, and incubated with BD Cytoperm Plus Buffer followed by an additional short fixation with BD Cytofix/Cytoperm Buffer. The incorporated BrdU was exposed by treatment with 30 µg DNase for 1 hour at 37^{o}C and probed with FITC-conjugated

anti-BrdU antibody (eBioscience) for 20 minutes at room temperature.

Cell death analysis was performed according to Annexin V-FITC Apoptosis Detection Kit (BioVision). Briefly, bone marrow cells were obtained from femurs and tibias and erythrocytes were lysed in RBC lysis buffer (10 mM Tris-HCl, 0.83% NH_4Cl, pH 7.3). Cells were stained with various surface markers as mentioned in the figure legends. Then, cells were stained by Annexin V-FITC in binding buffer (10 mM HEPES/NaOH, 150 mM NaCl, 5 mM KCl, 1mM $MgCl_2$, 2 mM $CaCl_2$, pH7.4) at room temperature for 15 minutes.

Methylcellulose culture

Methylcellulose culture was performed as previously described (66). Briefly, bone marrow was harvested from femurs and tibias and erythrocytes were lysed in RBC lysis buffer. Then, 5×10^4 bone marrow cells were resuspended in Methylcult H4100 (StemCell Technologies) supplemented with BSA, FBS, Insulin and Transferrin, with the following cytokines/plate: SCF (R&D, 450 ng), IL3 (R&D, 18 ng), IL6 (R&D, 9 ng) and erythropoietin (R&D, 5.4 Unit). Cells were plated in 35-mm dishes and incubated in a humidified atmosphere at 37°C, 5% CO_2. Typical colonies were photographed using a Leica DM IRBE inverted wild field microscope (Vanderbilt Cell Imaging Shared Resource). After six days, the cultures were washed with PBS, counted, and replated at the same density. The captured image was analyzed by Photoshop CS3 to measure the diameter of the

compact center of each GEMM or GM colony.

γH2A.X immunofluorescence and intra-cellular staining

Bone marrow was harvested from femurs and tibias and erythrocytes were lysed in RBC lysis buffer. Then, 5-10 × 10^4 bone marrow cells were centrifuged onto a glass coverslip by cytospin. Then, cells were fixed by 3% paraformaldehyde/2% sucrose solution and permeabilized by Triton X-100 solution (0.5% Triton X-100, 20 mM HEPES pH7.4, 50 mM NaCl, 3 mM $MgCl_2$, 300 mM Sucrose). γH2A.X-positive cells were detected by immunofluorescence using Alexa Fluor 488-conjugated anti-phospho-Histone H2A.X (Ser139) (Cell signaling, #9719). The cells were examined using a Leica DM IRBE inverted wild field microscope (Vanderbilt Cell Imaging Shared Resource).

For γH2A.X flow cytometry analysis, bone marrows were obtained from femurs and tibias and erythrocytes were lysed in RBC lysis buffer. Bone marrow cells were stained with various surface markers as mentioned in the figure legends. Then, cells were fixed and permeabilized with BD Cytofix/Cytoperm Buffer, and incubated with BD Cytoperm Plus Buffer followed by an additional short fixation with BD Cytofix/Cytoperm Buffer. Then, cells were stained with Alexa Fluor 488-conjugated anti-phospho-Histone H2A.X (Ser139) (Cell signaling) for 30 minutes at room temperature and γH2A.X-positive cells were detected by flow cytometry.

Competitive reconstitution in bone marrow transplantation

Congenic C57/BL6 mice recipient mice (CD45.1) were lethally irradiated with 9 Gy using a ^{137}Cs source. Donor cells were obtained from *Bid* +/+ (CD45.2) and *Bid* -/- (CD45.2) mice following 6-month HU treatment. Bone marrows were obtained from femurs and tibias and erythrocytes were lysed in RBC lysis buffer. Then, cells were stained with lineage markers (CD3, B220, TER119 and Gr-1) for 20 minutes on ice. Lineage+ cells were depleted by Dynabeads Sheep anti-Rat IgG (Invitrogen) and lineage- cells were counted. 1×10^6 lineage- bone marrow cells from either wild type or *Bid* -/- C57/BL6 mice (CD45.2+) following 6-month HU treatment together with 1×10^6 lineage- bone marrow cells from normal wild type C57/BL6 mice (CD45.1+) were equally transplanted into 10 lethally irradiated recipients (CD45.1+) by intravenous injection. Hematopoietic reconstitution was detected followed 2 and 4 months after the transplantation. Peripheral blood from the recipient mice was subjected to Lymphocyte Separation Medium (MP Biomedicals) and lymphocytes were collected after centrifugation at 3000 rpm for 30 minutes. The lymphocytes were washed once with PBS, stained by anti-PE-CD45.1 and anti-FITC-CD45.2 antibodies, and analyzed in flow cytometry.

CHAPTER III

PROAPOPTOTIC BID MEDIATES THE ATR-DIRECTED DNA DAMAGE RESPONSE TO REPLICATIVE STRESS*

Introduction

The BCL-2 family of proteins regulates the intrinsic pathway of programmed cell death or apoptosis. The BH3-only members of the family function as sensors, relaying death signals to the core apoptotic machinery at the mitochondria. BH3-only BH3-interacting domain death agonist (BID) has a unique function in apoptosis to interconnect the death receptors of the extrinsic pathway to the mitochondrial amplification loop of the intrinsic pathway (31,32). Despite the potent role of BID in apoptosis, *Bid* -/- mice develop normally, but show deregulated myeloid homeostasis, culminating in a clonal disorder closely resembling human chronic myelomonocytic leukemia (CMML) (66). *Bid* -/- myeloid progenitor cells (MPCs) show an increased mitomycin c-induced chromosomal breaks (2), and *Bid* -/- leukemias show chromosomal abnormalities (66). Following DNA damage, ATM, and/or ATR phosphorylate Bid on Ser61/64 and Ser78, and this phosphorylation is required for proper regulation of S phase after DNA damage (2,3,93). Thus, BID has two distinct and separable functions in

*The research results in this chapter have been published as reference (4).

apoptosis and the DNA damage response.

A highly regulated response program senses and repairs DNA damage (1). Two phosphoinositide 3-kinase-related protein kinases (PIKKs), ATM, and ATR, sense DNA damage at the site of the DNA lesion and activate downstream transducers to engage the checkpoint and DNA repair machinery (1), or the apoptotic pathway (110). ATM responds primarily to double strand breaks, and ATR to replication protein A (RPA)-coated single-stranded DNA (ssDNA) by interaction with its stable binding partner ATRIP (108,110,125).

Stalled replication forks created by replicative stress produce a distinct DNA lesion comprised of RPA-coated ssDNA adjacent to a stretch of dsDNA. RPA recruits a multiprotein complex at the site of the DNA lesion, comprised of ATRIP, interacting with RPA via its checkpoint recruitment domain (CRD) and its stable binding partner ATR (242). RAD17 independently recruits the RAD9-HUS1-RAD1 complex (9-1-1 complex) to stalled replication forks (126,243). The 9-1-1 complex then recruits TopBP1 (127), to associate with ATRIP and ATR, and stimulate ATR kinase activity (128,129). Activated ATR phosphorylates a multitude of downstream effectors to initiate the complex cellular response to replicative stress, including activation of checkpoints, DNA repair, and apoptosis (124).

Proapoptotic BID functions in apoptosis as well as the DNA damage response (2,3,76). Several independent groups have demonstrated that Bid is found in the nucleus after DNA damage, is phosphorylated by ATM and/or ATR, and mediates

efficient activation of an S-phase checkpoint (2,3,80,81). BID has also been identified in a screen of proteins phosphorylated in response to DNA damage on consensus ATM/ATR phosphorylation sites (93). Furthermore, mice expressing mutated Nijmegen breakage syndrome 1 (NBS1) demonstrate defective ATM activation and BID phosphorylation (82). Nonetheless, the mechanism by which BID interacts within the DNA damage response is unknown, and there is some controversy in the literature, primarily concerning the generality of role of BID in DNA damage-induced apoptosis (77). Of note, transient knockdown (KD) of BID was not tested in the above studies, therefore, the differences may have been attributable to compensation of cells to the absence of BID in a given experimental setting. Indeed, a recent report showed defects (198) in S phase following replicative stress induced by thymidine in *BID* KD HCT116 cells.

In this study, I demonstrate that BID facilitates ATR signaling, acting at the DNA damage sensor complex in response to replicative stress. In the absence of BID, ATR function is limited, as measured by recruitment of ATR and ATRIP to chromatin and nuclear foci following hydroxyurea (HU), phosphorylation of ATR substrates, and recovery of DNA replication following replicative stress (stalled replication forks). In addition, BID is found in nuclear foci with RPA following HU-induced replicative stress, and associates with members of the DNA damage sensor complex, ATR, ATRIP, and RPA. Importantly, the ATR/ATRIP association with RPA is diminished in the absence of BID. Furthermore, BID-ATRIP

association is required for CHK1 phosphorylation and accumulation of ATRIP at nuclear foci following HU. Thus, I demonstrate that BID facilitates the response of the ATR-mediated pathway to replicative stress through association with ATRIP at DNA damage foci, functioning at the level of the sensor complex.

Results

Bid is expressed in tissues with proliferating cells

Previous results show increased chromosomal damage and increased sensitivity of *Bid* -/- MPCs after treatment with agents inducing replicative stress (2,66). Bid is highly expressed in tissues that contain proliferating cells, such as thymus, bone marrow, and spleen, as well as intestinal epithelium after DNA damage (244), but not in tissues comprised primarily of post-mitotic cells, such as brain and lungs (Figure 3-1 A). In addition, the expression level of Bid correlates with that of PCNA, a marker for cell proliferation (Figure 3-1 A). Bid is, therefore, expressed in settings, in which cells are undergoing proliferation.

Bid -/- bone marrow cells are more sensitive to replicative stress

I asked whether BID might have a role *in vivo* to monitor the response to replicative stress by treating mice with HU, a ribonucleotide reductase inhibitor that predominantly triggers activation of the ATR-mediated signaling pathway.

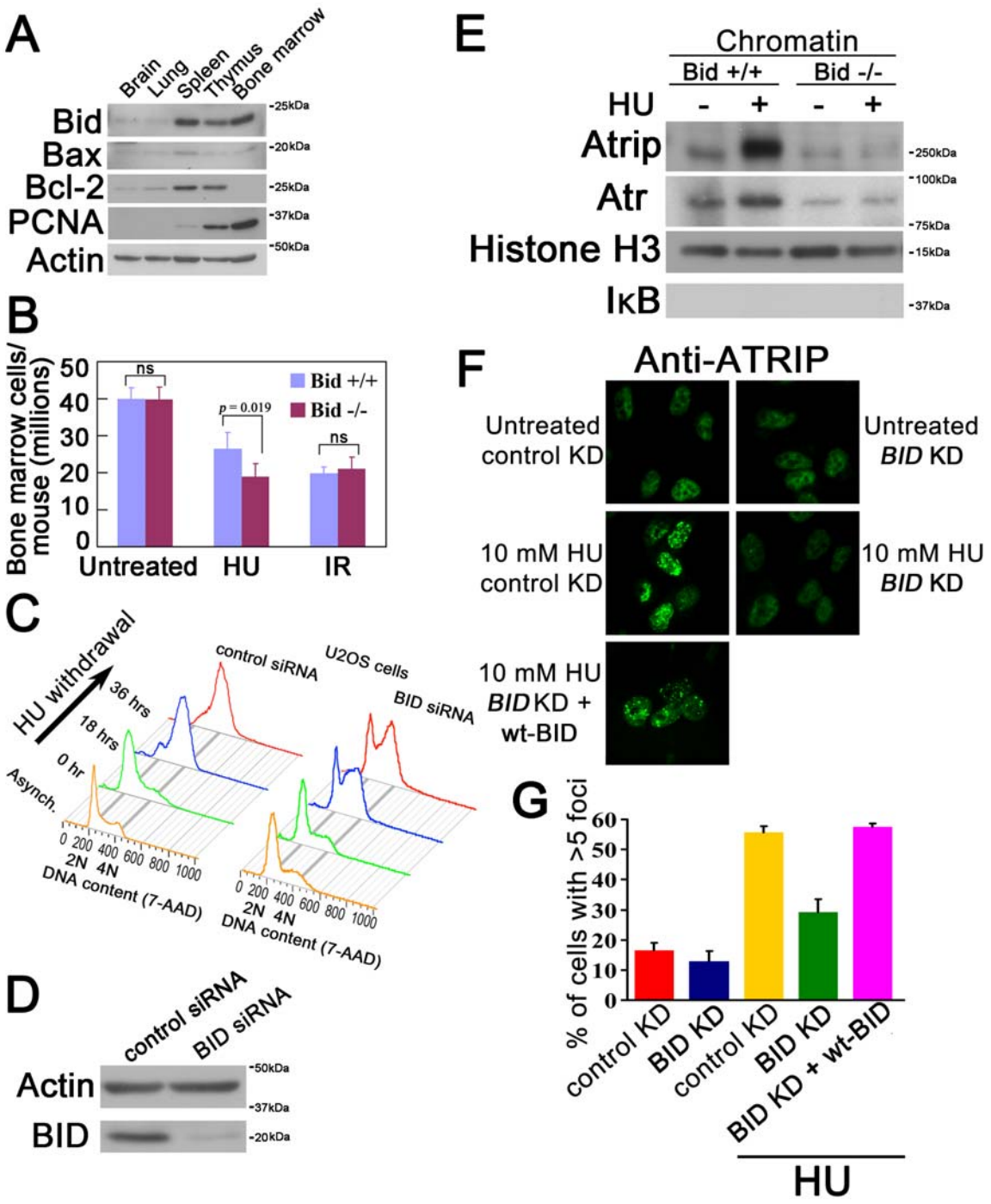

Figure 3-1. The cellular recovery from replicative stress and the HU-induced accumulation of ATRIP at nuclear foci are impaired in the absence of BID. (A) Bid is highly expressed in hematopoietic tissues. Tissues were harvested from wild type C57BL6 mice. Total cell lysates from the indicated tissues were resolved by SDS-PAGE and immunoblotted with the indicated antibodies. The molecular weight markers used in immunoblots are labeled on the right of the blots. (B) Bid -/- bone marrow cells are more sensitive to replicative stress. *Bid* +/+ and *Bid* -/- mice were injected with 100 mg/kg hydroxyurea (HU) for 3 consecutive days. Mice were killed and bone

marrow was harvested from mouse femurs and tibia at 24 h after the third injection. *Bid* +/+ and *Bid* -/- mice were irradiated with 2 Gy using a ^{137}Cs source. Mice were killed and bone marrow was harvested from mouse femurs and tibia 24 h after irradiation. Following lysis of red blood cells, viable bone marrow cells were identified by trypan blue exclusion and counted. N=15 mice for HU treatment and n=10 mice for irradiation treatment. Error bar=90% confidence interval. *p*-value is calculated by student's t-test. (C) U2OS cells were transfected with control siRNA or *BID* siRNA. After 2 days, cells were exposed to 10 mM HU for 24 h, and released into fresh media containing 1 μg/ml nocodazole for the indicated times. Cells were fixed and stained with 7-AAD and analyzed by flow cytometry. (D) U2OS cells were transfected with control siRNA or *BID* siRNA for 72 h. Cells were lysed and BID was detected in immunoblots. (E) *Bid* +/+ and *Bid* -/- MPCs were treated with 10 mM HU for 2 h. The chromatin fraction was isolated and extracts were resolved on SDS-PAGE and immunoblotted with the indicated antibodies. (F) U2OS cells were transfected with control siRNA or *BID* siRNA and wild type mouse Bid was introduced into the cells simultaneously with siRNA. Cells were treated with 10 mM HU for 5 h, fixed, and stained with anti-ATRIP antibody. Representative images of ATRIP staining were shown. (G) Quantitative analysis of ATRIP accumulation at nuclear foci following replicative stress. The percentage of cells with >5 clearly visible ATRIP nuclear foci was calculated for each cell type. More than 600 cells were counted in three independent experiments.

Hematopoietic progenitor cells proliferate and repopulate the bone marrow following insult, and are vulnerable to agents inducing replicative stress. *Bid* -/- but not *Bid* +/+ bone marrow cells are more sensitive to systemic treatment with 100 mg/kg HU *in vivo* (Figure 3-1 B), but not to a low dose of ionizing radiation (2 Gy), suggesting specific sensitivity to replicative stress. I, thus, demonstrate that BID has a role *in vivo* to mediate the response of bone marrow to HU-induced replicative stress.

BID has a role in recovery and completion of DNA replication following HU

One function of activated ATR that is distinct to ATR among the PIKKs is to facilitate cell cycle re-entry after the release of replicative stress (245). U2OS cells transfected with siRNA directed against *BID* (*BID* KD) or a control siRNA (control KD) were arrested in early S phase by 10 mM HU for 24 h. HU was washed out and cells were released into fresh medium with nocodazole to prevent cell division. Asynchronous *BID* KD and control KD U2OS cells showed similar cell cycle profiles at baseline (Figures 3-1 C, D). *BID* KD but not control KD U2OS cells demonstrated impaired DNA replication recovery and impaired progression through S phase (Figure 3-1 C, Figure 3-2 A), but no significant increase in apoptotic cells as measured by <2N DNA content (Figure 3-2 B). Thus, the recovery of DNA replication and completion of S phase after replicative stress was significantly impaired in the absence of BID further suggesting a defect in ATR

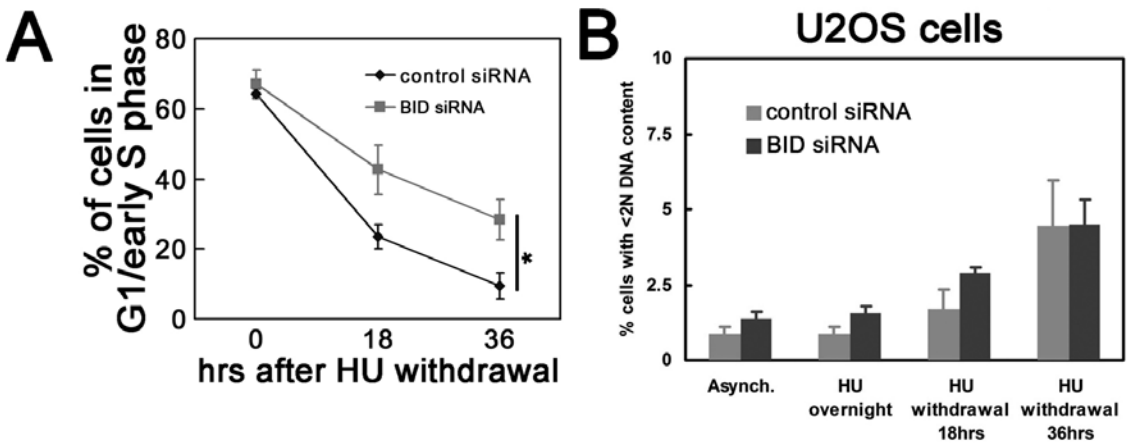

Figure 3-2. Cell cycle reentry is limited in *BID* KD cells. (A) The quantitative analysis of the arrested G1/early S phase cells following HU withdrawal in Fig 3-1 C. Data were collected from three independent experiments. *, $p<0.05$. (B) Hydroxyurea treatment does not result in significant increase of cell death in U2OS cells. U2OS cells transfected with control siRNA or *BID* siRNA for 72 hours were treated with 10 mM hydroxyurea overnight. Then, cells were released to fresh medium containing nocodazole. Cells were fixed and DNA content was detected by 7-AAD. Quantitative analysis of the percentage of cell with less than 2N DNA content was obtained from three independent experiments. Error bar=90% confidence interval.

activation in the absence of BID.

BID does not mediate TopBP1-directed ATR activation in vitro

To determine whether BID modulates TopBP1 activation of ATR, ATR-ATRIP was purified by immunoprecipitation (IP) from 293T cells, and incubated with purified TopBP1 AAD, γ-^{32}P-ATP, and Mcm2 as an ATR substrate (246,247), with and without BID (Figure 3-3 A). ATR-ATRIP phosphorylated BID and Mcm2, however, the presence of BID did not alter Mcm2 phosphorylation. Thus, BID is a substrate of ATR but does not modulate TopBP1-directed ATR activation in this *in vitro* system.

BID has a role in recruitment or maintenance of ATRIP to nuclear foci following replicative stress

In the presence of replicative stress, ATRIP and ATR are recruited to stalled replication forks and accumulate in nuclear foci. *Bid* -/- cells demonstrated decreased ATR/ATRIP accumulation in chromatin following HU relative to *Bid* +/+ cells (Figure 3-1 E). *BID* KD U2OS cells demonstrate decreased accumulation of ATRIP in HU-induced DNA damage foci (Figure 3-1 F, G). Importantly, reintroducing wild type BID into *BID* KD U2OS cells restored ATRIP accumulation at nuclear foci (Figure 3-1 F, G). No HU-induced increase in ATR or ATRIP levels was seen in control U2OS cells; a modest HU-induced increase in ATR protein

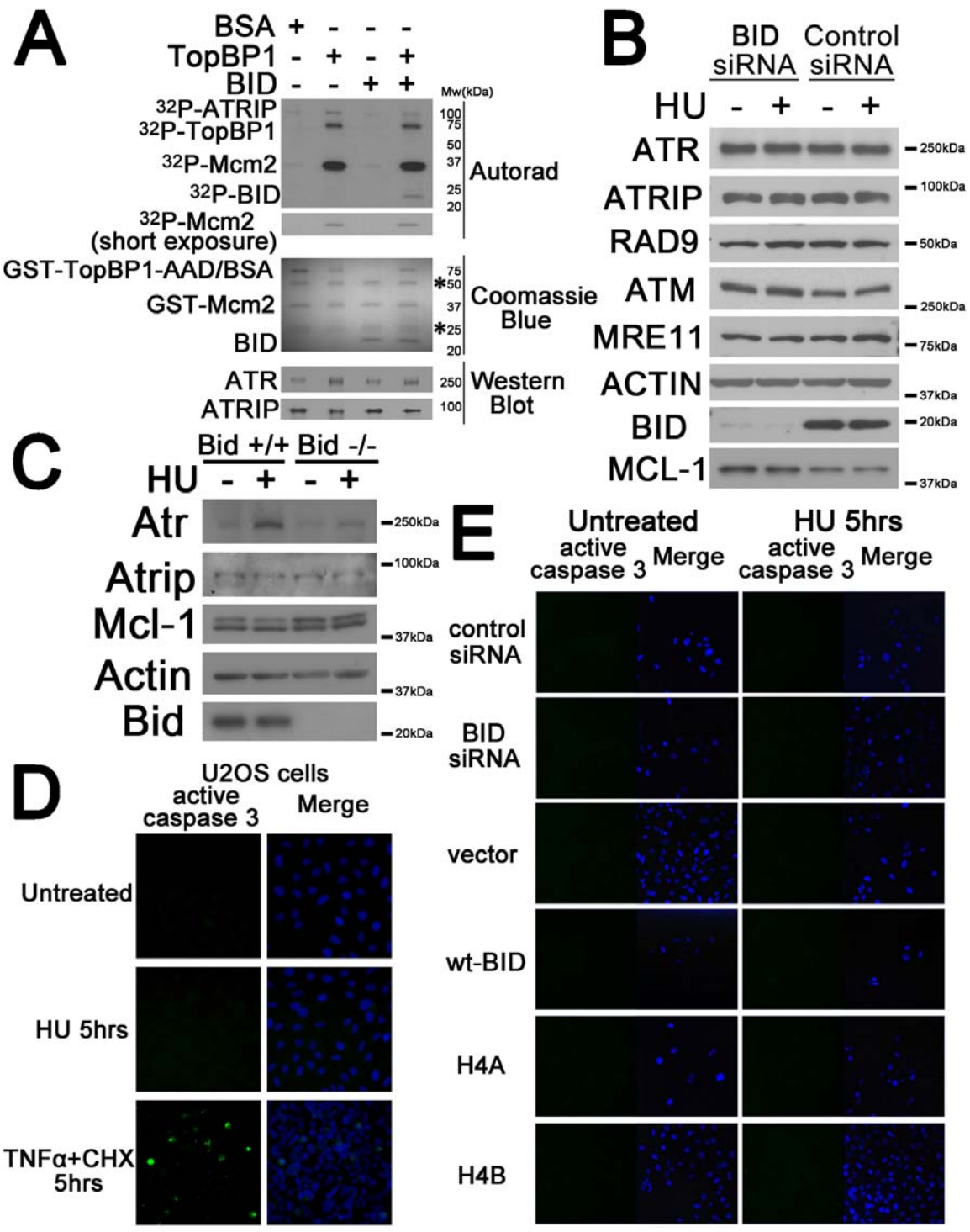

Figure 3-3. Expression of BID results in neither ATR activation in an *in vitro* system nor significant changes of cell death and sensor levels in U2OS cells. (A) BID does not facilitate TopBP1 activation of ATR *in vitro*. HA-ATRIP and myc-ATR were overexpressed in 293T cells, and isolated from whole cell extracts by immunoprecipitation with anti-HA conjugated agarose beads. Purified ATR/ATRIP was incubated with the activating domain of TopBP 1 (TopBP1 AAD), the ATR

substrate MCM2 peptide, and γ-^{32}P-ATP. Reactions were separated on SDS-PAGE, stained with Coomassie Blue, and exposed to film. Duplicate samples were separated on SDS-PAGE, and immuno-blotted with anti-ATR and anti-ATRIP. (B) The protein levels of various DNA damage sensors are not significantly changed in *BID* KD U2OS cells. U2OS cells were transfected with control siRNA or *BID* siRNA for 72 hours. Then the control knockdown and *BID* knockdown cells were treated with 10 mM hydroxyurea for 2 hours and various DNA damage sensors in ATM/ATR pathways were detected by immunoblots. (C) *Bid* +/+ and *Bid* -/- MPCs were treated with 10 mM hydroxyurea for 2 hours and various DNA damage sensors in ATR pathways were detected by immunoblots. (D) TNFα/CHX treatment but not hydroxyurea treatment significantly induces apoptosis in U2OS cells. U2OS cells were treated with 10 mM hydroxyurea or 10 ng/ml TNFα+25 μg/ml CHX for 5 hours. Cells were fixed and stained with anti-activated caspase 3 (Asp175) polyclonal antibody (Cell signaling, #9661) in immunofluorescence. DNA was stained by Hoechst. (E) Expression of wild type or mutated BID does not cause significant apoptosis in U2OS cells. U2OS cells transfected with control siRNA, *BID* siRNA, wild type or Helix 4 mutated BID were treated with 10 mM hydroxyurea for 5 hours. No obvious apoptotic cells were detected by activated caspase 3 in immunofluorescence. DNA was stained by Hoechst.

level was observed following DNA damage in *Bid* +/+ but not *Bid* -/- MPCs (Figure 3-3 B, C). The above data are consistent with a role for BID in recruitment or maintenance of ATR and ATRIP at nuclear foci following DNA damage.

Apoptosis activates DNAases. To rule out BID-induced apoptosis as the etiology of ATRIP accumulation at nuclear foci, I evaluated caspase 3 activation by immunofluorescence following reintroduction of BID (Figure 3-3 D, E). Death receptor stimulation but not HU treatment activates caspase 3 in U2OS cells. Reintroduction of BID +/+ to *BID* KD U2OS cells treated with HU does not activate caspase 3, indicating that the ATRIP accumulation at nuclear foci is not due to BID-induced apoptosis.

DNA damage-induced phosphorylation of ATR substrates is diminished in the absence of BID

I next evaluated phosphorylation of the ATR effectors, CHK1 and RPA32. Following HU treatment, CHK1 immunoblot displayed phosphatase-sensitive slower migrating bands that reacted with antibodies specific for phospho-CHK1 (S317) and (S345) (Figure 3-4 A, B, Figure 3-5 A). These bands were diminished in *Bid* -/- MPCs following HU treatment (Figure 3-4 A, B). To acutely decrease BID protein levels, siRNAs targeted against human *BID* and mouse *Bid* mRNA were introduced into human U2OS cells and mouse MPCs, respectively, decreasing BID levels to <20% of endogenous levels in U2OS cells using siRNA7, and nearly

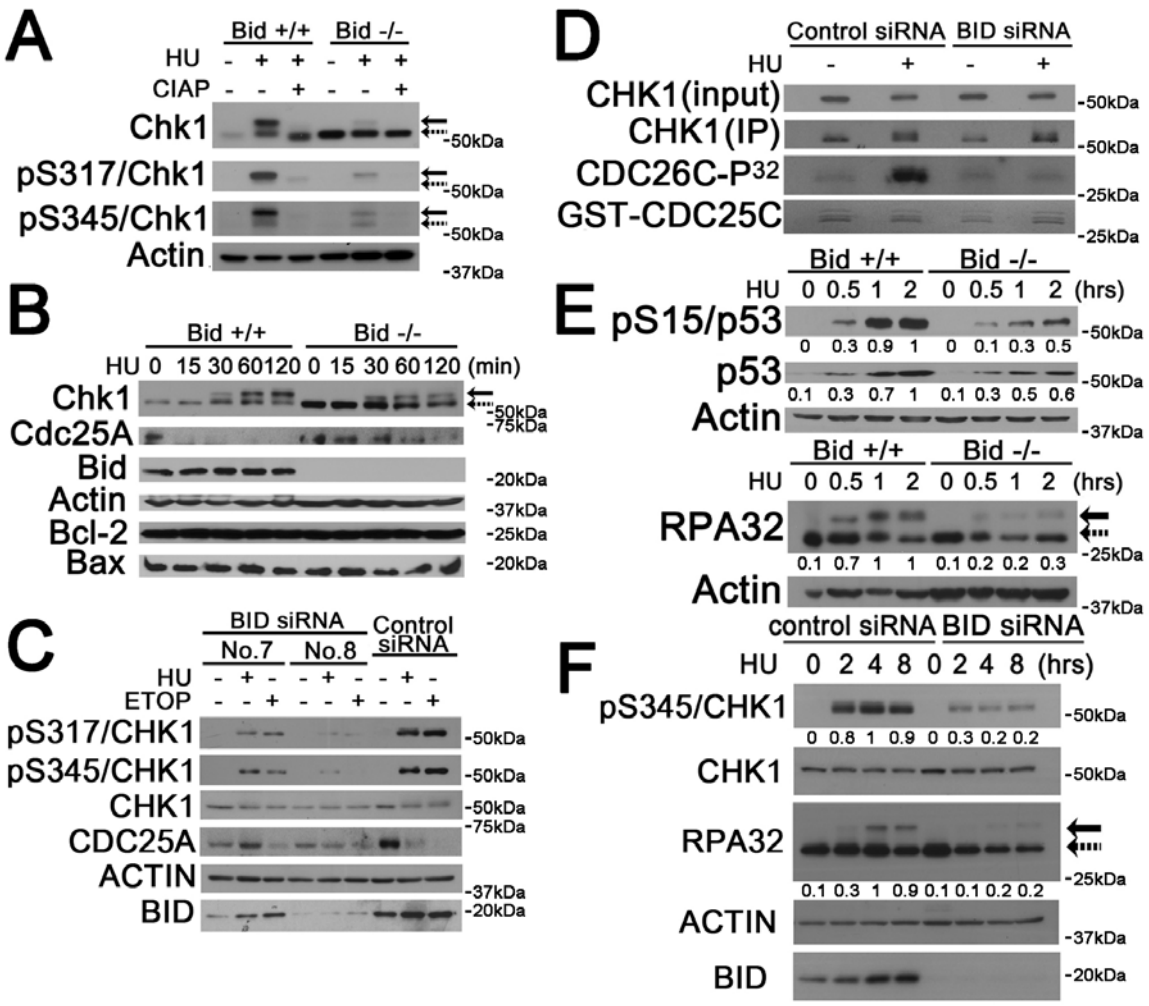

Figure 3-4. The phosphorylation of ATR substrates are diminished in *Bid* -/- and *BID* KD cells following replicative stress. (A) Phosphorylated mouse CHK1 presents as a shifted band. *Bid* +/+ and *Bid* -/- MPCs were treated with 10 mM HU for 2 h. Whole-cell extracts were incubated with 10 U Calf Intestinal Alkaline Phosphatase (Invitrogen)/100 µg lysate, resolved by SDS-PAGE and immunoblotted with anti-CHK1, anti-pCHK1 (S317), or anti-pCHK1 (S345) as indicated. Solid arrows denote the mobility of shifted phosphorylated CHK1, and dashed arrows denote the mobility of unphosphorylated CHK1. (B) *Bid* +/+ and *Bid* -/- MPCs were treated 10 mM HU for the indicated times. Total cell lysate was resolved by SDS-PAGE followed by immunoblotting with the indicated antibodies. (C) U2OS cells were treated with *BID*-specific siRNA No.7, *BID*-specific siRNA No.8, or control siRNA for 72 h. *BID* KD and control KD cells were treated with 10 mM HU or 25 µM ETOP for 2 h, and total cell lysate was resolved by SDS-PAGE followed by immunoblotting with the indicated antibodies. (D) U2OS cells transfected with control siRNA or *BID* siRNA (no. 8) for 72 h were treated with 10 mM HU for 2 h. Whole-cell lysates were immunoprecipitated with anti-CHK1 antibody, and the immunoprecipitated product was incubated with 1 µg GST-CDC25C protein, 10 µM cold ATP and 5 µCi γ-^{32}P-ATP in kinase buffer. CHK1 kinase reactions were resolved on SDS-PAGE, stained with SimplyBlue SafeStain (Invitrogen) to visualize GST-CDC25c

levels, and analyzed by autoradiography. (E) *Bid* +/+ and *Bid* -/- MPCs were treated 10 mM HU over time. Total cell lysate was resolved by SDS-PAGE followed by immunoblot with the indicated antibodies. Relative band intensity has been measured by densitometry analysis. (F) U2OS cells were transfected with control siRNA or *BID* siRNA for 72 h, and then treated with 10 mM HU over time. Total cell lysate was resolved by SDS-PAGE followed by immunoblot with the indicated antibodies. Solid arrow denotes the mobility of shifted phosphorylated RPA32, and dashed arrow denotes the mobility of unphosphorylated RPA32. Relative band intensity was measured by densitometry analysis.

completely using siRNA8 (Figure 3-4 C). *BID* KD U2OS cells (Figure 3-4 C) and MPCs (Figure 3-4 A, B, Figure 3-5 B, D) displayed diminished phosphorylated CHK1 following HU or etoposide (ETOP) treatment. Furthermore, the degree of decreased CHK1 phosphorylation correlated with the degree of *BID* KD. Interestingly, the CHK1 level is increased in *Bid* -/- MPCs (Figure 3-4A, B), but not in U2OS cells when *BID* was knocked down by siRNA (Figure 3-4 C), consistent with a compensatory increase in CHK1 levels in the setting of chronic absence of BID, but not when BID is lost acutely. These results implicate BID in mediating ATR function.

I next evaluated effectors of the DNA damage response, such as Cdc25A in *Bid* +/+ and *Bid* -/- cells. Cdc25A is phosphorylated by Chk1 following replicative stress, targeting it for degradation (248,249). Cdc25A degradation following DNA damage was delayed in *Bid* -/- MPCs as well as in *BID* KD U2OS cells (Figure 3-4 B, C, Figure 3-5 B). Interestingly, Cdc25A levels are increased in untreated *Bid* -/- MPCs but not in *BID* KD U2OS cells, consistent with a compensatory increase in Cdc25A levels in the setting of prolonged loss of Bid. These results implicate BID in mediating CHK1 function.

I further evaluated CHK1 kinase activity via IP of CHK1 from control siRNA and *BID* siRNA-transfected U2OS cells followed by incubation with GST-cdc25C and γ-^{32}P-ATP. The anti-CHK1 antibody immunoprecipitated both CHK1 and phosphorylated CHK1 (Figure 3-5 E, F). Following HU treatment, *BID* KD U2OS

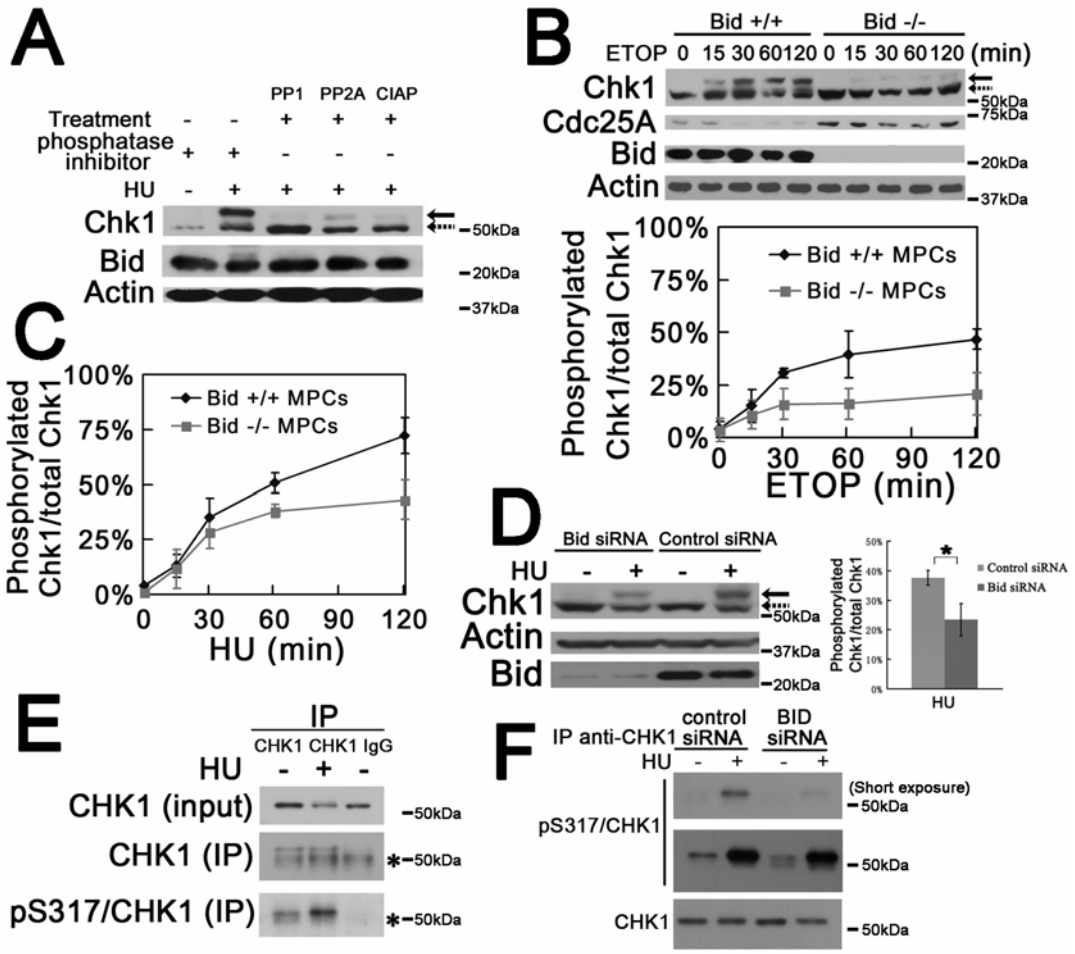

Figure 3-5. CHK1 phosphorylation is diminished in *Bid* -/- MPCs following DNA damage treatments. (A) Phosphorylated mCHK1 present as a shifted band in immunoblots. *Bid* +/+ MPCs were treated with 10 mM hydroxyurea for 2 hours. Cells were lysed in RIPA buffer with or without phosphatase inhibitors. The indicated protein phosphatases (PP1, protein phosphatase type; PP2A, protein phosphatase types 2A; CIAP, calf intestine alkaline phosphatase) were added to 400 µg cell lysate and incubated at 30^{o}C for 30 minutes. Protein extracts were resolved by SDS-PAGE and immunoblotted with anti-CHK1 antibody. Solid arrow denotes the mobility of shifted band corresponding to phosphorylated CHK1, and dashed arrow denotes the mobility of unshifted band corresponding to CHK1. (B) *Bid* +/+ and *Bid* -/- MPCs were treated 25 µM etoposide for the indicated times. Total cell lysate was evaluated by SDS-PAGE followed by immunobloting with the indicated antibodies. The quantitative analysis of the ratio of pCHK1 to total CHK1 were collected from three independent experiments. (C) The quantitative analysis of the ratio of pCHK1 to total CHK1 in Fig 3-4B were collected from three independent experiments. (D) *Bid* +/+ MPCs were treated with *Bid*-specific siRNA or control siRNA using nucleofectin and incubated for 72 hours. *Bid* knockdown and control knockdown cells were treated with 10 mM hydroxyurea for 2 hrs, and total cell lysate was resolved by SDS-PAGE followed by immunobloting with the indicated antibodies. The quantitative analysis of the ratio of pCHK1 to total CHK1 were collected from three independent experiments. *, p<0.05.

cells demonstrated decreased kinase activity relative to control KD cells suggesting that the HU-induced CHK1 activity, or a kinase associated with CHK1, is decreased in the absence of BID (Figure 3-4 D). These results strongly suggest that HU-induced CHK1 activation is decreased in the absence of BID.

I next evaluated phosphorylation of the ATR targets p53 and RPA32 following replicative stress. p53 phosphorylation at Ser15 (Figure 3-4 E, Figure 3-6 A), and the HU-induced expression levels of the p53 target genes *p21* and *Noxa* were diminished (Figure 3-6 B) in *Bid* -/- MPCs following HU treatment. Furthermore, RPA32 phosphorylation was decreased in *Bid* -/- MPCs (Figure 3-4 E) and in U2OS cells upon siRNA KD of *BID* (Figure 3-4 F). Thus, in the absence of *BID*, phosphorylation of multiple ATR substrates was diminished, consistent with a role for BID in ATR activation.

In contrast, the autophosphorylation of ATM was normal in the absence of *BID* following ETOP treatment in U2OS cells (Figure 3-6 C), suggesting that BID does not have a major role in ATM activation. In addition, CHK1 phosphorylation was diminished in *BID*/*ATM* double KD U2OS cells as well as *BID* KD U2OS cells (Figure 3-6 D), suggesting that the function of BID in the ATR-mediated response is independent of ATM.

CHK1 phosphorylation increases in S phase. I observed no significant difference in the percentage of cells in S phase between *Bid* +/+ and *Bid* -/- cells (Figure 3-7 A, B). To stringently evaluate the status of CHK1 phosphorylation at a defined stage

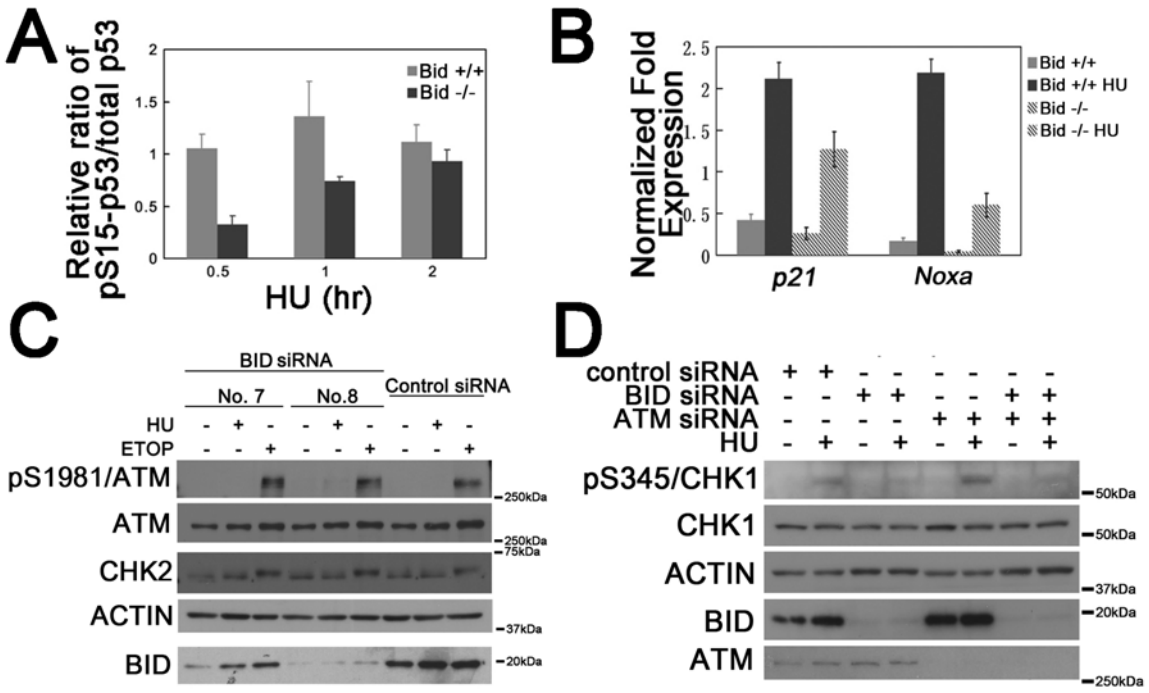

Figure 3-6. p53 phosphorylation is diminished in *Bid* -/- MPCs following DNA damage treatments. (A) The quantitative analysis of the ratio of pS15/p53 to total p53 in Fig 3-4E. (B) The transcription level of p53-target genes is diminished in *Bid* -/- MPCs following replicative stress. *Bid* +/+ and *Bid* -/- MPCs were treated 10 mM hydroxyurea for 3 hours. Total RNA was extracted and real-time PCR performed to detect the relative transcription levels of *p21* and *Noxa*. *Actin* was used as the reference. (The bars indicate the s.d., N=3) (C) ATM auto-phosphorylation is unaffected in the absence of *BID* following etoposide treatment. U2OS cells were treated with *BID*-specific siRNA No.7, *BID*-specific siRNA No.8 or control siRNA for 72 hours. *BID* knockdown and control knockdown cells were treated with 10 mM hydroxyurea or 25 μM etoposide for 2 hrs, and total cell lysate was resolved by SDS-PAGE followed by immunoblot with the indicated antibodies. (D) U2OS cells were transfected with control siRNA, *BID* siRNA and/or *ATM* siRNA for 72 hours. Then cells were treated with 10 mM hydroxyurea for 2 hours and CHK1 phosphorylation was detected by immunoblots.

of the cell cycle, I performed intra-cellular phospho-CHK1 staining with 7-AAD co-staining followed by flow cytometry. *Bid* -/- cells showed decreased numbers of phospho-CHK1+ cells, and the mean fluorescence index of phospho-CHK1 staining was significantly decreased relative to *Bid* +/+ cells within the total cell population and in cells in late S/G2/M (Figure 3-7 D, K), demonstrating on a per cell basis that phospho-CHK1 is decreased in *Bid* -/- cells. Thus, the differences in CHK1 phosphorylation observed in *Bid* -/- cells were not because of an alteration of the cell cycle profile (250-252).

BID associates with ATR/ATRIP/RPA

The findings outlined above implicate a role for BID very early in the DNA damage response, at the level of ATR activation and recruitment to DNA damage foci. Qiong Shi, therefore, examined the ability of BID to associate with the DNA damage sensor complex, composed of ATR, ATRIP, and RPA. ATR, ATRIP, and RPA co-immunoprecipitated with Bid from nuclear extracts, and this co-IP was enhanced after HU treatment (Figure 3-8 A). Mouse but not human BID co-migrates with the immunoglobulin light chain on SDS-PAGE, therefore, she performed the reverse IP in U2OS cells. When endogenous ATRIP or RPA was immunoprecipitated from the nuclear fraction of U2OS cells, BID was detected in the immunoprecipitated product (Figure 3-8 B, C). The anti-BID antibody did not nonspecifically precipitate DNA as shown by immunoblotting with anti-RUNX1

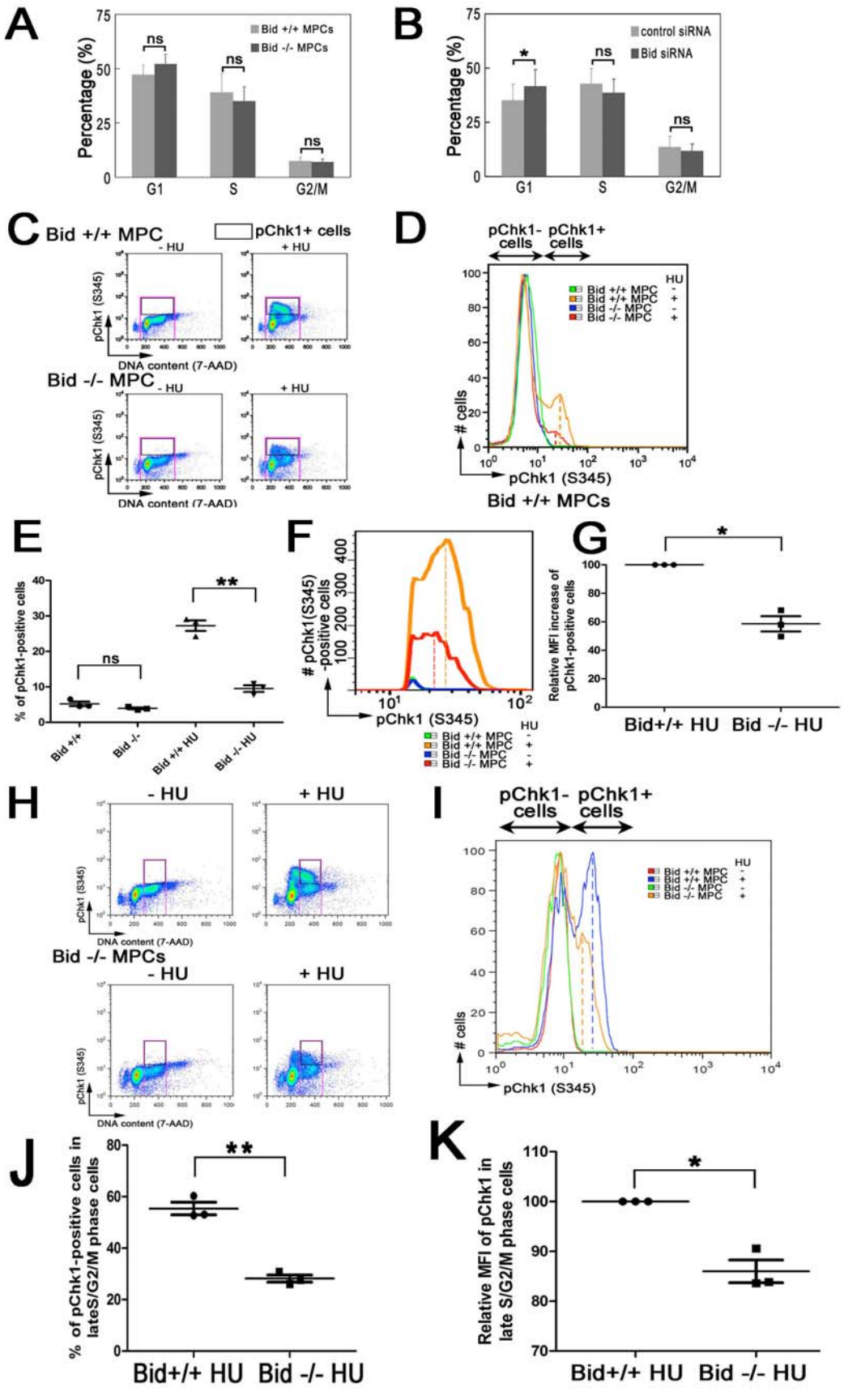
A
Percentage (%)
Bid +/+ MPCs
Bid -/- MPCs
ns
G1
S
G2/M
B
control siRNA
Bid siRNA
*
C
Bid +/+ MPC
pChk1+ cells
- HU
+ HU
pChk1 (S345)
DNA content (7-AAD)
Bid -/- MPC
D
pChk1- cells
pChk1+ cells
HU
cells
pChk1 (S345)
Bid +/+ MPCs
E
% of pChk1-positive cells
**
Bid +/+
Bid -/-
Bid +/+ HU
Bid -/- HU
F
pChk1(S345) -positive cells
G
Relative MFI increase of pChk1-positive cells
Bid+/+ HU
Bid -/- HU
H
Bid -/- MPCs
I
J
% of pChk1-positive cells in lateS/G2/M phase cells
K
Relative MFI of pChk1 in late S/G2/M phase cells

Figure 3-7. CHK1 phosphorylation is diminished in *Bid* -/- MPCs by flow cytometry. (A) The cell cycle profile is similar between *Bid* +/+ and *Bid* -/- MPCs. *Bid* +/+ and *Bid* -/- MPCs were labeled with BrdU for 45 minutes. Then cells were fixed and permeabilized with BD Cytofix/Cytoperm Buffer. BrdU was detected by intracellular staining with FITC-conjugated anti-BrdU antibody (BD Pharmingen). DNA was stained by 7-AAD. Then cells were analyzed by flow cytometry. Quantitative analysis of the cell cycle data was obtained from eight independent experiments. Error bar=90% confidence interval. *p* value is calculated by student's t-test. (B) U2OS cells transfected with control siRNA or *BID* siRNA were labeled with BrdU for 2 hours and analyzed by flow cytometry. Quantitative analysis of the cell cycle data was obtained from six independent experiments. Error bar=90% confidence interval. *p* value is calculated by student's t-test. (C) *Bid* +/+ and *Bid* -/- MPCs were treated with 10 mM hydroxyurea for 2 hours. Then cells were fixed and permeabilized with BD Cytofix/Cytoperm Buffer. CHK1 phosphorylation was detected by intracellular staining with anti-pCHK1 (S345) antibody (Cell signaling, #2348) and Alexa Fluor 488 conjugated Goat anti-Rabbit IgG antibody (Invitrogen). DNA was stained by 7-AAD. pCHK1-postive cells were gated as black rectangle. (D) pCHK1-positive cells were gated based on the hydroxyurea-induced population. The peak of pCHK1-positive *Bid* +/+ and *Bid* -/- cells was shown as yellow and red dash line, respectively. (E) Quantitative analysis of the percentage of pCHK1-positive cells from three independent experiments. Error bar, S.E.M. *p* value is calculated by student's t-test. **, $p<0.01$. (F) Gating on pCHK1-positive cells, *Bid* +/+ MPCs significantly increased pCHK1-positive population following hydroxyurea treatment. (G) Quantitative analysis of the relative mean fluorescence intensity (MFI) increase of pCHK1 signal by hydroxyurea in pCHK1-positive cells from three independent experiments. The HU-induced MFI increase of pCHK1 signal from pCHK1-positive *Bid* +/+ MPCs was set as 100 arbitrarily. Error bar, S.E.M. *p* value is calculated by student's t-test. *, $p<0.05$. (H) CHK1 phosphorylation is diminished in *Bid* -/- MPCs with high DNA content. *Bid* +/+ and *Bid* -/- MPCs were treated with 10 mM hydroxyurea for 2 hours. Then cells were fixed and permeabilized with BD Cytofix/Cytoperm Buffer. CHK1 phosphorylation was detected by intracellular staining with anti-pCHK1 (S345) antibody (Cell signaling, #2348) and Alexa Fluor 488 conjugated Goat anti-Rabbit IgG antibody (Invitrogen). DNA was stained by 7-AAD. Late S/G2/M phase cells (high DNA content) were gated. pCHK1-postive cells were gated as black rectangle. (I) pCHK1-positive cells were gated based on the hydroxyurea-induced population. The peak of pCHK1-positive *Bid* +/+ and *Bid* -/- cells was shown as blue and yellow dash line, respectively. (J) Quantitative analysis of the percentage of pCHK1-positive cells in late S/G2/M phase cells (high DNA content) following hydroxyurea treatments from three independent experiments. Error bar, S.E.M. *p* value is calculated by student's t-test. **, $p<0.01$. (K) Quantitative analysis of the relative mean fluorescence intensity (MFI) of pCHK1 signal in late S/G2/M phase cells (high DNA content) following hydroxyurea treatments from three independent experiments. The MFI of pCHK1 signal from *Bid* +/+ MPCs was set as 100 arbitrarily. Error bar, S.E.M. *p* value is calculated by student's t-test. *, $p<0.05$.

antibody. The above results are consistent with an association of BID with the RPA complex at stalled replication forks following replicative stress.

The BID/ATR/ATRIP/RPA association does not require DNA

To determine whether the association of BID with the RPA/ATR/ATRIP complex requires DNA, Qiong Shi isolated nuclear extracts from HU-treated *Bid* +/+ and *Bid* -/- MPCs and incubated the extracts with DNAase. There is no change in the association of Bid with ATR or RPA70 following DNAase treatment (Figure 3-8 D), indicating that the association of Bid with RPA/ATR/ATRIP is not dependent on intact DNA.

BID is found at nuclear foci with RPA following HU

The above results implicate a role for BID at the site of DNA damage following replicative stress, at stalled replication forks. To determine whether BID is present at these structures following DNA damage, Clinton Bertram synchronized *Bid* -/- MEFs stably expressing FlagHA-tagged BID (FHA/BID MEFs) in G1 by incubation in reduced serum (0.1% FBS) medium for 24 h, then released the cells into complete medium (10% FBS; Figure 3-8 E). The population of S-phase cells was enriched 17 h after release (Figure 3-8 E), whereupon cells were left untreated or treated with 1 mM HU for 1 h. Immunofluorescence using antibodies to HA and RPA32 revealed the presence of Bid and RPA32 in nuclear foci in synchronized

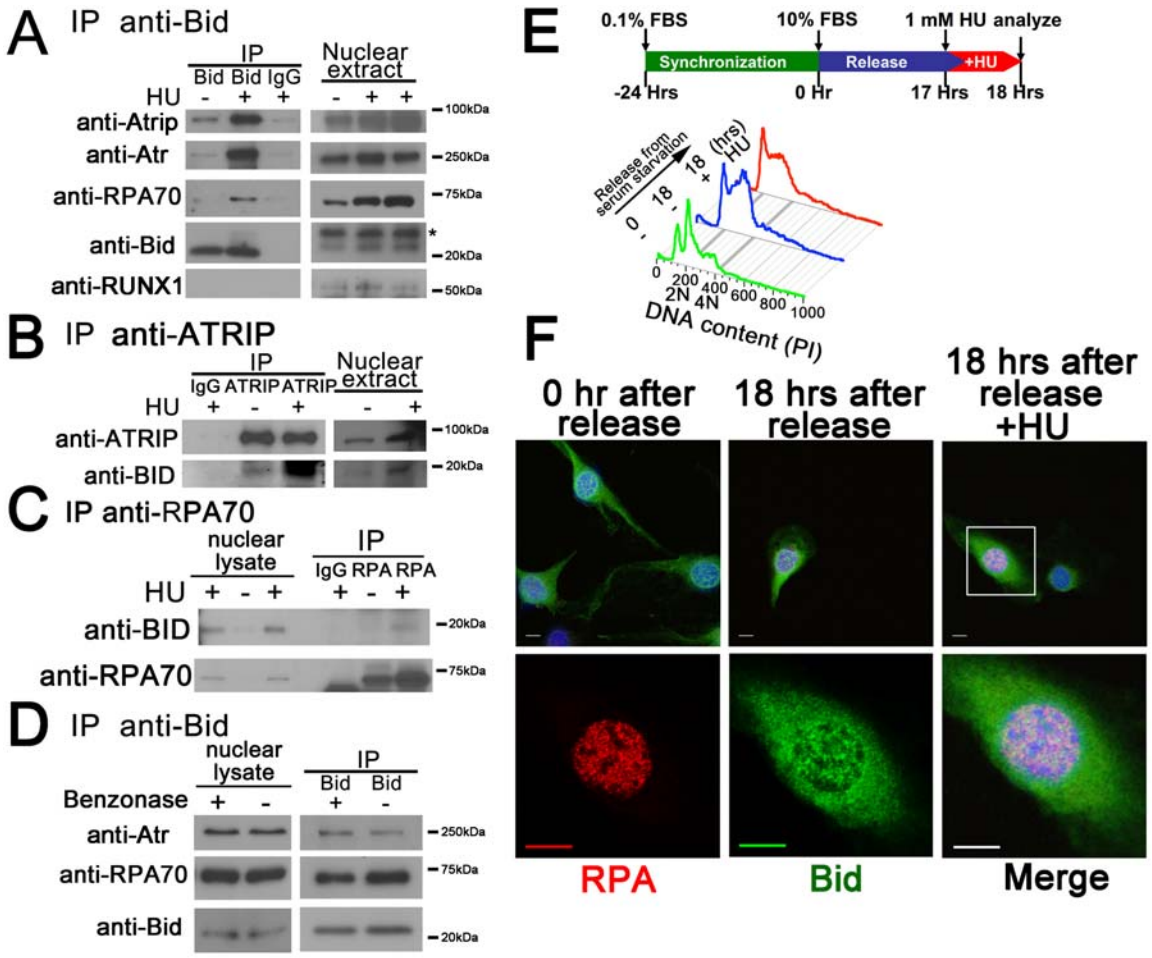

Figure 3-8. BID associates and co-localizes with ATR/ATRIP/RPA complex following replicative stress. (A) *Bid* +/+ and *Bid* -/- MPCs were treated with 10 mM HU for 2 h. BID was immunoprecipitated from nuclear extracts using biotin-conjugated anti-BID antibody and streptavidin–agarose beads. Samples were analyzed using SDS-PAGE followed by immunoblotting with the indicated antibodies. The asterisk (*) indicates a crossreacting band. Transcription factor RUNX1 was used as a negative control. (B) U2OS cells were treated with 10 mM HU for 2 h. Cells were harvested, and ATRIP was immunoprecipitated from nuclear extracts using anti-ATRIP (401) antibody. Immunoprecipitates were analyzed using SDS-PAGE followed by immunoblotting with anti-BID and anti-ATRIP antibodies. (C) U2OS cells were treated with 10 mM HU for 2 h. Cells were harvested, and RPA was immunoprecipitated from nuclear extracts using anti-RPA70 antibody. Immunoprecipitates were resolved by SDS-PAGE followed by immunoblotting with anti-BID and anti-RPA70 antibodies. (D) The interaction between Bid and ATR complex is independent of DNA. *Bid* +/+ MPCs were treated with 10 mM HU for 2 h. Then, the nuclear fraction was purified and incubated with 250U Benzonase Nuclease (Novagen). Then, Bid was immunoprecipitated from nuclear extracts using biotin-conjugated anti-BID antibody and streptavidin-agarose beads. Samples were analyzed using SDS-PAGE followed by immunoblotting with the indicated antibodies. (E) *Bid* -/- MEFs harboring HA-tagged BID were

synchronized in low serum medium (0.1% FBS-DMEM) for 24 h. Following synchronization, cells were released into complete medium (10% FBS–DMEM). At 17 h after release, cells were left untreated (18 h serum) or treated for 1 h with 1 mM HU (18 h serum plus HU). Then, cells were fixed and stained for anti-HA and anti-RPA32 antibodies. Representative images in (F) were captured by a Zeiss LSM 510 inverted confocal microscopy. Scale bars represent 10 μm. The experiments in (A)-(D) in this figure are performed and finished by Qiong Shi. The experiments in (E)-(F) in this figure are designed and finished by Clinton Bertram.

FHA/BID cells treated with HU, but not in untreated cells, or serum-starved cells (Figure 3-8 F). Bid is thus present in the region of stalled replication forks following HU treatment.

BID helix 4 associates with ATRIP

To determine the domain of BID that associates with ATRIP, various BID mutants were transiently overexpressed in 293T cells with HA-tagged ATRIP (Figure 3-9 A). Cells that were untreated or treated with HU were harvested, and BID was immunoprecipitated from total cell extracts. Interestingly, BID mutants targeting the well-studied BH3 domain and phosphorylation sites still associated with ATRIP (Figure 3-9 B). Successive deletion of α-helices beginning at the C terminus of BID revealed that the BID-ATRIP association was maintained and enhanced following DNA damage even in the absence of helices 5-8, but not helix 4 (data not shown). On the basis of nuclear magnetic resonance structure of BID (Figure 3-9 C), Leu105, Leu109, Gln112, and Asn115 in helix 4 are on the outer face of the protein, providing a candidate surface to interact with other proteins.29, 30 Site-directed mutagenesis of Leu105 and Leu109 to polar cysteine residues (BID/H4A), or mutation of Gln112 and Asn115 to alanine residues (BID/H4B), severely diminished the BID-ATRIP association (Figure 3-9 A, D). Mutating residues in the loop between helices 4 and 5 by mutating Ser117 and Ser119 to alanines (loop A) or mutating Glu120, Glu121, and Asp122 to glycines (loop B) had

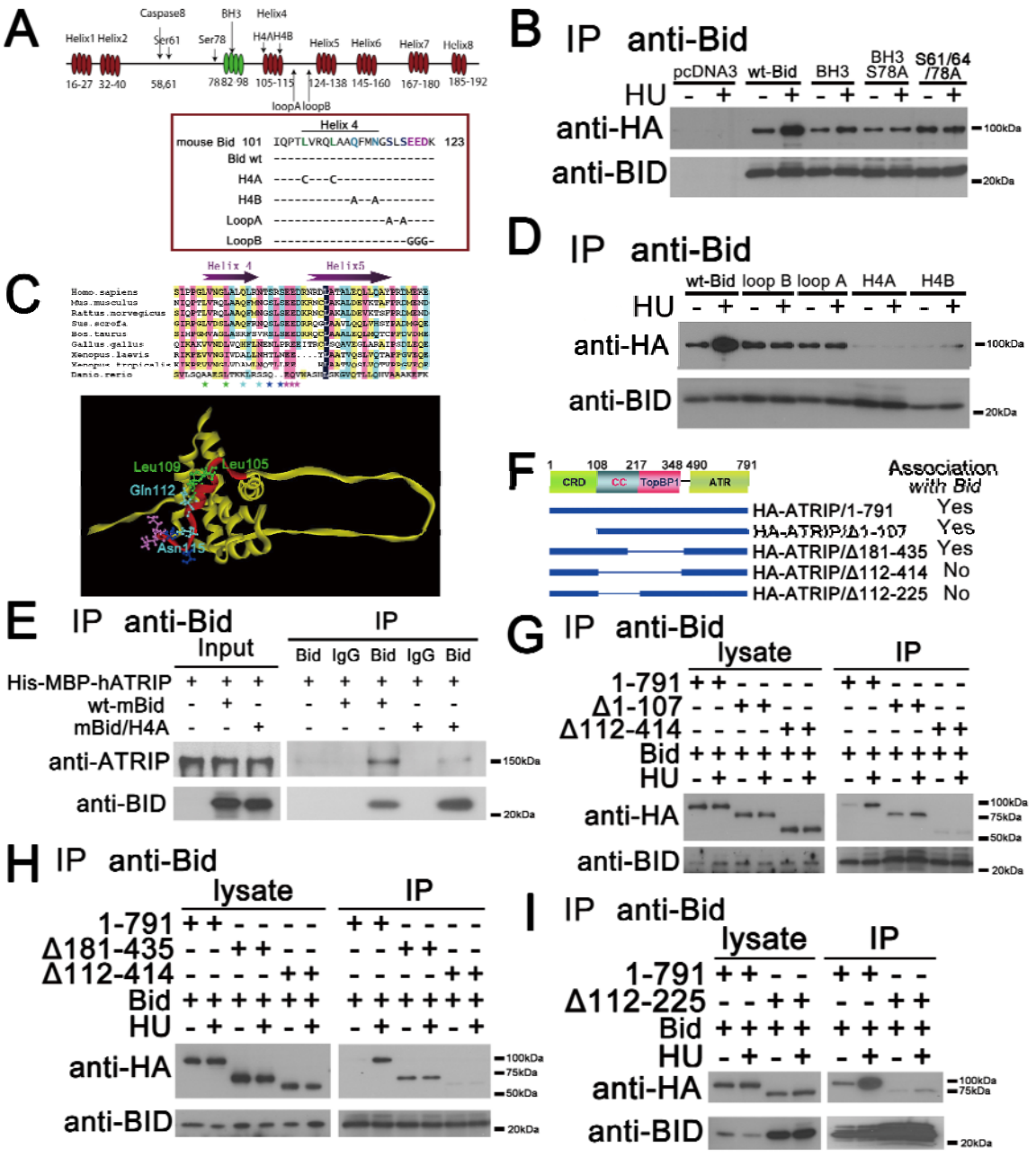

Figure 3-9. The helix 4 domain of BID interacts with the coiled-coil domain of ATRIP. (A) Schematic illustration of mouse Bid structure. (B) Cells (293T) were co-transfected with HA-ATRIP/pLPCX, and either wild type BID, or BID mutated in the BH3 domain or BID mutated in the ATM/ATR consensus phosphorylation sites. BID was immunoprecipitated from whole-cell extracts using anti-BID antibody. Samples were resolved on SDS-PAGE followed by immunoblotting with the indicated antibodies. (C) Sequence alignment of the helix 4 and helix 5 of BID among different species. Helix 4 and Helix 5 are labeled as purple arrows. The GenBank accession numbers of the sequences used here are: Homo sapiens (NM_197966), Mus musculus (NM_007544), Rattus norvegicus (NM_022684), Gallus gallus (NM_204552), Danio rerio (NM_001079826), Sus scrofa

(NM_001030535), Xenopus laevis (NM_001095594), Xenopus tropicalis (NM_001097226), and Bos taurus (NM_001075446). The alignment was performed by Clustal X. The Leu105 and Leu109 in helix 4 are labeled as green stars. The Gln112 and Asn115 in helix are labeled as cyan stars. Loop A amino acids are dark blue, Loop B amino acids are pink. The same amino acids are labeled in the nuclear magnetic resonance structure of BID. Helix 4 is denoted in red, and is on an exposed surface of BID. The BH3 domain is facing out of the page. (D) Cells (293T) were co-transfected with HA-ATRIP/pLPCX, and wild type BID or BID harboring mutations in helix 4: mutation of green stars to polar cysteine residues (H4A), or of cyan stars to alanine residues (H4B), or of dark blue stars at the end of helix 4 to alanine residues (loop A), or of pink stars in the loop region between helices 4 and 5 to glycine (loop B) BID was immunoprecipitated from whole-cell extracts and samples were analyzed as above. (E) Wild type or helix 4-mutated BID and His-MBP-ATRIP protein were purified from *E.coli*. BID (10 μg) and 100 μg His-MBP-ATRIP protein were incubated in binding buffer at room temperature for 30 minutes. BID was immunoprecipitated using anti-BID antibody, and the immunoprecipitated proteins were resolved on SDS-PAGE and immunoblotted with the indicated antibodies. (F) Schematic illustration of ATRIP structure. CRD, checkpoint recruitment domain. CC, coiled-coil domain. TopBP1, TopBP1-interacting domain. ATR, ATR-binding domain. (G-I) Wild type BID and HA-tagged full-length or various truncated ATRIP constructs were overexpressed in human 293T cells. Then the cells were treated with 10 mM HU for 2 h and BID was immunoprecipitated by anti-BID antibody. The immunoprecipitated products were detected by anti-BID and anti-HA antibodies. The experiments in this figure are performed and finished by Qiong Shi.

a less severe effect (Figure 3-9 A, D). Finally, I purified *Escherichia coli*-expressed BID and His-MBP-fused ATRIP. BID, but not BID/H4A or BID/H4B immunoprecipitated with full-length ATRIP (Figure 3-9 E). The above data indicate that BID interacts with ATRIP, and this interaction is dependent on an intact BID helix 4. Of note, BID helix 4 is highly conserved between human, mouse, and rat (Figure 3-9 C), underscoring its potential importance, and raising the possibility that the function of BID in the DNA damage signaling pathway might be a unique characteristic of BID among BCL-2 family members.

BID binds to the ATRIP coiled-coil domain

To determine the domain of ATRIP required for the association with BID, various HA-tagged ATRIP mutants (253), were tested for BID-ATRIP association in 293T cells as above (Figure 3-9 F, I). Deletion of the first 107 amino acids of ATRIP, including the CRD or amino acids 181-435 (TopBP1-binding domain) had no effect on the association of BID with ATRIP (Figure 3-9 G). Deletion of amino acids 112-414 significantly decreased the BID-ATRIP association (Figure 3-9 G, H). Although the deletion of ATRIP amino acids 112-225 resulted in decreased stability of the protein (253), the association of ATRIPΔ112-225 with BID is decreased. As the BID-ATRIP association was preserved in deletions involving the TopBP1 domain, but not in deletions involving amino acids 112-225, the above data are most consistent with an association of BID with the ATRIP coiled-coil

domain. Cells harboring ATRIP/Δ112-225 mutant showed defects in CHK1 phosphorylation and ATRIP nuclear foci following replicative stress (253).

BID helix 4 mutants maintain cell death activity

BID/H4A and BID/H4B maintain a comparable ability to bind to BCL-2 and MCL-1, as well as the ability to be cleaved by caspase 8 (Figure 3-10 A, C). I further tested the ability of these helix 4 mutants to induce cell death by stably introducing BID +/+ and BID/H4A and H4B into U2OS cells. siRNA KD of endogenous BID but not control KD resulted in protection from TRAIL/cycloheximide-induced cell death. Trail-induced cell death was restored by re-introduction of BID +/+ or BID/H4A and BID/H4B but not BID mutated in the BH3 domain (Figure 3-10 D). Thus, BID helix 4 mutants are able to be cleaved by caspases and to induce cell death following death receptor stimulation, providing further evidence that the structure and cell death function of BID helix 4 mutants is intact (Figure 3-10 A, D and data not shown). Furthermore, the two functions of BID, cell death and DNA damage can be structurally separated, providing additional evidence that the DNA damage and apoptotic functions of BID are distinct.

BID helix 4 mediates the ATR-directed DNA damage response

To further define the role of BID helix 4 in the ATR-directed DNA damage response, I reintroduced BID/H4A or BID/H4B into *BID* KD U2OS cells, and

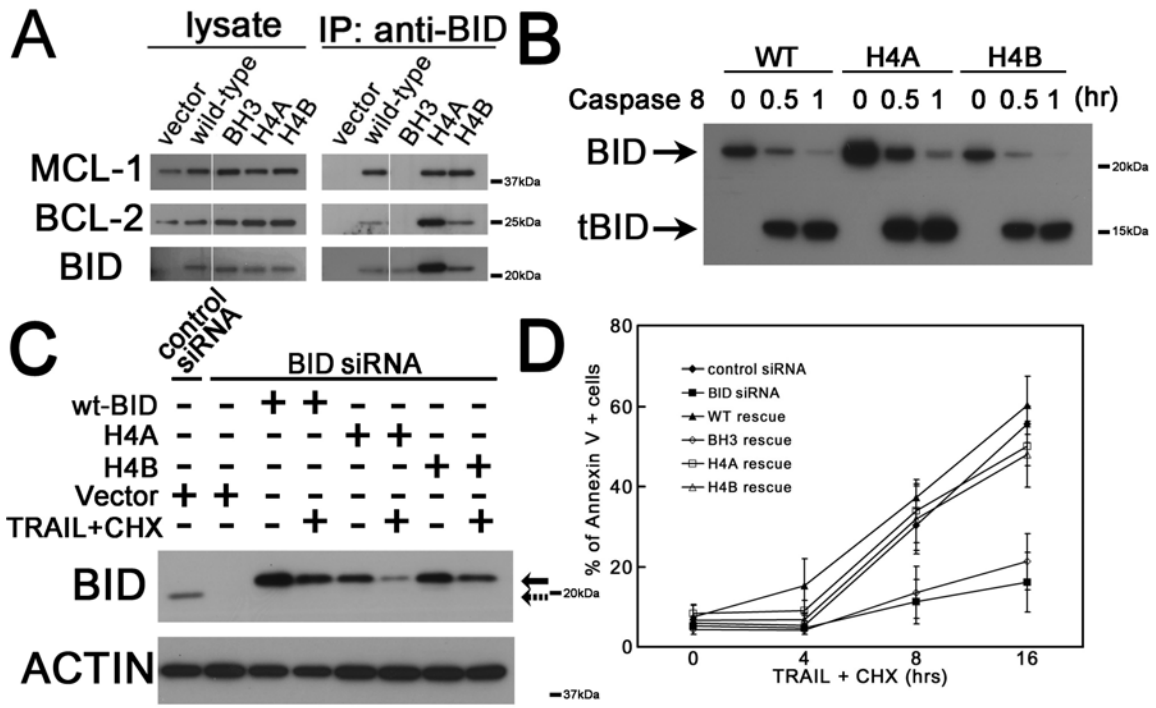

Figure 3-10. Mutations in helix 4 domain of BID do not significantly change the function of BID in the extrinsic cell death pathway. (A) Helix 4 mutated BID binds with other BCL-2 family proteins. Cells (293T) were transfected with wild type BID or helix 4-mutated BID. BID was immunoprecipitated from whole-cell extracts. Immunoprecipitates were resolved by SDS-PAGE followed by immunoblotting with anti-BID, anti-BCL-2 and anti-MCL-1 antibodies. All the samples were run in the same gel with interrupted lanes deleted. (B) Helix 4-mutated BID show similar sensitivity as wild type BID to caspase 8. Purified wild type and two helix 4 BID mutants (H4A and H4B) were cleaved by active caspase 8 (Millipore) *in vitro* for 0.5 and 1 h. The full-length and truncated BID in reaction products were analyzed by anti-BID antibody in immunoblots. (C) U2OS cells overexpressing HA-tagged wild type or helix 4-mutated BID was transfected with *BID* siRNA for 72 h. Silent mutations were introduced in the *BID* siRNA-target region so that only endogenous BID was knocked down by *BID* siRNA. Then, cells were treated with 50 ng/ml TRAIL and 5 μg/ml cycloheximide (CHX) for 4 h. Total cell lysate was analyzed by SDS-PAGE followed by immunoblotting with anti-BID antibody. Solid and dashed arrows denote endogenous BID and overexpressed BID, respectively. (D) Cells harboring helix 4-mutated BID show similar sensitivity to TRAIL/CHX treatment. U2OS cells overexpressing HA-tagged wild type or various BID mutations was transfected with *BID* siRNA for 72 h. Then, cells were treated with 50 ng/ml TRAIL and 5 μg/ml CHX over time. The apoptotic cells were detected by Annexin V-FITC Apoptosis Detection Kit (BioVision, Mountain View, CA, USA).

evaluated HU-induced accumulation of ATRIP at nuclear foci, CHK1 phosphorylation, DNA damage, and recovery and completion of DNA replication. BID helix 4 mutants failed to restore HU-induced accumulation of ATRIP at DNA damage foci (Figure 3-11 A, B) or CHK1 phosphorylation in *BID* KD U2OS cells (Figure 3-11 C). To assess DNA damage following replicative stress, I performed alkaline Comet assays following HU treatment. *BID* KD U2OS cells demonstrated increased DNA damage relative to control KD cells as measured by tail moment. Expression of BID +/+ but not BID/H4A or BID/H4B in *BID* KD U2OS cells restored DNA damage levels to those observed in control KD cells. (Figure 3-11 D). In addition, BID +/+ but not BID/H4A or BID/H4B rescued the recovery and completion of DNA replication in *BID* KD U2OS cells following HU (Figure 3-11 E, F). Taken together, these results are consistent with a role for BID in ATR activation, mediated by an interaction of BID helix 4 with ATRIP.

The RPA/ATR/ATRIP association is decreased in the absence of BID

To determine whether Bid alters the association of ATR/ATRIP and RPA, Qiong Shi immunoprecipitated RPA70 or ATR from nuclear extracts of HU-treated *Bid* +/+ and *Bid* -/- MPCs. The association of ATR/ATRIP and RPA was decreased in the absence of Bid (Figure 3-12 A). My data are most consistent with a role for Bid to facilitate ATR signaling through modulating the DNA damage sensor complex.

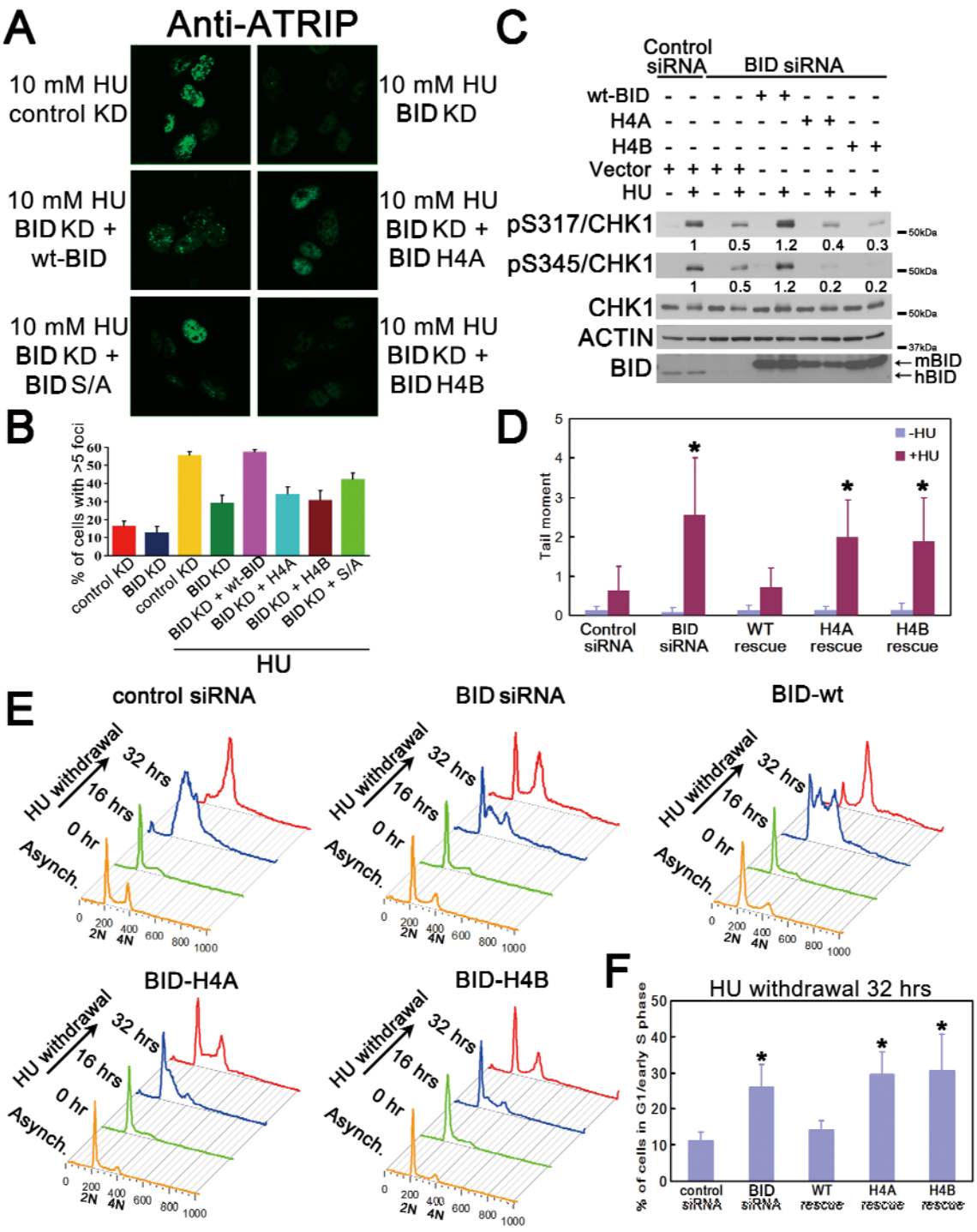

Figure 3-11. An intact BID helix 4 is required for BID's function following HU treatment. (A) U2OS cells transfected with control siRNA or *BID* siRNA, and *BID* KD cells with rescue by wt-BID, H4A, H4B or phospho-mutated (S/A) BID were treated with 10 mM HU for 5 h, fixed, and stained with anti-ATRIP antibody. Representative images of ATRIP staining were shown. (B) Quantitative analysis of ATRIP accumulation at nuclear foci following replicative stress. The percentage of cells with >5 clearly visible ATRIP nuclear foci was calculated for each cell type. More than 600 cells

were counted in three independent experiments. (C) U2OS cells were treated with control siRNA or *BID* siRNA for 72 h. Wild type mouse BID, BID/H4A, BID/H4B, or vector alone was introduced into the cells simultaneously with siRNA. Cells were treated with 10 mM HU for 2 h. Total cell lysate was resolved on SDS-PAGE and immunoblotted as above. Relative band intensity of pCHK1 signal has been measured by densitometry analysis. (D) U2OS cells overexpressing HA-tagged wild type or helix 4-mutated hBID was transfected with *BID* siRNA for 72 h. Silent mutations were introduced in the *BID* siRNA-target region so that only endogenous BID was knocked down by *BID* siRNA. Then, cells were treated with HU overnight. The untreated and treated cells were collected in ice-cold PBS and detected in alkaline comet assay. At least 60 randomly chosen comets/sample were analyzed by CometScore Program Version 1.5. **p*<0.05. (E) U2OS cells overexpressing HA-tagged wild type or helix 4-mutated hBID was transfected with *BID* siRNA for 72 h. Silent mutations were introduced in the *BID* siRNA-target region so that only endogenous BID was knocked down by *BID* siRNA. Then, cells were treated with HU for overnight and released into fresh media containing 1 μg/ml nocodazole for the indicated times. Cells were fixed and stained with propidium iodide. Live cells were gated on FSC/SSC and analyzed by flow cytometry. The quantitative analysis of the arrested G1/early S phase cells following 32 h HU withdrawal was shown in (F). **p*<0.05. (F) The quantitative analysis of the arrested G1/early S-phase cells following HU withdrawal in (E). Data were collected from three independent experiments. **p*<0.05.

Discussion

The BH3-only BCL-2 family members serve as sensors for cellular damage, transducing death signals to the multidomain family members at the mitochondria. These proapoptotic BH3-only proteins may function by participating in fundamental cellular processes (2,254-256) in position to sense potentially catastrophic perturbations in cell function and signal to the core apoptotic machinery. BID has been shown to be a substrate of ATM/ATR and loss of BID results in an aberrant S-phase response to DNA damage (2-5,80,257).

In this study, I demonstrate that BID functions at a remarkably proximal position in the ATR-mediated DNA damage response to replicative stress, associating with ATR, ATRIP, and RPA, in the DNA damage sensor complex. In my study, *Bid* -/- and *BID* KD cells exhibit several phenotypes consistent with limited ATR function following replicative stress: (1) *Bid* -/- cells are hypersensitive to replicative stress *in vitro*, *ex vivo* (2) and *in vivo* (Figure 3-1 B); (2) cell cycle re-entry ability is limited in *BID* KD cells following HU withdrawal (Figure 3-1 C); (3) chromatin-bound ATR and ATRIP are significantly decreased following treatment with HU (Figure 3-1 E); (4) activation of the ATR substrates CHK1 and RPA is decreased (Figure 3-4); and (5) the association of ATR/ATRIP and RPA is diminished in the absence of BID (Figure 3-12 A). The data presented above clearly place BID in the DNA damage response at the level of the sensor complex, and are consistent with a role for BID

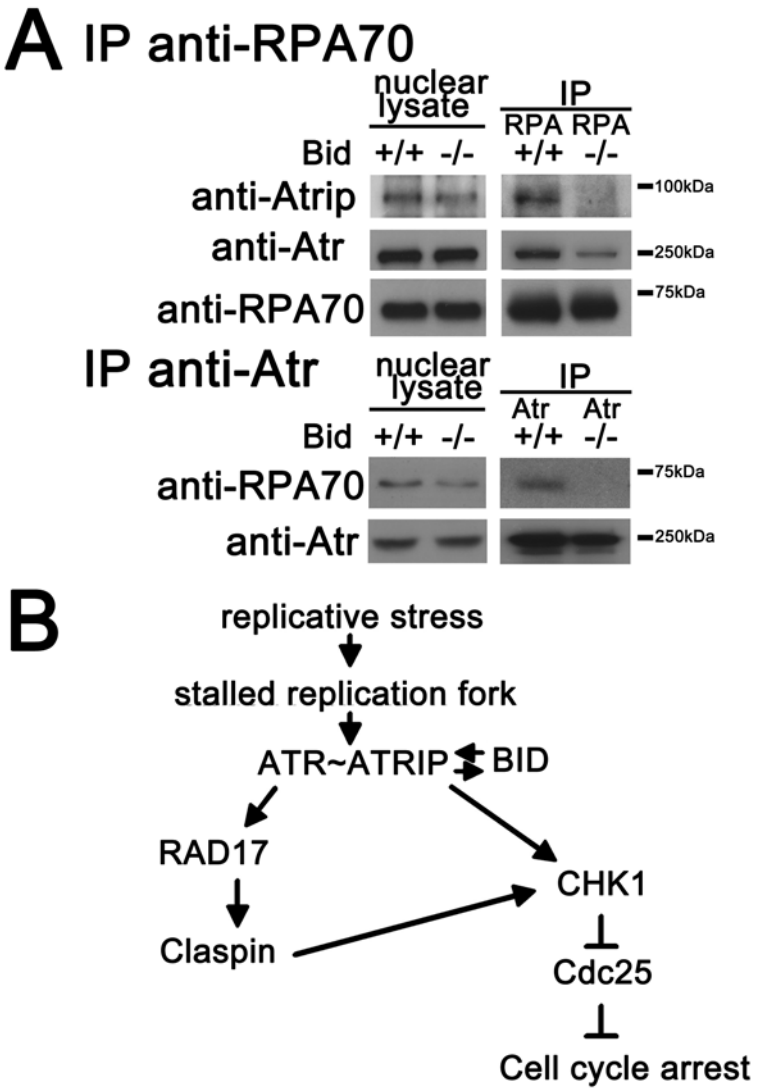

Figure 3-12. A proposed model for BID in the ATR-mediated DNA damage response to replicative stress. (A) The damage complex is unstable in *Bid* -/- MPCs following HU treatment. *Bid* +/+ and *Bid* -/- MPCs were treated with 10 mM HU for 2 h. Then, the nuclear fraction was purified and RPA or ATR was immunoprecipitated from nuclear extracts. The immunoprecipitated samples were analyzed using SDS-PAGE followed by immunoblotting with the indicated antibodies. (B) Schematic model of a proposed role for BID in the ATR-mediated DNA damage signaling pathway. BID serves as a mediator in the ATR-directed response to replicative stress at the level of ATR/ATRIP activation. BID associates with the ATR/ATRIP complex via ATRIP. Thus, BID functions at the level of the sensor complex, to facilitate and amplify ATR-directed CHK1 activation and ensure rapid and efficient checkpoint activation.

in stabilization of the ATR/ATRIP DNA damage sensor complex at nuclear foci following replicative stress, potentially by acting as a bridging protein. Alternatively, BID may have a role in the stabilization of the replication fork after DNA damage.

Cells respond to stalled replication fork progression by activating signal transduction pathways to initiate a complex set of responses, including checkpoint activation, DNA repair, and in settings of irreparable DNA damage, programmed cell death or apoptosis (1). A multi-protein complex assembles in a highly coordinated and regulated manner at the site of the DNA lesion. RPA senses the accumulation of single-stranded DNA at stalled replication forks, and has a central role in checkpoint activation through interaction with ATRIP to recruit ATR to the site of the DNA lesion. A unified model for activation of ATR/ATRIP incorporating the current data in the literature on the role of the association with RPA-ssDNA has not yet developed. ATR-ATRIP bound to RPA-coated single stranded DNA is not sufficient for checkpoint activation, but requires the ordered recruitment of additional factors, including the 9-1-1 complex and TopBP1 for downstream signaling to effect the complex response to DNA damage (124,258). This study places BID, a member of the BCL-2 family, in association with key proteins of the sensor complex. I further demonstrate that BID has a role in the stable association of ATR/ATRIP and RPA, and in an efficient ATR-mediated DNA damage response following replicative stress.

Following genotoxic stress, ATM/ATR phosphorylate Bid at Ser61 and Ser78. in

this study, I found that mutation in Ser61/64/78 attenuates the induction of the BID-ATRIP interaction following HU, but does not abrogate the interaction (Figure 3-9 B). In addition, reintroduction of S61/64/78A mutated Bid only partially rescues the defects of ATRIP nuclear foci in *BID* KD U2OS cells (Figure 3-11 A, B). Further investigation is required to clarify the detailed mechanism of BID phosphorylation in the DNA damage response.

Recently, MCL-1 has been demonstrated to be a novel mediator in the ATR-CHK1 pathway (259,260). Although the MCL-1 level is not significantly altered in *Bid* -/- and *BID* KD cells (Figure 3-3 B, C), the increased IP of BID/H4A with no corresponding increase in the amount of co-immunoprecipitated MCL-1 (Figure 3-10 A), suggests that binding of MCL-1 to BID/H4A (but not BID/H4B) might be reduced. Additional experiments will be required to evaluate the potential interaction of BID and MCL-1 in the DNA damage response.

The initial results differ from results reported by Kaufmann et al (77) with respect to the magnitude of sensitivity of *Bid* -/- cells to replicative stress (2,261). Kaufmann et al used different cell types and activation stimuli, thus the experiments are not directly comparable. Cells vary significantly in their apoptotic response to DNA damage, by both cell lineage as well as differentiation state due both to the percentage of cycling cells as well as the ‘hardwiring’ of the cell. Immature, rapidly cycling hematopoietic cells show a high propensity to undergo apoptosis. Fibroblasts are substantially more resistant. Moreover, redundancy in

the apoptotic pathway, particularly with respect to the role of a given BH3-only protein, results in variability of apoptotic outcome by cell signal and cell type. I expect that the differences observed between our group and Kaufmann et al were because of the cells and experimental parameters used. This is consistent with an effect that is cell type or context specific as I have proposed.

Distinct from cells defective in other classic mediators/effectors, such as ATRIP, RAD17, and Claspin, the CHK1 activation process is in fact initiated, albeit to a lesser extent, in *Bid* -/- cells following DNA damage treatment. Moreover, *Bid* -/- mice develop normally, whereas mice lacking the essential mediators/effectors (ATR, CHK1, RAD17) die early in embryonic development. The normal developmental program in the absence of BID may reflect the presence of redundancy or tissue/developmental stage specificity to the role of BID in ATR signaling. BID is present at high levels in hematopoietic cells, *Bid* -/- bone marrow is sensitive to *in vivo* HU, and *Bid* -/- mice develop CMML, consistent with a role for Bid in hematopoietic homeostasis and leukemogenesis. Although it is interesting to speculate that the location of BID as a participant in the DNA damage sensor complex places, it in position to have a key role in determining the fate of a cell following DNA damage, further studies will be necessary to dissect the roles of BID's apoptotic versus DNA damage function in this setting.

CHAPTER IV

BID BINDS TO REPLICATION PROTEIN A AND STIMULATES ATR FUNCTION FOLLOWING REPLICATIVE STRESS[#]

Introduction

The BCL-2 family of proteins regulates a mitochondrial-directed program of cellular destruction, used by multicellular organisms to dispose of unwanted or damaged cells. The BH3-only members such as BID, sense cellular stresses and initiate cell death by interacting with multi-domain BCL-2 members (7,254). Recent data suggest that these BH3-only members may possess additional functions in fundamental cellular processes, placing them in position to sense cellular damage (2,3,255,256).

BID has been demonstrated to play a pro-apoptotic role in multiple cellular stress-induced responses (31,32,79,86,87,97). However, a singular apoptotic function does not account for all of the current data regarding BID's function. BID is highly expressed in hematopoietic cells, and loss of BID impairs cell growth and increases sensitivity to replicative stress, consistent with a survival role to maintain genomic integrity following DNA damage treatments, especially replicative stress (2-4,261). *Bid* -/- mice spontaneously develop chronic

The research results in this chapter have been published as reference (5).

myelomonocytic leukemia with significant chromosomal abnormalities (66). Following replicative stress, BID associates with the ATR/ATRIP/RPA complex through BID helix 4 and the coiled-coil domain of ATRIP (4). BID's association with ATRIP facilitates ATR function as measured by CHK1 phosphorylation and recovery of DNA synthesis following hydroxyurea (4). Interestingly, the association between ATR/ATRIP and RPA is diminished in *Bid* -/- cells following replicative stress, suggesting that BID might function to maintain the DNA damage sensor complex containing RPA and ATR/ATRIP (4).

The assembly of the DNA damage sensor complex is a dynamic process involving the ordered recruitment of proteins to the single-stranded DNA generated by the uncoupled activity of DNA helicases and DNA polymerases (262). RPA, the primary eukaryotic single-strand DNA binding protein, serves as the initial sensor of replicative stress (159). RPA binds and coats the exposed single-stranded DNA (ssDNA), protecting it from nucleolytic damage and inhibiting formation of secondary structure (159).

The RPA is a modular protein composed of three subunits (RPA70, RPA32, and RPA14) organized into eight domains connected by flexible linkers. Motion between domains allows for optimal association with DNA and associated proteins during DNA processing (159,171,174,263,264). RPA binds ssDNA using four OB-fold domains that bind sequentially to DNA with a 5'-3' polarity (168,169). The binding affinities of each individual domain are weak, but together produce a

high binding affinity for ssDNA, K_d 10^{-9}-10^{-10} M (264). Scanning transmission electron microscopy and gel filtration studies have identified multiple conformations of RPA on DNA, further demonstrating the flexible nature of the protein (175). RPA also physically interacts with DNA processing factors through its protein-protein interaction modules, including RPA70N, RPA70AB, and RPA32C (159). RPA70N is a key protein interaction module for DNA damage response (DDR); a number of proteins involved in DDR have been shown to interact with this domain (148). In one model, RPA70N functions to recruit a series of checkpoint proteins to ssDNA, including RAD9 and ATRIP (148,159). RPA also maintains genomic stability by interaction with multiple proteins, including RAD51, the MRN complex, and the TIM/TIPIN complex (164,184,185), and prevents the generation of excessive ssDNA following replicative stress through recruitment of the annealing helicase SMARCAL1 (HARP) (186-189).

Following replicative stress, proteins of the DNA damage sensor complex are recruited to RPA-coated ssDNA. ATR/ATRIP and the 9-1-1 complexes are independently recruited to RPA-coated ssDNA (126). TopBP1, a key ATR activator, is then recruited to ssDNA by interaction with ATR/ATRIP and Rad9 to facilitate the formation of activated DNA damage sensor complex (127-129). The activated ATR then phosphorylates numerous substrates required for replicative stress-induced DNA damage response (93). ATR and its effectors maintain genomic integrity by arresting cell cycle, slowing origin firing, stabilizing replication

fork, and facilitating replication fork restart (124).

In my previous study, I demonstrated that BID interacts with the DNA damage sensor complex, including ATR-ATRIP and RPA *in vivo* and *in vitro* (4), and facilitates an efficient response to replicative stress through interaction of BID Helix 4 with ATRIP. In the present work, I demonstrate that the acidic N-terminal region of BID's Helix 5 (named RPA-ID, RPA-interacting domain) interacts with the basic cleft of RPA70N. In addition, BID stimulates recruitment of ATR-ATRIP to RPA-coated ssDNA. Interestingly, association of RPA and PCNA with chromatin is not maintained in the absence of BID. I further demonstrate that the BID-RPA interaction is important for normal ATR function following replicative stress.

Results

BID interacts with the N-terminal domain of RPA70

My previous study demonstrated that BID facilitates an efficient DNA damage response to replicative stress. I further demonstrated that the association of ATRIP and RPA with chromatin is diminished in the absence of BID (4). As RPA plays a key function to sense ssDNA and to recruit the proteins involved in checkpoint response and DNA repair, I asked whether BID might interact with the DNA damage response machinery through association with RPA.

To evaluate the ability of BID to interact with the RPA, the protein was expressed

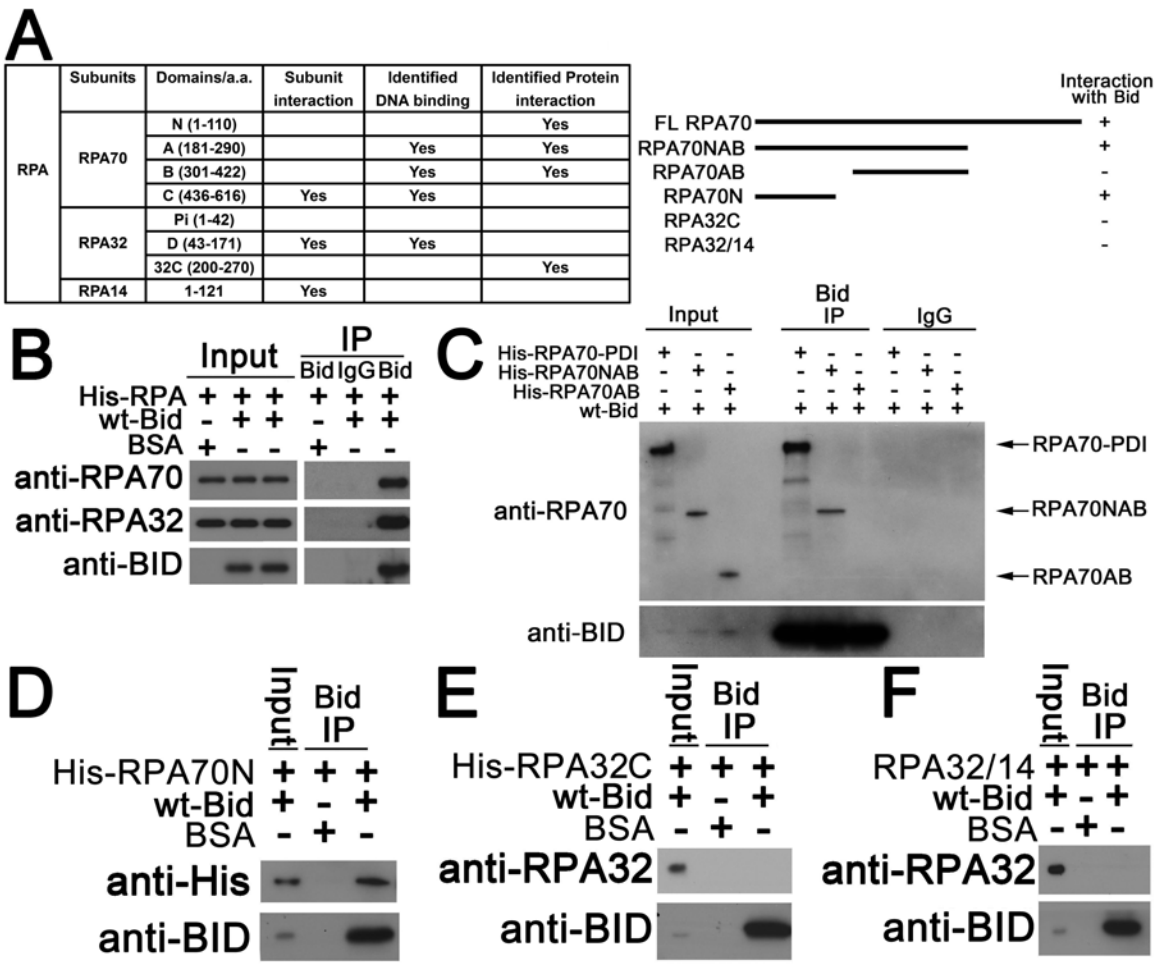

Figure 4-1. BID interacts with the N terminal domain of RPA70 *in vitro*. (A) Schematic diagram of the functional domains of RPA. The interactions between BID and various RPA domains are summarized. (B) BID interacts with RPA. Purified recombinant mouse BID and His-tagged RPA were incubated in binding buffer at room temperature for 30 minutes. BID was immunoprecipitated using anti-BID antibody, and the immunoprecipitated proteins were resolved on SDS-PAGE and immunoblotted with the indicated antibodies. (C) BID interacts with RPA70. Purified recombinant mouse BID was incubated with His-tagged RPA70-PDI fusion protein, His-tagged RAP70NAB domain, or His-tagged RPA70AB domain as in (B). BID was immunoprecipitated using anti-BID antibody, and the immunoprecipitated proteins were resolved on SDS-PAGE and immunoblotted with the indicated antibodies. (D) BID interacts with the N domain of RPA70. Purified recombinant mouse BID and His-tagged RPA70N domain (1 - 168 aa) were incubated as in (B). BID was immunoprecipitated using anti-BID antibody, and the immunoprecipitated proteins were resolved on SDS-PAGE and immunoblotted with the indicated antibodies. (E) BID does not interact with the C domain of RPA32. Purified recombinant mouse BID and His-tagged RPA32/C domain were incubated as in (B). BID was immunoprecipitated using anti-BID antibody, and the immunoprecipitated proteins were resolved on SDS-PAGE and immunoblotted with the indicated antibodies. (F) BID does not interact with RPA32/RPA14 domains. Purified recombinant mouse

BID and RPA32/14 subunits were incubated as in (B). BID was immunoprecipitated using anti-BID antibody, and the immunoprecipitated proteins were resolved on SDS-PAGE and immunoblotted with the indicated antibodies.

in *E. coli* and purified (Figure 4-1 A) (159). The purified RPA was incubated with purified recombinant mouse Bid and immunoprecipitated with anti-BID antibody. The immunoprecipitated product was resolved on SDS-PAGE and immunoblotted with the indicated antibodies. My experiments showed BID associates with RPA *in vitro* (Figure 4-1 B). As noted above, RPA70N, RPA70AB, and RPA32C are the protein interaction modules of RPA (Figure 4-1 A) (159). To identify the domain(s) that associate with BID, various RPA domain constructs were overexpressed in *E. coli* and purified (Figure 4-2), then evaluated for association with BID by immunoprecipitation. As the expression of the RPA70 subunit of RPA in *E. coli* is completely insoluble (265), I used the PDI-fusion system to express full-length RPA70 subunit and successfully purified soluble RPA70 in *E. coli*. To assess BID-RPA70 interaction, wild type BID was incubated with His-tagged RPA70-PDI fusion protein, His-tagged RPA70NAB, His-tagged RPA70AB or His-tagged RPA70N. After BID was immunoprecipitated by anti-BID antibody, the RPA70-PDI fusion, RPA70NAB and RPA70N were detected in the immunoprecipitated products, but not RPA70AB (Figure 4-1 C, D). These results suggest that BID interacts with the RPA70N domain. To evaluate whether BID may also associate with RPA32C, wild type BID was incubated with purified His-tagged RPA32C or RPA32/14. After BID was immunoprecipitated by anti-BID antibody, no significant RPA32C or RPA32/14 was found in the immunoprecipitated product (Figure 4-1 E, F), suggesting that BID does not interact with RPA32C. As controls, I established

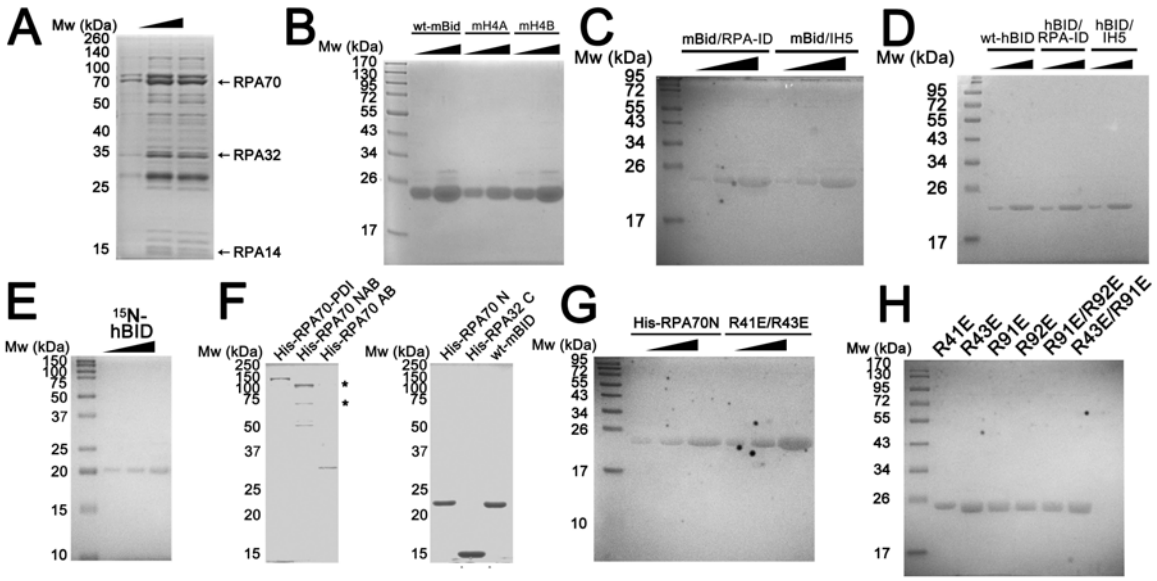

Figure 4-2. Purified recombinant protein from *E. coli* in this study. (A) His-tagged RPA. (B) Wild type mouse Bid and two Helix 4 domain Bid mutants. H4A: L105C/L109C; H4B: Q112A/N115A. (C) Mouse Bid with mutations in RPA-ID region (E120G/E121G/D122G) and in IH5 region (D132A/E133A). (D) Wild type human BID and BID mutations in RPA-ID (E120G/E121G/D122G/D126A) region and in IH5 (E132A/Q133A) region. (E) ^{15}N-labeled human BID. (F) His-tagged RPA70-PDI fusion protein, His-tagged RPA70NAB, His-tagged RPA70/AB, His-tagged RPA70N, and His-tagged RPA32/C. Asterisks denote two contaminating proteins. (G) His-tagged wild type RPA70N and RPA70N harboring R41E/R43E mutation. (H) His-tagged RPA70N harboring R41E, R43E, R91E, R92E, R91E/R92E, or R43E/R91E mutation.

that when BID was incubated with His-tagged PDI (Figure 4-3 A) or His-tagged MBP (Figure 4-3 B), followed by immunoprecipitation with anti-BID antibody, no significant His-tagged PDI (Figure 4-3 A) or His-tagged MBP (Figure 4-3 B) was detected in the immunoprecipitated product. Accordingly, I conclude that BID specifically interacts with the RPA70N domain.

The acidic N-terminal region of Helix 5 of BID interacts with the basic cleft of RPA70N

RPA70N has been demonstrated to play an important role in sensing and recruiting various DNA damage response factors to ssDNA following replicative stress. The basic cleft of RPA70N serves as a docking surface for a series of checkpoint proteins, including RAD9 and ATRIP, which interact primarily through charge-charge interactions (148). To further characterize the interaction between BID and RPA70N, ^{15}N-^{1}H HSQC (heteronuclear single quantum correlation) NMR was employed to map the interaction surfaces on the two proteins. This approach has been used extensively in the case of RPA to characterize binding interactions (148,178,236). In these experiments, one of the two binding partners is produced with enrichment in the NMR active ^{15}N isotope and ^{15}N-^{1}H-HSQC NMR spectra are acquired as the unlabeled binding partner is titrated into the solution. The assay is effective because the NMR chemical shift is extremely sensitive to electronic environment, so when a molecule that interacts with the labeled

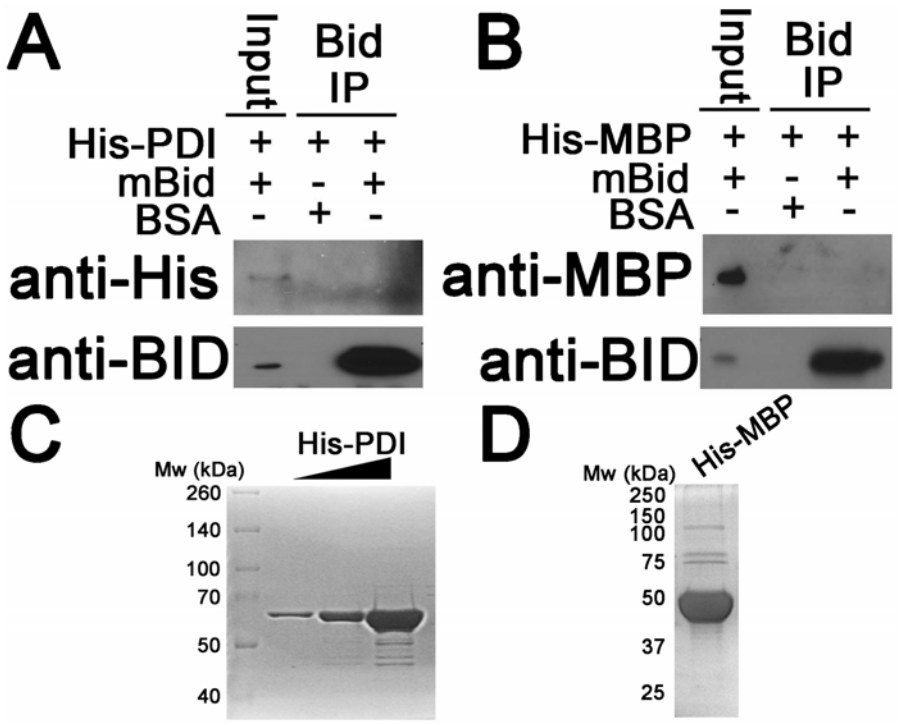

Figure 4-3. Bid does not interact with PDI or MBP. (A) Purified recombinant mouse Bid and His-tagged PDI were incubated in binding buffer at room temperature for 30 minutes. Bid was immunoprecipitated using anti-BID antibody, and the immunoprecipitated proteins were resolved on SDS-PAGE and immunoblotted with the indicated antibodies. (B) Purified recombinant mouse Bid and His-tagged MBP were incubated in binding buffer at room temperature for 30 minutes. Bid was immunoprecipitated using anti-BID antibody, and the immunoprecipitated proteins were resolved on SDS-PAGE and immunoblotted with the indicated antibodies. (C) Purified recombinant His-tagged human PDI from *E. coli*. (D) Purified recombinant His-tagged MBP from *E. coli*.

protein is added to the solution the chemical shifts of signals from residues at the binding interface are perturbed. It should be noted that additional chemical shift perturbations may arise as a result of changes in the structure of the labeled protein that are induced by the interactions with the binding partner.

Titration of ^{15}N-labled RPA70N with BID gave rise to a select set of chemical shift perturbations in ^{15}N-^{1}H HSQC NMR spectra (Figure 4-4 A), which indicated a specific binding interaction. The effects were within the fast exchange regime on the NMR time scale, which meant that chemical shift assignments could be traced from the continuous shifting of signals. The RPA70N residues most affected were mapped onto the structure of RPA70N (Figure 4-4 B), and include Arg31, Ile33, Arg43, Leu44, Arg92 and Tyr118. These residues are all located in the basic cleft of RPA70N, indicating that the binding site for BID on RPA70N is similar to that of ATRIP, MRE11, and RAD9 (148,242). A reciprocal titration of RPA70N into ^{15}N-labeled BID was also performed. The residues with the most significant chemical shift perturbations were located in Helices 4 and 5 and the loop between them, including Arg118, Ser119, Glu120, Glu121, Asp 122, Asp126, Leu127, Thr129, Ala130, and Gln133 (Figure 4-4 C, D). This region is termed the RPA interacting domain (RPA-ID) of BID.

Having used NMR to map the residues involved in the interaction between BID and RPA70N, Sivaraja Vaithiyalingam turned to computational docking using these data to guide the generation of a structural model of the complex. The

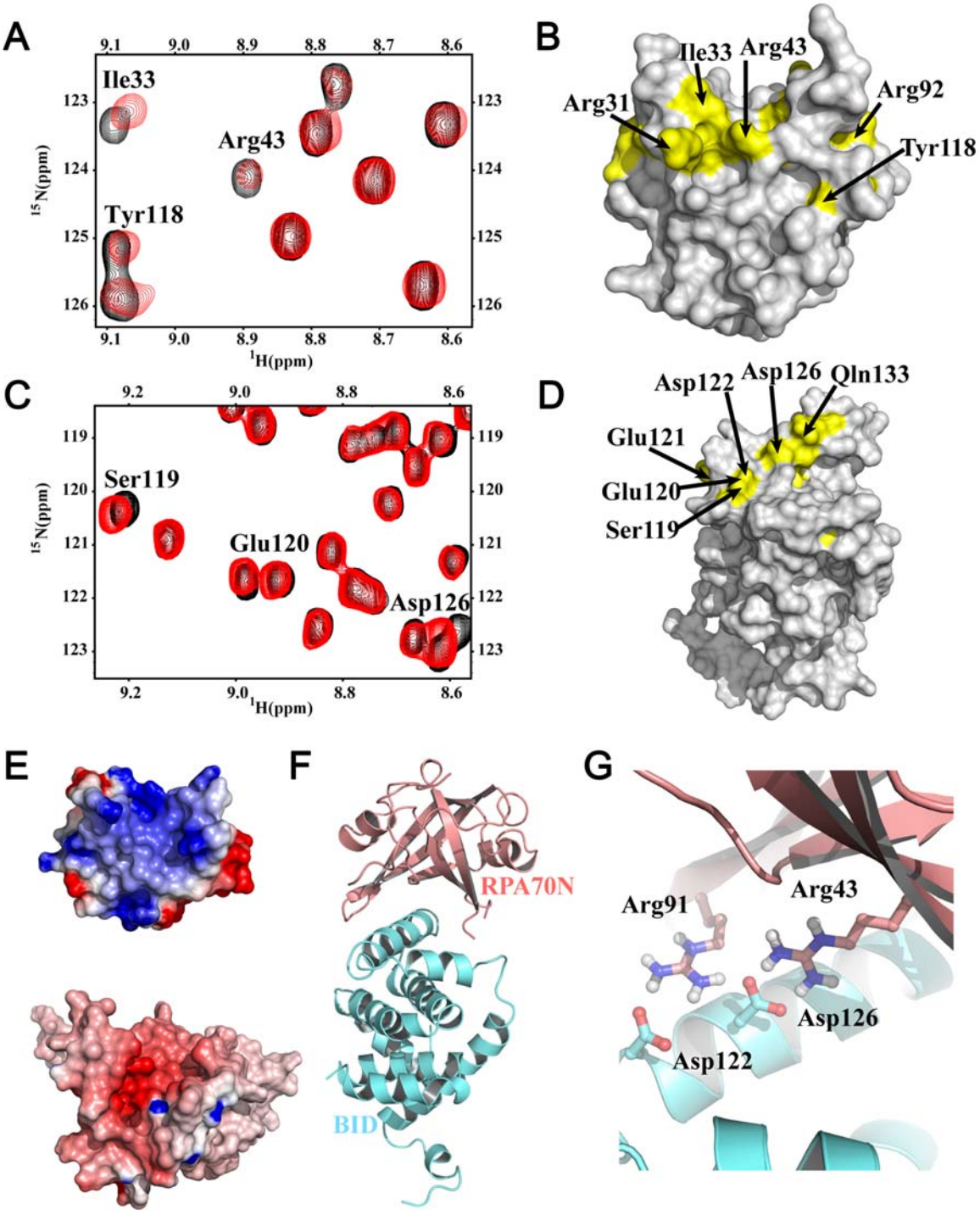

Figure 4-4. NMR analysis of the interaction of RPA70N and BID. (A) Identification of the RPA70N residues in the BID binding site. Overlaid ^{15}N-^{1}H HSQC spectra of 15N-labled RPA70N (1 - 120 aa) in the absence (black) and presence (red) of BID. (B) Map of RPA70N residues (yellow) perturbed upon the addition of BID on the structure of RPA70N. (C) Identification of the BID residues in the RPA70N interaction domain. Binding of RPA70N with BID monitored on the ^{15}N-^{1}H HSQC spectra of ^{15}N-labled BID in the absence (black) and presence (red) of RPA70N. (D) Map of BID

residues (yellow) perturbed upon the addition of RPA70N on the structure of BID. (F) Electrostatic complementarity of the RPA70N (top) and BID (bottom) binding sites. (E) NMR-based model of the complex of BID with RPA70N. Ribbon representation of PA70N and BID are colored in salman red and cyan, respectively. (G) A close up view of the model of the BID-RPA70N complex. The whole experiments and models in this figure are designed and finished by Sivaraja Vaithiyalingam.

program HADDOCK (High Ambiguity Driven biomolecular DOCKing) was used for this purpose (239,240). Interface restraints were generated for residues that exhibited significant chemical shift perturbations or broadening and also had side chains with >50% solvent accessibility. An overview of the model of the BID-RPA70N complex is shown in Figure 4-4 E-G. A comparison of the electrostatic surfaces in the binding region of the two proteins show there is a significant electrostatic complimentarity (Figure 4-4 F). For example, there are a number of specific salt bridges in the model, in particular from acidic residues in RPA-ID of BID (e.g. Glu121, Asp122, Asp126) and basic residues in the basic cleft region of RPA70N (e.g. Arg43, Arg91) (Figure 4-4G).

The structural model suggests key amino acids in the basic cleft region of RPA70N interact with acidic residues in the RPA-ID of BID. To test these predictions, a series of RPA70N and BID mutations were prepared and interactions were tested by co-immunoprecipitation experiments. Introduction of mutations in RPA70N basic residues Arg43 and Arg91 significantly impaired the BID-RPA70N interaction (Figure 4-5 A). Interestingly, although NMR chemical shift perturbations are observed for the Arg41 and Arg92 residues, mutation of these residues results in little to no effect on the BID-RPA70N interaction (Figure 4-5 A). These observations confirm the validity of the model as residues 41 and 92 do not face directly into the BID interaction interface and chemical shift perturbations can be attributed to changes induced by the binding of adjacent

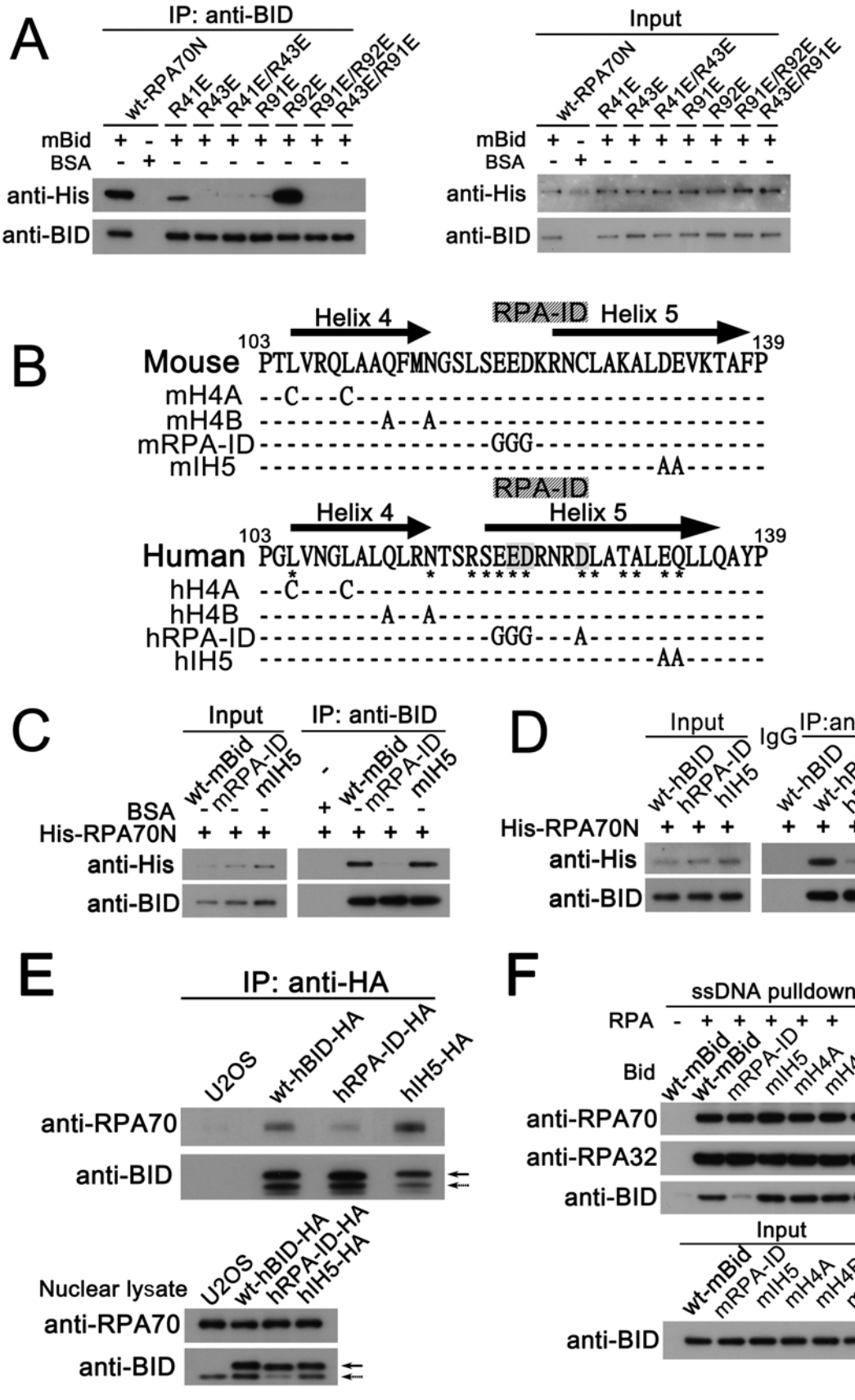
A
IP: anti-BID
Input
wt-RPA70N
R41E
R43E
R41E/R43E
R91E
R92E
R91E/R92E
R43E/R91E
mBid
BSA
anti-His
anti-BID
B
Helix 4
RPA-ID
Helix 5
Mouse
mH4A
mH4B
mRPA-ID
mIH5
Human
hH4A
hH4B
hRPA-ID
hIH5
C
Input
IP: anti-BID
wt-mBid
mRPA-ID
mIH5
BSA
His-RPA70N
anti-His
anti-BID
D
Input
IgG
IP:anti-BID
wt-hBID
hRPA-ID
hIH5
His-RPA70N
anti-His
anti-BID
E
IP: anti-HA
U2OS
wt-hBID-HA
hRPA-ID-HA
hIH5-HA
anti-RPA70
anti-BID
Nuclear lysate
F
ssDNA pulldown
RPA
Bid
wt-mBid
mRPA-ID
mIH5
mH4A
mH4B
mBH3
anti-RPA70
anti-RPA32
anti-BID
Input

Figure 4-5. Mutations in the RPA-ID of BID or the basic cleft region of RPA70N impair BID-RPA70N interaction. (A) BID interacts with the basic cleft of RPA70N. Purified recombinant His-tagged wild type RPA70N or RPA70N mutated at residues 41, 43, 91, 92- charged residues located around the RPA basic cleft region was incubated with BID in binding buffer at room temperature for 30 minutes. BID was immunoprecipitated using anti-BID antibody, and the immunoprecipitated proteins were resolved on SDS-PAGE and immunoblotted with the indicated antibodies. (B) Schematic diagram of the RPA-ID and IH5 mutated BID. Glu121, Asp122 and Asp126 in the RPA-ID region of BID are marked. (C) The BID RPA-ID region interacts with RPA70N. Purified recombinant His-tagged wild type RPA70N was incubated with wild type, RPA-ID or IH5 mutated mouse Bid in binding buffer at room temperature for 30 minutes. Bid was immunoprecipitated using anti-BID antibody, and the immunoprecipitated proteins were resolved on SDS-PAGE and immunoblotted with the indicated antibodies. (D) Purified recombinant His-tagged wild type RPA70N was incubated with wild type, RPA-ID or IH5 mutated human BID in binding buffer at room temperature for 30 minutes. BID was immunoprecipitated using anti-BID antibody, and the immunoprecipitated proteins were resolved on SDS-PAGE and immunoblotted with the indicated antibodies. (E) Mutation in RPA-ID region of BID impairs BID-RPA interaction in U2OS cells. U2OS cells harboring HA-tagged wild type hBID or mutated hBID in RPA-ID or IH5 region were treated with 10 mM hydroxyurea for 5 hours. Then, the expressed HA-tagged BID was immunoprecipitated from purified nuclear extracts by anti-HA antibody and RPA70 was detected in the immunoprecipitated products. The HA-tagged mutated hBID and endogenous hBID are labeled as solid and dashed arrows, respectively. (F) Biotinylated ssDNA was incubated with streptavidin beads for 30 minutes at 4^{o}C. Then, the pull-down products were incubated with His-tagged RPA in the presence of wild type or mutated mouse BID for 1 hour at 4^{o}C and the pull-down products were resolved on SDS-PAGE and immunoblotted with the indicated antibodies.

residues to BID. I note some chemical shift perturbations in BID residues were observed for residues outside of the RPA-ID, particularly in Helix 4 and Helix 5. These effects are also attributable to a secondary effect induced by the binding of RPA70N to the BID RPA-ID. To test the involvement of the RPA-ID of BID in the BID-RPA70N interaction, acidic residues in the RPA-ID of BID were mutated. As a control, acidic residues inside of Helix 5 (IH5) (Figure 4-5 B), were also tested. In the BID-RPA70N co-IP experiments, wild type BID and IH5 mutants were found to interact with RPA70N, but RPA-ID mutated human or mouse BID did not (Figure 4-5 B-D). These results further support the BID-RPA70N structural model in which the acidic RPA-ID primarily contacts the basic cleft region of RPA70N.

To investigate whether mutation in RPA-ID region of BID impairs BID-RPA interaction at the endogenous level, U2OS cells harboring HA-tagged wild type hBID or mutated hBID in RPA-ID or IH5 region were treated with hydroxyurea to induce replicative stress. Then, the expressed HA-tagged BID was immunoprecipitated from purified nuclear extracts by anti-HA antibody and RPA70 was detected in the immunoprecipitated products. RPA-ID mutated BID significantly deceased BID-RPA interaction while wild type and IH5 mutated BID show an intact BID-RPA interaction following replicative stress (Figure 4-5 E). Interestingly, the immunoprecipitation of HA-tagged nuclear BID also immunoprecipitates endogenous BID (Figure 4-5 E), suggesting that BID might form an oligomer in the nucleus.

I further evaluated the ability of wild type BID and BID mutants in the RPA-ID or the IH5 to associate with RPA bound to ssDNA. An 80-nucleotide 3'-biotinylated DNA oligomer was incubated with streptavidin agarose and then coated with His-tagged RPA. Wild type BID or BID mutated in the RPA-ID or the IH5 was incubated with the RPA-coated ssDNA and pulled down by streptavidin agarose. Wild type BID and IH5 mutated BID but not the RPA-ID mutant were found in the pull-downs (Figure 4-5 F). Additional controls were performed on mutants in other functional domains of BID (i.e. BH3 domain and Helix 4 domain) and these also do not significantly impair the BID-RPA70N interaction (Figure 4-6). The above results confirm the importance of the BID RPA-ID for the interaction of RPA70N with BID.

The RPA-ID of BID is important for normal ATR function following replicative stress

The N terminal domain of RPA70 has been demonstrated to play a crucial role in the ATR-mediated DNA damage response (125,148). Cells harboring RPA70-R41E/R43E exhibit significantly diminished ATR-mediated CHK1 phosphorylation following UV treatment (148). To test whether the BID-RPA interaction is important for normal ATR function, wild type BID or an RPA-ID mutant BID was reintroduced into *BID* KD U2OS cells. Compared with mouse Bid, the RPA-ID region of human BID harbors an additional acidic amino acid (D126),

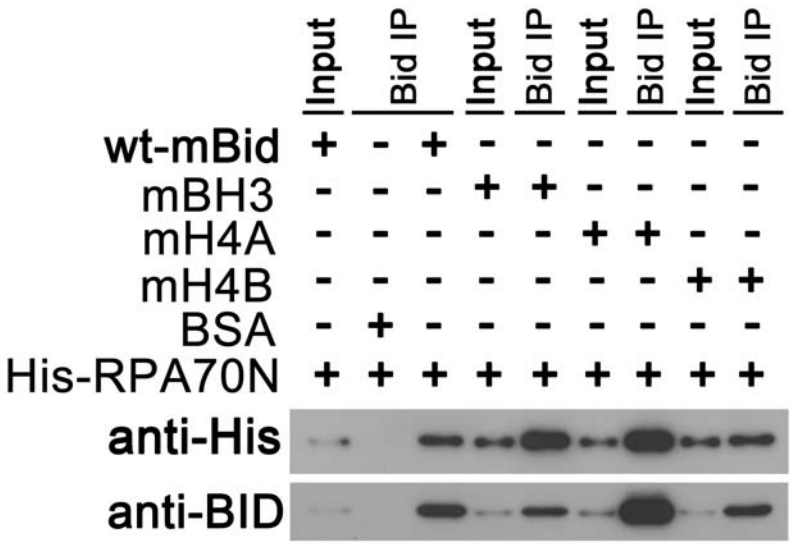

Figure 4-6. Mutations in the BH3 or Helix 4 region of BID do not impair the BID-RPA70N interaction. Purified recombinant His-tagged wild type RPA70N was incubated with wild type mouse Bid, or Bid harboring mutations in the Bid BH3 domain (I93A/G94A/D95A/E96A) or Bid Helix 4 domain (H4A: L105C/L109C; H4B: Q112A/N115A) in binding buffer at room temperature for 30 minutes. Bid was immunoprecipitated using anti-BID antibody, and the immunoprecipitated proteins were resolved on SDS-PAGE and immunoblotted with the indicated antibodies.

which displays an obvious chemical shift perturbation in NMR HSQC spectrum upon adding RPA70N. Therefore, I also mutated Asp 126 to Ala in human RPA-ID mutated BID (Figure 4-5 B).

One unique ATR function is to facilitate cell cycle re-entry after release from replicative stress (124). U2OS cells harboring wild type, RPA-ID or IH5 mutated human BID were transfected with *BID*-targeted siRNA to knock down endogenous BID. Then, cells were arrested in early S phase by 10 mM HU overnight and released into fresh medium with nocodazole to prevent cell division. *BID* KD U2OS cells demonstrated impaired DNA recovery of replication and progression through S phase (Figure 4-7 A). Expression of wild type and IH5 mutated BID but not RPA-ID mutated BID rescued the recovery and completion of DNA synthesis in *BID* KD U2OS cells (Figure 4-7 A, B), suggesting that the BID-RPA association is important for normal ATR function following replicative stress.

ATR signals to downstream effectors in the DDR through phosphorylation of key substrates. Following HU-induced replicative stress, the phosphorylation of ATR substrates (i.e. CHK1 and RPA32) was diminished in *BID* KD U2OS cells (4) (Figure 4-7 C), suggesting that ATR kinase activity is limited in the absence of BID. Reintroduction of wild type but not the RPA-ID mutated BID rescued the defects of ATR substrate phosphorylation (Figure 4-7 C), suggesting that the RPA-ID of BID is important for normal ATR activity in the cellular response to replicative stress.

Following replicative stress, ATR phosphorylates numerous substrates to

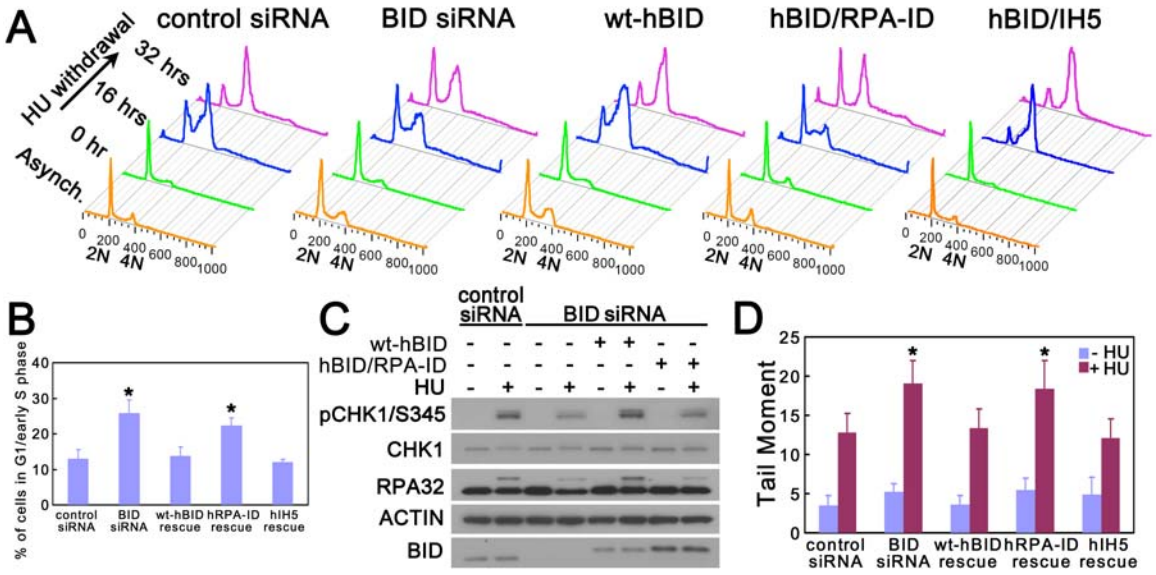

Figure 4-7. The RPA-ID of BID is important for normal ATR function following replicative stress. (A) An intact RPA-ID region of BID is required for normal recovery of DNA synthesis following hydroxyurea withdrawal. U2OS cells overexpressing HA-tagged wild type, RPA-ID or IH5 mutated human BID were transfected with *BID* siRNA for 72 hours. Then, cells were treated with 10 mM hydroxyurea overnight and released into fresh media containing 1 μg/ml nocodazole for the indicated times. Cells were fixed and stained with propidium iodide. Live cells were analyzed by flow cytometry gated on FSC/SSC. The quantitative analysis of the arrested G1/early S phase cells following 32-hour HU withdrawal was shown in (B). *, $p < 0.05$. (C) An intact RPA-ID region of BID is important for normal ATR substrate phosphorylation following hydroxyurea treatment. U2OS cells overexpressing HA-tagged wild type BID or RPA-ID mutated human BID were transfected with *BID* siRNA for 72 hours. Silent mutations were introduced into the *BID* siRNA-targeted region so that only endogenous BID was knocked down by *BID* siRNA. Then, cells were treated with 10 mM hydroxyurea for 5 hrs, protein extracts were resolved on SDS-PAGE and immunoblotted with anti-phospho-CHK1 and anti-RPA32. (D) U2OS cells overexpressing HA-tagged wild type, RPA-ID or IH5 mutated human BID was transfected with *BID* siRNA for 72 hours. Silent mutations were introduced into the *BID* siRNA-targeted region so that only endogenous BID was knocked down by *BID* siRNA. Then, cells were treated with 10 mM hydroxyurea overnight. The untreated and treated cells were collected in ice-cold PBS and detected in alkaline comet assay (Trevigen). The samples were run in Alkaline Electrophoresis Solution at 21 V for 30 minutes. At least 60 randomly-chosen comets per sample were analyzed by CometScore Program Version 1.5. *, $p < 0.05$.

maintain the stalled replication fork and genomic integrity. To detect the DNA damage level following replicative stress, U2OS cells harboring wild type or RPA-ID mutated human BID were transfected with *BID*-targeted siRNA to knock down endogenous BID. Then, cells were treated with HU overnight. In the *BID* KD U2OS cells, the DNA damage level is significantly increased following HU treatment (Figure 4-7 D). Reintroduction of wild type but not the RPA-ID mutated BID rescued the increased DNA damage level (Figure 4-7 D), suggesting that the RPA-ID of BID is important to maintain genomic integrity following replicative stress.

The Helix 4 domain interacts with the coiled-coil region of ATRIP following replicative stress, and reintroduction of Helix 4 mutated BID into *BID* KD cells cannot rescue the defects in cell cycle re-entry ability, ATR substrate phosphorylation and DNA damage level (4).These results suggest that both the BID-ATRIP and the BID-RPA interactions are important for BID's function in the ATR-mediated DNA damage signaling pathways.

RPA-ID mutated BID maintains pro-apoptotic function

To investigate whether mutations in the RPA-ID affect BID's cell death function, purified wild type BID or RPA-ID mutant was incubated with purified caspase 8, the initiator caspase responsible for cleaving BID following death receptor activation. Purified recombinant wild type BID and RPA-ID mutant show similar

sensitivity to caspase 8 *in vitro* (Figure 4-8 A). Furthermore, incubation of BID with RPA70N did not change the sensitivity of BID to caspase 8 (Figure 4-8 B) in this *in vitro* assay. In addition, truncated BID showed similar interaction with RPA70 as full-length BID (Figure 4-8 C), suggesting that cleavage of BID by caspase 8 does not impair BID-RPA interaction *in vitro*. These results are consistent with distinct separation of the RPA-ID and caspase cleavage site of BID. To determine if mutation in the RPA-ID resulted in loss of interaction with other apoptosis factors, I evaluated the ability of RPA-ID mutant to associate with BCL-2 and MCL-1 (Figure 4-8 D, E). Wild type Bid or RPA-ID mutated mouse Bid was expressed in 293T cells, and immunoprecipitated with anti-BID antibody. The immunoprecipitated product was resolved on SDS-PAGE and immunoblotted with anti-BCL-2 and anti-MCL-1. I found that the RPA-ID mutant associates with both BCL-2 and MCL-1 (Figure 4-8 D), suggesting that mutation does not disrupt the global structure of Bid, but maintains the ability to bind other BCL-2 family members. Similar results were also observed in U2OS cells stably expressing wild type or RPA-ID mutated human BID (Figure 4-8 E). In addition, TRAIL-induced cell death was restored by re-introduction of wild type and RPA-ID mutated human BID but not BH3 domain-mutated human BID (Figure 4-8 F), suggesting that RPA-ID mutated BID maintains its pro-apoptotic function. The above results are consistent with biological and biochemical separation of the functions of BID in cell death and the DNA damage response.

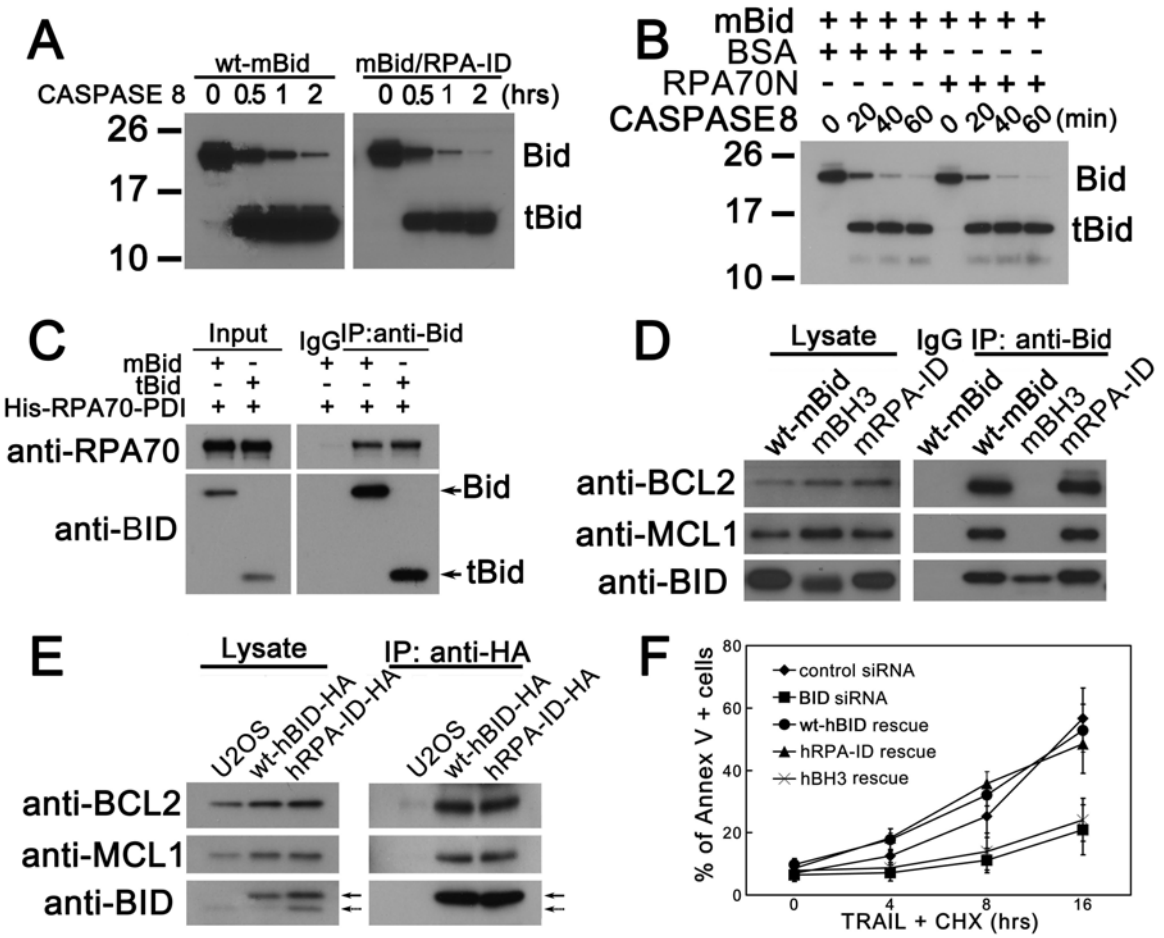

Figure 4-8. Mutation in RPA-ID region of BID does not significantly alter BID's apoptotic function in the extrinsic cell death pathway. (A) Caspase 8 cleaves RPA-ID mutated BID. Purified wild type and RPA-ID mutated mouse Bid were incubated with active caspase 8 (Millipore) *in vitro* for 0.5, 1 and 2 hours. The reaction products were resolved by SDS-PAGE and immunoblotted with anti-BID antibody. (B) Incubation with RPA does not affect Bid's sensitivity to Caspase 8 *in vitro*. Purified wild type mouse Bid was incubated with active caspase 8 in the presence of RPA or BSA for 20, 40 and 60 minutes. The reaction products were resolved by SDS-PAGE and immunoblotted with anti-BID antibody. (C) Cleaved Bid binds with RPA *in vitro*. Purified recombinant mouse Bid was first incubated with activated caspase 8 for 4 hours at 37oC. Then, the cleaved Bid was incubated with purified recombinant His-tagged RPA70-PDI fusion protein and *in vitro* co-IP assay was performed. (D) RPA-ID mutated Bid binds to other BCL-2 family proteins. 293T cells were transfected with wild type Bid or RPA-ID mutated mouse Bid for 48 hours. Then Bid was immunoprecipitated from whole-cell extracts with anti-BID antibody. The immunoprecipitated products were resolved by SDS-PAGE followed by immunoblotting with anti-BID, anti-MCL1 and anti-BCL2 antibodies. (E) U2OS cells overexpressing HA-tagged wild type or RPA-ID mutated human BID were lysed and HA-tagged BID was immunoprecipitated from whole-cell extracts with anti-HA antibody. The immunoprecipitated products were resolved by SDS-PAGE followed by immunoblotting with anti-BID, anti-MCL1 and anti-BCL2 antibodies. The HA-tagged mutated hBID

and endogenous hBID are labeled as solid and dashed arrows, respectively. (F) Cells harboring RPA-ID-mutated BID show similar sensitivity to TRAIL/CHX treatment. U2OS cells overexpressing HA-tagged wild type or RPA-ID mutated human BID were transfected with *BID* siRNA for 72 hours. Then, cells were treated with 50 ng/ml TRAIL and 5 μg/ml CHX for the indicated times. The apoptotic cells were detected using the Annexin V-FITC Apoptosis Detection Kit (BioVision).

RPA and PCNA are not maintained at the stalled replication fork in BID KD cells

Following replicative stress, the ATR-mediated DNA damage response stabilizes stalled replication forks and facilitates replication re-entry. In my previous study, *BID* KD cells demonstrated limited replication re-entry following replicative stress, and decreased association of ATR-ATRIP and RPA, suggesting the possibility that BID may be involved at the replication fork. To evaluate the role of BID on association of replication fork proteins with chromatin following replicative stress, U2OS cells transfected with control siRNA or *BID*-targeted siRNA were treated with HU. Cells were then harvested at the indicated time points, chromatin fractions were isolated and resolved on SDS-PAGE, and immunoblotted with the indicated antibodies detecting factors involved in the replication fork. Consistent with my previous result, replicative stress induced an accumulation of ATR-ATRIP on the chromatin fraction in control KD but not *BID* KD U2OS cells (Figure 4-9 A). As a key ssDNA sensor, RPA accumulated in chromatin fractions in both control KD and *BID* KD U2OS cells. However, following treatment with HU, the accumulation of RPA on chromatin was significantly diminished in *BID* KD U2OS cells, most notably at four and eight hours of HU treatment (Figure 4-9 A).

Following replicative stress, *BID* KD cells demonstrated increased DNA damage level (Figure 4-7 D). As ATR signal contributes to genomic integrity by stabilization of stalled replication fork (124), I asked whether the replication fork is

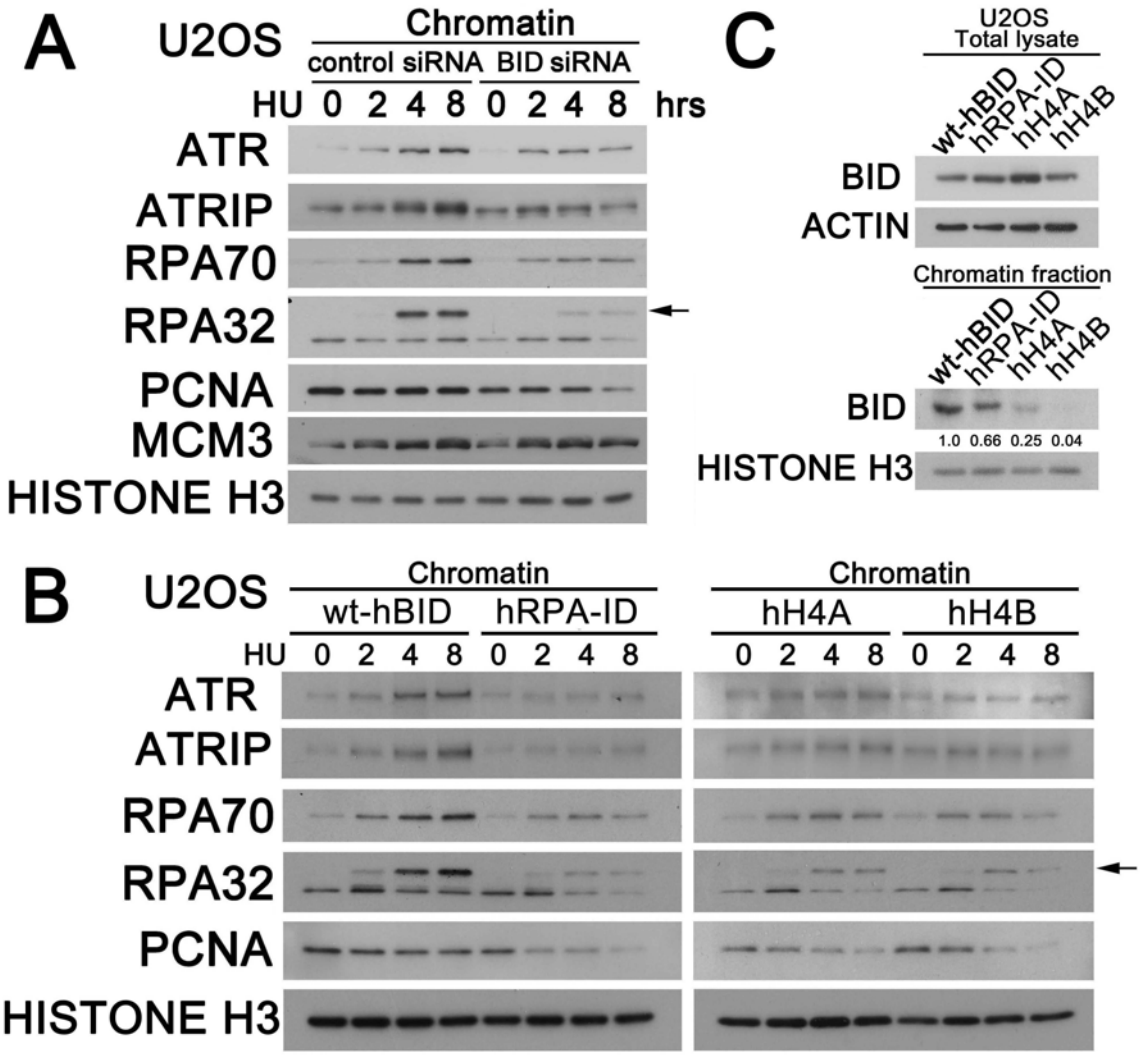

Figure 4-9. The stability of replication fork is diminished in *BID* KD cells following replicative stress. (A) U2OS cells were transfected with control siRNA or *BID* siRNA for 72 hours. Then cells were treated with 10 mM hydroxyurea over time and the chromatin fraction was purified and resolved on SDS-PAGE and immunoblotted with the indicated antibodies to various factors involved in the replication fork. (B) U2OS cells overexpressing HA-tagged wild type hBID, RPA-ID mutated hBID, or Helix 4 mutated hBID were transfected with *BID* siRNA for 72 hours. Overexpressed BID and BID mutants harbors silent mutations in the *BID* siRNA-targeted region to evade siRNA knockdown and thus only endogenous BID was knocked down by *BID* siRNA. Then, cells were treated with 10 mM hydroxyurea over time and chromatin fraction was purified, resolved on SDS-PAGE and immunoblotted with the indicated antibodies. (C) U2OS cells used in (B), overexpressing HA-tagged wild type hBID, RPA-ID mutated hBID, or Helix 4 mutated hBID harboring silent mutations to evade siRNA knockdown, were transfected with *BID* siRNA for 72 hours. Then, cells were treated with 10 mM hydroxyurea for 5 hours and the chromatin fraction was purified, resolved on SDS-PAGE and immunoblotted with anti-BID antibody.

stable in the absence of BID. Strikingly, the maintenance of PCNA, a key co-factor of DNA polymerase delta in the replication fork, was significantly reduced in the *BID* KD chromatin fraction at eight hours post HU treatment, while PCNA was well-maintained in control KD chromatin four hours post HU treatment (Figure 4-9 A). Of note, the total level of PCNA in *BID* KD cells was not significantly changed following HU treatment over time (Figure 4-10). Interestingly, chromatin-bound minichromosome maintenance complex 3 (MCM3) was maintained normally in *BID* KD cells following HU treatment, indicating that BID plays a minimal role to maintain the helicase on chromatin. This defect can be rescued by re-introduction of wild type BID but not by the RPA-ID mutated or Helix 4 mutated BID (Figure 4-9 B). In addition, the chromatin-bound RPA-ID or Helix 4 mutated BID was significantly diminished following replicative stress (Figure 4-9 C). These above results are consistent with decreased stability of the protein complex involved in the DNA damage response at stalled replication forks in the absence of BID. Furthermore, both the BID-ATRIP and BID-RPA interactions are important for BID's function to maintain the DNA damage sensor complex.

BID facilitates the RPA-ATRIP interaction in vitro in a dose-dependent manner

Following replicative stress, BID associates with ATR/ATRIP/RPA complex. The association between ATR/ATRIP and RPA is diminished in *Bid* -/- cells (4). To investigate the mechanism of BID's regulation of the ATR/ATRIP/RPA complex,

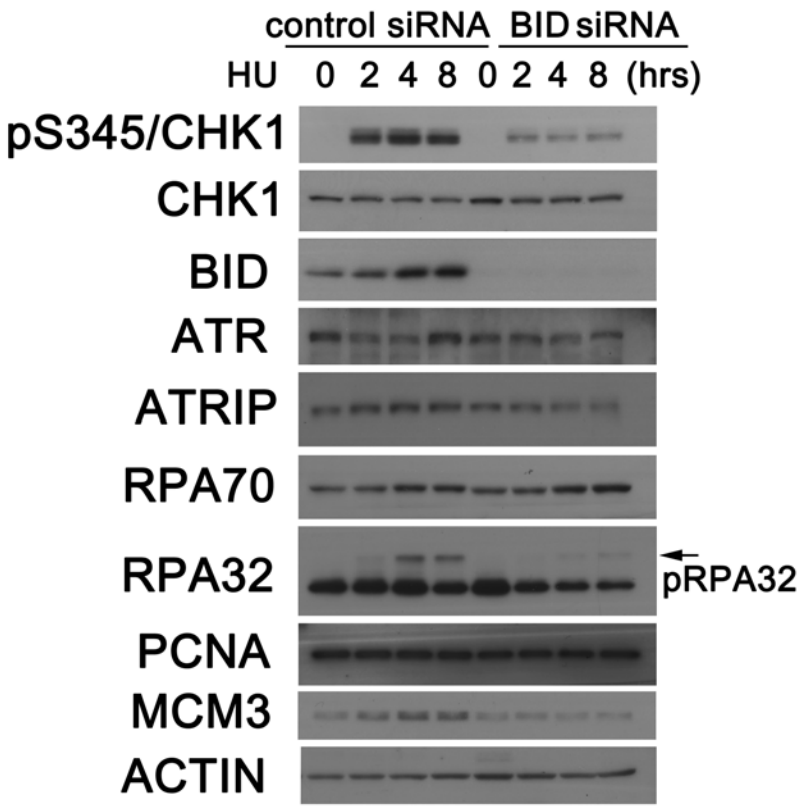

Figure 4-10. The protein levels of various factors involved in the replication fork are not significantly changed in *BID* KD cells following replicative stress. U2OS cells were transfected with control siRNA or *BID* siRNA for 72 hours. Then cells were treated with 10 mM HU for the indicated times. Then, cells were lysed, protein extracts were resolved by SDS-PAGE and immunoblotted with the indicated antibodies. Solid arrows denote shifted bands in immunoblots that match the predicted position of phosphorylated CHK1 or RPA32.

the ATRIP-RPA interaction was evaluated in the absence or presence of purified recombinant BID. Interestingly, low concentrations of BID stimulate binding of HA-ATRIP in the nuclear lysate to GST-RPA70N while high concentrations of BID compete with HA-ATRIP binding to GST-RPA70N (Figure 4-11 A). In addition, the induction of HA-ATRIP bound to GST-RPA70N was also observed in HU-treated nuclear lysate, although to a lesser extent (Figure 4-11 B). It is worthwhile to note that HU treatment dramatically increases the binding ability of HA-ATRIP to GST-RPA70N (Figure 4-11 B), suggesting that a more stable ATR/ATRIP-RPA complex is formed following replicative stress. Mutations in either the RPA-ID or the Helix 4 region of BID impair BID's ability to facilitate the RPA-ATRIP interaction in this *in vitro* system (Figure 4-11 C), which is consistent with my finding that BID facilitates formation of the DNA damage sensor complex *in vivo*, both through the BID-ATRIP interaction and the BID-RPA interaction.

Discussion

Although the BCL-2 family of proteins was first characterized as sensors and/ortransducers that function at the mitochondria to activate the intrinsic apoptosis pathway, accumulating data has implicated increasing numbers of BCL-2 family members that function in the nucleus following DNA damage. BCL-2 plays a role to suppress DNA double strand-break repair and V(D)J recombination

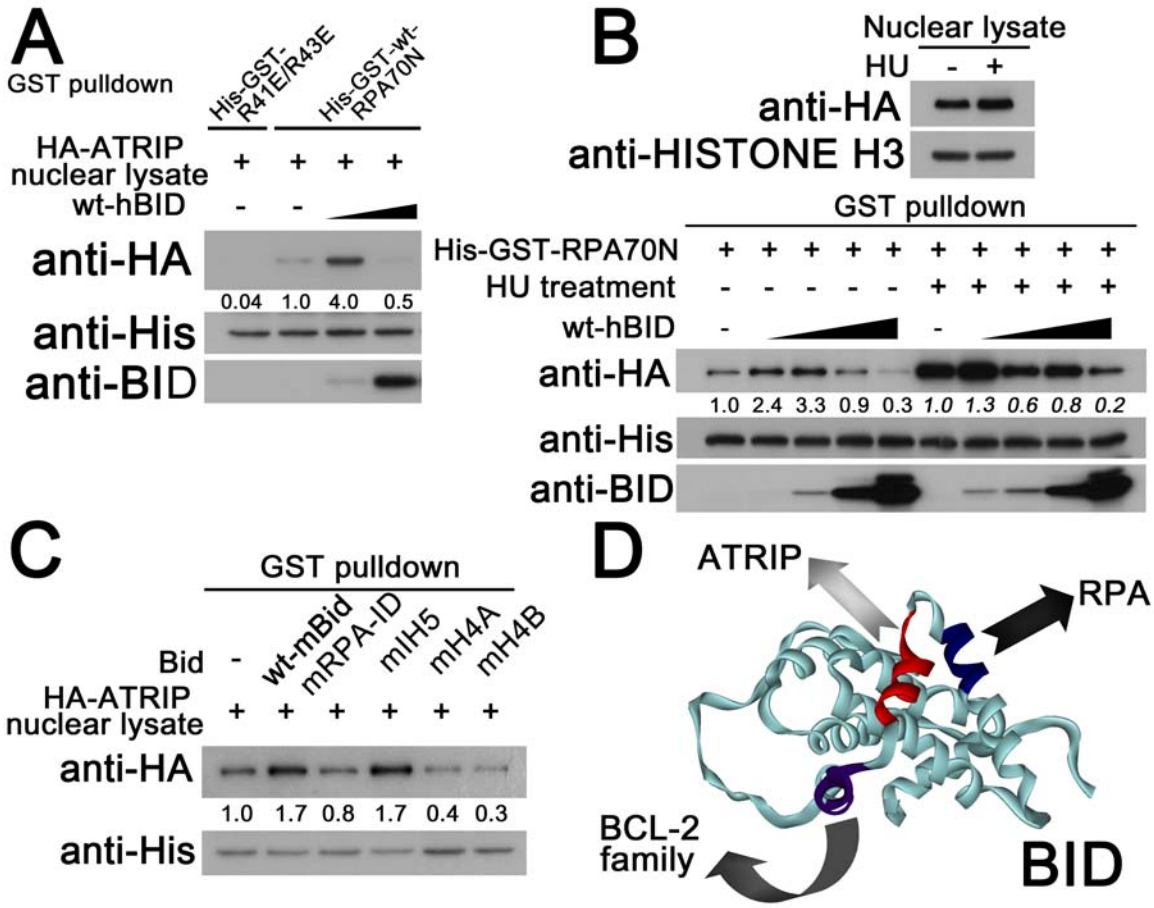

Figure 4-11. BID facilitates the RPA-ATRIP interaction *in vitro* in a dose-dependent manner. (A) 250 pmol His-GST fused wild type RPA70N or RPA70N harboring R41E/R43E mutations was bound to Glutathione-Agarose beads. Then, the nuclear fraction was purified from U2OS cells stably expressing HA-tagged ATRIP. The nuclear lysate was incubated with the RPA70N or RPA70NR41E/R43E beads in the presence of 50 or 1250 pmol purified human BID at room temperature for 1 hour. The GST-pulldown product was resolved on SDS-PAGE and immunoblotted with the indicated antibodies. (B) 250 pmol His-GST fused wild type RPA70N was bound to Glutathione-Agarose beads. Then, U2OS cells stably expressing HA-tagged ATRIP were left untreated or treated with 10 mM HU for 5 hours and the nuclear fraction was purified. The nuclear lysate was incubated with the RPA70N Glutathione-Agarose beads in the presence of 10, 50, 250, 1250 pmol purified human BID at room temperature for 1 hour. The GST-pulldown product was resolved on SDS-PAGE and immunoblotted with the indicated antibodies. (C) 250 pmol His-GST fused wild type RPA70N was bound to Glutathione-Agarose beads. Then, the nuclear fraction was purified from U2OS cells stably expressing HA-tagged ATRIP. The nuclear lysate was incubated with the RPA70N Glutathione-Agarose beads in the presence of 10 pmol purified wild type mouse Bid or Bid mutated in the RPA-ID, IH5, H4A (L105C/L109C) and H4B (Q112A/N115A) regions at room temperature for 1 hour. The GST-pulldown product was resolved on SDS-PAGE and immunoblotted with the indicated antibodies. (D) A structural view of the functional domains of BID. The BH3, Helix4 and RPA-ID domain are labeled in the solution of

human BID (PDB accession code: 2BID) to interact with BCL-2 family, ATRIP, and RPA, respectively. The different structural domains of BID mediate different functions of BID in either programmed cell death or DNA damage signaling pathways.

by interaction with Ku70 and Ku86 via its BH1 and BH4 domains (266). Following etoposide treatment, MCL-1 is found in the DNA damage complex containing NBS1 and γH2A.X to facilitate ATR-dependent CHK1 phosphorylation (259,260,267). The accumulation of nuclear MCL-1 in response to DNA damage is mediated by interaction with the IEX-1 protein (268). AVEN, a BCL-XL-interacting protein, functions as an ATM activator to inhibit G2/M progression (269). In addition to these anti-apoptotic members, I have shown that BID, a pro-apoptotic BH3-only protein, associates with the DNA damage sensor complex (4). Interestingly, following replicative stress, BID interacts with the DNA damage sensor complex (i.e. ATRIP and RPA) by its unique Helix 4 and RPA-ID regions, which are not shared by any other BCL-2 family members, supporting the notion that this function in the cellular response to replicative stress is unique to BID. It is worthwhile to notice that the dual functions of BID in programmed cell death and DNA damage signaling pathways are mediated by distinct domains in structure (Figure 4-11 D). Following death stimuli, BH3 domain plays a critical role for BID to facilitate its interaction with other BCL-2 family protein. Following genotoxic stress, the Helix4 and RPA-ID domain plays an important role for BID to facilitate its interaction with ATRIP and RPA in the DNA damage sensor complex, respectively (Figure 4-11 D).

As the direct sensor of single-stranded DNA, RPA plays a crucial role in ATR-mediated DNA damage response to replicative stress (125). RPA binds to

exposed ssDNA and recruits other checkpoint proteins to form an activated DNA damage sensor complex. It is important to note that although I find a primary interaction of BID with RPA70N, it is also possible that other regions of RPA may participate in the interaction with BID. Following replicative stress, the ATR-ATRIP complex and the RAD9-HUS1-RAD1 complex (9-1-1) are recruited independently to RPA-coated ssDNA (126,243). The function of RPA in the ATR recruitment/activation process is predominantly mediated by its RPA70N domain, and RAD9 and ATRIP compete for the same basic cleft region of RPA70N *in vitro* (148). However, both RAD9 and ATRIP are essential positive regulators for normal ATR-mediated response *in vivo* (108,148), and are required to initiate and maintain the activated DNA damage sensor complex on chromatin. Both the length of ssDNA and the structure of the damaged DNA have also been reported to be important factors to initiate the ATR-mediated checkpoint response (270-272). Together, these results suggest that a higher order structure is required for a robust checkpoint response (273). In my studies, the association between ATR-ATRIP and RPA is diminished in *Bid* -/- cells following replicative stress (4), and BID stimulates the association of ATRIP with RPA on chromatin, suggesting that BID plays a role *in vivo* to maintain the high-order structure of DNA damage sensor complex.

My studies also showed that chromatin-bound PCNA is significantly diminished in *BID* KD cells following replicative stress (Figure 4-9). Although PCNA is prone

to release from stalled replication forks in the absence of BID, the chromatin-bound MCM3 is maintained normally in *BID* KD cells (Figure 4-9). These results are consistent with the observation that although *Bid* -/- cells double more slowly, DNA replication can function, and *Bid* -/- mice are viable (4,76), with defects predominantly in hematopoietic homeostasis. My results are most consistent with a role for BID in the response to replicative stress, functioning as a novel mediator to help coordinate an efficient response to this cellular damage.

CHAPTER V

Bid PRESERVES THE MOUSE HEMATOPOIETIC SYSTEM FOLLOWING HYDROXYUREA-INDUCED REPLICATIVE STRESS^

Introduction

Hematopoietic stem cells (HSCs) are the multipotent cells responsible for maintaining the entire blood system over the lifespan of an organism. Following stress induced by trauma or toxin, hematopoietic stem cells are mobilized to expand the pool of multipotent progenitors that rapidly proliferate and repopulate the hematopoietic system. Hematopoietic homeostasis therefore requires that the production of cells and the removal of damaged or superfluous cells be carefully balanced and coordinated (200,220). Loss of stem cell regulation with increased self-renewal is a defining step in malignant transformation, while loss of self-renewal capacity results in hematopoietic failure. In both cases, the consequence for the organism is catastrophic.

The central role of HSCs for hematopoietic maintenance requires stringent protection of genomic integrity, while maintaining the ability to repopulate the hematopoietic system. HSCs are subject to genotoxic stress through both extrinsic sources such as environmental toxins and radiation, as well as DNA

^ The research results in this chapter have been submitted as reference (6).

damage arising from essential functions of the cell, including DNA damage arising during DNA replication.

Cells respond to DNA damage through activation of a highly regulated signaling program that results in activation of cell cycle checkpoints, DNA repair programs, and apoptosis in the setting of irreparable damage. ATM initiates the DNA damage response to double-strand breaks (DSB) induced by agents such as ionizing radiation (1). ATR mediates the DNA damage response (DDR) to single stranded DNA (ssDNA) generated during replicative stress. The ribonucleotide reductase inhibitor hydroxyurea (HU) stimulates the ATR-directed DDR by depleting nucleotide pools, resulting in stalled replication forks. ATR is also essential for DNA replication, in addition to regulating the DDR to replicative stress (124,125). Cells with defects in ATR pathways show increased sensitivity to DNA-damaging agents causing replicative stress such as HU (129,274,275).

Recently, two groups investigated the response of HSCs and committed progenitor cells to DNA damage induced by ionizing radiation in mouse and human systems, respectively (105,107). Murine hematopoietic stem and progenitor cells (HSPCs-lin-/c-kit+/Sca-1+/Flk2-) resist IR-induced apoptosis and preferentially utilize error-prone non-homologous end joining for DNA repair (105). Human HSPCs isolated from human cord blood upregulate p53 in response to DNA damage and are removed by apoptosis (107). In both systems, HSCs demonstrated decreased repopulating ability following IR. HSCs thus appear to

maintain longterm genomic integrity at the expense of repopulating ability.

The dynamic nature of the hematopoietic system places it in a vulnerable position with respect to genomic damage during DNA replication (210). Following hematopoietic stress, hematopoietic stem cells are mobilized, and enter the cell cycle to produce the rapidly cycling hematopoietic progenitors that replenish the hematopoietic compartment. Thus, in the setting of bone marrow stress requiring stem cell mobilization, both the HSCs as well as the committed progenitors are vulnerable to replicative stress-induced DNA damage. Indeed, defects in cell cycle checkpoint result in excessive mobilization of HSCs and depletes their self-renewal function in serial bone marrow transplantation (219). A number of key factors in the DNA damage/repair pathways play an important role to maintain genomic integrity and stem cell function (222). Atr conditional knockout mice demonstrated premature aging defects with significantly decreased LSK (Lin-Scal+ckit+) population and thymic progenitors (145). Atm -/- mice demonstrate progressive bone marrow failure due to a depletion of LSK cells as well as HSC function (123). Mice harboring a hypermorphic mutant allele of p53 display reduced proliferating HSC population in aging with limited HSC function (223). In addition, mice with deficiencies in DNA repair, including nucleotide excision repair, telomere maintenance, non-homologous end-joining, have diminished hematopoietic stem cell function with age (224,225), suggesting that the accumulation of endogenous DNA damage limits stem cell function in a cell

autonomous fashion. Besides DNA damage/repair factors, other cytoprotective properties have been proposed to protect HSCs from genotoxic stresses, including maintenance of quiescence by regulation of lipid raft clustering (226) and maintenance of a low metabolism level to prevent reactive oxygen species (227-229).

Pro-apoptotic Bid is highly expressed in the hematopoietic system and regulates myeloid homeostasis and tumorigenesis (4,66). Bid is a highly potent activator of intrinsic apoptosis following multiple cellular stresses (31,32,66,76,86,87,97,98), however, a singular apoptotic function does not account for all of the current data regarding Bid's function. *Bid* -/- myeloid progenitor cells display decreased viability in culture (2,4). Cultured *Bid* -/- activated T cells and myeloid progenitor cells (MPCs) are hypersensitive to HU but not IR treatment *in vitro* (2). *Bid* -/- bone marrow is hypersensitive to intraperitoneal injection of HU but not to IR *in vivo* (4), consistent with an impaired DDR to replicative stress. Indeed, *Bid* -/- MPCs and BID KD U2OS cells demonstrate limited ATR function following hydroxyurea treatment (4). Furthermore, Bid associates with the ATR/ATRIP/RPA complex (4), and the association between ATR/ATRIP and RPA is significantly diminished in *Bid* -/- cells following replicative stress (4), suggesting that Bid plays a role to maintain the DNA damage sensor complex. Bid is thus positioned to play a role in the DDR response to replicative stress in the hematopoietic system.

In this study, I investigated the response of wild type and *Bid* -/- HSCs and committed progenitors to replicative stress. I found that HU-stressed hematopoietic progenitor cells are preferentially depleted. HSCs maintain normal cell numbers, but display increased BrdU incorporation, consistent with mobilization to replace the MPCs eliminated by replicative stress. Under conditions of repeated replicative stress, the LSK and MPC cell populations are expanded. Interestingly, in wild type mice, this expanded HSC pool competes adequately to repopulate lethally irradiated recipient mice.

Consistent with a role for Bid in the DDR to replicative stress, *Bid* -/- hematopoietic progenitor cells demonstrate increased cell death and increased DNA damage. In addition, *Bid* -/- LSK cells demonstrate increased proliferation, consistent with increased mobilization following replicative stress-induced homeostatic recovery. *Bid* -/- bone marrow forms abnormal immature colonies and exhibits an abnormal growth potential in methylcellulose cultures. Following long-term HU treatment, the HSC-enriched LSK and myeloid progenitor cell populations are significantly diminished in *Bid* -/- mice and γH2A.X-positive cells are significantly increased in *Bid* -/- bone marrow. In addition, longterm HU-stressed *Bid* -/- bone marrow displays defective repopulating ability in competitive repopulation experiments consistent with diminished stem cell function. My studies are most consistent with Bid facilitating normal ATR function to maintain replication fork and genomic integrity in the cycling progenitor cells

following replicative stress. Proper control of replicative-stress-induced progenitor cell death thus prevents excessive mobilization of HSCs and resultant depletion of HSC function (6).

Results

MPC but not LSK cell populations are decreased in mouse bone marrow following hydroxyurea treatment

The impact of DNA damage induced by IR on HSC function has recently been evaluated in both mouse and human systems. HSCs and MPCs are also subjected to DNA damage induced by replicative stress over the lifetime of an organism. To investigate the impact of DNA damage induced by replicative stress on HSC function, I treated mice with hydoxyurea (HU) to deplete nucleotide pools, thus selectively depleting the replicating MPCs. HU treatment has been demonstrated to increase cycling of the HSC-enriched LSK population *in vivo* (231), presumably by a mobilization of HSCs to compensate for the depletion of the progenitor cell population. *Bid* -/- mice were chosen as a model to investigate the physiological function of ATR-mediated DDR in the hematopoietic system.

Bid +/+ and *Bid* -/- mice were treated with HU by intraperitoneal injection for three consecutive days and the regulation of hematopoiesis was studied. LSK (Lin-Sca1+ckit+) and MPC (Lin-Scal-ckit+) cells were evaluated by

immunostaining and flow cytometry (211,212). The lineage (Lin) cocktail consists of: CD3, B220, Ter119, Gr-1. Lin-, c-kit+, Sca-1- cells were stained for CD34 and FcγII/III to delineate subpopulations of progenitor cells. HSCs were defined as Lin-, c-kit^{high}, Sca-1^{high}. Megakaryocyte-erythroid progenitors (MEPs) were defined as Lin^{-}c-kit^{high}Sca-1^{low}CD34^{-}FcγII/III^{lo}, granulocyte-monocyte progenitors (GMPs) were defined as Lin^{-}c-kit^{high}Sca-1^{low}CD34^{+}FcγII/III^{high}, and common myeloid progenitors (CMPs) were defined as Lin^{-}c-kit^{high}Sca-1^{low}CD34^{+}FcγII/III^{lo} (209). Following HU treatment, the MPC populations (CMP, GMP, MEP) were significantly diminished in *Bid* -/- bone marrow (Figure 5-1 A, B), which is consistent with the previous finding that cultured *Bid* -/- MPCs are hypersensitive to HU (2). Interestingly, no obvious alteration was observed in the HSC-enriched LSK population (Figure 5-1 C), consistent with their quiescent state.

Apoptosis is not increased in wild type MPC and LSK cells despite increased BrdU incorporation following HU

To investigate the apoptotic response of MPCs and LSKs to replicative stress, *Bid* +/+ and *Bid* -/- mice were injected with 100 mg/kg/day HU intraperitoneally daily for three days, and the bone marrow was analyzed by flow cytometry on Day four. Using this treatment schedule, both LSK and MPC populations demonstrated only a modestly increased percentage of Annexin V-positive cells (Figure 5-2 A, B). Strikingly, *Bid* -/- bone marrow demonstrated increased

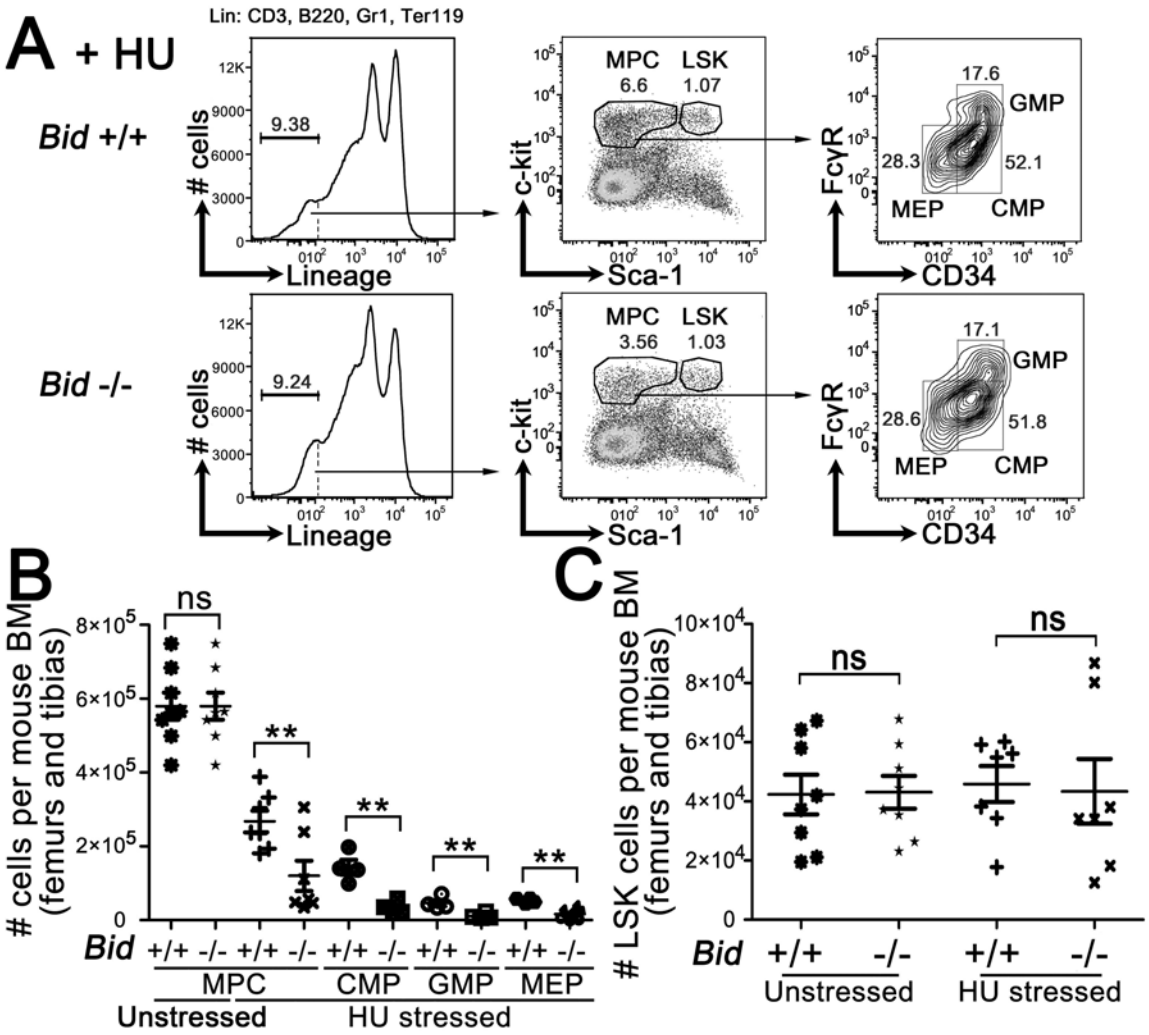

Figure 5-1. *Bid* -/- MPC but not LSK cell population is diminished following hydroxyurea treatment. (A) *Bid* +/+ and *Bid* -/- mice were treated with HU for three consecutive days and bone marrow was harvested from femurs and tibias 24 hours after the third injection. Cells were first stained with lineage marker (biotinylated CD3, B220, Gr-1 and Ter119) and then stained with c-kit, Sca1, CD34 and FcγRII/III. MPC and LSK cells were gated as Lin-Sca1-ckit+ and Lin-Scal+ckit+ population, respectively. GMP, CMP, and MEP cells were gated as CD34+FcγR+, CD34+FcγR-, and CD34-FcγR- population from MPC cells, respectively. Representative results were shown. (B) MPC, CMP, GMP and MEP population cell number was counted and quantitative analysis was shown. (C) LSK population cell number was counted and quantitative analysis was shown. **, $p < 0.01$. Error bar, SEM.

Annexin V-positive MPC and LSK cells following HU treatment (Figure 5-2 A, B).

To investigate the proliferation of MPCs and LSKs following HU, *Bid* +/+ and *Bid* -/- mice were treated with HU for three consecutive days and then the bone marrow was labeled with BrdU for 1 hour by intraperitoneal injection. Following HU, both LSK and MPC populations demonstrate significantly increased BrdU incorporation compared with untreated mice (Figure 5-2 C, D), which is consistent with mobilization of HSC and MPC cells to replenish cells depleted by HU (231). Interestingly, HU-stressed LSK but not MPC populations in *Bid* -/- bone marrow demonstrated significantly increased BrdU incorporation (Figure 5-2 C, D), consistent with increased mobilization of *Bid* -/- LSK cells to replenish the observed increased loss of *Bid* -/- MPCs to HU in *Bid* -/- mice.

This increased LSK apoptosis is consistent with the observed increase in BrdU incorporation of *Bid* -/- LSK cells. In addition, ATR function, mediated by Bid, is important to facilitate cell cycle re-entry after the release of replicative stress (124). It is also possible that apoptotic *Bid* -/- LSK cells might display delayed clearance *in vivo*.

Hydroxyurea-stressed Bid -/- bone marrow forms abnormal immature colonies in methylcellulose culture

To further evaluate the function of HU-stressed hematopoietic cells, bone marrow marrow from HU-stressed *Bid* +/+ and *Bid* -/- mice was harvested and cultured in

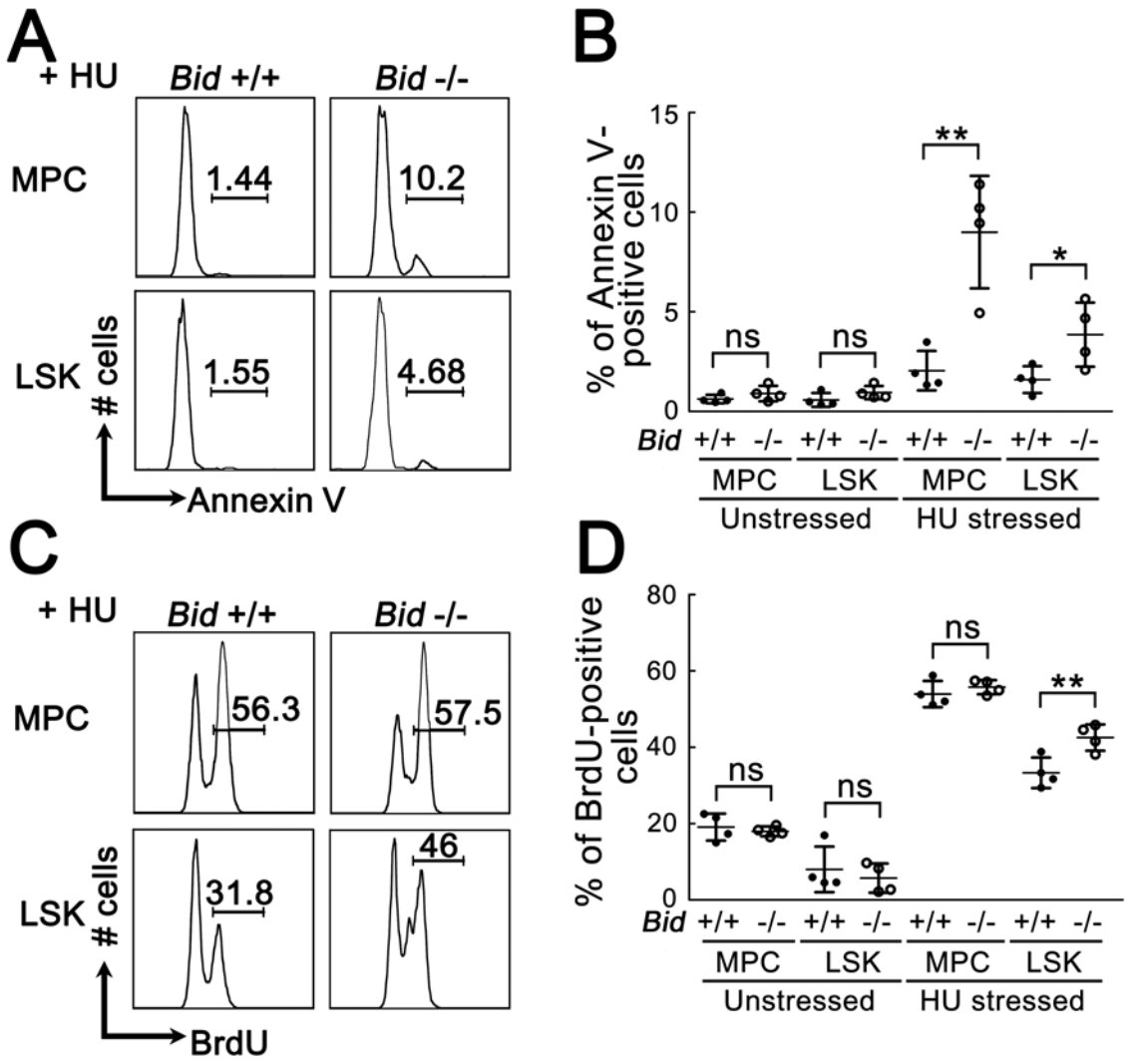

Figure 5-2. Cycling and apoptotic LSK cell population is increased in *Bid* -/- bone marrow following hydroxyurea treatment. (A) *Bid* +/+ and *Bid* -/- mice were treated with HU for three consecutive days. Bone marrow was harvested from femurs and tibias 24 hours after the third injection. Cells were stained with surface markers (CD3, B220, Gr-1, Ter-119, c-kit, Sca-1) first and apoptotic cells were detected by Annexin V-FITC Apoptosis Detection Kit. Annexin V-positive cells in various populations were analyzed by flow cytometry and representative results were shown. (B) The percentage of Annexin V-positive cells in LSK and MPC population was counted and quantitative analysis was shown. (C) *Bid* +/+ and *Bid* -/- mice were treated with HU for three consecutive days. 23 hours after the third HU injection, mice were treated with 100 µl 10 mg/ml BrdU solution for 1 hour by intraperitoneal injection. Bone marrow cells were stained with surface markers (CD3, B220, Gr-1, Ter-119, c-kit, Sca-1). After fixation and permeabilization, cells were treated with DNase for 1 hour at 37^{o}C and stained with anti-BrdU antibody for 20 minutes at room temperature. The incorporation of BrdU in various populations was analyzed by flow cytometry and representative results were shown. (D) The percentage of BrdU-positive cells in LSK and MPC population was counted and quantitative analysis was shown. *, $p < 0.05$; **, $p < 0.01$. Error bar, SEM.

methylcellulose supplemented with interleukin 3 (IL3), interleukin 6 (IL6), stem cell factor (SCF) and erythropoietin (EPO). These conditions support differentiation of hematopoietic cells through the myeloid lineage (207). Colony morphology reflects the cell types in the colony, and thus reflects the differentiative capacity of the cell of origin. GEMM colonies (colony-forming unit of granulocyte/erythrocyte/ macrophage/megakaryocyte) are formed from HSCs and CMPs; GM colonies (colony-forming unit of granulocyte/macrophage) are formed from GMPs; G and M colonies are generated from granulocyte and macrophage cells, respectively (209). Strikingly, markedly increased GEMM colonies were observed in *Bid* -/- cultures on Day 4 after the bone marrow was plated (Figure 5-3 A, B), consistent with the increased proliferation noted in *Bid* -/- HSCs and MPCs. In addition, immature colonies (GEMM and GM colonies) but not mature colonies (G and M colonies) were significantly increased in *Bid* -/- methylcellulose cultures (Figure 5-3 C, D). To evaluate the regenerative capacity of HU-stressed progenitor cells, methylcellulose cultures were serially replated at 7-day intervals. Interestingly, *Bid* -/- but not *Bid* +/+ bone marrow displayed a prolonged colony forming ability (Figure 5-3 E, F). These results suggest that *Bid* -/- immature HSC/MPC populations may possess an abnormal proliferative potential and/or decreased apoptosis *ex vivo* following HU stress. Of note, although unstressed *Bid* -/- bone marrow demonstrates increased colony forming ability, most notable in the third plating, ultimately it does not display increased regenerative capacity and is

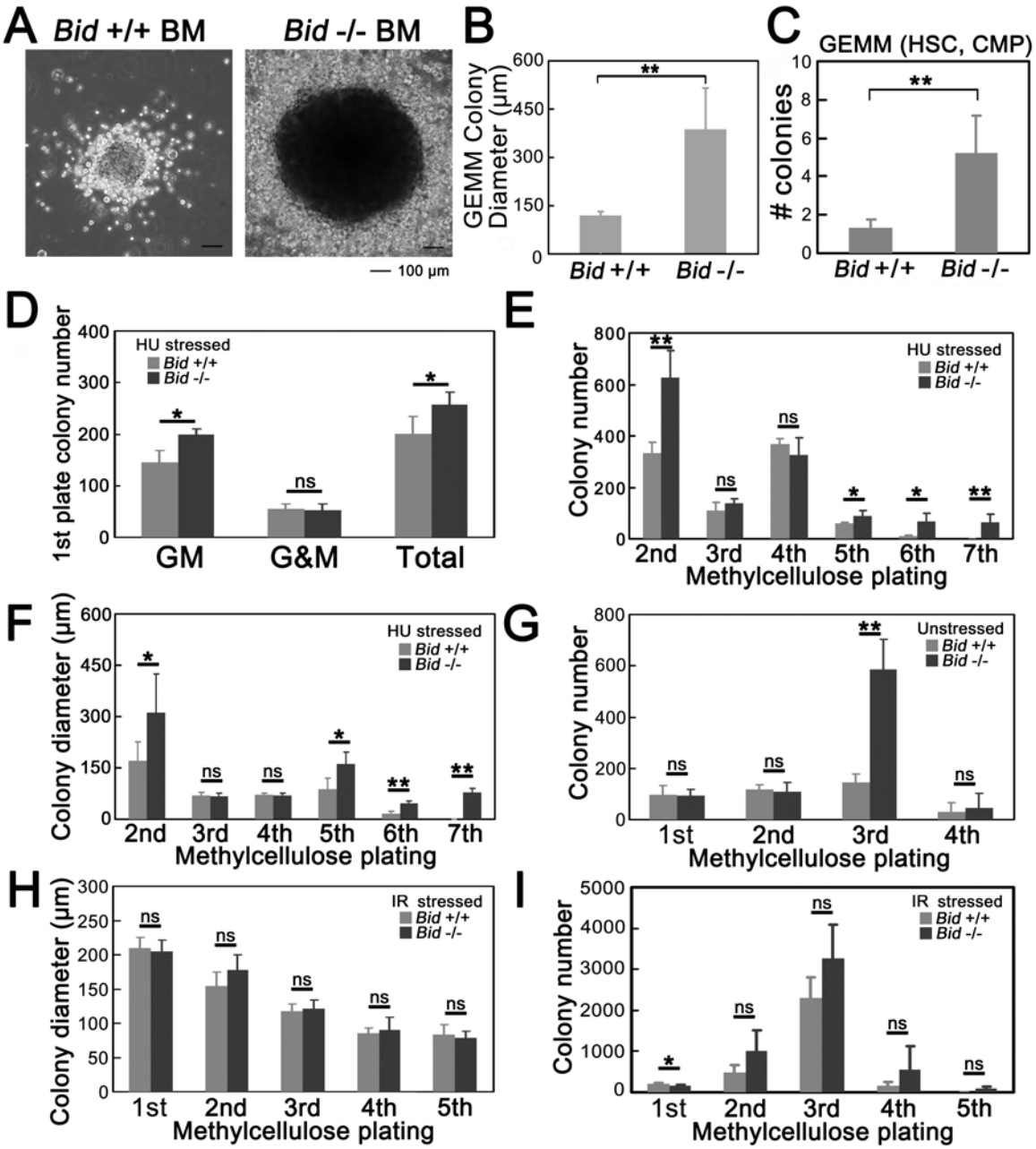

Figure 5-3. Hydroxyurea-stressed *Bid* -/- bone marrow forms abnormal immature colonies in methylcellulose culture. (A) Hydroxyurea-stressed *Bid* -/- bone marrow forms bigger GEMM colonies in methylcellulose culture. *Bid* +/+ and *Bid* -/- mice were treated with HU for three consecutive days and bone marrow was harvested from femurs and tibias 24 hours after the third injection. Bone marrow cells were cultured in methylcellulose culture and representative GEMM colonies were shown on Day 4 after plating. (B) More than 5 or all representative GEMM colonies in each plate were photographed in 1st methylcellulose plating and the colony diameter was measured. Three independent experiments were performed with n = 5 in each set. (C) GEMM colony number was counted in 1st methylcellulose plating. (D) GM, G colony and M colony, and total colony number was counted in 1st methylcellulose plating. (E) Total colony number was

counted in methylcellulose re-plating process. (F) More than 5 or all representative GM colonies in each plate were photographed in each methylcellulose re-plating process and the colony diameter was measured. Three independent experiments were performed with n = 5 in each set. (G) Unstressed *Bid* +/+ and *Bid* -/- mice were sacrificed and bone marrow cells were cultured in methylcellulose culture. Total colonies number was counted. n = 5. (H) *Bid* -/- bone marrow exhibits similar colony formation ability in methylcellulose culture following IR treatment. IR-stressed *Bid* -/- bone marrow forms normal GEMM colonies in methylcellulose culture. *Bid* +/+ and *Bid* -/- mice were irradiated with 2 Gy using a ^{137}Cs source. Mice were sacrificed and bone marrow was harvested 24 hours after irradiation. Bone marrow cells were cultured in methylcellulose culture. Two independent experiments were performed with n = 5 in each set. Various colonies were captured in methylcellulose plating process and the colony diameter was measured. GEMM colonies were captured in 1st plating (Day 7) and GM colonies were captured in re-plating. More than 5 or all representative colonies in each plate were photographed in each methylcellulose plating process and the colony diameter was measured. (I) Total colony number was counted in methylcellulose plating process. *, $p < 0.05$; **, $p < 0.01$. Error bar, SD.

exhausted after the 4th plate (Figure 5-3 G).

To determine if the increased replating capacity of *Bid* -/- bone marrow was specific to treatment with HU, *Bid* +/+ and *Bid* -/- mice were irradiated with low dose IR (2 Gy). Bone marrow from IR-stressed *Bid* +/+ and *Bid* -/- mice was harvested and cultured in methylcellulose culture. Both *Bid* +/+ and *Bid* -/- bone marrow demonstrate modestly increased replating ability following IR relative to unstressed bone marrow. Distinct from HU-stress, IR-stressed *Bid* -/- and *Bid* +/+ bone marrow showed similar GEMM colony size in the 1st methylcellulose culture (Figure 5-3 H) and similar colony formation ability in methylcellulose replating (Figure 5-3 I). Overall, the phenotype in IR-stressed *Bid* -/- bone marrow is consistent with my previous finding that Bid plays a minimum role in the ATM-directed DDR, the predominant DDR to IR activation (4).

I have previously demonstrated that *Bid* -/- cells display limited ATR function and increased sensitivity to replicative stress (2,4,5). Furthermore, bone marrow of *Bid* -/- mice displays increased sensitivity to intraperitoneal injection of HU but not to IR (4), and *Bid* -/- but not *Bid* +/+ MPC and LSK cells demonstrate increased annexin V+ cells following HU (Figure 5-2 A, B). Thus, I favor model that the formation of large GEMM colonies in *Bid* -/- methylcellulose cultures is due to increased proliferation of LSKs and MPCs. I can not exclude protection from apoptosis due to loss of Bid in this *ex vivo* culture system.

MPC and LSK cell populations increase following six months of HU treatment and Bid -/- MPC and LSK populations are decreased relative to Bid +/+ populations

Enforced mobilization of HSCs from quiescence to a cycling state results in the depletion of stem cell self-renewal function (218,219). Following HU-induced hematopoietic recovery, *Bid* -/- HSCs demonstrate increased BrdU incorporation, consistent with increased mobilization to compensate for the depletion of progenitor cell populations. To determine whether long-term HU treatment results in the depletion of HSC function in *Bid* -/- mice, *Bid* +/+ and *Bid* -/- mice were treated with HU by intraperitoneal injection for three days, and allowed to recover for seven days. This regimen was repeated for 6 months (see Methods for details) (199).

Both *Bid* +/+ and *Bid* -/- mice survived six months of HU treatment, although a gradual loss of body weight (Figure 5-4 A) and a trend towards decrease in HU sensitivity (Figure 5-4 B) were observed in *Bid* -/- mice. After six months, cell populations in the bone marrow were analyzed by flow cytometry. Both MPC and LSK cell populations were increased relative to untreated mice. Notably, both MPC and LSK cell populations were diminished in *Bid* -/- mice compared with those in *Bid* +/+ mice (Figure 5-4 A-D). Among myeloid progenitor cells, only the GMP population was significantly diminished in *Bid* -/- mice compared to the *Bid* +/+ mice (Figure 5-5 D). GMP cells are the most rapidly proliferating cells in themyeloid system (221), and thus are the most vulnerable to replicative stress. *Bid*

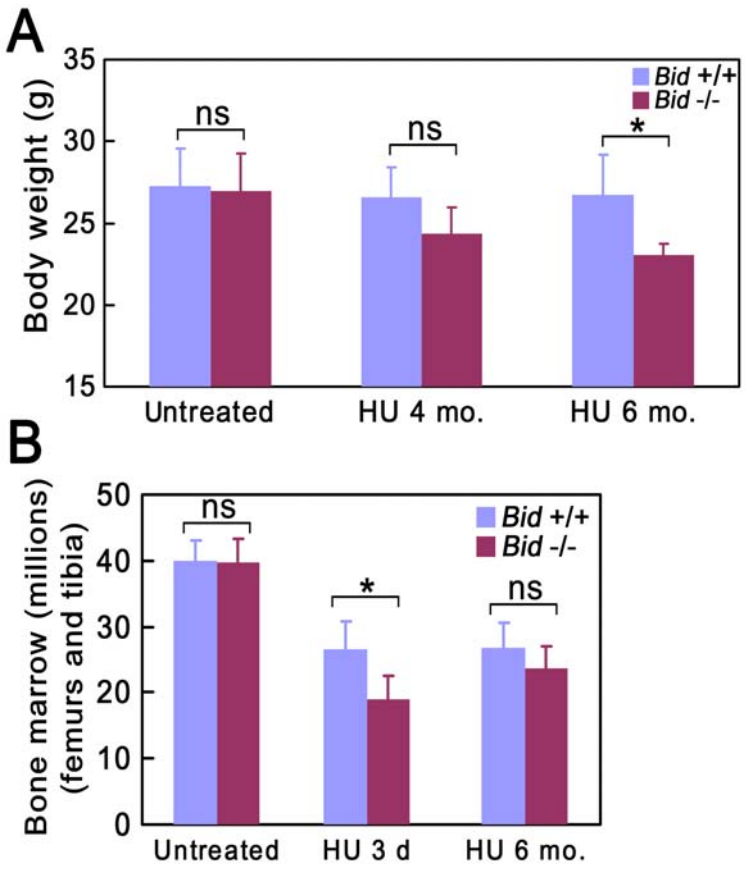

Figure 5-4. The body weight and bone marrow number in *Bid* +/+ and *Bid* -/- mice following long-term HU treatment. (A) Wild type and *Bid* -/- C57/BL6 mice (6-8 weeks old) were treated with 100 mg/kg/day hydroxyurea by intraperitoneal injection for three consecutive days. After three-consecutive-day-HU treatment, mice were released from HU treatment for 7 days and subjected to HU treatment again for three consecutive days. Mice were continuously treated with HU for 4 or 6 month and the body weight was measured. *, $p < 0.05$; n = 5. Error bar, SD. (B) Mice were sacrificed and bone marrow was harvested from femurs and tibias 24 hours after last HU injection. After erythrocytes were lysed in RBC lysis buffer, bone marrow cell number was counted by Trypan Blue. *, $p < 0.05$; Untreated, n = 5; HU 3 days, n = 15; HU 6 month, n = 10. Error bar, SD.

-/- GMP cells showed persistent defects following long-term HU treatment. It is worthwhile to note that long-term HU treatment significantly induced both LSK and MPC populations compared with untreated mice (Figure 5-5 B, C). Interestingly an expanded MPC and LSK population is also observed in unstressed aged mice (276,277). This increase may reflect compensation for decreased function following longterm replicative stress or aging.

Bid -/- bone marrow exhibits increased γH2A.X staining following six months of HU treatment

To investigate the effect of long-term HU on the hematopoietic system, bone marrow was harvested from *Bid* +/+ and *Bid* -/- mice treated for six months with HU as above and cultured in methylcellulose. Similar GEMM colony number and size were observed in *Bid* -/- and *Bid* +/+ cultures (Figure 5-6 A, B), suggesting that the excessive mobilization of the LSK population is attenuated following long-term HU treatment. In addition, similar colony formation ability was observed between *Bid* +/+ and *Bid* -/- in methylcellulose replating (Figure 5-6 B), suggesting that the progenitor cell competency was not severely impaired following long-term HU treatment.

Replicative stress has been demonstrated to induce genomic instability and accumulate DNA damage at the cellular level(124). γH2A.X is phosphorylated following DNA damage, and can be detected by immunofluorescence and flow

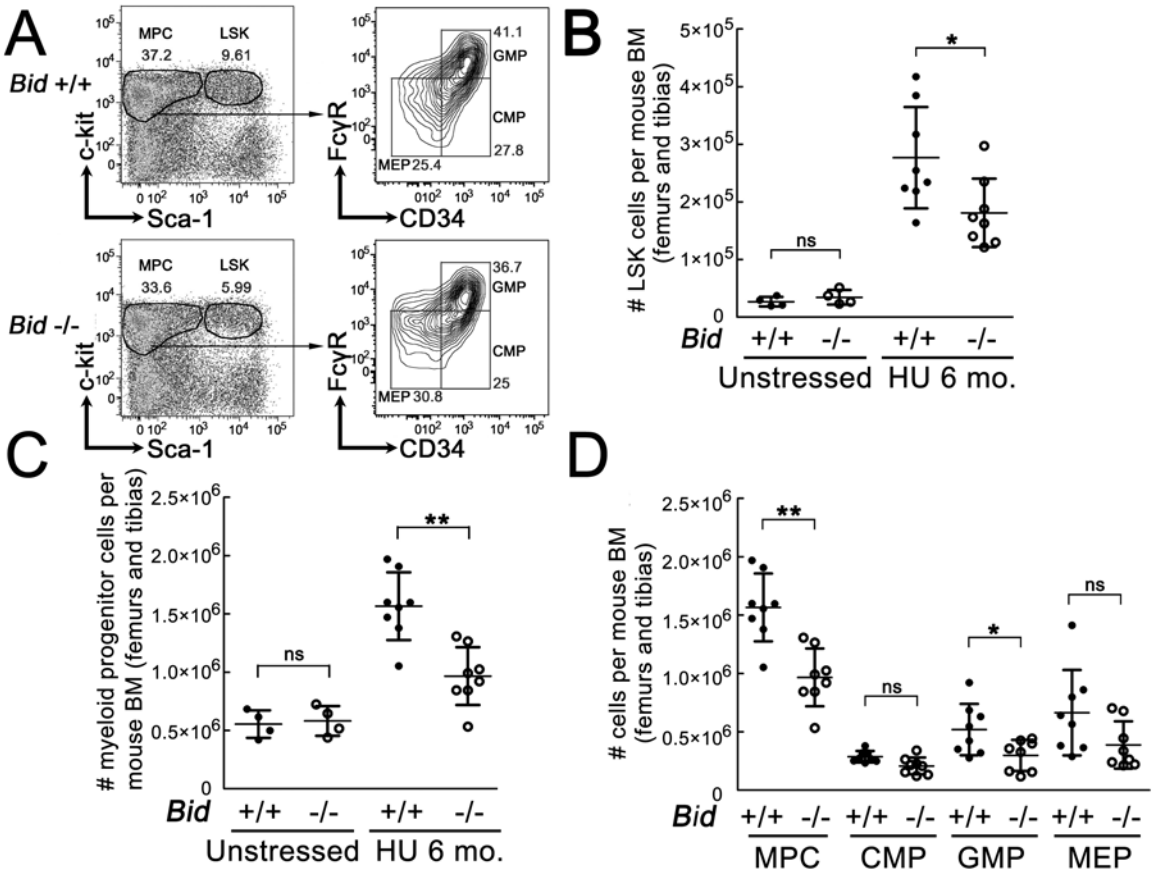

Figure 5-5. *Bid* -/- MPC and LSK cell population is diminished following long-term HU treatment. (A) *Bid* +/+ and *Bid* -/- mice were continuously treated with HU for 6 month and bone marrow was harvested from femurs and tibias 24 hours after last HU injection. Cells were first stained with lineage marker (biotinylated CD3, B220, Gr-1 and Ter119) and then stained with c-kit, Sca1, CD34 and FcγRII/III. MPC and LSK cells were gated as Lin-Sca1-ckit+ and Lin-Scal+ckit+ population, respectively. GMP, CMP, and MEP cells were gated as CD34+FcγR+, CD34+FcγR-, and CD34-FcγR- population from MPC cells, respectively. Representative results were shown. (B) LSK population cell number was counted and quantitative analysis was shown. (C) MPC population cell number was counted and quantitative analysis was shown. (D) CMP, GMP and MEP population cell number was counted and quantitative analysis was shown. *, $p < 0.05$; **, $p < 0.01$. Error bar, SEM.

cytometry (Figure 5-7). DNA damage levels were detected by γH2A.X staining following six months of HU treatment. The γH2A.X-positive cells measured by immunofluorescence were significantly increased in *Bid* -/- bone marrow (Figure 5-6 C-E), suggesting that DNA damage is accumulated in *Bid* -/- bone marrow following long-term HU treatment. To further identify the cell populations harboring γH2A.X-positive cells, *Bid* +/+ and *Bid* -/- bone marrow was stained with surface markers and γH2A.X-positive cells were detected by intra-cellular staining with anti-γH2A.X antibody by flow cytometry. Interestingly, γH2A.X-positive cells were significantly increased in *Bid* -/- MPCs but not the LSKs (Figure 5-6 F, G), suggesting that the accumulated γH2A.X-positive cells in *Bid* -/- bone marrow were generated at the progenitor cell level. Different DNA repair mechanisms have been reported between HSC and MPC following DSBs (105). My results are consistent cycling HSCs and MPCs utilizing a different mechanism to maintain the replication fork following replicative stress. Alternatively, HSCs may have a lower threshold for apoptosis or preferentially differentiate upon accumulation of DNA damage.

Stem cell function is diminished in Bid -/- bone marrow following six months of HU treatment

Given the relationship between HSC mobilization and stem cell functional depletion (218,219), I asked whether the self-renewal function of HSCs was altered in *Bid* +/+

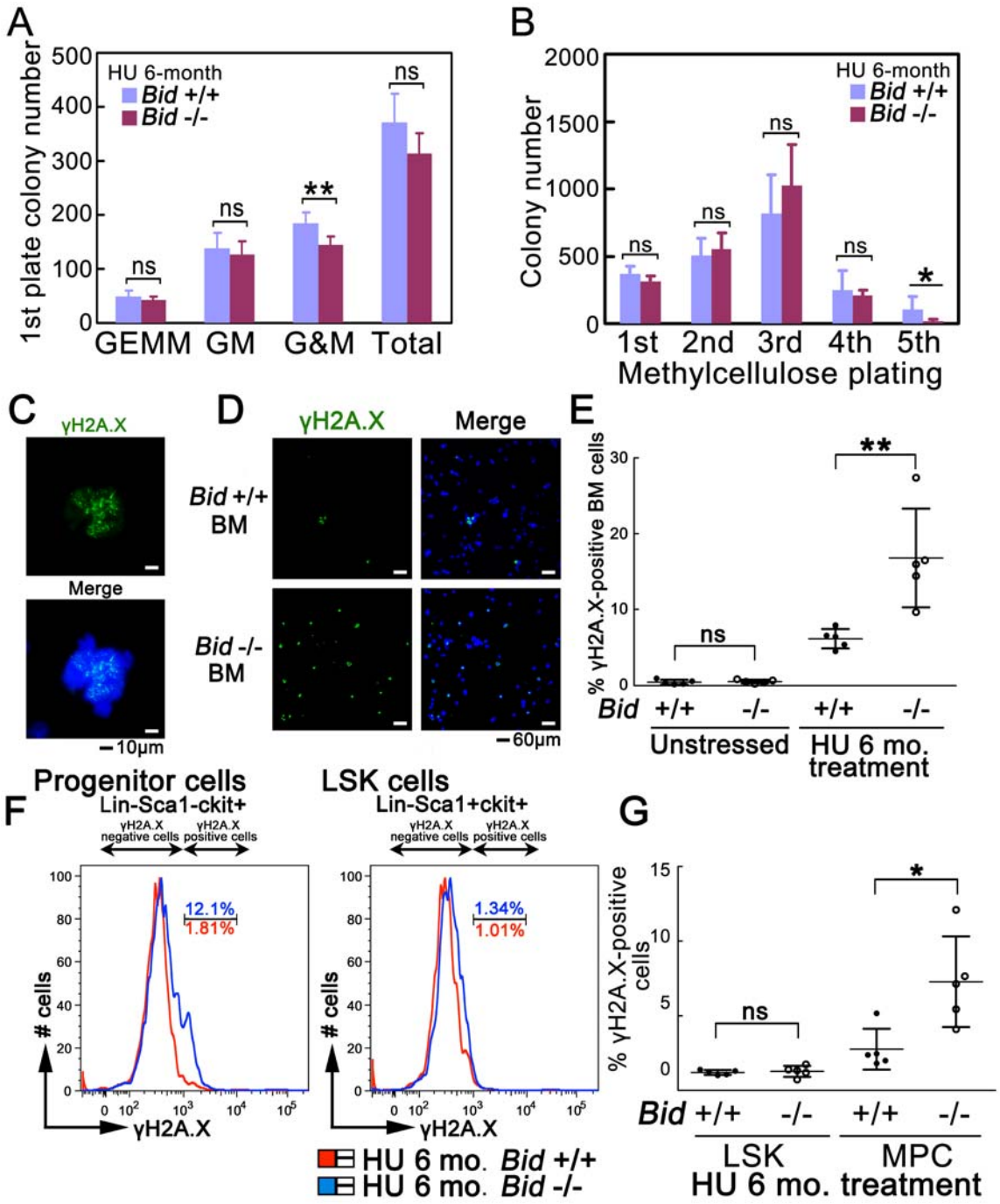

Figure 5-6. *Bid* -/- bone marrow exhibit increased γH2A.X staining following 6-month HU treatment. (A) *Bid* -/- bone marrow exhibits similar colony formation ability as *Bid* +/+ in methylcellulose culture. *Bid* +/+ and *Bid* -/- mice were treated with HU for 6 month and bone marrow was harvested from femurs and tibias 24 hours after last HU injection. Bone marrow cells were cultured in methylcellulose culture and various colonies were counted on Day 7 after plating according to colony morphology. Two independent experiments were performed with n = 5 in each set. (B) Total colony number was counted in methylcellulose re-plating process. (C-D) *Bid* -/- bone marrow

exhibit increased γH2A.X staining following 6-month HU treatment. *Bid* +/+ and *Bid* -/- mice were treated with HU for 6 month and bone marrow was harvested from femurs and tibias 24 hours after last HU injection. Bone marrow cells were fixed, permeabilized and stained by Alexa Fluor 488-conjugated anti-phospho-Histone H2A.X (Ser139). Typical γH2A.X foci were observed in *Bid* -/- bone marrow (C, high resolution image). Representative figures of γH2A.X staining in around 100 bone marrow cells were shown in (D). DNA was detected by Hoechst stain (blue). (E) γH2A.X-positive bone marrow cells were counted from 150-300 cells/mice and quantitative analysis was calculated from 5 mice. (F) *Bid* -/- MPC but not HSC population exhibits increased γH2A.X staining following 6-month HU treatment. *Bid* +/+ and *Bid* -/- mice were treated with HU for 6 month and bone marrow was harvested. Cells were first stained with surface marker (CD3, B220, Gr-1, Ter119, c-kit and Sca-1). Then, cells were fixed and permeabilized and then stained with anti-phospho-Histone H2A.X (Ser139) for 30 minutes at room temperature and γH2A.X-positive cells was detected by flow cytometry. γH2A.X-positive cells were gated as Alexa Fluor 488 intensity > 103 (See explanation in Fig. S2B). Representative figures were shown. (G) The percentage of γH2A.X-positive cells in MPC and LSK population was analyzed from 5 mice and quantitative analysis was shown. *, $p < 0.05$; **, $p < 0.01$. error bar, (A-B), SD; (E and G), SEM.

and *Bid* -/- mice following six months of HU treatment by competitive bone marrow reconstitution. Lineage-depleted *Bid* +/+ (CD45.2) and *Bid* -/- (CD45.2) bone marrow cells were transplanted into lethally irradiated recipient mice (CD45.1) with equal amounts of lineage-depleted competitor bone marrow cells (CD45.1). The reconstitution of the hematopoietic system was detected by the CD45.2/CD45.1 ratio in peripheral blood from the recipient mice over time (66) (Figure 5-8 A). The percentage of CD45.2+ cells in *Bid* -/- peripheral blood was significantly diminished compared with *Bid* +/+ cells, as demonstrated by the decreased CD45.2/CD45.1 ratio in the recipient mice for the *Bid* -/- but not the *Bid* +/+ test populations (Figure 5-8 B, C). As a control, no defect in the reconstitution capacity was observed in untreated *Bid* -/- bone marrow in a competitive reconstitution assay, but rather a slight competitive advantage (66), suggesting that the diminished HSC function is due to long-term HU treatment. Distinct from the HSC exhaustion noted in other mouse models (219,224), the reconstitution capacity of *Bid* -/- HSCs is only impaired following long-term HU treatment. Consistent with this thesis, *Bid* -/- MPCs but not HSCs display increased cell death following HU, suggesting that the increased death of *Bid* -/- MPCs triggers mobilization of *Bid* +/+ HSCs. Of note, *Bid* -/- hematopoietic cells display a defect in radioresistant DNA synthesis so I can not rule out a contribution from an additional cell cycle checkpoint defect of *Bid* -/- HSCs.

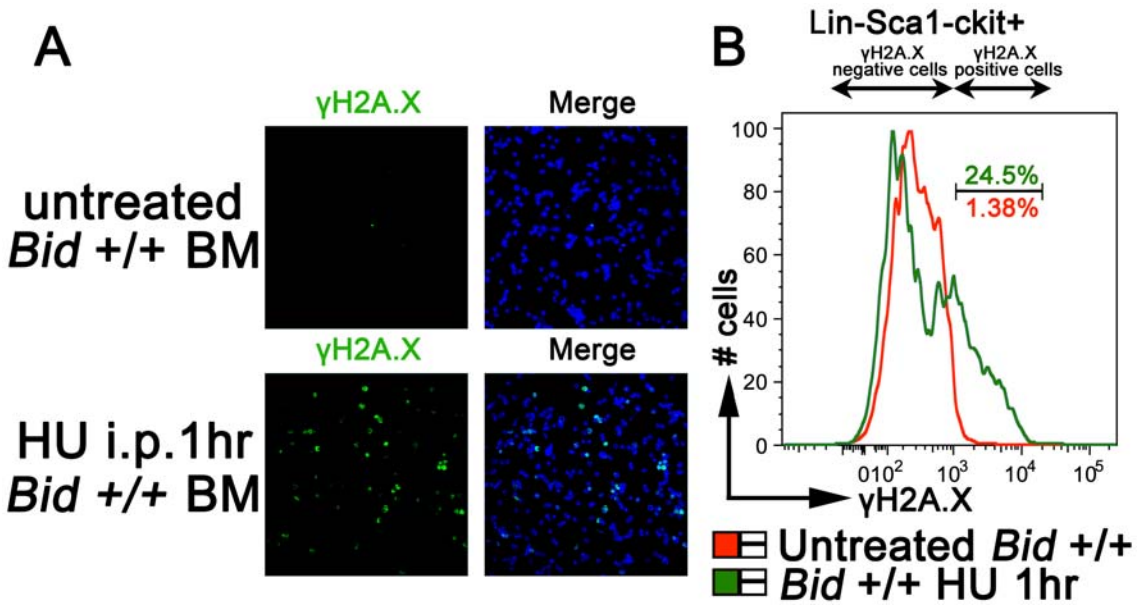

Figure 5-7. Test of anti-phospho-Histone H2A.X in immunofluorescence and intra-cellular staining in flow cytometry. (A) *Bid* +/+ mice were treated with 100 mg/kg/day hydroxyurea by intraperitoneal injection for 1 hour. Mice were sacrificed and bone marrow was harvested from femurs and tibias. Cells were centrifuged onto a glass coverslip by cytospin. Then, cells were fixed by 3% paraformaldehyde/2% sucrose solution and permeabilized by Triton X-100 solution. γH2A.X-positive cells was detected by immunofluorescence using Alexa Fluor 488-conjugated anti-phospho-Histone H2A.X. DNA was detected by Hoechst stain (blue). (B) *Bid* +/+ mice were treated with 100 mg/kg/day hydroxyurea by intraperitoneal injection for 1 hour. Mice were sacrificed and bone marrow was harvested from femurs and tibias. After erythrocytes were lysed in RBC lysis buffer, bone marrow cells were stained with lineage marker (biotinylated CD3, B220, Gr-1 and Ter119). Then cells were staining with APC-conjugated anti-c-kit, PE-Cy7-conjugated anti-Sca1 and Pacific blue-conjugated streptavidin. Cells were fixed and permeabilized with BD Cytofix/Cytoperm Buffer, and incubated with BD Cytoperm Plus Buffer followed by an additional short fixation with BD Cytofix/Cytoperm Buffer. Then, cells were stained with Alexa Fluor 488-conjugated anti-phospho-Histone H2A.X (Ser139) for 30 minutes at room temperature and γH2A.X-positive cells was detected by flow cytometry. γH2A.X-positive cells were significantly increased in myeloid progenitor cell population (Lin-Sca1-ckit+) upon HU treatment, suggesting that anti-phospho-Histone H2A.X is a specific antibody against γH2A.X signals in flow cytometry. Based on the induced γH2A.X-positive cell population, γH2A.X-positive cells were gated as Alexa Fluor 488 intensity > 10^3.

Discussion

Hematopoietic stem cells are susceptible to genotoxic stress from multiple etiologies. DSBs and replicative stress are two kinds of well-established DNA damage. Recently, the response of HSC and MPCs to IR has been studied *in vivo* (105,107) in both mice and humans. Two distinct PI3Kinase-like kinases regulate the DDR to double strand breaks and replicative stress, ATM and ATR, respectively. Bid has been shown to mediate the ATR-directed response to replicative stress. In this study, I use *Bid* -/- mice as a model to investigate how defects in ATR-mediated DDR impact the maintenance of the hematopoietic system following replicative stress. My results are most consistent with the following model: the hypersensitivity of *Bid* -/- MPCs to HU treatment results in an excessive depletion of the MPC population, which mobilizes HSCs to compensate for this defect (Figure 5-8 D). Following long-term HU treatment, the continuous mobilization of HSCs in *Bid* -/- mice leads to exhaustion of the HSC population, leading to a diminished LSK and MPC population (Figure 5-8 D).

As Bid has been demonstrated to play a survival role in MPCs following replicative stress (2), it is surprising that *Bid* -/- mice survived following six months of HU treatment. Several possible reasons might explain this compensatory ability of *Bid* -/- HSCs. First, in unstressed conditions, *Bid* -/- bone marrow exhibits a competitive advantage in bone marrow competitive reconstitution

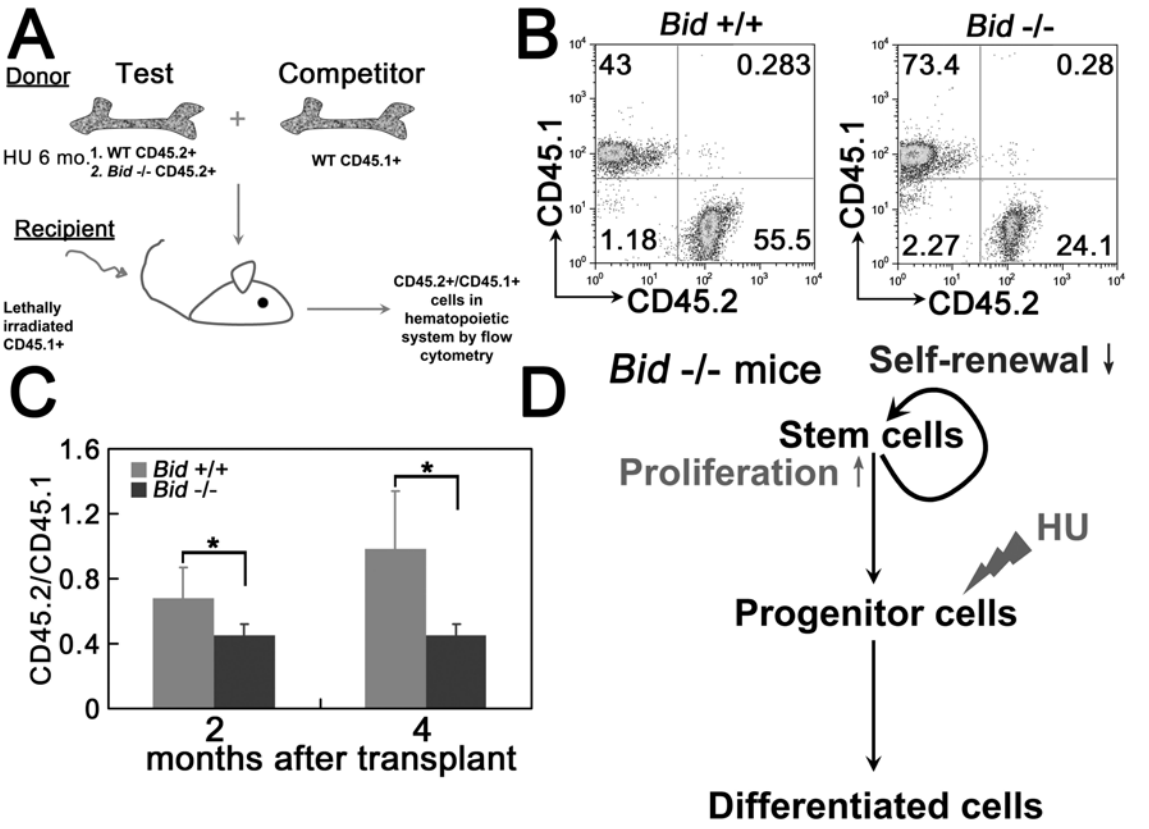

Figure 5-8. Stem cell function is diminished in *Bid* -/- bone marrow following 6-month HU treatment. (A) Experimental design. Following 6 month HU treatment, *Bid* +/+ and *Bid* -/- mice (CD45.2) were sacrificed and bone marrow were obtained from femurs and tibias. Lineage+ cells were depleted by Dynabeads Sheep anti-Rat IgG. 1×10^5 lineage- bone marrow cells from either *Bid* +/+ or *Bid* -/- mice (CD45.2+) following HU treatment together with 1×10^5 lineage- bone marrow "Competitor" cells (CD45.1+) were transplanted into lethally irradiated recipients (CD45.1+) by intravenous injection. Hematopoietic reconstitution was detected followed 2 and 4 months after the transplantation. (B) Peripheral blood was obtained from the recipient mice transplanted from *Bid* +/+ or *Bid* -/- mice following 6-month HU treatment. The lymphocytes were stained by anti-CD45.1 and anti-CD45.2 antibodies, and analyzed in flow cytometry. Representative figure was shown. (C) The ratio of CD45.2-positive cells vs. CD45.1-positive cells in the peripheral blood of recipient mice after 4-month transplantation was calculated and quantitative analysis was shown. *, $p < 0.05$; n = 10. error bar, SD. (D) Proposed model of Bid's function in hematopoietic system following replicative stress. In *Bid* +/+ mice, Bid facilitates normal ATR function to maintain replication fork and genomic integrity in the cycling progenitor cells following replicative stress. In *Bid* -/- mice, *Bid* -/- myeloid progenitor cells are hypersensitive to replicative stress. The excessive depletion of myeloid progenitor cells results in an over mobilization of hematopoietic stem cells to compensate this defect in *Bid* -/- progenitor cells. Long-term HU treatment causes an extended proliferation of HSCs and resultant depletion of stem cell self-renewal function in *Bid* -/- mice.

assays (66), suggesting that the self-renewal capacity might be augmented in *Bid* -/- HSCs potentially due to the loss of the pro-apoptotic function of Bid. Secondly, according to the immortal DNA strand hypothesis (278), it is quite possible that the DNA segregation is asymmetrical in mitotic HSCs and the undamaged parental strands are maintained in HSCs populations, which might explain the low DNA damage level in the LSK population following long-term HU treatment (Figure 5-6 F, G). Thirdly, the compensated increase of LSK/MPC populations following long-term HU treatment (Figure 5-5 B, C) might limit the damage efficiency of HU to MPC population and lead to a diminished mobilization pressure of HSC to replicative stress. Lastly, although HU- induces the DNA damage response within 1 hour (Figure 5-7), the half-life is only 3-4 hours *in vivo* (230). The rapid elimination of HU might limit its function, i.e., it can only stall replication fork rather than cause fork collapse *in vivo*. As no significantly increased γH2A.X-positive cells were observed in the *Bid* -/- LSK population following long-term HU treatment (Figure 5-6 F, G), the function of Bid in the regulation of HSCs might not be a cell autonomous effect. Interestingly, Bid has been demonstrated to be highly expressed in the GMP population rather than LSK population (105), which also suggests that Bid might play a preferential role in GMPs.

ATR has been demonstrated to play important roles in maintenance of genomic integrity in proliferating cells, as well as in normal DNA replication (124). Germline deletion of ATR results in early embryonic lethality (141,142). Conditional *Atr* -/-

mice showed defects in tissue homeostasis with aging-related phenotypes and exhaustion of tissue-specific stem and progenitor cells (143-145). However, compared with its role in the normal cell cycle, the ATR-mediated signaling pathway functions diversely following replicative stress. Although the DNA damage response was severely impaired, cells harboring mutated RPA70 (148) or ATRIP (129) showed a quite normal cell cycle profile. *Bid* -/- cells demonstrated limited ATR function following replicative stress, however, no obvious defects were observed in the cell cycle profile of *Bid* -/- cells (4) or development of *Bid* -/- mice (66). In addition, *Atr* -/- Arabidopsis develops normally and growth retardation is only observed when the plants are challenged with replicative stress (149). In this study, no obvious aging defects were observed in long-term HU stressed *Bid* -/- mice and one-year aged untreated *Bid* -/- mice show a similar percentage of LSKs and MPCs as *Bid* +/+ mice (Figure 5-9). These results are consistent with my previous finding that the major function of Bid in the ATR response is DNA damage-induced (4).

Bid has been demonstrated to play dual roles in both programmed cell death and the replicative stress-induced response (2,4,31,32). The two distinct functions of Bid are mediated by distinct functional domains (2,4,5), manuscript submitted. The apoptotic function of Bid is predominantly mediated by its caspase-cleavage sites (31) and BH3 domain (73), while Bid executes its function in the DNA damage signaling pathways by its ATM/ATR phosphorylation sites (2,3) and its

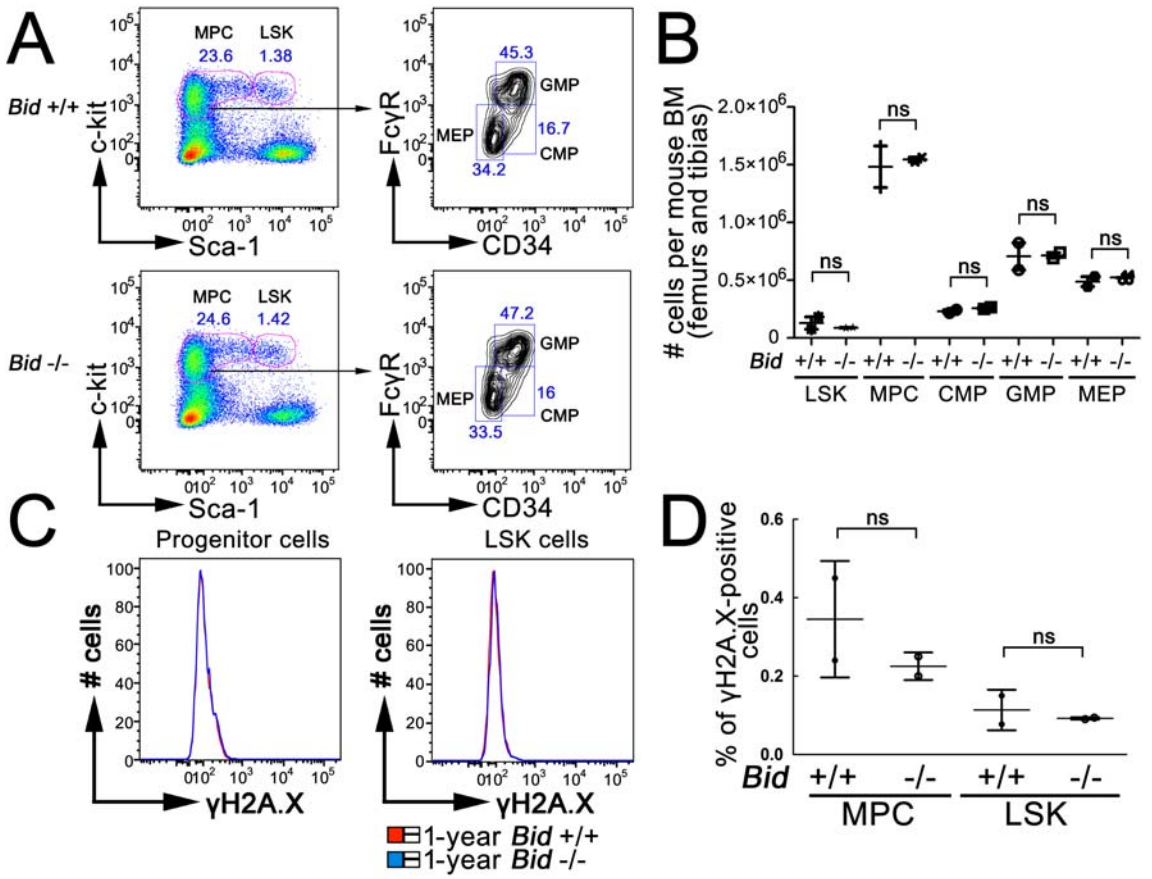

Figure 5-9. Aged *Bid* -/- mice show similar MPC and LSK population as *Bid* +/+. (A) One-year old *Bid* +/+ and *Bid* -/- mice were sacrificed and bone marrow was harvested from femurs and tibias. Cells were first stained with lineage marker (biotinylated CD3, B220, Gr-1 and Ter119) and then stained with c-kit, Sca1, CD34 and FcγRII/III. MPC and LSK cells were gated as Lin-Sca1-ckit+ and Lin-Scal+ckit+ population, respectively. GMP, CMP, and MEP cells were gated as CD34+FcγR+, CD34+FcγR-, and CD34-FcγR- population from MPC cells, respectively. Representative results were shown. (B) LSK, MPC, GMP, CMP, MEP population cell number was counted and quantitative analysis was shown. (C) One-year old *Bid* +/+ and *Bid* -/- mice were sacrificed and bone marrow was harvested. Cells were first stained with surface marker (CD3, B220, Gr-1, Ter119, c-kit and Sca-1). Then, cells were fixed and permeabilized and then stained with anti-phospho-Histone H2A.X (Ser139) for 30 minutes at room temperature and γH2A.X-positive cells was detected by flow cytometry. Representative results were shown. (D) The percentage of γH2A.X-positive cells in MPC and LSK population was analyzed and quantitative analysis was shown. Error bar, SEM.

unique Helix 4 and RPA-ID domain (4,5). *Bid* -/- mice spontaneously develop chronic myelomonocytic leukemia (CMML) and the tumor cells display chromosomal aberrations (66). Since both cell death and DNA damage signaling pathways are important for tissue homeostasis and genomic integrity, it will be interesting to determine which function of Bid directs the tumor suppressor function of Bid *in vivo*. It is likely that both the apoptotic and DNA damage function of Bid work synergistically to maintain hematopoiesis. My studies are most consistent with Bid facilitating normal ATR function to maintain replication fork and genomic integrity in the cycling progenitor cells following replicative stress, which prevents excessive mobilization of HSCs and resultant depletion of HSC function.

First identified in non-Hodgkin lymphomas (39), BCL-2 and its family have been demonstrated to play crucial roles in maintenance of hematopoiesis (279). Ectopic expression or knockout of various BCL-2 family proteins predominantly results in defects in hematopoietic system, suggesting that the regulation of hematopoiesis is dependent on BCL-2 family (279). Besides sensing and transducing various survival or death signals to mitochondria to regulate apoptosis, more and more “non-canonical” functions of BCL-2 family members have been identified (254). For example, BCL-2 and MCL-1 have been demonstrated to play a role in DSBs repair and DNA damage checkpoint signal pathway, respectively (259,266). Investigating the physiological function of these novel properties of BCL-2 members will deepen our understanding of BCL-2

family in hematopoietic system, which is quite important in future pharmaceutics and therapeutics.

CHAPTER VI

SUMMARY AND FUTURE DIRECTIONS

Summary

BID, a BH3-only BCL-2 family member, was first identified as a pro-apoptotic protein to transduce death receptor signals to the core apoptotic machinery by activation of BAX/BAK at mitochondria (31,32,73). Recent evidence suggests that BID also maintains genomic integrity following DNA damage treatments. *Bid* -/- mice spontaneously develop chronic myelomonocytic leukemia with significant chromosomal abnormalities (66). Following genotoxic stress, Bid is found in the nucleus to be phosphorylated by the PI-3-like kinases ATM and/or ATR (2,3). Furthermore, *Bid* -/- cells show an intra-S phase checkpoint defect manifest by abnormal radio-resistant DNA synthesis (2,3). In addition, *Bid* -/- myeloid progenitor cells show increased chromosomal breaks and quadriradials following mitomycin c treatment and increased sensitivity to chemotherapy agents inducing replicative stress (2), suggesting that Bid might play a survival role following replicative stress. Although the function of BID in the apoptotic pathway has been extensively studied, relatively little is known about BID's role in the DNA damage response, therefore I focus on the function of BID in DNA damage signaling

pathway in my thesis work. Following replicative stress, single-stranded DNA is sensed by RPA and ATR/ATRIP is recruited and activated at RPA-coated ssDNA (124,176). The ATR signals activate cell cycle checkpoints, maintain the replication fork, and slow origin firing by phosphorylation of numerous ATR substrates (124). Since ATR plays a crucial role to maintain genomic integrity following replicative stress, the function of BID in ATR-mediated pathway is investigated in this present thesis.

Using genetic tools (e.g., knockout of Bid and knockdown of BID), I first demonstrated that BID facilitates the ATR-mediated DNA damage response by various functional assays. Following replicative stress, *Bid* -/- and *BID* KD cells demonstrate limited ATR function as manifest by diminished phosphorylation of ATR substrates, reduced recovery of DNA synthesis, reduced ATRIP nuclear foci, and defects in chromatin-bound ATR, ATRIP, RPA and PCNA (4). Then, using cell biology and biochemical tools, I demonstated that BID co-localizes with RPA in nuclear foci and associates with the ATR/ATRIP/RPA complex following replicative stress (4). In addition, the Helix 4 domain of BID interacts with the coiled-coil domain of ATRIP and this association is required for normal ATR function (4). Interestingly, the association between ATR/ATRIP and RPA is significantly diminished in *Bid* -/- cells following replicative stress (4), suggesting that Bid plays a role to maintain the DNA damage sensor complex.

As a ssDNA-binding protein, RPA is the direct sensor of DNA damage in the

ATR-mediated response following replicative stress (125). To further investigate the mechanism by which BID functions in the ATR pathway, I investigated the interaction between BID and RPA. I found that BID stimulates the association of RPA with components of the DNA damage sensor complex through interaction with the basic cleft of the N terminal domain of the RPA70 subunit (5). Based on the chemical shift perturbation in two-dimensional ^{1}H-^{15}N HSQC spectrum, the basic cleft region of RPA70N and the acidic region in the N-terminus of BID's Helix 5 domain (named RPA-ID domain) are characterized as the potential BID-RPA70N interaction surface (5). Modeling of the BID-RPA70N complex with the binding information obtained from the NMR HSQC spectrum was performed using HADDOCK software (5). Mutations in the key amino acids in the basic cleft region of RPA70N or in the RPA-ID region of BID significantly impair the BID-RPA70N interaction, which is consistent with the model generated from the NMR experiment (5). Disruption of the BID-RPA interaction impairs association of ATR-ATRIP with chromatin as well as ATR function as measured by CHK1 activation and recovery of DNA replication following hydroxyurea (HU) (5). I further demonstrate that association of BID with RPA stimulates association of ATR/ATRIP to the DNA damage sensor complex in an *in vitro* assay (5). I propose a model in which BID associates with RPA, and stimulates the recruitment and/or stabilization of ATR-ATRIP to the DNA damage sensor complex.

Hematopoietic stem cells (HSCs) possess longterm self-renewal capacity and

multipotent differentiative capacity, to maintain the hematopoietic system. Long term hematopoietic homeostasis requires effective control of genotoxic damage to maintain HSC function and prevent propagation of deleterious mutations (210,280). As Bid is highly expressed in the hematopoietic system and *Bid* -/- mice spontaneously develop chronic myelomonocytic leukemia, I focus on the Bid's function in the hematopoietic system following DNA damage treatment. Here I investigate the response of murine HSCs to longterm replicative stress by hydroxyurea (HU). The serine/threonine kinase ATR initiates the DNA damage response to replicative stress. The pro-apoptotic BCL-2 family member Bid facilitates this response in hematopoietic cells (6). Bone marrow from HU-treated wild type mice demonstrates increased replating capacity relative to untreated wild type bone marrow (6). Following longterm HU treatment, the MPC and HSC populations expand and maintain longterm competitive repopulating ability (6). *Bid* -/- MPCs demonstrate increased sensitivity to HU and are depleted. *Bid* -/- HSCs demonstrate increased BrdU incorporation, and *Bid* -/- bone marrow demonstrates increased replating ability consistent with increased mobilization of HSCs and early progenitor cells (6). Following longterm HU treatment, *Bid* -/- MPCs and HSCs are relatively depleted, and bone marrow from *Bid* -/- mice displays increased DNA damage and decreased longterm competitive repopulating ability (6). Thus, HSCs and MPCs maintain function in the setting of increased replicative stress by expanding and repairing the DNA damage. *Bid* -/-

mice, deficient in the ATR-mediated DNA damage response, lose HSC function following longterm HU treatment.

Overall, my studies establish a direct role for the BH3-only BCL-2 family member, BID, at the damage sensor level to facilitate the ATR-directed cellular response to replicative stress both *in vitro* and *in vivo*. The significance of my thesis work is summarized below.

✧ Clarify the function of BID in the DNA damage response. BID has been demonstrated to play a role in the maintenance of genomic integrity and the DNA damage-induced checkpoint response (2,3), however, the detailed mechanism and function of BID in the DNA damage response are unknown and controversial results were reported in this field. My thesis work significantly increases our understanding of how BID functions in the DNA damage signaling pathways, especially in the ATR-mediated response. In the cell death field, although the mechanism by which BCL-2 family members transduce the apoptotic response at the mitochondria is well-established, the mechanism by which a damage signal is sensed and relayed to the mitochondria is still not understood. The present thesis provides an excellent model of a pro-apoptotic BH3-only molecule involved in the damage sensor complex to directly sense cellular stress. BID participates in the DNA damage sensor complex by physical interactions with the core DNA damage sensor proteins (i.e., ATRIP and RPA), which sense ssDNA and initiate a DNA

damage response directly following replicative stress. Although the detailed molecular mechanism is still not completely clear, the discovery of the association between BID and ATR/ATRIP/RPA provides a crucial clue to the function of BID in the stalled replication fork and DNA damage sensor complex following replicative stress. In addition, the exploration of pro-apoptotic BID as a novel regulator in the ATR-directed response extends our understanding of how cell fate is determined in response to DNA damage by elucidating the cross-talk between DNA damage sensing machinery and cell death signaling pathways. The investigation of the function of pro-apoptotic BID in the nucleus following genotoxic stress will deepen our understanding of how BH3-only molecules function in sensing various cellular stresses. Given the emerging interest in BH3-mimetics in cancer treatment, this is important information for clinical therapy as well as drug design.

✧ Map the functional domains of BID in the DNA damage response. In structure, the BCL2 family proteins are characterized by their homologous BH domains and the BH3-only molecules harbor only one BH3 domain. To transduce stress/death signals to mitochondria, the BH3-only molecules interact with other BCL-2 family by the BH3 domain; however, it was still unclear how BH3-only molecules sense various cellular stresses at the structural level. Several post-translational modifications have been reported to facilitate detection of various stimuli, including phosphorylation, cleavage and

myristoylation, by BH3-only proteins (31,32,84,88,91). However, except for the BH3 domain, no other functional domains of BID have been identified and characterized that mediate interactions with other proteins. My findings advance the field through identification of two novel functional domains of BID, Helix 4 and RPA-ID domains, which mediate the interaction with ATRIP and RPA, respectively (4,5). This finding provides further evidence that the dual functions of BID in apoptosis and DNA damage response are mediated by distinct regions of the protein (Table 4). The present work consolidates my model that the dual functions of BID in programmed cell death and ATR-mediated DNA damage response are mediated by its different structural domains (Table 4). These domains provide a framework with which to identify and investigate such “damage-sensing domains” in other BCL-2 family proteins.

✧ Provide an animal model to investigate the regulation and homeostasis of hematopoietic system following replicative stress. Although various DNA damage responses have been well-established at the cellular level, very few studies focus on the physiological and pathological response to DNA damage at the animal level. In this present thesis, I used *Bid* +/+ and *Bid* -/- mice as a model to investigate the *in vivo* function of Bid to replicative stress (6). *Bid* -/- bone marrow shows a hypersensitivity to *in vivo* HU treatment and long-term HU treatment impairs the ability of HSCs to maintain their function in *Bid* -/-

mice (6). As *Bid* -/- mice spontaneously develop chronic myelomonocytic leukemia and the tumor cells display chromosomal aberrations (66), Bid plays a tumor suppressor role and contributes to hematopoietic homeostasis. A purely apoptotic role for Bid cannot account for all of the current data regarding Bid's function, and my thesis work provides additional physiological evidence to support my model that Bid facilitates ATR-mediated DNA damage response (6). It is quite possible that the dual roles of Bid in both apoptosis and DNA damage signaling pathways contribute synergistically to the tumor suppressor function of Bid *in vivo*.

Table 4. Dual functions of BID in both apoptotic and DNA damage response.

Pathway	Apoptosis	DNA damage
Cellular stress	Death receptor	Replicative stress
Character	Senor	Sensor/Mediator
Protein interaction	BCL-2 family (i.e. BCL-2, MCL-1, BAX/BAK)	DNA damage sensor complex (i.e. ATR/ATRIP, RPA)
Post-translational modification	Asp 59 cleavage (Caspase 8); Gly60 myristoylation (N-myristoyltransferase)	Ser61/64, Ser78 phosphorylation (ATM/ATR)
Functional domain	Helix 3 (BH3)	Helix 4; RPA-ID
Localization	Mitochondria	Chromatin
Function	Programmed cell death	Genomic integrity
Family	BCL-2 family	Unknown

Future directions

How does BID work?

Although my results are consistent with a model that BID facilitates ATRIP-RPA interaction *in vivo* (Figure 3-12 A) and *in vitro* (Figure 4-11 A-C), the detailed molecular mechanism is still elusive. Several possible models at the molecular level are proposed below. It is worthwhile to note that all these models are not mutually exclusive and BID might function at multiple levels in the DNA damage sensor complex.

- ✧ BID might function as an "RPA activator" to facilitate certain conformational changes of RPA70N. After ATRIP is recruited, BID releases from this RPA-ATRIP complex (Figure 6-1 A). However, no obvious structure change has been observed in RPA70N upon adding other binding partners *in vitro*.
- ✧ BID might function as an adaptor to stabilize ATR/ATRIP complex to multiple RPA molecules (Figure 6-1 B). BID interacts with ATRIP and RPA by its Helix 4 and RPA-ID regions, respectively. However, it is still unclear whether one BID molecule binds with ATRIP and RPA simultaneously or not. To investigate BID-RPA-ATRIP complex directly, the chromatin fraction from HU-stressed *Bid* +/+ cells could be purified and then fractionated by various biochemical separation, such as size exclusion chromatography and sucrose density gradient centrifugation. Then the molecular weight of the complex harboring BID, RPA and ATR/ATRIP could be estimated. The limitation of this procedure is that the DNA damage sensors are quite large (>500kDa) and many other factors are involved in this complex. Alternatively, an *in vitro* reconstitution

assay with purified BID, RPA, and ATRIP might be performed to detect the molecular weight of the complex. The limitation of this procedure is that, by far, it is very difficult to purify high-pure ATR and ATRIP proteins.

- ✧ BID interacts with other unknown factors to stabilize ATR/ATRIP complex binding to RPA (Fig. 6-1 C). In my studies, I found that BID facilitates RPA-ATRIP interaction *in vitro* in a dose-dependent manner. At low molar ratio, BID facilitate ATRIP bound to RPA while it competes with ATRIP at high molar ratio (Figure 4-11 A-B). Interestingly, the binding ability of ATRIP to RPA is much more induced by hydroxyurea treatment than by incubation with BID (Figure 4-11 B), suggesting that other factors are involved in this DNA damage sensor complex to facilitate the formation of stable RPA-ATR/ATRIP complex *in vivo*. Further studies need to be performed to clarify how the high-order structure of DNA damage sensor complex is maintained and how BID functions in the DNA damage sensor complex.
- ✧ Although ATRIP is predominantly in the form of an ATR-ATRIP heterodimer by hydrodynamic methods (281), ATRIP could form oligomers by its coiled-coil domain (Δ112-225) as demonstrated by co-IP assay (253). Following replicative stress, BID interacts with the coiled-coil domain of ATRIP. Thus, it is possible that BID facilitates or stabilizes ATRIP oligomerization on RPA-coated ssDNA following replicative stress (Figure 6-1 D).

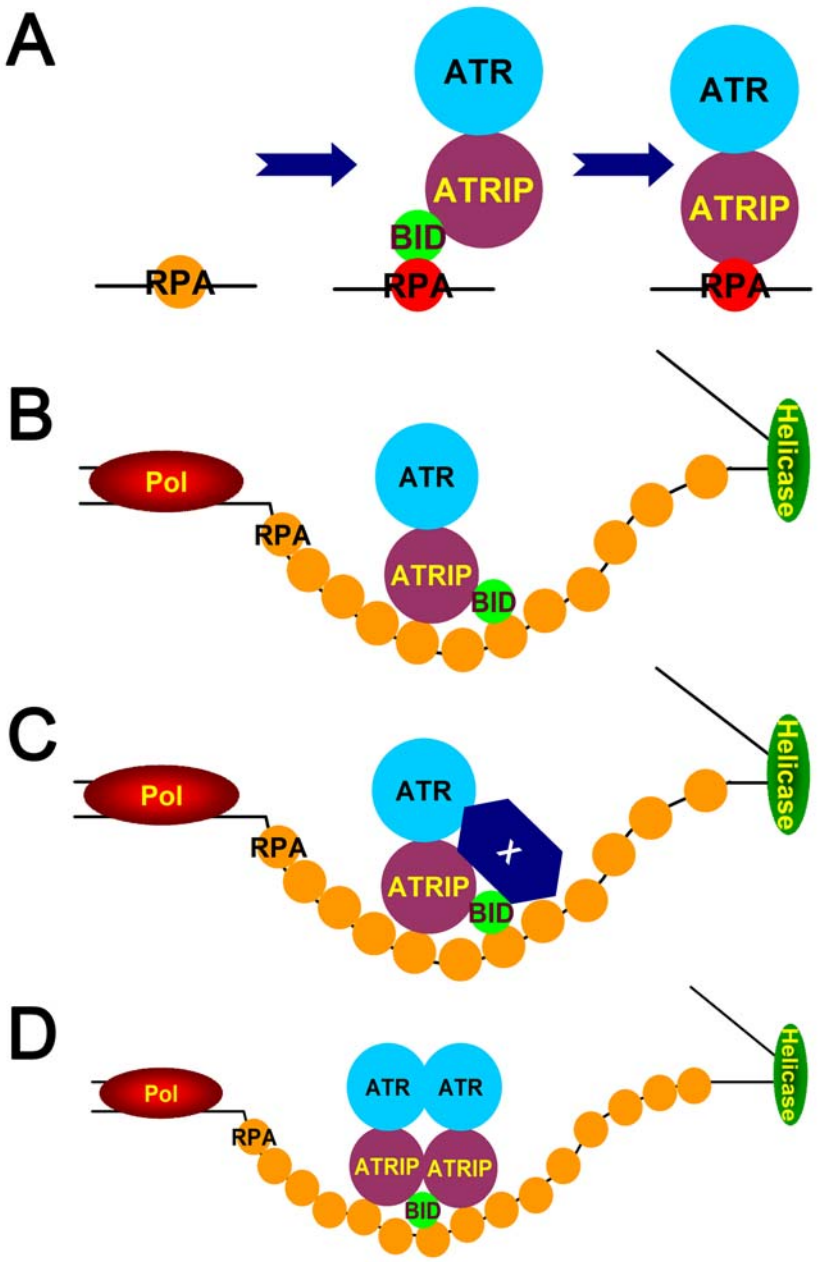

Figure 6-1. Proposed working models for BID to facilitate ATRIP-RPA association at the molecular level. (A) “RPA activator” model. BID might interact with RPA and facilitate certain conformational change of RPA70N, which makes RPA70N bind to ATRIP easily. After ATRIP is recruited, BID releases from this RPA-ATRIP complex. (B) “Adaptor” model. BID might function as an adaptor to stabilize ATR/ATRIP complex binding to multiple RPA molecules. Pol, DNA polymerase. (C) “X”model. BID interacts with other unknown factors to stabilize ATR/ATRIP complex binding to RPA. (D) “ATRIP oligomerization” model. As ATRIP could form oligomers by its coiled-coil domain (Δ112-225) and BID associates with the coiled-coli domain of ATRIP following replicative stress, it is possible that BID facilitates or stabilizes ATRIP oligomerization on RPA-coated ssDNA following replicative stress.

In addition to activation of cell cycle checkpoint, ATR signals also maintain genomic integrity by controlling origin firing and stabilizing stalled replication forks following replicative stress (282). In yeast, Mec1 (ATR) and RecQ helicase has been reported to maintain DNA pol α and pol ε in the replication fork by a density isotope substitution method and chromatin immunoprecipitation assay (283,284). In addition, the mediator in ATR pathway, Mrc1 (Claspin), has been found to interact with DNA pol ε and Mcm complex, which stabilizes Pol2 at stalled replication forks following replicative stress (285). However, due to technical limitation, it is still difficult to investigate the stalled replication fork directly in mammalian cells (286). In my study, chromatin-bound PCNA is significantly diminished in *BID* KD cells following replicative stress (Figure 4-9). Although PCNA is prone to release from stalled replication fork in the absence of BID, the chromatin-bound MCM3 is maintained normally in *BID* KD cells (Figure 4-9). It will be interesting to investigate whether the unstable replication fork in ATR function-limited cells is attributed to the release of certain key components (e.g. PCNA) from the replisome or to a global dissociation of the replisome from chromatin. It is also worthwhile to investigate whether BID associates with certain key factors in various DNA polymerases to maintain the stalled replication fork following replicative stress.

Why BID?

Although BID has been demonstrated to play dual roles in both apoptosis and the ATR-mediated DNA damage response, it is worthwhile to think about the significance of these functions of BID in evolution. ATR-mediated DNA damage response is quite conserved from yeast to human. However, apoptosis only occurs in multicellular organisms and BID is only identified in vertebrates, which leaves a question as to why BID is involved in the DNA damage response.

In apoptosis, BCL-2 family proteins function as sensors to sense and relay various cellular stresses to mitochondria to initiate programmed cell death. Apoptosis and BCL-2 family proteins have been demonstrated to play important roles in the maintenance of tissue homeostasis and prevention of tumorigenesis in metazoans. It is a challenge for multicellular organisms to maintain their tissue homeostasis by efficient clearance of damaged or irreparable cells and exquisite preservation of unstressed or repaired cells simultaneously, which is not a problem for unicellular organisms (e.g. yeast). Thus, it is reasonable to speculate that more and more complicated mechanisms are involved in higher organisms to regulate the DNA damage response elaborately, especially DNA damage-induced programmed cell death.

Following DNA damage, cells maintain genomic integrity by two major decision programs. Cell cycle checkpoint is first executed to arrest cell cycle progression, which cooperates with the DNA repair process to ensure cell survival. If the damage is overwhelming, cells then initiate apoptosis to eliminate injured cells. It

is still unclear how such a critical control point is established to decide cell fate from survival to death following genotoxic stress. Based on the studies from our lab and other research groups, BID might be such a feasible candidate to participate in both checkpoint responses following DNA damage. First, BID functions as a survival factor to facilitate ATR-mediated DNA damage checkpoint as well as maintenance of replication fork. Following prolonged or severe DNA damage, BID might be released from the DNA damage sensor complex or stalled replication fork to execute its apoptotic function at mitochondria. As caspase 2 has been reported in the nucleus and caspase 2 cleaves BID *in vitro* (86,87,193), it is very interesting to investigate whether nuclear BID is cleaved by caspase 2 or not following prolonged replicative stress. However, as apoptosis is quite a context-dependent cellular response, different cell types or culture condition might utilize distinct mechanism to decide cell fate following cellular stress.

Except for its BH3 domain, BID does not share any homologous domains with other proteins. Accordingly, it is important to study how these unique damage sensing domains are generated in evolution. It is worthwhile to search the protein or cDNA databases to explore and identify the invertebrate BID homologues harboring Helix 4 or RPA-ID regions.

Functions in ATR pathway

In my thesis studies, the functions of various factors in the ATR-mediated

signaling pathways have been detected in *Bid* -/- and *BID* KD cells, including ATR, ATRIP, RPA, TopBP1, p53, CHK1 and CDC25A (4). However, the functions of 9-1-1, RAD17 and Claspin were not detected directly. To further clarify the function of BID in the ATR-mediated response, it is necessary to detect the recruitment of the 9-1-1 complex to ssDNA as well as the interaction among 9-1-1, RAD17 and Claspin in *BID* KD cells. In addition, it will provide us much additional information by detection of the post-translational modifications of various DNA damage sensors in *BID* KD cells following replicative stress, such as RAD17 phosphorylation.

Following replicative stress, checkpoint protein RAD17 is phosphorylated by ATR at Ser635 and Ser645 residues (132,287,288) prior to CHK1 activation. The phosphorylated RAD17 binds with and regulates the phosphorylation of Claspin by ATR following genotoxic stress (132). The phosphorylated Claspin recruits CHK1 and facilitates CHK1 to be phosphorylated by ATR exclusively (131). Interestingly, cells harboring S635A/S645A mutated RAD17 exhibit a quite similar phenotype as BID -/- cells, including intra-S checkpoint defects, genomic instability, hypersensitivity to replication stress, and unstable CHK1 phosphorylation (132). Accordingly, it is worthwhile to investigate whether RAD17-Claspin function is normal or not in *BID* KD cells and whether BID interacts with RAD17 or Claspin directly in the DNA damage sensor complex following replicative stress.

Although signaling pathways are thought to be conserved, individual proteins might be diversely regulated in different species. In ATR-mediated pathway, a unique feature has been reported for human ATR in Seckel syndrome. In humans, Seckel syndrome is “a rare autosomal recessive disorder characterized by growth retardation, microcephaly with mental retardation, and a characteristic 'bird-headed' facial appearance” (ncbi.nlm.nih.gov). In molecular genetics, Seckel syndrome locus has been assigned to 3q22.1-q24 (289) and a mutation in the exon 9 of *ATR* gene is reported in Seckel patients (140). Intriguingly, the A2101G mutation inside exon 9 region of *ATR* gene is synonymous but significantly impairs the proper splicing of exons 8-10 via an unknown mechanism, producing a message with premature termination. This defect only occurs in human *ATR* as no phenotype is observed in mice harboring mouse *Atr* gene with similar mutation (143). Mice harboring human *ATR* exon 8-10 region with A2101G mutation recapitulate human Seckel syndrome, including decreased body weight, brain development defects and premature aging (143), indicating a unique mechanism by which the human *ATR* gene ensures its efficient expression. It is worthwhile to investigate whether similar human-specific mechanisms exist in other DNA damage sensor genes, which are quite important for human genetics and clinical investigation.

Except the ATR-Seckel mice, few studies have been performed to focus on the physiological and pathological functions of the ATR-mediated pathway using an

animal model because of the essential function of ATR/ATRIP in mammalian systems. Nevertheless, cells harboring mutated RPA70 (R41E/R43E)(148) showed a quite normal cell cycle profile but significant defects in ATR-mediated DNA damage response, which provides us an additional feasible model to investigate the RPA-ATR mediated DNA damage response *in vivo*. A mouse model harboring knockin RPA with mutation in the basic cleft region (e.g. R41E/R43E) might develop normally but exhibit severe defects following DNA damage treatments. Other feasible target proteins include, but not limited to, BID mutations in Helix 4 or RPA-ID region, ATRIP mutation in TopBP-binding domain, RAD17 mutation in ATM/ATR phosphorylation sites, and CHK1 mutation in S317 residue.

Other cell death proteins

Besides the canonical apoptotic function in mitochondria, more and more cell death proteins have been demonstrated to play additional roles in other signaling pathways following various cellular stresses (Table 5). BCL-2 has been reported to suppress DNA double strand-break repair and V(D)J recombination by interaction with Ku70 and Ku86 via its BH1 and BH4 domains (266). Following etoposide treatment, MCL-1 is found in the DNA damage complex containing NBS1 and γH2A.X to facilitate ATR-dependent CHK1 phosphorylation (259,260). In addition, the accumulation of nuclear MCL-1 in response to DNA damage is

mediated by interaction with IEX-1 (268). As BID interacts with BCL-2 and MCL-1 by its BH3 domain in cytoplasm, it is quite possible that BID might also interact with BCL-2 and MCL-1 in the nucleus or on the chromatin following genotoxic stress. As the function of MCL-1 on CHK1 phosphorylation is exclusive to ETOP but not HU treatment, it is interesting to investigate the function of BID/MCL-1 in processing DSBs to ssDNA.

Recently, BCL2L12 has been identified as a novel negative regulator of p53 to inhibit p53 transcription factor function following DNA damage response (290). p53 plays dual roles in DNA damage response. p53 activates cell cycle checkpoint and DNA repair proteins to fix the damage. On the other hand, p53 induces the expression of pro-apoptotic proteins to initiate programmed cell death. As BID might play similar roles in DNA damage response, it is possible that BID affects the transcription factor activity of p53 by interaction with other BCL-2 family proteins. Although it is less likely that BID acts as a transcription regulator directly, it is interesting to investigate how Bid -/- p53 -/- cells sense and transduce DNA damage signals to mitochondria.

AVEN, a BCL-XL-interacting protein, has been reported to function as an ATM activator to inhibit G2/M progression (269). Following various DNA damage treatments, BID is phosphorylated by ATM/ATR and the phosphorylation of BID is significantly diminished in *Atm* -/- cells. In my thesis studies, no obvious defects of ATM autophosphorylation (Figure 3-6 C) as well as CHK2 phosphorylation (data

not shown) were observed in *BID* KD cells following etoposide treatment, suggesting that BID plays a minimal role in ATM activation following DSBs. Nevertheless, ATM has also been demonstrated to play a role following oxidative stress *in vitro* and *in vivo* (122,123), and the cleavage of BID by caspase-2 has been demonstrated to be a critical apoptotic signal downstream of endoplasmic reticulum stress (87). Given the close relationship between ROS and ER stress, it is worthwhile to investigate whether BID plays a role at the sensor level following oxidative stress.

Importantly, most of the identifications of these novel functions are at the cellular level, and it is necessary to demonstrate the non-canonical function of these cell death proteins *in vivo* to clarify the physiological and/or pathological significance of these multifunctional proteins.

Table 5. Non-canonical functions of proteins in cell death pathways.

Protein name	Function	Interaction partner
AVEN	An novel ATM activator	ATM
BAX	Inhibit homologous recombination	Unknown
BID	Facilitate ATR function following replicative stress	ATR/ATRIP/RPA
BCL-2	Suppress DSB repair and V(D)J recombination	Ku70/Ku86
BCL2L12	Inhibits the p53 tumor suppressor	p53
MCL-1	Facilitate ATR-mediated CHK1 phosphorylation	CHK1
NOXA	Stimulates glucose consumption and enhance glucose turnover via the pentose phosphate pathway	CDK5

BID's phosphorylation

Following replicative stress, BID interacts with ATRIP and RPA by its Helix 4

and RPA-ID regions, respectively (Figure 3-9 and Figure 4-5). In addition, BID nulcera foci is only observed following DNA damage treatments (2,3) and the association between BID and the DNA damage sensor complex is significantly induced by hydroxyruea treatment in cells (Figure 3-8). It is still unclear how BID-ATRIP and BID-RPA interaction are regulated by DNA damage. Following DNA damage, BID is phosphorylated by ATM and/or ATR (2,3). Mutation in the ATM/ATR consensus phosphorylation sites (S61/64/78A) does not block BID-ATRIP interaction; however, this interaction is not induced by HU treatment (Figure 3-9 B). In addition, ATM/ATR consensus phosphorylation sites mutated BID only partially rescues ATRIP nuclear foci in *BID* KD U2OS cells following HU treatment (Figure 3-11 A, B). Based on these observations, it is reasonable to speculate that the phosphorylation of BID by ATM/ATR following DNA damage facilitate BID's association with the DNA damage sensor complex. In mechanism, the phosphorylation of BID might alter the flexible feature of the long loop region in BID, which might mediate BID to interact with other unknown factors in the DNA damage sensor complex. Alternatively, the phosphorylation of BID might stabilize BID in chromatin and increase its access to various DNA damage sensors. It is interesting to investigate the function of BID (e.g. phosphorylation, localization, interaction) in ATR- and/or ATM- deficient cells following various DNA damage treatments.

Clinical implications

Most of BID's regulation occurs at the post-translational level, and most studies of human tumors have relied on gene expression analysis therefore extensive data on BID in human tumors is not available. Nonetheless, one study in cervical cancer did indicate a correlation of BID expression with clinical outcome. High expression of BID has been reported as an adverse prognostic factor for radiotherapy outcome in carcinoma of the cervix (291), suggesting that BID might play a survival role for cancer cells following DNA damage treatment. In addition, 6.0% of gastric carcinomas have been reported to associate with mutations in *BID* gene (either frameshift or missense mutations), and one mutation in 342G results in a frameshift at the end of Helix 4 domain, which loses the RPA-ID region of BID (292). These observations provide a link between my results and cancer pathophysiology.

Bid -/- cells exhibit a hypersensitivity to chemotherapy drugs inducing replicative stress and the function of BID in the DNA damage response is mediated by its association with ATRIP and RPA in the damage sensor complex. A pharmaceutical inhibitor might be developed to mimic and block the BID-ATRIP or BID-RPA interaction, which might be used in clinic combination therapy with HU to increase DNA damage level and kill rapid proliferating tumor cells efficiently.

REFERENCES

1. **Sancar, A., L. A. Lindsey-Boltz, K. Unsal-Kacmaz, and S. Linn**. 2004. Molecular mechanisms of mammalian DNA repair and the DNA damage checkpoints. Annual Review of Biochemistry **73**:39-85.

2. **Zinkel, S. S., K. E. Hurov, C. Ong, F. M. Abtahl, A. Gross, and S. J. Korsmeyer**. 2005. A role for proapoptotic BID in the DNA-damage response. Cell **122**:579-591.

3. **Kamer, I., R. Sarig, Y. Zaltsman, H. Niv, G. Oberkovitz, L. Regev, G. Haimovich, Y. Lerenthal, R. C. Marcellus, and A. Gross**. 2005. Proapoptotic BID is an ATM effector in the DNA-damage response. Cell **122**:593-603.

4. **Liu, Y., C. C. Bertram, Q. Shi, and S. S. Zinkel**. 2011. Proapoptotic Bid mediates the Atr-directed DNA damage response to replicative stress. Cell Death Differ **18**:841-852.

5. **Liu, Y., S. Vaithiyalingam, Q. Shi, W. J. Chazin, and S. Zinkel**. 2011. BID binds to replication protein A and stimulates ATR function following replicative stress. Molecular and Cellular Biology. (In press)

6. **Liu, Y., A. Aiello, and S. Zinkel**. 2011. Bid preserves the mouse hematopoietic system following hydroxyurea-induced replicative stress. (Submitted)

7. **Danial, N. N. and S. J. Korsmeyer**. 2004. Cell death: Critical control points. Cell **116**:205-219.

8. **Edinger, A. L. and C. B. Thompson**. 2004. Death by design: apoptosis, necrosis and autophagy. Current Opinion in Cell Biology **16**:663-669.

9. **Kerr, J. F., A. H. Wyllie, and A. R. Currie**. 1972. Apoptosis: a basic biological phenomenon with wide-ranging implications in tissue kinetics. Br. J. Cancer **26**:239-257.

10. **Li, M. O., M. R. Sarkisian, W. Z. Mehal, P. Rakic, and R. A. Flavell**. 2003. Phosphatidylserine receptor is required for clearance of apoptotic cells. Science **302**:1560-1563.

11. **Riedl, S. J. and Y. G. Shi**. 2004. Molecular mechanisms of caspase regulation during apoptosis. Nature Reviews Molecular Cell Biology **5**:897-907.

12. **Galluzzi, L. and G. Kroemer**. 2008. Necroptosis: A Specialized Pathway of Programmed Necrosis. Cell **135**:1161-1163.

13. **Levine, B. and D. J. Klionsky**. 2004. Development by self-digestion: Molecular mechanisms and biological functions of autophagy. Developmental Cell **6**:463-477.

14. **Levine, B.** 2007. Cell biology - Autophagy and cancer. Nature **446**:745-747.

15. **Shamas-Din, A., H. Brahmbhatt, B. Leber, and D. W. Andrews**. 2011. BH3-only proteins: Orchestrators of apoptosis. Biochimica et Biophysica Acta-Molecular Cell Research **1813**:508-520.

16. **Lomonosova, E. and G. Chinnadurai**. 2008. BH3-only proteins in apoptosis and beyond: an overview. Oncogene **27**:S2-S19.

17. **Youle, R. J. and A. Strasser**. 2008. The BCL-2 protein family: opposing activities that mediate cell death. Nature Reviews Molecular Cell Biology **9**:47-59.

18. **Li, P., D. Nijhawan, I. Budihardjo, S. M. Srinivasula, M. Ahmad, E. S. Alnemri, and X. D. Wang**. 1997. Cytochrome c and dATP-dependent formation of Apaf-1/caspase-9 complex initiates an apoptotic protease cascade. Cell **91**:479-489.

19. **Jiang, X. J. and X. D. Wang**. 2000. Cytochrome c promotes caspase-9 activation by inducing nucleotide binding to Apaf-1. Journal of Biological Chemistry **275**:31199-31203.

20. **Tait, S. W. G. and D. R. Green**. 2010. Mitochondria and cell death: outer membrane permeabilization and beyond. Nature Reviews Molecular Cell Biology **11**:621-632.

21. **Llambi, F. and D. R. Green**. 2011. Apoptosis and oncogenesis: give and take in the BCL-2 family. Current Opinion in Genetics & Development **21**:12-20.

22. **Bogner, C., B. Leber, and D. W. Andrews**. 2010. Apoptosis: embedded in membranes. Curr. Opin. Cell Biol. **22**:845-851.

23. **Rodriguez, J. and Y. Lazebnik**. 1999. Caspase-9 and APAF-1 form an active holoenzyme. Genes & Development **13**:3179-3184.

24. **Du, C. Y., M. Fang, Y. C. Li, L. Li, and X. D. Wang**. 2000. Smac, a mitochondrial protein that promotes cytochrome c-dependent caspase activation by eliminating IAP inhibition. Cell **102**:33-42.

25. **Verhagen, A. M., P. G. Ekert, M. Pakusch, J. Silke, L. M. Connolly, G. E. Reid, R. L. Moritz, R. J. Simpson, and D. L. Vaux**. 2000. Identification of DIABLO, a mammalian protein that promotes apoptosis by binding to and antagonizing IAP proteins. Cell **102**:43-53.

26. **Suzuki, Y., Y. Imai, H. Nakayama, K. Takahashi, K. Takio, and R. Takahashi**. 2001. A serine protease, HtrA2, is released from the mitochondria and interacts with XIAP, inducing cell death. Molecular Cell **8**:613-621.

27. **Li, L. Y., L. Luo, and X. D. Wang**. 2001. Endonuclease G is an apoptotic DNase when released from mitochondria. Nature **412**:95-99.

28. **Susin, S. A., H. K. Lorenzo, N. Zamzami, I. Marzo, B. E. Snow, G. M. Brothers, J. Mangion, E. Jacotot, P. Costantini, M. Loeffler, N. Larochette, D. R. Goodlett, R. Aebersold, D. P. Siderovski, J. M. Penninger, and G. Kroemer**. 1999. Molecular characterization of mitochondrial apoptosis-inducing factor. Nature **397**:441-446.

29. **Chipuk, J. E. and D. R. Green**. 2008. How do BCL-2 proteins induce mitochondrial outer membrane permeabilization? Trends in Cell Biology **18**:157-164.

30. **Wajant, H.** 2002. The Fas signaling pathway: More than a paradigm. Science **296**:1635-1636.

31. **Li, H. L., H. Zhu, C. J. Xu, and J. Y. Yuan**. 1998. Cleavage of BID by caspase 8 mediates the mitochondrial damage in the Fas pathway of apoptosis. Cell **94**:491-501.

32. **Luo, X., I. Budihardjo, H. Zou, C. Slaughter, and X. D. Wang**. 1998. Bid, a Bcl2 interacting protein, mediates cytochrome c release from mitochondria in response to activation of cell surface death receptors. Cell **94**:481-490.

33. **Scaffidi, C., S. Fulda, A. Srinivasan, C. Friesen, F. Li, K. J. Tomaselli, K. M. Debatin, P. H. Krammer, and M. E. Peter**. 1998. Two CD95 (APO-1/Fas) signaling pathways. Embo Journal **17**:1675-1687.

34. **Cleary, M. L., S. D. Smith, and J. Sklar**. 1986. Cloning and structural analysis of cDNAs for bcl-2 and a hybrid bcl-2/immunoglobulin transcript resulting from the t(14;18) translocation. Cell **47**:19-28.

35. **Tsujimoto, Y., E. Jaffe, J. Cossman, J. Gorham, P. C. Nowell, and C. M. Croce**. 1985. Clustering of breakpoints on chromosome 11 in human B-cell neoplasms with the t(11;14) chromosome translocation. Nature **315**:340-343.

36. **Bakhshi, A., J. P. Jensen, P. Goldman, J. J. Wright, O. W. McBride, A. L. Epstein, and S. J. Korsmeyer**. 1985. Cloning the chromosomal breakpoint of t(14;18) human lymphomas: clustering around JH on chromosome 14 and near a transcriptional unit on 18. Cell **41**:899-906.

37. **Cleary, M. L. and J. Sklar**. 1985. Nucleotide sequence of a t(14;18) chromosomal

breakpoint in follicular lymphoma and demonstration of a breakpoint-cluster region near a transcriptionally active locus on chromosome 18. Proc. Natl. Acad. Sci. U. S. A **82**:7439-7443.

38. **Tsujimoto, Y. and C. M. Croce**. 1986. Analysis of the structure, transcripts, and protein products of bcl-2, the gene involved in human follicular lymphoma. Proc. Natl. Acad. Sci. U. S. A **83**:5214-5218.

39. **Tsujimoto, Y., J. Cossman, E. Jaffe, and C. M. Croce**. 1985. Involvement of the Bcl-2 Gene in Human Follicular Lymphoma. Science **228**:1440-1443.

40. **Vaux, D. L., S. Cory, and J. M. Adams**. 1988. Bcl-2 gene promotes haemopoietic cell survival and cooperates with c-myc to immortalize pre-B cells. Nature **335**:440-442.

41. **McDonnell, T. J., N. Deane, F. M. Platt, G. Nunez, U. Jaeger, J. P. McKearn, and S. J. Korsmeyer**. 1989. bcl-2-immunoglobulin transgenic mice demonstrate extended B cell survival and follicular lymphoproliferation. Cell **57**:79-88.

42. **Linette, G. P., Y. Li, K. Roth, and S. J. Korsmeyer**. 1996. Cross talk between cell death and cell cycle progression: BCL-2 regulates NFAT-mediated activation. Proceedings of the National Academy of Sciences of the United States of America **93**:9545-9552.

43. **Strasser, A.** 2005. The role of BH3-only proteins in the immune system. Nature Reviews Immunology **5**:189-200.

44. **Dewson, G., T. Kratina, H. W. Sim, H. Puthalakath, J. M. Adams, P. M. Colman, and R. M. Kluck**. 2008. To trigger apoptosis, Bak exposes its BH3 domain and homodimerizes via BH3 : Groove interactions. Molecular Cell **30**:369-380.

45. **Chipuk, J. E., T. Moldoveanu, F. Llambi, M. J. Parsons, and D. R. Green**. 2010. The BCL-2 family reunion. Mol. Cell **37**:299-310.

46. **Kuwana, T., M. R. Mackey, G. Perkins, M. H. Ellisman, M. Latterich, R. Schneiter, D. R. Green, and D. D. Newmeyer**. 2002. Bid, Bax, and lipids cooperate to form supramolecular openings in the outer mitochondrial membrane. Cell **111**:331-342.

47. **Wei, M. C., T. Lindsten, V. K. Mootha, S. Weiler, A. Gross, M. Ashiya, C. B. Thompson, and S. J. Korsmeyer**. 2000. tBID, a membrane-targeted death ligand, oligomerizes BAK to release cytochrome c. Genes Dev. **14**:2060-2071.

48. **Kim, H., M. Rafiuddin-Shah, H. C. Tu, J. R. Jeffers, G. P. Zambetti, J. J. D. Hsieh, and E. H. Y. Cheng**. 2006. Hierarchical regulation of mitochondrion-dependent

apoptosis by BCL-2 subfamilies. Nature Cell Biology **8**:1348-1358.

49. **Chipuk, J. E., J. C. Fisher, C. P. Dillon, R. W. Kriwacki, T. Kuwana, and D. R. Green**. 2008. Mechanism of apoptosis induction by inhibition of the anti-apoptotic BCL-2 proteins. Proc. Natl. Acad. Sci. U. S. A **105**:20327-20332.

50. **Lovell, J. F., L. P. Billen, S. Bindner, A. Shamas-Din, C. Fradin, B. Leber, and D. W. Andrews**. 2008. Membrane binding by tBid initiates an ordered series of events culminating in membrane permeabilization by Bax. Cell **135**:1074-1084.

51. **Letai, A., M. C. Bassik, L. D. Walensky, M. D. Sorcinelli, S. Weiler, and S. J. Korsmeyer**. 2002. Distinct BH3 domains either sensitize or activate mitochondrial apoptosis, serving as prototype cancer therapeutics. Cancer Cell **2**:183-192.

52. **Ren, D., H. C. Tu, H. Kim, G. X. Wang, G. R. Bean, O. Takeuchi, J. R. Jeffers, G. P. Zambetti, J. J. Hsieh, and E. H. Cheng**. 2010. BID, BIM, and PUMA are essential for activation of the BAX- and BAK-dependent cell death program. Science **330**:1390-1393.

53. **Willis, S. N., J. I. Fletcher, T. Kaufmann, M. F. van Delft, L. Chen, P. E. Czabotar, H. Ierino, E. F. Lee, W. D. Fairlie, P. Bouillet, A. Strasser, R. M. Kluck, J. M. Adams, and D. C. Huang**. 2007. Apoptosis initiated when BH3 ligands engage multiple Bcl-2 homologs, not Bax or Bak. Science **315**:856-859.

54. **Willis, S. N. and J. M. Adams**. 2005. Life in the balance: how BH3-only proteins induce apoptosis. Current Opinion in Cell Biology **17**:617-625.

55. **Villunger, A., E. M. Michalak, L. Coultas, F. Mullauer, G. Bock, M. J. Ausserlechner, J. M. Adams, and A. Strasser**. 2003. p53- and drug-induced apoptotic responses mediated by BH3-only proteins Puma and Noxa. Science **302**:1036-1038.

56. **Dijkers, P. F., R. H. Medema, J. W. J. Lammers, L. Koenderman, and P. J. Coffer**. 2000. Expression of the pro-apoptotic Bcl-2 family member Bim is regulated by the forkhead transcription factor FKHR-L1. Current Biology **10**:1201-1204.

57. **Zha, J. P., H. Harada, E. Yang, J. Jockel, and S. J. Korsmeyer**. 1996. Serine phosphorylation of death agonist BAD in response to survival factor results in binding to 14-3-3 not BGL-X(L). Cell **87**:619-628.

58. **Xiang, Z., A. A. Ahmed, C. Moller, K. Nakayama, S. Hatakeyama, and G. Nilsson**. 2001. Essential role of the prosurvival bcl-2 homologue A1 in mast cell survival after allergic activation. Journal of Experimental Medicine **194**:1561-1569.

59. **Hamasaki, A., F. Sendo, K. Nakayama, N. Ishida, I. Negishi, K. Nakayama, and S. Hatakeyama**. 1998. Accelerated neutrophil apoptosis in mice lacking A1-a, a subtype of the bcl-2-related A1 gene. Journal of Experimental Medicine **188**:1985-1992.

60. **Ranger, A. M., J. P. Zha, H. Harada, S. R. Datta, N. N. Danial, A. P. Gilmore, J. L. Kutok, M. M. Le Beau, M. E. Greenberg, and S. J. Korsmeyer**. 2003. Bad-deficient mice develop diffuse large B cell lymphoma. Proceedings of the National Academy of Sciences of the United States of America **100**:9324-9329.

61. **Knudson, C. M., K. S. K. Tung, W. G. Tourtellotte, G. A. J. Brown, and S. J. Korsmeyer**. 1995. Bax-Deficient Mice with Lymphoid Hyperplasia and Male Germ-Cell Death. Science **270**:96-99.

62. **Lindsten, T., A. J. Ross, A. King, W. X. Zong, J. C. Rathmell, H. A. Shiels, E. Ulrich, K. G. Waymire, P. Mahar, K. Frauwirth, Y. F. Chen, M. Wei, V. M. Eng, D. M. Adelman, M. C. Simon, A. Ma, J. A. Golden, G. Evan, S. J. Korsmeyer, G. R. MacGregor, and C. B. Thompson**. 2000. The combined functions of proapoptotic Bcl-2 family members Bak and Bax are essential for normal development of multiple tissues. Molecular Cell **6**:1389-1399.

63. **Veis, D. J., C. M. Sorenson, J. R. Shutter, and S. J. Korsmeyer**. 1993. Bcl-2-Deficient Mice Demonstrate Fulminant Lymphoid Apoptosis, Polycystic Kidneys, and Hypopigmented Hair. Cell **75**:229-240.

64. **Print, C. G., K. L. Loveland, L. Gibson, T. Meehan, A. Stylianou, N. Wreford, D. De Kretser, D. Metcalf, F. Kontgen, J. M. Adams, and S. Cory**. 1998. Apoptosis regulator Bcl-w is essential for spermatogenesis but appears otherwise redundant. Proceedings of the National Academy of Sciences of the United States of America **95**:12424-12431.

65. **Ma, A., J. C. Pena, B. Chang, E. Margosian, L. Davidson, F. W. Alt, and C. B. Thompson**. 1995. Bclx Regulates the Survival of Double-Positive Thymocytes. Proceedings of the National Academy of Sciences of the United States of America **92**:4763-4767.

66. **Zinkel, S. S., C. C. Ong, D. O. Ferguson, H. Iwasaki, K. Akashi, R. T. Bronson, J. L. Kutok, F. W. Alt, and S. J. Korsmeyer**. 2003. Proapoptotic BID is required for myeloid homeostasis and tumor suppression. Genes & Development **17**:229-239.

67. **Bouillet, P., D. Metcalf, D. C. S. Huang, D. M. Tarlinton, T. W. H. Kay, F. Kontgen, J. M. Adams, and A. Strasser**. 1999. Proapoptotic Bcl-2 relative bim required for certain apoptotic responses, leukocyte homeostasis, and to preclude autoimmunity.

Science **286**:1735-1738.

68. **Bouillet, P., J. F. Purton, D. I. Godfrey, L. C. Zhang, L. Coultas, H. Puthalakath, M. Pellegrini, S. Cory, J. M. Adams, and A. Strasser**. 2002. BH3-only Bcl-2 family member Bim is required for apoptosis of autoreactive thymocytes. Nature **415**:922-926.

69. **Villunger, A., C. Scott, P. Bouillet, and A. Strasser**. 2003. Essential role for the BH3-only protein Bim but redundant roles for Bax, Bcl-2, and Bcl-w in the control of granulocyte survival. Blood **101**:2393-2400.

70. **Fischer, S. F., P. Bouillet, K. O'Donnell, A. Light, D. M. Tarlinton, and A. Strasser**. 2007. Proapoptotic BH3-only protein Bim is essential for developmentally programmed death of germinal center-derived memory B cells and antibody-forming cells. Blood **110**:3978-3984.

71. **Opferman, J. T., A. Letai, C. Beard, M. D. Sorcinelli, C. C. Ong, and S. J. Korsmeyer**. 2003. Development and maintenance of B and T lymphocytes requires antiapoptotic MCL-1. Nature **426**:671-676.

72. **Opferman, J. T., H. Iwasaki, C. C. Ong, H. Suh, S. Mizuno, K. Akashi, and S. J. Korsmeyer**. 2005. Obligate role of anti-apoptotic MCL-1 in the survival of hematopoietic stem cells. Science **307**:1101-1104.

73. **Wang, K., X. M. Yin, D. T. Chao, C. L. Milliman, and S. J. Korsmeyer**. 1996. BID: A novel BH3 domain-only death agonist. Genes & Development **10**:2859-2869.

74. **McDonnell, J. M., D. Fushman, C. L. Milliman, S. J. Korsmeyer, and D. Cowburn**. 1999. Solution structure of the proapoptotic molecule BID: A structural basis for apoptotic agonists and antagonists. Cell **96**:625-634.

75. **Chou, J. J., H. L. Li, G. S. Salvesen, J. Y. Yuan, and G. Wagner**. 1999. Solution structure of BID, an intracellular amplifier of apoptotic signaling. Cell **96**:615-624.

76. **Yin, X. M., K. Wang, A. Gross, Y. G. Zhao, S. Zinkel, B. Klocke, K. A. Roth, and S. J. Korsmeyer**. 1999. Bid-deficient mice are resistant to Fas-induced hepatocellular apoptosis. Nature **400**:886-891.

77. **Kaufmann, T., L. Tai, P. G. Ekert, D. C. S. Huang, F. Norris, R. K. Lindemann, R. W. Johnstone, V. M. Dixit, and A. Strasser**. 2007. The BH3-only protein bid is dispensable for DNA darnage- and replicative stress-induced apoptosis or cell-cycle arrest. Cell **129**:423-433.

78. **Shelton, S. N., M. E. Shawgo, and J. D. Robertson**. 2009. Cleavage of Bid by

Executioner Caspases Mediates Feed Forward Amplification of Mitochondrial Outer Membrane Permeabilization during Genotoxic Stress-induced Apoptosis in Jurkat Cells. Journal of Biological Chemistry **284**:11247-11255.

79. **Maas, C., V. E. de, S. W. Tait, and J. Borst**. 2011. Bid can mediate a pro-apoptotic response to etoposide and ionizing radiation without cleavage in its unstructured loop and in the absence of p53. Oncogene 30:3636-3647.

80. **Song, G., G. G. Chen, D. K. F. Chau, J. Miao, and P. B. S. Lai**. 2008. Bid exhibits S phase checkpoint activation and plays a pro-apoptotic role in response to etoposide-induced DNA damage in hepatocellular carcinoma cells. Apoptosis **13**:693-701.

81. **Oberkovitz, G., L. Regev, and A. Gross**. 2007. Nucleocytoplasmic shuttling of BID is involved in regulating its activities in the DNA-damage response. Cell Death and Differentiation **14**:1628-1634.

82. **Stracker, T. H., M. Morales, S. S. Couto, H. Hussein, and J. H. J. Petrini**. 2007. The carboxy terminus of NBS1 is required for induction of apoptosis by the MRE11 complex. Nature **447**:218-221.

83. **Pradhan, S., H. K. Kim, C. J. Thrash, M. A. Cox, S. K. Mantena, J. H. Wu, M. Athar, S. K. Katiyar, C. A. Elmets, and L. Timares**. 2008. A critical role for the proapoptotic protein bid in ultraviolet-induced immune suppression and cutaneous apoptosis. Journal of Immunology **181**:3077-3088.

84. **Zha, J. P., S. Weiler, K. J. Oh, M. C. Wei, and S. J. Korsmeyer**. 2000. Posttranslational N-myristoylation of BID as a molecular switch for targeting mitochondria and apoptosis. Science **290**:1761-1765.

85. **Denisov, A. Y., G. Chen, T. Sprules, T. Moldoveanu, P. Beauparlant, and K. Gehring**. 2006. Structural model of the BCL-w-BID peptide complex and its interactions with phospholipid micelles. Biochemistry **45**:2250-2256.

86. **Bonzon, C., L. Bouchier-Hayes, L. J. Pagliari, D. R. Green, and D. D. Newmeyer**. 2006. Caspase-2-induced apoptosis requires bid cleavage: A physiological role for bid in heat shock-induced death. Molecular Biology of the Cell **17**:2150-2157.

87. **Upton, J. P., K. Austgen, M. Nishino, K. M. Coakley, A. Hagen, D. Han, F. R. Papa, and S. A. Oakes**. 2008. Caspase-2 cleavage of BID is a critical apoptotic signal downstream of endoplasmic reticulum stress. Molecular and Cellular Biology **28**:3943-3951.

88. **Desagher, S., A. Osen-Sand, S. Montessuit, E. Magnenat, F. Vilbois, A. Hochmann, L. Journot, B. Antonsson, and J. C. Martinou**. 2001. Phosphorylation of bid by casein kinases I and II regulates its cleavage by caspase 8. Molecular Cell **8**:601-611.

89. **Mandic, A., K. Viktorsson, L. Strandberg, T. Heiden, J. Hansson, S. Linder, and M. C. Shoshan**. 2002. Calpain-mediated bid cleavage and calpain-independent Bak modulation: Two separate pathways in cisplatin-induced apoptosis. Molecular and Cellular Biology **22**:3003-3013.

90. **Cirman, T., K. Oresic, G. D. Mazovec, V. Turk, J. C. Reed, R. M. Myers, G. S. Salvesen, and B. Turk**. 2004. Selective disruption of lysosomes in HeLa cells triggers apoptosis mediated by cleavage of bid by multiple papain-like lysosomal cathepsins. Journal of Biological Chemistry **279**:3578-3587.

91. **Sutton, V. R., J. E. Davis, M. Cancilla, R. W. Johnstone, A. A. Ruefli, K. Sedelies, K. A. Browne, and J. A. Trapani**. 2000. Initiation of apoptosis by granzyme B requires direct cleavage of bid, but not direct granzyme B-mediated caspase activation. J. Exp. Med. **192**:1403-1414.

92. **Simmen, T., J. E. Aslan, A. D. Blagoveshchenskaya, L. Thomas, L. Wan, Y. Xiang, S. F. Feliciangeli, C. H. Hung, C. M. Crump, and G. Thomas**. 2005. PACS-2 controls endoplasmic reticulum-mitochondria communication and Bid-mediated apoptosis. Embo Journal **24**:717-729.

93. **Matsuoka, S., B. A. Ballif, A. Smogorzewska, E. R. McDonald, K. E. Hurov, J. Luo, C. E. Bakalarski, Z. M. Zhao, N. Solimini, Y. Lerenthal, Y. Shiloh, S. P. Gygi, and S. J. Elledge**. 2007. ATM and ATR substrate analysis reveals extensive protein networks responsive to DNA damage. Science **316**:1160-1166.

94. **Gonzalvez, F., F. Pariselli, O. Jalmar, P. Dupaigne, F. Sureau, M. Dellinger, E. A. Hendrickson, S. Bernard, and P. X. Petit**. 2010. Mechanistic Issues of the Interaction of the Hairpin-Forming Domain of tBid with Mitochondrial Cardiolipin. Plos One **5**.

95. **Lutter, M., M. Fang, X. Luo, M. Nishijima, X. S. Xie, and X. D. Wang**. 2000. Cardiolipin provides specificity for targeting of tBid to mitochondria. Nature Cell Biology **2**:754-756.

96. **Esposti, M. D., I. M. Cristea, S. J. Gaskell, Y. Nakao, and C. Dive**. 2003. Proapoptotic Bid binds to monolysocardiolipin, a new molecular connection between mitochondrial membranes and cell death. Cell Death Differ. **10**:1300-1309.

97. **Plesnila, N., S. Zinkel, D. A. Le, S. min-Hanjani, Y. Wu, J. Qiu, A. Chiarugi, S. S. Thomas, D. S. Kohane, S. J. Korsmeyer, and M. A. Moskowitz**. 2001. BID mediates neuronal cell death after oxygen/ glucose deprivation and focal cerebral ischemia. Proc. Natl. Acad. Sci. U. S. A **98**:15318-15323.

98. **Wei, Q., X. M. Yin, M. H. Wang, and Z. Dong**. 2006. Bid deficiency ameliorates ischemic renal failure and delays animal death in C57BL/6 mice. Am. J. Physiol Renal Physiol **290**:F35-F42.

99. **Bai, L., H. M. Ni, X. Chen, D. DiFrancesca, and X. M. Yin**. 2005. Deletion of Bid impedes cell proliferation and hepatic carcinogenesis. Am. J. Pathol. **166**:1523-1532.

100. **Bernstein, C., H. Bernstein, C. M. Payne, and H. Garewal**. 2002. DNA repair/pro-apoptotic dual-role proteins in five major DNA repair pathways: fail-safe protection against carcinogenesis. Mutation Research-Reviews in Mutation Research **511**:145-178.

101. **Soutoglou, E. and T. Misteli**. 2008. Activation of the Cellular DNA Damage Response in the Absence of DNA Lesions. Science **320**:1507-1510.

102. **Norbury, C. J. and I. D. Hickson**. 2001. Cellular responses to DNA damage. Annual Review of Pharmacology and Toxicology **41**:367-401.

103. **Akhtar, R. S., Y. Geng, B. J. Klocke, and K. A. Roth**. 2006. Neural precursor cells possess multiple p53-dependent apoptotic pathways. Cell Death and Differentiation **13**:1727-1739.

104. **Coultas, L. and A. Strasser**. 2000. The molecular control of DNA damage-induced cell death. Apoptosis **5**:491-507.

105. **Mohrin, M., E. Bourke, D. Alexander, M. R. Warr, K. Barry-Holson, M. M. Le Beau, C. G. Morrison, and E. Passegue**. 2010. Hematopoietic Stem Cell Quiescence Promotes Error-Prone DNA Repair and Mutagenesis. Cell Stem Cell **7**:174-185.

106. **Seita, J., D. J. Rossi, and I. L. Weissman**. 2010. Differential DNA Damage Response in Stem and Progenitor Cells. Cell Stem Cell **7**:145-147.

107. **Milyavsky, M., O. I. Gan, M. Trottier, M. Komosa, O. Tabach, F. Notta, E. Lechman, K. G. Hermans, K. Eppert, Z. Konovalova, O. Ornatsky, E. Domany, M. S. Meyn, and J. E. Dick**. 2010. A Distinctive DNA Damage Response in Human Hematopoietic Stem Cells Reveals an Apoptosis-Independent Role for p53 in

Self-Renewal. Cell Stem Cell **7**:186-197.

108. **Cortez, D., S. Guntuku, J. Qin, and S. J. Elledge**. 2001. ATR and ATRIP: Partners in checkpoint signaling. Science **294**:1713-1716.

109. **Bakkenist, C. J. and M. B. Kastan**. 2003. DNA damage activates ATM through intermolecular autophosphorylation and dimer dissociation. Nature **421**:499-506.

110. **Falck, J., J. Coates, and S. P. Jackson**. 2005. Conserved modes of recruitment of ATM, ATR and DNA-PKcs to sites of DNA damage. Nature **434**:605-611.

111. **Lee, J. H. and T. T. Paull**. 2005. ATM activation by DNA double-strand breaks through the Mre11-Rad50-Nbs1 complex. Science **308**:551-554.

112. **Kim, S. T., D. S. Lim, C. E. Canman, and M. B. Kastan**. 1999. Substrate specificities and identification of putative substrates of ATM kinase family members. Journal of Biological Chemistry **274**:37538-37543.

113. **Traven, A. and J. Heierhorst**. 2005. SQ/TQ cluster domains: concentrated ATM/ATR kinase phosphorylation site regions in DNA-damage-response proteins. Bioessays **27**:397-407.

114. **Abraham, R. T.** 2004. PI 3-kinase related kinases: 'big' players in stress-induced signaling pathways. Dna Repair **3**:883-887.

115. **Perry, J. and N. Kleckner**. 2003. The ATRs, ATMs, and TORs are giant HEAT repeat proteins. Cell **112**:151-155.

116. **Falck, J., N. Mailand, R. G. Syljuasen, J. Bartek, and J. Lukas**. 2001. The ATM-Chk2-Cdc25A checkpoint pathway guards against radioresistant DNA synthesis. Nature **410**:842-847.

117. **Dunphy, W. G. and A. Kumagai**. 1991. The Cdc25 Protein Contains An Intrinsic Phosphatase-Activity. Cell **67**:189-196.

118. **Gautier, J., M. J. Solomon, R. N. Booher, J. F. Bazan, and M. W. Kirschner**. 1991. Cdc25 Is A Specific Tyrosine Phosphatase That Directly Activates P34Cdc2. Cell **67**:197-211.

119. **Gu, Y., J. Rosenblatt, and D. O. Morgan**. 1992. Cell cycle regulation of CDK2 activity by phosphorylation of Thr160 and Tyr15. EMBO J. **11**:3995-4005.

120. **Savitsky, K., A. Barshira, S. Gilad, G. Rotman, Y. Ziv, L. Vanagaite, D. A. Tagle, S. Smith, T. Uziel, S. Sfez, M. Ashkenazi, I. Pecker, M. Frydman, R. Harnik, S. R.**

Patanjali, A. Simmons, G. A. Clines, A. Sartiel, R. A. Gatti, L. Chessa, O. Sanal, M. F. Lavin, N. G. J. Jaspers, A. Malcolm, R. Taylor, C. F. Arlett, T. Miki, S. M. Weissman, M. Lovett, F. S. Collins, and Y. Shiloh. 1995. A Single Ataxia-Telangiectasia Gene with A Product Similar to Pi-3 Kinase. Science **268**:1749-1753.

121. **Barlow, C., S. Hirotsune, R. Paylor, M. Liyanage, M. Eckhaus, F. Collins, Y. Shiloh, J. N. Crawley, T. Ried, D. Tagle, and A. WynshawBoris**. 1996. Atm-deficient mice: A paradigm of ataxia telangiectasia. Cell **86**:159-171.

122. **Guo, Z., S. Kozlov, M. F. Lavin, M. D. Person, and T. T. Paull**. 2010. ATM Activation by Oxidative Stress. Science **330**:517-521.

123. **Ito, K., A. Hirao, F. Arai, S. Matsuoka, K. Takubo, I. Hamaguchi, K. Nomiyama, K. Hosokawa, K. Sakurada, N. Nakagata, Y. Ikeda, T. W. Mak, and T. Suda**. 2004. Regulation of oxidative stress by ATM is required for self-renewal of haematopoietic stem cells. Nature **431**:997-1002.

124. **Cimprich, K. A. and D. Cortez**. 2008. ATR: an essential regulator of genome integrity. Nature Reviews Molecular Cell Biology **9**:616-627.

125. **Zou, L. and S. J. Elledge**. 2003. Sensing DNA damage through ATRIP recognition of RPA-ssDNA complexes. Science **300**:1542-1548.

126. **Zou, L., D. Cortez, and S. J. Elledge**. 2002. Regulation of ATR substrate selection by Rad17-dependent loading of Rad9 complexes onto chromatin. Genes & Development **16**:198-208.

127. **Delacroix, S., J. M. Wagner, M. Kobayashi, K. Yamamoto, and L. M. Karnitz**. 2007. The Rad9-Hus1-Rad1 (9-1-1) clamp activates checkpoint signaling via TopBP1. Genes & Development **21**:1472-1477.

128. **Kumagai, A., J. Lee, H. Y. Yoo, and W. G. Dunphy**. 2006. TopBP1 activates the ATR-ATRIP complex. Cell **124**:943-955.

129. **Mordes, D. A., G. G. Glick, R. Zhao, and D. Cortez**. 2008. TopBP1 activates ATR through ATRIP and a PIKK regulatory domain. Genes & Development **22**:1478-1489.

130. **Liu, Q. H., S. Guntuku, X. S. Cui, S. Matsuoka, D. Cortez, K. Tamai, G. B. Luo, S. Carattini-Rivera, F. DeMayo, A. Bradley, L. A. Donehower, and S. J. Elledge**. 2000. Chk1 is an essential kinase that is regulated by Atr and required for the G(2)/M DNA damage checkpoint. Genes & Development **14**:1448-1459.

131. **Jeong, S. Y., A. Kumagai, J. Lee, and W. G. Dunphy**. 2003. Phosphorylated claspin interacts with a phosphate-binding site in the kinase domain of Chk1 during ATR-mediated activation. Journal of Biological Chemistry **278**:46782-46788.

132. **Wang, X., L. Zou, T. Lu, S. Bao, K. E. Hurov, W. N. Hittelman, S. J. Elledge, and L. Li**. 2006. Rad17 phosphorylation is required for claspin recruitment and Chk1 activation in response to replication stress. Molecular Cell **23**:331-341.

133. **Katsuragi, Y. and N. Sagata**. 2004. Regulation of Chk1 kinase by autoinhibition and ATR-mediated phosphorylation. Molecular Biology of the Cell **15**:1680-1689.

134. **Smits, V. A. J., P. M. Reaper, and S. P. Jackson**. 2006. Rapid PIKK-dependent release of Chk1 from chromatin promotes the DNA-damage checkpoint response. Current Biology **16**:150-159.

135. **Shimada, M., H. Niida, D. H. Zineldeen, H. Tagami, M. Tanaka, H. Saito, and M. Nakanishi**. 2008. Chk1 is a histone H3 threonine 11 kinase that regulates DNA damage-induced transcriptional repression. Cell **132**:221-232.

136. **Sanchez, Y., C. Wong, R. S. Thoma, R. Richman, R. Q. Wu, H. PiwnicaWorms, and S. J. Elledge**. 1997. Conservation of the Chk1 checkpoint pathway in mammals: Linkage of DNA damage to Cdk regulation through Cdc25. Science **277**:1497-1501.

137. **Peng, C. Y., P. R. Graves, R. S. Thoma, Z. Wu, A. S. Shaw, and H. Piwnica-Worms**. 1997. Mitotic and G2 checkpoint control: regulation of 14-3-3 protein binding by phosphorylation of Cdc25C on serine-216. Science **277**:1501-1505.

138. **Leung-Pineda, V., C. E. Ryan, and H. Piwnica-Worms**. 2006. Phosphorylation of Chk1 by ATR is antagonized by a Chk1-regulated protein phosphatase 2A circuit. Molecular and Cellular Biology **26**:7529-7538.

139. **Zhang, Y. W., D. M. Otterness, G. G. Chiang, W. L. Xie, Y. C. Liu, F. Mercurio, and R. T. Abraham**. 2005. Genotoxic stress targets human Chk1 for degradation by the ubipuitin-proteasome pathway. Molecular Cell **19**:607-618.

140. **O'Driscoll, M., V. L. Ruiz-Perez, C. G. Woods, P. A. Jeggo, and J. A. Goodship**. 2003. A splicing mutation affecting expression of ataxia-telangiectasia and Rad3-related protein (ATR) results in Seckel syndrome. Nature Genetics **33**:497-501.

141. **Brown, E. J. and D. Baltimore**. 2000. ATR disruption leads to chromosomal

fragmentation and early embryonic lethality. Genes & Development **14**:397-402.

142. **de Klein, A., M. Muijtjens, R. van Os, Y. Verhoeven, B. Smit, A. M. Carr, A. R. Lehmann, and J. H. J. Hoeijmakers**. 2000. Targeted disruption of the cell-cycle checkpoint gene ATR leads to early embryonic lethality in mice. Current Biology **10**:479-482.

143. **Murga, M., S. Bunting, M. F. Montana, R. Soria, F. Mulero, M. Canamero, Y. Lee, P. J. McKinnon, A. Nussenzweig, and O. Fernandez-Capetillo**. 2009. A mouse model of ATR-Seckel shows embryonic replicative stress and accelerated aging. Nature Genetics **41**:891-898.

144. **Ruzankina, Y., D. W. Schoppy, A. Asare, C. E. Clark, R. H. Vonderheide, and E. J. Brown**. 2009. Tissue regenerative delays and synthetic lethality in adult mice after combined deletion of Atr and Trp53. Nature Genetics **41**:1144-1149.

145. **Ruzankina, Y., C. Pinzon-Guzman, A. Asare, T. Ong, L. Pontano, G. Cotsarelis, V. P. Zediak, M. Velez, A. Bhandoola, and E. J. Brown**. 2007. Deletion of the developmentallv essential gene ATR in adult mice leads to age-related phenotypes and stem cell loss. Cell Stem Cell **1**:113-126.

146. **Niida, H., Y. Katsuno, B. Banerjee, M. P. Hande, and M. Nakanishi**. 2007. Specific role of Chk1 phosphorylations in cell survival and checkpoint activation. Molecular and Cellular Biology **27**:2572-2581.

147. **Zou, Y., Y. Y. Liu, X. M. Wu, and S. M. Shell**. 2006. Functions of human replication protein A (RPA): From DNA replication to DNA damage and stress responses. Journal of Cellular Physiology **208**:267-273.

148. **Xu, X., S. Vaithiyalingam, G. G. Glick, D. A. Mordes, W. J. Chazin, and D. Cortez**. 2008. The Basic Cleft of RPA70N Binds Multiple Checkpoint Proteins, Including RAD9, To Regulate ATR Signaling. Molecular and Cellular Biology **28**:7345-7353.

149. **Culligan, K., A. Tissier, and A. Britt**. 2004. ATR regulates a G2-phase cell-cycle checkpoint in Arabidopsis thaliana. Plant Cell **16**:1091-1104.

150. **Paulsen, R. D. and K. A. Cimprich**. 2007. The ATR pathway: Fine-tuning the fork. Dna Repair **6**:953-966.

151. **Sartori, A. A., C. Lukas, J. Coates, M. Mistrik, S. Fu, J. Bartek, R. Baer, J. Lukas, and S. P. Jackson**. 2007. Human CtIP promotes DNA end resection. Nature **450**:509-514.

152. **Yu, X. C. and J. J. Chen**. 2004. DNA damage-induced cell cycle checkpoint control

requires CtIP, a phosphorylation-dependent binding partner of BRCA1 C-terminal domains. Molecular and Cellular Biology **24**:9478-9486.

153. **Cuadrado, M., B. Martinez-Pastor, M. Murga, L. I. Toledo, P. Gutierrez-Martinez, E. Lopez, and O. Fernandez-Capetillo**. 2006. ATM regulates ATR chromatin loading in response to DNA double-strand breaks. Journal of Experimental Medicine **203**:297-303.

154. **Zaugg, K., Y. W. Su, P. T. Reilly, Y. Moolani, C. C. Cheung, R. Hakem, A. Hirao, S. J. Elledge, and T. W. Mak**. 2007. Cross-talk between Chk1 and Chk2 in double-mutant thymocytes. Proceedings of the National Academy of Sciences of the United States of America **104**:3805-3810.

155. **Wobbe, C. R., L. Weissbach, J. A. Borowiec, F. B. Dean, Y. Murakami, P. Bullock, and J. Hurwitz**. 1987. Replication of Simian Virus-40 Origin-Containing Dna Invitro with Purified Proteins. Proceedings of the National Academy of Sciences of the United States of America **84**:1834-1838.

156. **Wold, M. S. and T. Kelly**. 1988. Purification and Characterization of Replication Protein-A, A Cellular Protein Required for Invitro Replication of Simian Virus-40 Dna. Proceedings of the National Academy of Sciences of the United States of America **85**:2523-2527.

157. **Fairman, M. P. and B. Stillman**. 1988. Cellular Factors Required for Multiple Stages of Sv40 Dna-Replication Invitro. Embo Journal **7**:1211-1218.

158. **Wold, M. S.** 1997. Replication protein A: A heterotrimeric, single-stranded DNA-binding protein required for eukaryotic DNA metabolism. Annual Review of Biochemistry **66**:61-92.

159. **Fanning, E., V. Klimovich, and A. R. Nager**. 2006. A dynamic model for replication protein A (RPA) function in DNA processing pathways. Nucleic Acids Research **34**:4126-4137.

160. **He, Z. G., L. A. Henricksen, M. S. Wold, and C. J. Ingles**. 1995. Rpa Involvement in the Damage-Recognition and Incision Steps of Nucleotide Excision-Repair. Nature **374**:566-569.

161. **Li, L., X. Y. Lu, C. A. Peterson, and R. J. Legerski**. 1995. An Interaction Between the Dna-Repair Factor Xpa and Replication Protein-A Appears Essential for Nucleotide Excision-Repair. Molecular and Cellular Biology **15**:5396-5402.

162. **Matsuda, T., M. Saijo, I. Kuraoka, T. Kobayashi, Y. Nakatsu, A. Nagai, T. Enjoji,**

C. Masutani, K. Sugasawa, F. Hanaoka, A. Yasui, and K. Tanaka. 1995. Dna-Repair Protein Xpa Binds Replication Protein-A (Rpa). Journal of Biological Chemistry **270**:4152-4157.

163. **Sung, P.** 1994. Catalysis of Atp-Dependent Homologous Dna Pairing and Strand Exchange by Yeast Rad51 Protein. Science **265**:1241-1243.

164. **Stauffer, M. E. and W. J. Chazin**. 2004. Physical interaction between replication protein A and Rad51 promotes exchange on single-stranded DNA. Journal of Biological Chemistry **279**:25638-25645.

165. **Sung, P. and D. L. Robberson**. 1995. Dna Strand Exchange Mediated by A Rad51-Ssdna Nucleoprotein Filament with Polarity Opposite to That of Reca. Cell **82**:453-461.

166. **Bochkarev, A. and E. Bochkareva**. 2004. From RPA to BRCA2: lessons from single-stranded DNA binding by the OB-fold. Current Opinion in Structural Biology **14**:36-42.

167. **Theobald, D. L., R. M. Mitton-Fry, and D. S. Wuttke**. 2003. Nucleic acid recognition by OB-fold proteins. Annual Review of Biophysics and Biomolecular Structure **32**:115-133.

168. **Iftode, C. and J. A. Borowiec**. 2000. 5 ' -> 3 ' molecular polarity of human replication protein A (hRPA) binding to pseudo-origin DNA substrates. Biochemistry **39**:11970-11981.

169. **de Laat, W. L., E. Appeldoorn, K. Sugasawa, E. Weterings, N. G. J. Jaspers, and J. H. J. Hoeijmakers**. 1998. DNA-binding polarity of human replication protein A positions nucleases in nucleotide excision repair. Genes & Development **12**:2598-2609.

170. **Bochkarev, A., R. A. Pfuetzner, A. M. Edwards, and L. Frappier**. 1997. Structure of the single-stranded-DNA-binding domain of replication protein A bound to DNA. Nature **385**:176-181.

171. **Cai, L. F., M. Roginskaya, Y. X. Qu, Z. G. Yang, Y. Xu, and Y. Zou**. 2007. Structural characterization of human RPA sequential binding to single-stranded DNA using ssDNA as a molecular ruler. Biochemistry **46**:8226-8233.

172. **Kim, C. S., B. F. Paulus, and M. S. Wold**. 1994. Interactions of Human Replication Protein-A with Oligonucleotides. Biochemistry **33**:14197-14206.

173. **Bochkareva, E., S. Korolev, S. P. Lees-Miller, and A. Bochkarev**. 2002. Structure

of the RPA trimerization core and its role in the multistep DNA-binding mechanism of RPA. Embo Journal **21**:1855-1863.

174. **Bochkareva, E., V. Belegu, S. Korolev, and A. Bochkarev**. 2001. Structure of the major single-stranded DNA-binding domain of replication protein A suggests a dynamic mechanism for DNA binding. Embo Journal **20**:612-618.

175. **Blackwell, L. J., J. A. Borowiec, and I. A. Mastrangelo**. 1996. Single-stranded-DNA binding alters human replication protein a structure and facilitates interaction with DNA-dependent protein kinase. Molecular and Cellular Biology **16**:4798-4807.

176. **Mordes, D. A. and D. Cortez**. 2008. Activation of ATR and related PIKKs. Cell Cycle **7**:2809-2812.

177. **Bochkareva, E., L. Kaustov, A. Ayed, G. S. Yi, Y. Lu, A. Pineda-Lucena, J. C. C. Liao, A. L. Okorokov, J. Milner, C. H. Arrowsmith, and A. Bochkarev**. 2005. Single-stranded DNA mimicry in the p53 transactivation domain interaction with replication protein A. Proceedings of the National Academy of Sciences of the United States of America **102**:15412-15417.

178. **Arunkumar, A. I., V. Klimovich, X. H. Jiang, R. D. Ott, L. Mizoue, E. Fanning, and W. J. Chazin**. 2005. Insights into hRPA32 C-terminal domain-mediated assembly of the simian virus 40 replisome. Nature Structural & Molecular Biology **12**:332-339.

179. **Han, Y. F., Y. M. Loo, K. T. Militello, and T. Melendy**. 1999. Interactions of the papovavirus DNA replication initiator proteins, bovine papillomavirus type 1 E1 and simian virus 40 large T antigen, with human replication protein A. Journal of Virology **73**:4899-4907.

180. **Weisshart, K., P. Taneja, and E. Fanning**. 1998. The replication protein A binding site in simian virus 40 (SV40) T antigen and its role in the initial steps of SV40 DNA replication. Journal of Virology **72**:9771-9781.

181. **Vassin, V. M., R. W. Anantha, E. Sokolova, S. Kanner, and J. A. Borowiec**. 2009. Human RPA phosphorylation by ATR stimulates DNA synthesis and prevents ssDNA accumulation during DNA-replication stress. Journal of Cell Science **122**:4070-4080.

182. **Olson, E., C. J. Nievera, V. Klimovich, E. Fanning, and X. H. Wu**. 2006. RPA2 is a direct downstream target for ATR to regulate the S-phase checkpoint. Journal of Biological Chemistry **281**:39517-39533.

183. **Sogo, J. M., M. Lopes, and M. Foiani**. 2002. Fork reversal and ssDNA accumulation at stalled replication forks owing to checkpoint defects. Science **297**:599-602.

184. **Robison, J. G., J. Elliott, K. Dixon, and G. G. Oakley**. 2004. Replication protein A and the Mre11 center dot Rad50 center dot Nbs1 complex co-localize and interact at sites of stalled replication forks. Journal of Biological Chemistry **279**:34802-34810.

185. **Unsal-Kacmaz, K., P. D. Chastain, P. P. Qu, P. Minoo, M. Cordeiro-Stone, A. Sancar, and W. K. Kaufmann**. 2007. The human Tim/Tipin complex coordinates an intra-S checkpoint response to UV that slows replication fork displacement. Molecular and Cellular Biology **27**:3131-3142.

186. **Bansbach, C. E., R. Betous, C. A. Lovejoy, G. G. Glick, and D. Cortez**. 2009. The annealing helicase SMARCAL1 maintains genome integrity at stalled replication forks. Genes & Development **23**:2405-2414.

187. **Ciccia, A., A. L. Bredemeyer, M. E. Sowa, M. E. Terret, P. V. Jallepalli, J. W. Harper, and S. J. Elledge**. 2009. The SIOD disorder protein SMARCAL1 is an RPA-interacting protein involved in replication fork restart. Genes & Development **23**:2415-2425.

188. **Yusufzai, T., X. D. Kong, K. Yokomori, and J. T. Kadonaga**. 2009. The annealing helicase HARP is recruited to DNA repair sites via an interaction with RPA. Genes & Development **23**:2400-2404.

189. **Yuan, J. S., G. Ghosal, and J. J. Chen**. 2009. The annealing helicase HARP protects stalled replication forks. Genes & Development **23**:2394-2399.

190. **Shieh, S. Y., J. Ahn, K. Tamai, Y. Taya, and C. Prives**. 2000. The human homologs of checkpoint kinases Chk1 and Cds1 (Chk2) phosphorylate p53 at multiple DNA damage-inducible sites. Genes & Development **14**:289-300.

191. **Shieh, S. Y., M. Ikeda, Y. Taya, and C. Prives**. 1997. DNA damage-induced phosphorylation of p53 alleviates inhibition by MDM2. Cell **91**:325-334.

192. **Moll, U. M., S. Wolff, D. Speidel, and W. Deppert**. 2005. Transcription-independent pro-apoptotic functions of p53. Current Opinion in Cell Biology **17**:631-636.

193. **Tinel, A. and J. Tschopp**. 2004. The PIDDosome, a protein complex implicated in activation of caspase-2 in response to genotoxic stress. Science **304**:843-846.

194. **Konishi, A., S. Shimizu, J. Hirota, T. Takao, Y. H. Fan, Y. Matsuoka, L. L. Zhang,**

Y. Yoneda, Y. Fujii, A. I. Skouitchi, and Y. Tsujimoto. 2003. Involvement of histone H1.2 in apoptosis induced by DNA double-strand breaks. Cell **114**:673-688.

195. **Harkin, D. P., J. M. Bean, D. Miklos, Y. H. Song, V. B. Truong, C. Englert, F. C. Christians, L. W. Ellisen, S. Maheswaran, J. D. Oliner, and D. A. Haber**. 1999. Induction of GADD45 and JNK/SAPK-dependent apoptosis following inducible expression of BRCA1. Cell **97**:575-586.

196. **Thangaraju, M., S. H. Kaufmann, and F. J. Couch**. 2000. BRCA1 facilitates stress-induced apoptosis in breast and ovarian cancer cell lines. Journal of Biological Chemistry **275**:33487-33496.

197. **Sidi, S., T. Sanda, R. D. Kennedy, A. T. Hagen, C. A. Jette, R. Hoffmans, J. Pascual, S. Imamura, S. Kishi, J. F. Amatruda, J. P. Kanki, D. R. Green, A. A. D'Andrea, and A. T. Look**. 2008. Chk1 suppresses a caspase-2 apoptotic response to DNA damage that bypasses p53, Bcl-2, and caspase-3. Cell **133**:864-877.

198. **Myers, K., M. E. Gagou, P. Zuazua-Villar, R. Rodriguez, and M. Meuth**. 2009. ATR and Chk1 Suppress a Caspase-3-Dependent Apoptotic Response Following DNA Replication Stress. Plos Genetics **5**.

199. **Venezia, T. A., A. A. Merchant, C. A. Ramos, N. L. Whitehouse, A. S. Young, C. A. Shaw, and M. A. Goodell**. 2004. Molecular signatures of proliferation and quiescence in hematopoietic stem cells. Plos Biology **2**:1640-1651.

200. **Kondo, M., A. J. Wagers, M. G. Manz, S. S. Prohaska, D. C. Scherer, G. E. Beilhack, J. A. Shizuru, and I. L. Weissman**. 2003. Biology of hematopoietic stem cells and progenitors: Implications for clinical application. Annual Review of Immunology **21**:759-806.

201. **Weissman, I. L., D. J. Anderson, and F. Gage**. 2001. Stem and progenitor cells: Origins, phenotypes, lineage commitments, and transdifferentiations. Annual Review of Cell and Developmental Biology **17**:387-403.

202. **McGrath, K. E. and J. Palis**. 2005. Hematopoiesis in the yolk sac: more than meets the eye. Exp. Hematol. **33**:1021-1028.

203. **Medvinsky, A. and E. Dzierzak**. 1996. Definitive hematopoiesis is autonomously initiated by the AGM region. Cell **86**:897-906.

204. **Muller, A. M., A. Medvinsky, J. Strouboulis, F. Grosveld, and E. Dzierzak**. 1994. Development of hematopoietic stem cell activity in the mouse embryo. Immunity.

1:291-301.

205. **Tavassoli, M.** 1991. Embryonic and fetal hemopoiesis: an overview. Blood Cells **17**:269-281.

206. **Ciofani, M. and J. C. Zuniga-Pflucker**. 2007. The thymus as an inductive site for T lymphopoiesis. Annu. Rev. Cell Dev. Biol. **23**:463-493.

207. **Ogawa, M.** 1993. Differentiation and Proliferation of Hematopoietic Stem-Cells. Blood **81**:2844-2853.

208. **Metcalf, D., G. R. Johnson, and Mandel T.E.** 1979. Colony formation in agar by multipotential hemopoietic cells. Journal of Cellular Physiology **98**:401-420.

209. **Akashi, K., D. Traver, T. Miyamoto, and I. L. Weissman**. 2000. A clonogenic common myeloid progenitor that gives rise to all myeloid lineages. Nature **404**:193-197.

210. **Reya, T., S. J. Morrison, M. F. Clarke, and I. L. Weissman**. 2001. Stem cells, cancer, and cancer stem cells. Nature **414**:105-111.

211. **Spangrude, G. J., S. Heimfeld, and I. L. Weissman**. 1988. Purification and Characterization of Mouse Hematopoietic Stem-Cells. Science **241**:58-62.

212. **Ikuta, K. and I. L. Weissman**. 1992. Evidence that hematopoietic stem cells express mouse c-kit but do not depend on steel factor for their generation. Proceedings of the National Academy of Sciences of the United States of America **89**:1502-1506.

213. **Osawa, M., K. Hanada, H. Hamada, and H. Nakauchi**. 1996. Long-term lymphohematopoietic reconstitution by a single CD34-low/negative hematopoietic stem cell. Science **273**:242-245.

214. **Morrison, S. J. and I. L. Weissman**. 1994. The long-term repopulating subset of hematopoietic stem cells is deterministic and isolatable by phenotype. Immunity. **1**:661-673.

215. **Ehninger, A. and A. Trumpp**. 2011. The bone marrow stem cell niche grows up: mesenchymal stem cells and macrophages move in. J. Exp. Med. **208**:421-428.

216. **Fliedner, T. M.** 1998. The role of blood stem cells in hematopoietic cell renewal. Stem Cells **16 Suppl 1**:13-29.

217. **Whetton, A. D. and G. J. Graham**. 1999. Homing and mobilization in the stem cell

niche. Trends Cell Biol. **9**:233-238.

218. **Orford, K. W. and D. T. Scadden**. 2008. Deconstructing stem cell self-renewal: genetic insights into cell-cycle regulation. Nature Reviews Genetics **9**:115-128.

219. **Cheng, T., N. Rodrigues, H. M. Shen, Y. G. Yang, D. Dombkowski, M. Sykes, and D. T. Scadden**. 2000. Hematopoietic stem cell quiescence maintained by p21(cip1/waf1). Science **287**:1804-1808.

220. **Zon, L. I.** 2008. Intrinsic and extrinsic control of haematopoietic stem-cell self-renewal. Nature **453**:306-313.

221. **Passegue, E., A. J. Wagers, S. Giuriato, W. C. Anderson, and I. L. Weissman**. 2005. Global analysis of proliferation and cell cycle gene expression in the regulation of hematopoietic stem and progenitor cell fates. Journal of Experimental Medicine **202**:1599-1611.

222. **Niedernhofer, L. J.** 2008. DNA repair is crucial for maintaining hematopoietic stem cell function. Dna Repair **7**:523-529.

223. **Dumble, M., L. Moore, S. M. Chambers, H. Geiger, G. Van Zant, M. A. Goodell, and L. A. Donehower**. 2007. The impact of altered p53 dosage on hematopoietic stem cell dynamics during aging. Blood **109**:1736-1742.

224. **Rossi, D. J., D. Bryder, J. Seita, A. Nussenzweig, J. Hoeijmakers, and I. L. Weissman**. 2007. Deficiencies in DNA damage repair limit the function of haematopoietic stem cells with age. Nature **447**:725-729.

225. **Nijnik, A., L. Woodbine, C. Marchetti, S. Dawson, T. Lambe, C. Liu, N. P. Rodrigues, T. L. Crockford, E. Cabuy, A. Vindigni, T. Enver, J. I. Bell, P. Slijepcevic, C. C. Goodnow, P. A. Jeggo, and R. J. Cornall**. 2007. DNA repair is limiting for haematopoietic stem cells during ageing. Nature **447**:686-690.

226. **Yamazaki, S., A. Iwama, S. I. Takayanagi, Y. Morita, K. Eto, H. Ema, and H. Nakauchi**. 2006. Cytokine signals modulated via lipid rafts mimic niche signals and induce hibernation in hematopoietic stem cells. Embo Journal **25**:3515-3523.

227. **Tothova, Z., R. Kollipara, B. J. Huntly, B. H. Lee, D. H. Castrillon, D. E. Cullen, E. P. McDowell, S. Lazo-Kallanian, I. R. Williams, C. Sears, S. A. Armstrong, E. Passegue, R. A. DePinho, and D. G. Gilliland**. 2007. FoxOs are critical mediators of hematopoietic stem cell resistance to physiologic oxidative stress. Cell **128**:325-339.

228. **Miyamoto, K., K. Y. Araki, K. Naka, F. Arai, K. Takubo, S. Yamazaki, S.**

Matsuoka, T. Miyamoto, K. Ito, M. Ohmura, C. Chen, K. Hosokawa, H. Nakauchi, K. Nakayama, K. I. Nakayama, M. Harada, N. Motoyama, T. Suda, and A. Hirao. 2007. Foxo3a is essential for maintenance of the hematopoietic stem cell pool. Cell Stem Cell **1**:101-112.

229. **Simsek, T., F. Kocabas, J. K. Zheng, R. J. DeBerardinis, A. I. Mahmoud, E. N. Olson, J. W. Schneider, C. C. Zhang, and H. A. Sadek**. 2010. The Distinct Metabolic Profile of Hematopoietic Stem Cells Reflects Their Location in a Hypoxic Niche. Cell Stem Cell **7**:380-390.

230. **Yarbro, J. W.** 1992. Mechanism of Action of Hydroxyurea. Seminars in Oncology **19**:1-10.

231. **Uchida, N., A. M. Friera, D. P. He, M. J. Reitsma, A. S. Tsukamoto, and I. L. Weissman**. 1997. Hydroxyurea can be used to increase mouse c-kit(+)Thy-1.1(lo)Lin(-/lo)Sca-1(+) hematopoietic cell number and frequency in cell cycle in vivo. Blood **90**:4354-4362.

232. **Wang, J., H. Iwasaki, A. Krivtsov, P. G. Febbo, A. R. Thorner, P. Ernst, E. Anastasiadou, J. L. Kutok, S. C. Kogan, S. S. Zinkel, J. K. Fisher, J. L. Hess, T. R. Golub, S. A. Armstrong, K. Akashi, and S. J. Korsmeyer**. 2005. Conditional MLL-CBP targets GMP and models therapy-related myeloproliferative disease. EMBO J. **24**:368-381.

233. **Mendez, J. and B. Stillman**. 2000. Chromatin association of human origin recognition complex, Cdc6, and minichromosome maintenance proteins during the cell cycle: Assembly of prereplication complexes in late mitosis. Molecular and Cellular Biology **20**:8602-8612.

234. **Xiang, J., D. Chao, and S. Korsmeyer**. 1996. BAX-induced cell death may not require interleukin 1 beta-converting enzyme-like proteases. Proceedings of the National Academy of Sciences of the United States of America **93**:14559-14563.

235. **Liu, Y., T. J. Zhao, Y. B. Yan, and H. M. Zhou**. 2005. Increase of soluble expression in Escherichia coli cytoplasm by a protein disulfide isomerase gene fusion system. Protein Expression and Purification **44**:155-161.

236. **Mer, G., A. Bochkarev, R. Gupta, E. Bochkareva, L. Frappier, C. J. Ingles, A. M. Edwards, and W. J. Chazin**. 2000. Structural basis for the recognition of DNA repair proteins UNG2, XPA, and RAD52 by replication factor RPA. Cell **103**:449-456.

237. **Jiang, X. H., V. Klimovich, A. I. Arunkumar, E. B. Hysinger, Y. D. Wang, R. D. Ott,**

G. D. Guler, B. Weiner, W. J. Chazin, and E. Fanning. 2006. Structural mechanism of RPA loading on DNA during activation of a simple pre-replication complex. Embo Journal **25**:5516-5526.

238. **Namiki, Y. and L. Zou**. 2006. ATRIP associates with replication protein A-coated ssDNA through multiple interactions. Proceedings of the National Academy of Sciences of the United States of America **103**:580-585.

239. **Dominguez, C., R. Boelens, and A. M. Bonvin**. 2003. HADDOCK: a protein-protein docking approach based on biochemical or biophysical information. J. Am. Chem. Soc. **125**:1731-1737.

240. **de Vries, S. J., A. D. van Dijk, M. Krzeminski, D. M. van, A. Thureau, V. Hsu, T. Wassenaar, and A. M. Bonvin**. 2007. HADDOCK versus HADDOCK: new features and performance of HADDOCK2.0 on the CAPRI targets. Proteins **69**:726-733.

241. **Hubbard, S. J. and J. M. Thornton**. 1993. "NACCESS"Computer Program, Department of Biochemistry and Molecular Biology, University College London.

242. **Ball, H. L., M. R. Ehrhardt, D. A. Mordes, G. G. Glick, W. J. Chazin, and D. Cortez**. 2007. Function of a conserved checkpoint recruitment domain in ATRIP proteins. Molecular and Cellular Biology **27**:3367-3377.

243. **Bermudez, V. P., L. A. Lindsey-Boltz, A. J. Cesare, Y. Maniwa, J. D. Griffith, J. Hurwitz, and A. Sancar**. 2003. Loading of the human 9-1-1 checkpoint complex onto DNA by the checkpoint clamp loader hRad17-replication factor C complex in vitro. Proceedings of the National Academy of Sciences of the United States of America **100**:1633-1638.

244. **Sax, J. K., P. Fei, M. E. Murphy, E. Bernhard, S. J. Korsmeyer, and W. S. El-Deiry**. 2002. BID regulation by p53 contributes to chemosensitivity. Nat. Cell Biol. **4**:842-849.

245. **Casper, A. M., P. Nghiem, M. F. Arlt, and T. W. Glover**. 2002. ATR regulates fragile site stability. Cell **111**:779-789.

246. **Cortez, D., G. Glick, and S. J. Elledge**. 2004. Minichromosome maintenance proteins are direct targets of the ATM and ATR checkpoint kinases. Proc. Natl. Acad. Sci. U. S. A **101**:10078-10083.

247. **Yoo, H. Y., A. Shevchenko, A. Shevchenko, and W. G. Dunphy**. 2004. Mcm2 is a direct substrate of ATM and ATR during DNA damage and DNA replication checkpoint responses. J. Biol. Chem. **279**:53353-53364.

248. **Sorensen, C. S., R. G. Syluasen, J. Falck, T. Schroeder, L. Ronnstrand, K. K. Khanna, B. B. Zhou, J. Bartek, and J. Lukas**. 2003. Chk1 regulates the S phase checkpoint by coupling the physiological turnover and ionizing radiation-induced accelerated proteolysis of Cdc25A. Cancer Cell **3**:247-258.

249. **Boutros, R., C. Dozier, and B. Ducommun**. 2006. The when and wheres of CDC25 phosphatases. Current Opinion in Cell Biology **18**:185-191.

250. **Fisher, D. and M. Mechali**. 2004. Sleeping policemen for DNA replication? Nat. Cell Biol. **6**:576-577.

251. **Kastan, M. B. and J. Bartek**. 2004. Cell-cycle checkpoints and cancer. Nature **432**:316-323.

252. **Maya-Mendoza, A., E. Petermann, D. A. Gillespie, K. W. Caldecott, and D. A. Jackson**. 2007. Chk1 regulates the density of active replication origins during the vertebrate S phase. EMBO J. **26**:2719-2731.

253. **Ball, H. L. and D. Cortez**. 2005. ATRIP oligomerization is required for ATR-dependent checkpoint signaling. Journal of Biological Chemistry **280**:31390-31396.

254. **Zinkel, S., A. Gross, and E. Yang**. 2006. BCL2 family in DNA damage and cell cycle control. Cell Death and Differentiation **13**:1351-1359.

255. **Cheng, W. C., S. B. Berman, I. Ivanovska, E. A. Jonas, S. J. Lee, Y. Chen, L. K. Kaczmarek, F. Pineda, and J. M. Hardwick**. 2006. Mitochondrial factors with dual roles in death and survival. Oncogene **25**:4697-4705.

256. **Danial, N. N., L. D. Walensky, C. Y. Zhang, C. S. Choi, J. K. Fisher, A. J. Molina, S. R. Datta, K. L. Pitter, G. H. Bird, J. D. Wikstrom, J. T. Deeney, K. Robertson, J. Morash, A. Kulkarni, S. Neschen, S. Kim, M. E. Greenberg, B. E. Corkey, O. S. Shirihai, G. I. Shulman, B. B. Lowell, and S. J. Korsmeyer**. 2008. Dual role of proapoptotic BAD in insulin secretion and beta cell survival. Nat. Med. **14**:144-153.

257. **Ta, V. B. T., K. Bezstarosti, J. A. A. Demmers, T. Maculins, K. Schellekens, D. C. van Gent, and S. P. Persengiev**. 2008. Proapoptotic Bid Association with Mre11-Rad50-Nbs1 Complex is Indispensable for Checkpoint Activation after DNA Damage. Available from Nature Precedings <http://hdl. handle. net/10101/npre. 2007. 1203. 1>.

258. **Burrows, A. E. and S. J. Elledge**. 2008. How ATR turns on: TopBP1 goes on ATRIP with ATR. Genes Dev. **22**:1416-1421.

259. **Jamil, S., S. Mojtabavi, P. Hojabrpour, S. Cheah, and V. Duronio**. 2008. An essential role for MCL-1 in ATR-mediated CHK1 phosphorylation. Molecular Biology of the Cell **19**:3212-3220.

260. **Jamil, S., C. Stoica, T. L. Hackett, and V. Duronio**. 2010. MCL-1 localizes to sites of DNA damage and regulates DNA damage response. Cell Cycle **9**:2843-2855.

261. **Zinkel, S. S., K. E. Hurov, and A. Gross**. 2007. Bid plays a role in the DNA damage response. Cell **130**:9-10.

262. **Segurado, M. and J. A. Tercero**. 2009. The S-phase checkpoint: targeting the replication fork. Biol. Cell **101**:617-627.

263. **Arunkumar, A. I., M. E. Stauffer, E. Bochkareva, A. Bochkarev, and W. J. Chazin**. 2003. Independent and coordinated functions of replication protein A tandem high affinity single-stranded DNA binding domains. J. Biol. Chem. **278**:41077-41082.

264. **Bhattacharya, S., M. V. Botuyan, F. Hsu, X. Shan, A. I. Arunkumar, C. H. Arrowsmith, A. M. Edwards, and W. J. Chazin**. 2002. Characterization of binding-induced changes in dynamics suggests a model for sequence-nonspecific binding of ssDNA by replication protein A. Protein Sci. **11**:2316-2325.

265. **Henricksen, L. A., C. B. Umbricht, and M. S. Wold**. 1994. Recombinant Replication Protein-A - Expression, Complex-Formation, and Functional-Characterization. Journal of Biological Chemistry **269**:11121-11132.

266. **Wang, Q. H., F. Q. Gao, W. S. May, Y. D. Zhang, T. Zhang, and X. M. Deng**. 2008. Bcl2 negatively regulates DNA double-strand-break repair through a nonhomologous end-joining pathway. Molecular Cell **29**:488-498.

267. **Jamil, S., R. Sobouti, P. Hojabrpour, M. Raj, J. Kast, and V. Duronio**. 2005. A proteolytic fragment of Mcl-1 exhibits nuclear localization and regulates cell growth by interaction with Cdk1. Biochemical Journal **387**:659-667.

268. **Pawlikowska, P., I. Leray, B. de Laval, S. Guihard, R. Kumar, F. Rosselli, and F. Porteu**. 2010. ATM-dependent expression of IEX-1 controls nuclear accumulation of Mcl-1 and the DNA damage response. Cell Death and Differentiation **17**:1739-1750.

269. **Guo, J. Y., A. Yamada, T. Kajino, J. Q. Wu, W. Tang, C. D. Freel, J. Feng, B. N. Chau, M. Z. Wang, S. S. Margolis, H. Y. Yoo, X. F. Wang, W. G. Dunphy, P. M. Irusta, J. M. Hardwick, and S. Kornbluth**. 2008. Aven-dependent activation of ATM following DNA damage. Current Biology **18**:933-942.

270. **Choi, J. H., L. A. Lindsey-Boltz, M. Kemp, A. C. Mason, M. S. Wold, and A. Sancar**. 2010. Reconstitution of RPA-covered single-stranded DNA-activated ATR-Chk1 signaling. Proceedings of the National Academy of Sciences of the United States of America **107**:13660-13665.

271. **MacDougall, C. A., T. S. Byun, C. Van, M. C. Yee, and K. A. Cimprich**. 2007. The structural determinants of checkpoint activation. Genes & Development **21**:898-903.

272. **Van, C., S. Yan, W. M. Michael, S. Waga, and K. A. Cimprich**. 2010. Continued primer synthesis at stalled replication forks contributes to checkpoint activation. Journal of Cell Biology **189**:233-246.

273. **Nam, E. A. and D. Cortez**. 2011. ATR signalling: more than meeting at the fork. Biochem. J. **436**:527-536.

274. **Cliby, W. A., C. J. Roberts, K. A. Cimprich, C. M. Stringer, J. R. Lamb, S. L. Schreiber, and S. H. Friend**. 1998. Overexpression of a kinase-inactive ATR protein causes sensitivity to DNA-damaging agents and defects in cell cycle checkpoints. Embo Journal **17**:159-169.

275. **Wright, J. A., K. S. Keegan, D. R. Herendeen, N. J. Bentley, A. M. Carr, M. F. Hoekstra, and P. Concannon**. 1998. Protein kinase mutants of human ATR increase sensitivity to UV and ionizing radiation and abrogate cell cycle checkpoint control. Proceedings of the National Academy of Sciences of the United States of America **95**:7445-7450.

276. **Morrison, S. J., A. M. Wandycz, K. Akashi, A. Globerson, and I. L. Weissman**. 1996. The aging of hematopoietic stem cells. Nature Medicine **2**:1011-1016.

277. **Rossi, D. J., D. Bryder, J. M. Zahn, H. Ahlenius, R. Sonu, A. J. Wagers, and I. L. Weissman**. 2005. Cell intrinsic alterations underlie hematopoietic stem cell aging. Proceedings of the National Academy of Sciences of the United States of America **102**:9194-9199.

278. **Cairns, J.** 1975. Mutation Selection and Natural-History of Cancer. Nature **255**:197-200.

279. **Opferman, J. T. and S. J. Korsmeyer**. 2003. Apoptosis in the development and maintenance of the immune system. Nature Immunology **4**:410-415.

280. **Lobo, N. A., Y. Shimono, D. Qian, and M. F. Clarke**. 2007. The biology of cancer stem cells. Annual Review of Cell and Developmental Biology **23**:675-699.

281. **Unsal-Kacmaz, K. and A. Sancar**. 2004. Quaternary structure of ATR and effects

of ATRIP and replication protein A on its DNA binding and kinase activities. Molecular and Cellular Biology **24**:1292-1300.

282. **Friedel, A. M., B. L. Pike, and S. M. Gasser**. 2009. ATR/Mec1: coordinating fork stability and repair. Current Opinion in Cell Biology **21**:237-244.

283. **Cobb, J. A., L. Bjergbaek, K. Shimada, C. Frei, and S. M. Gasser**. 2003. DNA polymerase stabilization at stalled replication forks requires Mec1 and the RecQ helicase Sgs1. Embo Journal **22**:4325-4336.

284. **Cobb, J. A., T. Schleker, V. Rojas, L. Bjergbaek, J. A. Tercero, and S. M. Gasser**. 2005. Replisome instability, fork collapse, and gross chromosomal rearrangements arise synergistically from Mec1 kinase and RecQ helicase mutations. Genes & Development **19**:3055-3069.

285. **Lou, H. Q., M. Komata, Y. Katou, Z. Y. Guan, C. C. Reis, M. Budd, K. Shirahige, and J. L. Campbell**. 2008. Mrc1 and DNA Polymerase epsilon Function Together in Linking DNA Replication and the S Phase Checkpoint. Molecular Cell **32**:106-117.

286. **Sirbu, B. M., F. B. Couch, J. T. Feigerle, S. Bhaskara, S. W. Hiebert, and D. Cortez**. 2011. Analysis of protein dynamics at active, stalled, and collapsed replication forks. Genes Dev. **25**:1320-1327.

287. **Bao, S. D., R. S. Tibbetts, K. M. Brumbaugh, Y. N. Fang, D. A. Richardson, A. Ali, S. M. Chen, R. T. Abraham, and X. F. Wang**. 2001. ATR/ATM-mediated phosphorylation of human Rad17 is required for genotoxic stress responses. Nature **411**:969-974.

288. **Post, S., Y. C. Weng, K. Cimprich, L. B. Chen, Y. Xu, and E. Y. H. P. Lee**. 2001. Phosphorylation of serines 635 and 645 of human Rad17 is cell cycle regulated and is required for G(1)/S checkpoint activation in response to DNA damage. Proceedings of the National Academy of Sciences of the United States of America **98**:13102-13107.

289. **Goodship, J., H. Gill, J. Carter, A. Jackson, M. Splitt, and M. Wright**. 2000. Autozygosity mapping of a seckel syndrome locus to chromosome 3q22. 1-q24. Am. J. Hum. Genet. **67**:498-503.

290. **Stegh, A. H., C. Brennan, J. A. Mahoney, K. L. Forloney, H. T. Jenq, J. P. Luciano, A. Protopopov, L. Chin, and R. A. DePinho**. 2010. Glioma oncoprotein Bcl2L12 inhibits the p53 tumor suppressor. Genes & Development **24**:2194-2204.

291. **Green, M. M., G. J. Hutchison, H. R. Valentine, R. J. Fitzmaurice, S. E. Davidson,**

R. D. Hunter, C. Dive, C. M. West, and I. J. Stratford. 2005. Expression of the proapoptotic protein Bid is an adverse prognostic factor for radiotherapy outcome in carcinoma of the cervix. Br. J. Cancer **92**:449-458.

292. **Lee, J. H., Y. H. Soung, J. W. Lee, W. S. Park, S. Y. Kim, Y. G. Cho, C. J. Kim, S. H. Seo, H. S. Kim, S. W. Nam, N. J. Yoo, S. H. Lee, and J. Y. Lee**. 2004. Inactivating mutation of the pro-apoptotic gene BID in gastric cancer. Journal of Pathology **202**:439-445.